School of Chemical and Environmental Engineering
Technical University of Crete
Doctoral Studies in Environmental Engineering
Laboratory of Aquatic Chemistry

PhD Thesis
Advanced Studies on the Detection and Fate of Organic Pollutants in water

Nikolitsa Solomou

Advisory Committee
Professor ELEFTHERIA PSYLLAKI – Supervisor
Associate Professor PARASKEVI PANAGIOTOPOULOU
Professor LORENA VIDAL MARTINEZ

CHANIA
July 2023

Examination Committee

ELEFTHERIA PSYLLAKI – Supervisor

Professor,

School of Chemical and Environmental Engineering,

Technical University of Crete,

Chania, Greece

PARASKEVI PANAGIOTOPOULOU – Advisory Committee

Associate Professor,

School of Chemical and Environmental Engineering,

Technical University of Crete,

Chania, Greece

LORENA VIDAL MARTINEZ – Advisory Committee

Professor,

Department of Analytical Chemistry, Nutrition and Food Sciences,

University of Alicante,

Alicante, Spain

NIKOS KALOGERAKIS

Professor,

School of Chemical and Environmental Engineering,

Technical University of Crete,

Chania, Greece

NIKOLAOS NIKOLAIDIS

Professor,

School of Chemical and Environmental Engineering,

Technical University of Crete,

Chania, Greece

DANAI VENIERI

Associate Professor,

School of Chemical and Environmental Engineering,

Technical University of Crete,

Chania, Greece

APOSTOLOS GIANNIS

Assistant Professor,

School of Chemical and Environmental Engineering,

Technical University of Crete,

Chania, Greece

In loving memory of my father L.S.

Acknowledgements

Foremost, I would like to express my deepest gratitude to my supervisor Professor, Elefteria Psillakis for her guidance, support, patience and faith in me and my potential as a new researcher throughout my studies. Her immense knowledge and motivation, as well as her attention to detail, helped me to successfully conclude my research and broadened my horizons towards the envisioning of my future work prospects.

I would also like to express my sincere appreciation to the advisory committee, Associate Professor Paraskevi Panagiotopoulou and Professor Lorena Vidal, for their excellent cooperation, encouragement and overall insights throughout my studies and preparation of my thesis.

I would also like to thank the rest of my thesis committee, Professor N. Kalogerakis, Professor N. Nikolaidis, Associate Professor D. Venieri and Assistant Professor A. Giannis, for taking the time to evaluate my thesis and participate in the examination.

From the bottom of my heart, I would like to say a big thank you to all my lab mates who became lifetime friends to me and with whom I shared this exciting and at times challenging experience. Their presence in my everyday life during my research years in the lab was the constituent that kept me on track.

I am deeply indebted to my family, my loving mother and father. They loved me unconditionally and supported me emotionally and financially all through these years.

I could not have undertaken this journey without my father, my personal hero and the biggest fighter I know. He was my beacon of hope through my darkest times with his infectious positivity and incomparable sense of humor. He was the reason I decided to excel academically and although he is greatly missed from my life, he is the reason my morale was never bent. As most of the times, words fail to describe what our hearts know to be true, I can only say: “This is for you, dad”.

TABLE OF CONTENTS

TABLE OF FIGURES

TABLE OF TABLES

ΠΕΡΙΛΗΨΗ

Η παρούσα διδακτορική διατριβή προσανατολίζεται στη διερεύνηση του ευρύτερου θέματος των προηγμένων μελετών ανίχνευσης και παρακολούθησης της τύχης των οργανικών ρύπων στο υδάτινο περιβάλλον. Η επίτευξη αυτού του στόχου υλοποιείται με τη χρήση διαφόρων επιστημονικών μέσων, που κυμαίνονται από την καθιέρωση καινοτόμων τεχνικών μικροεκχύλισης υπό ατμοσφαιρική πίεση καθώς και υπό συνθήκες κενού σχετικά με την παρουσία αρωματικών υδρογονανθράκων στα εκπλύματα νερού και προϊόντων καπνού, έως την προκαλούμενη από την UVC αποικοδόμηση τόσο μίας διαδεδομένης φαρμακευτικής ουσίας (σιλαστατίνη) όσο και της νικοτίνης σε φυσικό νερό και επεξεργασμένα λύματα, όπου μελετάται διεξοδικά η κινητική της φωτοαποικοδόμησης των ουσιών αυτών.

Στο **Κεφάλαιο 1** παρουσιάζονται εισαγωγικά θέματα. Επιδεικνύεται μια ολοκληρωμένη ανασκόπηση της προετοιμασίας δείγματος και της ταξινόμησης των πιο δημοφιλών τεχνικών εκχύλισης. Ιδιαίτερη προσοχή δίνεται στις τεχνικές προετοιμασίας δείγματος χωρίς διαλύτες και πιο συγκεκριμένα στις αρχές SPME και SBSE, στους δύο τρόπους δειγματοληψίας τους (άμεσος και στον υπερκείμενο χώρο) και στις παραμέτρους βελτιστοποίησης που εφαρμόζονται για την επίτευξη βέλτιστων αποδόσεων εκχύλισης σε κάθε τεχνική. Έμφαση δίνεται στην επίδραση του κενού στη δειγματοληψία μικροεκχύλισης υπερκείμενου χώρου, ως εναλλακτικό τρόπο επιτάχυνσης της κινητικής μιας διαδικασίας εκχύλισης και ως εκ τούτου επίτευξης ταχύτερων χρόνων εξισορρόπησης. Η ανάπτυξη του θεωρητικού μοντέλου παρουσιάζεται μαζί με αρχές σχετικά με την (αν)εξαρτησία από την πίεση στην ισορροπία και την εξάρτηση από την πίεση σε συνθήκες προ-ισορροπίας δειγματοληψίας υπερκείμενου χώρου από δείγματα νερού και του K_H κριτηρίου. Η HiSorb Sorptive Extraction ως τεχνική μικροεκχύλισης στερεής φάσης αναφέρεται επίσης εδώ. Τέλος, το θέμα της φωτοαποικοδόμησης εξετάζεται σε θεωρητική βάση, καλύπτοντας τους μηχανισμούς αποδόμησης και τις διαδικασίες φωτόλυσης καθώς και τις βασικές αρχές της φωτόλυσης, την κινητική των διαδικασιών αποδόμησης και τους μηχανισμούς αντίδρασης που παρατηρούνται κατά τις φωτολυτικές διαδικασίες.

Στο **Κεφάλαιο 2** παρουσιάζεται το δημοσιευμένο άρθρο με τίτλο: ***Προσροφητική εκχύλιση υπερκείμενου χώρου υποβοηθούμενη από κενό: Θεωρητικοί παράγοντες και απόδειξη της ιδέας εκχύλισης πολυκυκλικών αρωματικών υδρογονανθράκων από δείγματα νερού.*** Σε αυτή την μελέτη, προτείνουμε τη δειγματοληψία HSSE υπό συνθήκες κενού ως την πλέον κατάλληλη για τη μείωση των χρόνων επίτευξης ισορροπίας. Συνεπώς, παρουσιάζεται ένα θεωρητικό μοντέλο που περιγράφει την εξάρτηση από την πίεση της επονομαζόμενης μεθόδου HSSE με υποβοήθηση κενού

(Vac-HSSE) και το οποίο προβλέπει τη μείωση των χρόνων επίτευξης ισορροπίας ως επακόλουθο της μείωσης της πίεσης δειγματοληψίας. Εκμεταλλευόμαστε τη θεωρητική διατύπωση για να καταλήξουμε σε ορισμένα γενικά συμπεράσματα για την HSSE σχετικά με τη σχέση μεταξύ των φυσικών χαρακτηριστικών της ράβδου ανάδευσης, των ρυθμών πρόσληψης και των χρόνων εξισορρόπησης. Οι θεωρητικές προβλέψεις επαληθεύτηκαν πειραματικά χρησιμοποιώντας υδατικά διαλύματα με ναφθαλίνιο, ακεναφθένιο και φθορανθένιο ως αναλυόμενες ενώσεις. Τα αποτελέσματα της θερμοκρασίας δειγματοληψίας και του χρόνου εκχύλισης υπό συνθήκες κενού αλλά και κανονικής πίεσης διερευνήθηκαν διεξοδικά. Το θετικά συνδυασμένο αποτέλεσμα της θέρμανσης του δείγματος υπό χαμηλή πίεση δειγματοληψίας έδειξε ότι η υψηλή υγρασία δεν επηρέασε την απόδοση της φάσης εκχύλισης, ένα φαινόμενο που παρατηρείται συχνά στη μικροεκχύλιση στερεής φάσης υπερκείμενου χώρου. Τα προφίλ χρόνου εκχύλισης που κατασκευάστηκαν στους 25 και 55 ^{o}C απέδειξαν την ουσιαστική βελτίωση στην κινητική εκχύλισης με Vac-HSSE σε σύγκριση με την μέθοδο HSSE σε ατμοσφαιρική πίεση. Τα αποτελέσματα για το ναφθαλίνιο (για το οποίο υφίσταται η γενική παραδοχή ότι εξατμίζεται σχετικά γρήγορα από το δείγμα νερού) παρείχαν την απόδειξη ότι σε 1 atm η αντίσταση από πλευράς αέριας φάσης περιόριζε την πρόσληψη της αναλυόμενης ουσίας από τη ράβδο ανάδευσης και ότι αυτός ο περιορισμός έχει τη δυνατότητα να εξαλειφθεί αποτελεσματικά με την υιοθέτηση της προσέγγισης δειγματοληψίας σε συνθήκες κενού. Οι επιταχύνσεις στην επίτευξη ισορροπίας που σημειώθηκαν για τις αναλυόμενες ενώσεις του ακεναφθενίου και του φθορανθενίου υποδηλώνουν ότι οι περιορισμοί της αέριας φάσης περιόριζαν τόσο τη διαδικασία εξάτμισης όσο και την διαδικασία πρόσληψης των δύο ουσιών. Η ξεχωριστή βελτιστοποίηση της μεθόδου HSSE υπό κάθε συνθήκη πίεσης απέδωσε μικρότερο χρόνο δειγματοληψίας στην περίπτωση της Vac-HSSE σε σύγκριση με την διαδικασία HSSE σε ατμοσφαιρική πίεση (30 λεπτά έναντι 60 λεπτών αντίστοιχα). Οι αναλυτικές επιδόσεις των δύο βελτιστοποιημένων μεθόδων αξιολογήθηκαν και συνήχθη το συμπέρασμα ότι η Vac-HSSE δρούσε παρόμοια (ναφθαλίνιο και ακεναφθένιο) ή καλύτερα (φθορανθένιο) από την υπό κανονικές συνθήκες HSSE στο μισό χρόνο δειγματοληψίας που θα χρειαζόταν.

Στο **Κεφάλαιο 3** παρουσιάζεται το δημοσιευμένο άρθρο με τίτλο: ***Ολικοί και βιοδιαθέσιμοι πολυκυκλικοί αρωματικοί υδρογονάνθρακες σε αχρησιμοποίητα και χρησιμοποιημένα θερμαινόμενα προϊόντα καπνού και συμβατικά τσιγάρα.*** Οι παρούσες μελέτες αναφέρουν, για πρώτη φορά, τις συνολικές και βιοδιαθέσιμες συγκεντρώσεις πολυκυκλικών αρωματικών υδρογονανθράκων (PAHs) σε αχρησιμοποίητα και σε χρησιμοποιημένα θερμαινόμενα προϊόντα καπνού (HnBs). Προκειμένου να επιτευχθούν άμεσες συγκρίσεις, διεξήχθησαν πανομοιότυπα σύνολα μελετών και για συμβατικά τσιγάρα (CC). Προσδιορίστηκαν πέντε PAHs χαμηλού

μοριακού βάρους στα HnBs σε ολικές συγκεντρώσεις που ήταν της ίδιας τάξης πριν και μετά τη διαδικασία θέρμανσης τους (Σ_5PAH=47,37±3,44 ng unit^{-1} και Σ_5PAH=69,36±5,78 ng unit^{-1} σε αχρησιμοποίητα και χρησιμοποιημένα HnBs, αντίστοιχα) . Η ατελής καύση οργανικών ουσιών κατά το κάπνισμα των CC, απέδωσε σημαντικά υψηλότερες ποσότητες PAHs, με το άθροισμά τους (Σ_{10}PAHs=1449±113ng unit^{-1}) να είναι >20 φορές μεγαλύτερο από εκείνο των HnBs. Ο καπνός και το φίλτρο αποδείχτηκαν τα πιο ρυπασμένα τμήματα των HnBs. Σε αχρησιμοποίητα CC, ο καπνός έφερε το υψηλότερο φορτίο PAHs, ενώ μετά το κάπνισμα τους, το φίλτρο ήταν το πιο ρυπασμένο μέρος τους, περιέχοντας ~80% της συνολικής ποσότητας των PAHs. Το ναφθαλίνιο αποδείχτηκε το πιο άφθονο σε ποσότητα από όλους τους PAHs ενώ εντοπίστηκε σε όλα τα προϊόντα καπνού. Παρά τις υψηλές ολικές συγκεντρώσεις PAHs που βρέθηκαν στα καπνισμένα CC, τα αθροίσματα των βιοδιαθέσιμων συγκεντρώσεων PAHs ήταν της ίδιας τάξης σε όλα τα ελεγμένα προϊόντα καπνού (Σ_5PAH=61,38±1,79ng unit^{-1} σε αχρησιμοποίητα HnBs, Σ_5PAH=70,87±7,67ng unit^{-1} σε χρησιμοποιημένα HnBs, Σ_4PAH=66,92±5,95ng unit^{-1} σε αχρησιμοποίητα CC και Σ_6PAH=47,94±1,26ng unit^{-1} σε χρησιμοποιημένα CC). Το εύρημα αυτό σχετίστηκε με το γεγονός ότι το κάπνισμα επηρεάζει την έκπλυση των PAHs από τα CC και καθυστερεί την εκρόφησή τους από τη στερεά μήτρα. Η προσαρμογή του pH, της περιεκτικότητας σε αλάτι και σε χουμικά οξέα σε τιμές που ανταποκρίνονται με τις αντίστοιχες του περιβάλλοντος, δεν επηρέασε την έκπλυση των PAHs στις 24 ώρες εμποτισμού των προϊόντων καπνού. Τέλος, η συμπεριφορά έκπλυσης των PAHs σε φυσικά ύδατα (νερό ποταμού, βρόχινο νερό και θαλασσινό νερό) βρέθηκε παρόμοια με εκείνη στο υπερκάθαρο νερό, επαληθεύοντας πειραματικά την ικανότητα των αποβλήτων προϊόντων καπνού να διοχετεύουν PAHs στο υδάτινο περιβάλλον.

Στο **Κεφάλαιο 4** παρουσιάζεται το δημοσιευμένο άρθρο με τίτλο: ***UV-254 αποικοδόμηση της νικοτίνης σε φυσικά νερά και εκπλύματα που παράγονται από αποτσίγαρα και θερμαινόμενα προϊόντα καπνού.*** Σε αυτή τη μελέτη, εξετάζεται για πρώτη φορά η UV_{254} φωτολυτική τύχη της νικοτίνης στο φυσικό νερό και στα εκπλύματα που παράγονται από συμβατικά τσιγάρα (CCs) και τα νέας γενιάς προϊόντα καπνού που θερμαίνονται αλλά δεν καίγονται (HnBs). Αρχικά μελετήθηκε η επίδραση της ακτινοβολίας UV_{254} στην μείωση της νικοτίνης στο υπερκάθαρο νερό. Η αντίδραση ήταν ψευδο-πρώτης τάξης σε σχέση με τη συγκέντρωση νικοτίνης σε χαμηλές συγκεντρώσεις, και μετατοπίστηκε σε χαμηλότερη τάξη σε υψηλότερες συγκεντρώσεις, ένα αποτέλεσμα που σχετίζεται με τον κορεσμό προσρόφησης. Αν και η απομάκρυνση της νικοτίνης ήταν γρήγορη, μόνο το 9,5% του συνολικού οργανικού άνθρακα αφαιρέθηκε μετά την ακτινοβόληση κάτι που μπορεί να εξηγηθεί λόγω του σχηματισμού παραπροϊόντων. Οι χημικές δομές έξι φωτο-προϊόντων εξάχθηκαν μέσω

αέριας και υγρής χρωματογραφίας σε συνδυασμό με φασματομετρία μάζας. Από τα αποτελέσματα βρέθηκε πως η κινητική της φωτοαποικοδόμησης εξαρτάται από το pH και οι ταχύτερες κινητικές καταγράφηκαν όταν κυριαρχούσε η μονοπρωτονιωμένη μορφή της νικοτίνης (pH = 5-8). Η παρουσία χουμικών οξέων βρέθηκε να καθυστερεί ελαφρώς την κινητική καθώς ανταγωνίζονταν τη νικοτίνη για την ακτινοβολία του λαμπτήρα, ενώ η παρουσία αλατιού δεν είχε καμία επίδραση στην άμεση φωτόλυση της νικοτίνης. Επίσης, πραγματοποιήθηκαν μελέτες άμεσης φωτόλυσης χρησιμοποιώντας φυσικά νερά. Σε σύγκριση με το υπερκάθαρο νερό, η φωτοαποδόμηση βρέθηκε να προχωρά ελαφρώς πιο αργά στο νερό του ποταμού, σε παρόμοια κινητική στο θαλασσινό νερό και σχετικά πιο γρήγορα στο νερό της βροχής. Η παρατήρηση σχετικά με το νερό της βροχής φαίνεται να οφείλεται στο χαμηλότερο pH του σε σύγκριση με τα υπόλοιπα φυσικά ύδατα που δοκιμάστηκαν. Τα εκπλύματα από χρησιμοποιημένα HnBs και χρησιμοποιημένα CC υποβλήθηκαν επίσης σε ακτινοβολία UV_{254} και βρέθηκε ότι η άμεση φωτόλυση προχωρούσε γρήγορα παρά την υψηλή πολυπλοκότητα αυτών των μητρών. Παραταύτα, ο συνολικός οργανικός άνθρακας του συστήματος παρέμεινε ο ίδιος μετά την ακτινοβόληση λόγω της αφθονίας των οργανικών ενώσεων και των φωτοπροϊόντων που σχηματίστηκαν. Με αφορμή τις παραπάνω έρευνες αναφέρουμε σε αυτό το άρθρο τη συμπεριφορά έκπλυσης της νικοτίνης από HnBs και CC. Μεταξύ άλλων, βρέθηκε ότι στα HnBs ~70% της συνολικής και βιοδιαθέσιμης περιεκτικότητας σε νικοτίνη παραμένει στα sticks καπνού μετά την χρήση ενώ αυτό το ποσοστό πέφτει στο 15% στα CC λόγω της μείωσης της μάζας τους μετά το κάπνισμα. Αυτό το εύρημα αποδεικνύει τη σημασία της σωστής απόρριψης των απορριμμάτων προϊόντων καπνού για την επίτευξη της πρόληψης της έκπλυσης της νικοτίνης στα υδάτινα σώματα.

Στο **Κεφάλαιο 5** παρουσιάζεται το δημοσιευμένο άρθρο με τίτλο: ***UVC-παρακινούμενη αποικοδόμηση της σιλαστατίνης σε φυσικό νερό και επεξεργασμένα λύματα.*** Αυτή η εργασία αναφέρει για πρώτη φορά τη φωτοαποικοδόμηση UVC της σιλαστατίνης, ενός αναστολέα της νεφρικής αφυδροπεπτιδάσης που συγχορηγείται με το αντιβιοτικό ιμιπενέμη. Αρχικά, παρασκευάστηκαν διαλύματα σιλαστατίνης σε διάφορες συγκεντρώσεις σε υπερκάθαρο νερό και η άμεση φωτόλυση της σιλαστατίνης παρακολουθήθηκε υπό ακτινοβολία 254 nm. Η αποικοδόμηση ήταν πιο αργή σε υψηλότερες αρχικές συγκεντρώσεις σιλαστατίνης, λόγω κορεσμού προσρόφησης. Από τα διάφορα εκλουόμενα φωτοπροϊόντα, μόνο ένα προσδιορίστηκε δοκιμαστικά ως οξειδωμένη σιλαστατίνη φερόμενη μια ομάδα σουλφοξειδίου. Η φωτόλυση UV-254 επιτεύχθηκε πιο γρήγορα σε χαμηλότερες τιμές pH, επειδή οι πρωτονιωμένες μορφές του μορίου (H_3A^+, H_2A) έχουν υψηλότερους συντελεστές απορρόφησης και υψηλότερες κβαντικές αποδόσεις φωτόλυσης από τις μη πρωτονιωμένες (HA., A_2^-). Η άμεση φωτόλυση της σιλαστατίνης δεν περιλαμβάνει

●OH, καθώς ένα τέτοιο σενάριο αποκλείστηκε από πειράματα στα οποία προστέθηκε τριτ-βουτανόλη ως παράγοντας δέσμευσης ●OH, ενώ από την άλλη μεριά η παρουσία χουμικών οξέων ανέστειλε τη φωτόλυση λόγω του ανταγωνισμού για απορρόφηση ακτινοβολίας. Η ίδια εξήγηση μπορεί εν μέρει να δοθεί σχετικά με την παρατήρηση ότι η κινητική φωτόλυσης της σιλαστατίνης ήταν πιο αργή σε δείγματα νερού βρύσης, ποταμών και επεξεργασμένων λυμάτων σε σύγκριση με το υπερκάθαρο νερό. Επιπροσθέτως, η κβαντική απόδοση άμεσης φωτόλυσης ήταν επίσης χαμηλότερη στις προαναφερόμενες μήτρες νερού σε σύγκριση με το υπερκάθαρο νερό. Παρόμοια ευρήματα που αφορούσαν την τρικλοζάνη και το ζιζανιοκτόνο 2-μεθυλο-4-χλωροφαινοξυοξικό οξύ σε προηγούμενες μελέτες υποδεικνύουν ότι τα συστατικά της μήτρας του νερού θα μπορούσαν να πραγματοποιήσουν είτε φυσική απόσβεση των διεγερμένων καταστάσεων της σιλαστατίνης είτε αντίστροφη αναγωγή σε σιλαστατίνη των μερικώς οξειδωμένων ενδιαμέσων αποικοδόμησης. Συνολικά, τα παρόντα αποτελέσματα αποδεικνύουν ότι η ακτινοβολία UVC είναι μια γρήγορη και αποτελεσματική διαδικασία για την αποδόμηση της σιλαστατίνης σε φυσικό νερό και επεξεργασμένα λύματα.

Στο **Κεφάλαιο 6** συνοψίζονται τα αποτελέσματα της παρούσας διατριβής οδηγώντας σε σημαντικά συμπεράσματα. Εξετάζονται επίσης μελλοντικοί στόχοι και προσανατολισμοί που θα μπορούσαν να παρθούν σε μελλοντική έρευνα στον συγκεκριμένο τομέα.

Στο **Κεφάλαιο 7** δίνονται υποστηρικτικές πληροφορίες για τα Κεφάλαια 2-5 οι οποίες παρουσιάζονται με τη μορφή σχημάτων, γραφημάτων και πινάκων σε ξεχωριστά παραρτήματα που αντιστοιχούν στα προαναφερθέντα κεφάλαια.

ABSTRACT

The present doctoral thesis is orientated towards the investigation of the broad topic of advanced studies of detection and monitoring of the fate of organic pollutants in the aquatic environment. The achievement of this objective is implemented using various scientific means, ranging from the establishment of novel microextraction techniques under atmospheric pressure as well as vacuum conditions regarding the presence of aromatic hydrocarbons in water and tobacco product leachates, to the UVC-induced degradation of a prominent pharmaceutical substance (cilastatin) and nicotine in natural water and treated waste water, where the photodegradation kinetics are studied thoroughly.

In **Chapter 1** introductory themes are being presented. A comprehensive review on sample preparation and classification of the most popular extraction techniques is demonstrated. The main focus is placed on solvent – free sample preparation techniques and more specifically on SPME and SBSE principles, their two sampling modes (direct and headspace) and the optimization parameters implemented to effectuate optimum extraction yields in each technique. Emphasis is then steered towards the effect of vacuum in headspace microextraction sampling as an alternative way of accelerating the kinetics of an extraction procedure and attaining therefore faster equilibration times. The development of the theoretical model is being presented along with principles regarding the pressure (in)dependence at equilibrium and pressure dependence at pre-equilibrium conditions of headspace sampling from water samples and the K_H criterion. HiSorb Sorptive Extraction as a solid phase microextraction technique is also being reported here. On a final note, the subject of photodegradation is examined on a theoretical basis covering degradation mechanisms and photolysis processes as well as basic principles of photolysis, the kinetics of degradation processes and the reaction mechanisms inspected during photolytic procedures.

Chapter 2 presents the published report titled: ***Vacuum-assisted headspace sorptive extraction: Theoretical considerations and proof-of-concept extraction of polycyclic aromatic hydrocarbons from water samples.*** In this work we propose HSSE sampling under vacuum conditions to reduce equilibration times. A theoretical model is presented that describes the pressure dependence of the so-called vacuum-assisted HSSE (Vac-HSSE) method, and predicts the reduction in equilibration times when lowering the sampling pressure. We take advantage of the theoretical formulation to reach some general conclusions for HSSE on the relationship between the physical characteristics of the stir bar, uptake rates and equilibration times. The theoretical

predictions were experimentally verified using water solutions spiked with naphthalene, acenaphthene and fluoranthene as model compounds. The effects of sampling temperature and extraction time under vacuum and regular pressure conditions were thoroughly investigated. The positive combined effect of heating the sample under low sampling pressure pointed that high humidity did not affect the performance of the extraction phase; an effect commonly recorded in headspace solid-phase microextraction. The extraction time profiles built at 25 and 55^{o}C visualized the substantial improvement in extraction kinetics with Vac-HSSE compared to the regular HSSE method. The results on naphthalene (assumed to evaporate relatively fast from the water sample) provided evidence that at 1 atm gas-sided resistance limited analyte uptake by the stir-bar and that this limitation could be effectively reduced by adopting the vacuum sampling approach. The accelerations of acenaphthene and fluoranthene suggested that gasphase constraints limited both the evaporation and analyte uptake processes. Independent method optimization of HSSE under each pressure condition yielded a shorter sampling time for Vac-HSSE compared to the regular HSSE procedure (30 min vs. 60 min respectively). The analytical performances of the two optimized methods were evaluated and it was concluded that Vac-HSSE was performing similar (naphthalene and acenaphthene) or better (fluoranthene) than regular HSSE in half the sampling time needed.

Chapter 3 presents the published report titled: ***Total and bioavailable polycyclic aromatic hydrocarbons in unused and operated heat-not-burn tobacco products and conventional cigarettes.*** The present studies report, for the first time, the total and bioavailable polycyclic aromatic hydrocarbons (PAHs) concentrations in unused and operated heat-not-burn (HnBs) tobacco products. To enable direct comparisons, identical sets of studies were conducted using conventional cigarettes (CCs). Five low-molecular PAHs were determined in HnBs at total concentrations that were of the same order before and after operation (Σ_5PAH = 47.37 ± 3.44 ng unit^{-1} and Σ_5PAH = 69.36 ± 5.78 ng unit^{-1} in unused and used HnBs, respectively). The incomplete combustion of organics during smoking of CCs, yielded substantially higher amounts of PAHs with their sum (Σ_{10}PAHs = 1449 ± 113 ng unit^{-1}) being >20 times larger than those in HnBs. The tobacco and filter were the most contaminated parts in HnBs. In unused CCs, tobacco had the highest PAHs load and after smoking, the spent filter was the most contaminated part, containing ∼80% of the total amount of PAHs. Naphthalene was the most abundant PAH detected in all tobacco products. Despite the high total PAH concentrations found in smoked CCs, the sums of the bioavailable PAH concentrations were of the same order in all tested tobacco products

(Σ_5PAH = 61.38 ± 1.79 ng unit^{-1} in unused HnBs, Σ_5PAH = 70.87 ± 7.67 ng unit^{-1} in used HnBs, Σ_4PAH = 66.92 ± 5.95 ng unit^{-1} in unused CCs, and Σ_6PAH = 47.94 ± 1.26 ng unit^{-1} in smoked CCs). This finding was related to smoking affecting PAHs' leachability from CCs and delaying their desorption from the solid matrix. Adjusting the pH, salt and humic acids content at environmentally relevant values did not affect PAHs leaching at 24 h of soaking. Finally, the leaching behavior of PAHs in natural waters (river water, rainwater, and seawater) was found similar to that in ultrapure water, experimentally verifying the ability of tobacco product waste to leach PAHs into the aquatic environment.

Chapter 4 presents the published report titled: ***UV-254 degradation of nicotine in natural waters and leachates produced from cigarette butts and heat-not-burn tobacco products.*** In this study, the UV_{254} photolytical fate of nicotine in natural water and leachates produced from conventional cigarettes (CCs) and the new generation heat-not-burn (HnBs) tobacco products is examined for the first time. The effect of UV_{254} irradiation on nicotine depletion in ultrapure water was initially studied. The reaction was pseudo first-order with respect to nicotine concentration at low concentrations and shifted to lower order at higher concentrations, an effect associated to absorption saturation. Although nicotine removal was fast, only 9.5% of the total organic carbon was removed after irradiation due to the formation of by-products. The chemical structures of six photo-products were derived by means of liquid and gas chromatography coupled to mass spectrometry. The photodegradation kinetics was found to depend on pH and faster kinetics were recorded when the monoprotonated form of nicotine was dominant (pH = 5–8). The presence of humic acids was found to slightly delay kinetics as they competed with nicotine for lamp irradiance, whereas the presence of salt had no effect on the direct photolysis of nicotine. Direct photolysis studies were also performed using natural waters. Compared to ultra-pure water, photodegradation was found to proceed slightly slower in river water, in similar kinetics in seawater, and relatively faster in rain water. The later was assumed to be due to the lower pH compared to the rest of the natural water tested. Leachates from used HnBs and smoked CCs were also submitted to UV_{254} irradiation and direct photolysis was found to proceed fast despite the high complexity of these matrices. Nonetheless, the total organic carbon in the system remained the same after irradiation due to the abundance of organics and photo-products formed. We take advantage of

the present investigations and report the leaching behavior of nicotine from HnBs and CCs. Among others, we found that in HnBs ~70% of the total and bioavailable nicotine content remains in the tobacco sticks after operation and this percentage drops to 15% in CCs due to the reduction in mass after smoking. This finding demonstrated the importance of properly disposing tobacco product waste to prevent nicotine leaching in water bodies.

Chapter 5 presents the published report titled: ***UVC-induced degradation of cilastatin in natural water and treated wastewater.*** This work reports for the first time the UVC photodegradation of cilastatin, a renal dehydropeptidase inhibitor co-adminstered with the imipenem antibiotic. Initially, solutions of cilastatin at varying concentrations were prepared in ultra-pure water and the direct photolysis of cilastatin was monitored under 254-nm irradiation. Degradation was slower at higher initial cilastatin concentrations, due to absorption saturation. Of the different eluting photoproducts, only one was tentatively identified as oxidized cilastatin bearing a sulfoxide group. UV-254 photolysis occurred faster at lower pH values, because the protonated forms of the molecule (H_3A^+, H_2A) have both higher absorption coefficients and higher photolysis quantum yields than the non-protonated ones (HA^-, A^{2-}). The direct photolysis of cilastatin does not involve •OH, as excluded by experiments in which t-butanol was added as •OH scavenger, whereas the presence of humic acids inhibited photolysis due to competition for radiation absorption. The same explanation partially accounts for the observation that the photolysis kinetics of cilastatin was slower in tap water, river water and treated wastewater samples compared to ultra-pure water. Moreover, the direct photolysis quantum yield was also lower in water matrices compared to ultra-pure water. Similar findings reported for triclosan and the herbicide 2-methyl-4-chlorophenoxyacetic acid in previous studies might suggest that the water matrix components could carry out either physical quenching of cilastatin's excited states or back-reduction to cilastatin of the partially oxidized degradation intermediates. Overall, the present results demonstrate that UVC irradiation is a fast and efficient process for the degradation of cilastatin in natural water and treated wastewater.

In **Chapter 6** the results of the present thesis are synopsized leading to important conclusions and an evaluation of the overall significance of the breakthroughs achieved here. Future objectives and orientations of research in this particular field are also considered.

In **Chapter 7** Supporting Information on Chapters 2-5 is being presented in the form of figures, graphs and tables in separate appendices per the aforementioned chapters.

CHAPTER 1: INTRODUCTION

1.1. SAMPLE PREPARATION

A complete analytical method involves of many stages from the sample collection, sample storage, sample preparation, instrumental analysis with identification and quantitative evaluation of the target analytes to the final presentation of the reported results (Berrueta et al., 1995).

Several issues need to be addressed prior to instrumental analysis including extraction and isolation of the target analytes, elimination of matrix interferences and separation of trace level compounds, to name a few (Nogueira, 2015; Pawliszyn, 2003; Xia et al., 2020). Sample preparation is essentially the analytical process that consists of an extraction procedure that involves the transfer, enrichment and isolation of the analytes of interest from the sample matrix. As a result, qualitative and quantitative evaluation of the analytes in question can be executed as they are transferred to a phase more compatible with the analytical instrument/detector (Nogueira, 2015; Pawliszyn, 2003; Xia et al., 2020). Thus, sample preparation through the last few decades has been rendered the backbone and core component of the whole analytical process, especially when monitoring low levels of organic environmental pollutants are in question, considering the complexity of environmental sample matrices characterized by their high amount of interferences (C. Ribeiro et al., 2014; Wardencki et al., 2007). In this respect significant efforts have been advanced through the years to develop fast and sensitive detection of organic pollutants which demand the implementation of robust analytical methods (C. Ribeiro et al., 2014). In this context, appropriate selection and optimization of the sample preparation procedure can greatly affect the reliability and accuracy of the final results (Schoenmakers, 2012).

Sample preparation is generally a very tedious and time-consuming step of the whole analytical method, estimated to account for the two thirds of the overall analytical time, while it can be the cause and source of much error and inaccuracy (Berrueta et al., 1995; Schoenmakers, 2012). Additionally, conventional extraction methods including liquid-liquid extraction (LLE), Soxhlet extraction, and solid-phase extraction (SPE), although still widely accepted by the scientific community, they entail the use of significant amounts of very expensive and environmentally unfriendly solvents (Trujillo-Rodríguez et al., 2020). Accordingly, basic principles of green analytical chemistry (GAC), involving the elimination to reduction of organic toxic solvents

(solventless extraction techniques), the elimination of reagents displaying high toxicity, the decrease of energy consumption and the low sample volume requirements for the successful effectuation of an analytical procedure, should be considered in modern "green" analytical chemistry (Nogueira, 2015; Wardencki et al., 2007).

Under these circumstances, ideas like miniaturization of extraction steps, automation, integration and simplification became the underlying conceptions for the effectuation of microscale or miniaturized versions of the aforementioned conventional extraction methods discussed above (C. Ribeiro et al., 2014; Schoenmakers, 2012; Trujillo-Rodríguez et al., 2020). For trace analysis, notably, direct microextraction of predominantly volatile and semi-volatile compounds from solid, liquid and gaseous matrices has been enabled through the years with the development of sorption-based methods as they have been proven as the best option for this particular group of analytes (Nogueira, 2015).

1.2. CLASSIFICATION OF EXTRACTION TECHNIQUES

Figure 1.1 gives a categorization of extraction techniques according to the fundamental principles that govern the different extraction approaches (Pawliszyn, 2003). Typically, the calibration step is omitted in an exhaustive extraction technique. This could be explained by the argument that the majority of the analytes of interest are transferred to the given extraction phase with the utilization of enormous amounts of it (Pawliszyn, 2003; Thurman & Mills, 1998). As an attempt to avoid time consuming processes as well as minimize the amount of solvents used for the effectuation of exhaustive removal, batch equilibrium techniques are as a general rule outweighed by flow-though techniques (Pawliszyn, 2003; Thurman & Mills, 1998). Essentially, the procedure that is pursued in both sorbent trap techniques and SPE, entails the passing of big bulks of volume of sample through a small cartridge packed with a sorbent material. This procedure results to an effective mass transfer (Pawliszyn, 2003; Thurman & Mills, 1998). Then, by desorption of the target compounds into a minimal solvent volume, enrichment of the analytes is carried out successfully (Pawliszyn, 2003; Thurman & Mills, 1998). The rinsing of the target analytes from the sample matrix is actualized with compressed and inert gas at atmospheric conditions, in SFE and purge-and-trap methods, correspondingly. In the Soxhlet extraction technique the solvent's boiling

point is the activator for the analytes of interest to be consistently removed by the solvent (Dean, 1998; Pawliszyn, 2003). In PFE techniques, small volumes of organic solvent are employed to accomplish enrichment alongside with extraction. This is explained by the enhanced elution strength and solvent capacity at elevated temperatures and pressures (Dean, 1998; Pawliszyn, 2003).

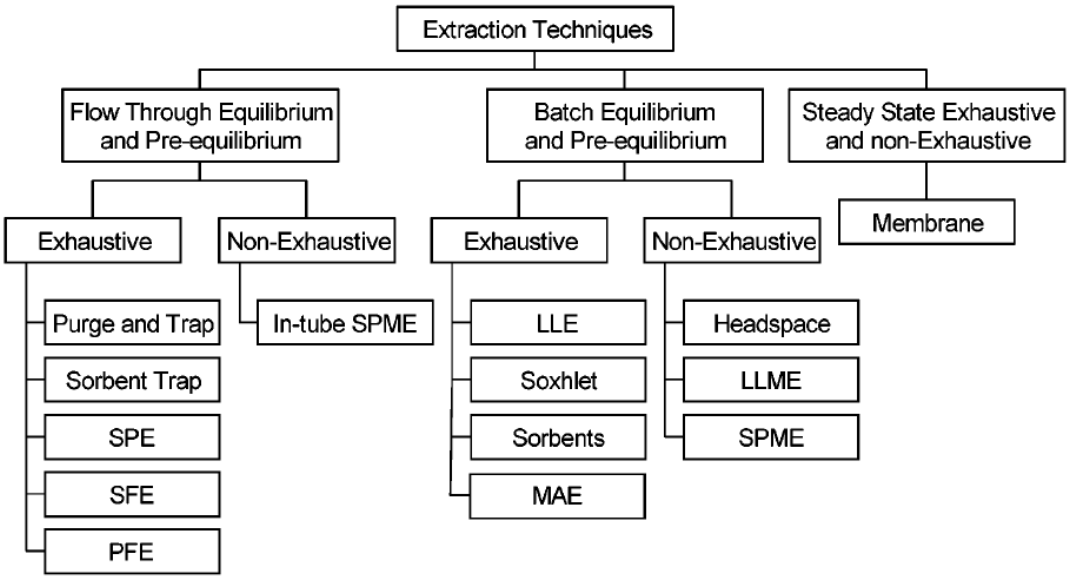

Figure 1.1. Classification of extraction techniques (Pawliszyn, 2003).

In non-exhaustive extraction approaches the capacity of the extracting phase is considered significantly small and inadequate to remove the bulk of the target analytes from the sample matrix, mainly due to the is the limited volume of the extractant with respect to the sample volume (Handley, 1999; Pawliszyn, 2003). Such small volumes of extractants have been utilized in microextraction techniques such as solvent microextraction (F. F. Cantwell & Losier, 2002), SPME (Pawliszyn, 1997), SBSE (Baltussen, Sandra, David, & Cramers, 1999) etc. A low sample matrix-extracting phase distribution constant has been recorded as well in gaseous headspace techniques (Vitenberg et al., 1984). Non-exhaustive techniques are categorized on the grounds of equilibrium, preequilibrium and permeation (Handley, 1999). The usage of a very small volume of extraction phase in relation to the sample volume or a low partition coefficient among the extraction phase and the sample matrix is what distinguishes equilibrium techniques from other methods (Bao & Dasgupta, 1992). Preequilibrium conditions are executed by breaking contact between the extraction phase and the sample matrix prior to the equilibrium (Pawliszyn, 2003). Lastly, in permeation techniques, a concurrent re-extraction of the analytes of interest ensures that constant

steady-state transfer of the target analytes is achieved successfully (Pawliszyn, 2003). Such an example could be the membrane extraction (Noble & Stern, 1995).

1.2.1. Liquid based extraction techniques

Liquid-liquid extraction (LLE), commonly known as solvent extraction, is a typical ternary system in the chemical engineering field. Its function is to separate chemicals from one solution to the other on the basis of the different solubility of the solute in two solvents (J. Zhang & Hu, 2013). The solute which is dissolved in diluent, is extracted from the diluent and dissolved into another solvent, the extractant. More specifically, initially the extractant solvent is added to the diluent (in which the solute is dissolved), which should be immiscible with the diluent (J. Zhang & Hu, 2013). The second step involves the mixing of the two aforementioned solvents in order to achieve significant improvement of their interface (J. Zhang & Hu, 2013). Then, most frequently, the extractant or diluent forms droplets as a result of the surface tension. The solute then chooses the host solvent in agreement with its different solubility in extractant and diluent. A well thought-out extraction system should have the solute primarily dissolved in the extractant, where from this point on, the solute can be collected from the extractant with evaporation or distillation (J. Zhang & Hu, 2013). Conventionally, the whole process is taking place in a separatory funnel (F. F. Cantwell & Losier, 2002; Craig & Craig, 1956; Irving & Williams, 1961). There the mixture of the two solvents is stirred while drops are disseminating between them. A conclusion of the agitation accomplishes drop fusion, and finally the bulk liquid phases are separated from one another (F. F. Cantwell & Losier, 2002; Craig & Craig, 1956; Irving & Williams, 1961). LLE in comparison with other batch-type phase distribution techniques provides significant linear sample capacities (F. F. Cantwell & Losier, 2002). Instant quantitative analysis either by a gas or liquid chromatographic system is yet another of its great advantages. Lastly, its immense use over the last few decades, which has been recorded in literature, makes information about LLE accessible to analytical scientists globally in comparison with other techniques (F. F. Cantwell & Losier, 2002).

However, LLE has some significant drawbacks that outweigh its aforesaid advantages. The use of substantial volumes of toxic organic solvents, the fairly large volumes of sample volumes demanded, the requirement of use of ultra-pure solvents, the formation

of emulsions and the fact that the whole procedure could be time consuming considering the necessity of multiple successive extraction processes required, are only a few of them (Berrueta et al., 1995).

1.2.2. Liquid based microextraction techniques

Over the last decades the increased demand for accurate and miniaturized methods of sample preparation within the analytical chemistry field has led to the development of liquid-phase microextraction (LPME) which ultimately utilizes small volumes of liquids and organic solvents to perform analytical extractions (Pawliszyn & Pedersen-Bjergaard, 2006). Accordingly, many analytical approaches on the base of solvent microextraction have been developed with new set-ups and techniques (Schoenmakers, 2012).

The most straightforward technique that derived from the LPME approach is called single drop microextraction (SDME). It was established in 1996 where the utilization of small single micro-droplets of water insoluble organic solvent suspended from the tip of GC micro-syringes was introduced for the first time (Jeannot & Cantwell, 1996; H. Liu & Dasgupta, 1996; Pawliszyn & Pedersen-Bjergaard, 2006).

In this technique, the micro-drop is either immersed in the aqueous sample or suspended to the headspace of the vial above the sample. Extractant volumes can vary from 1μL to 8μL while aqueous sample volumes range from 1 to 10mL. SDME is essentially considered an equilibrium technique (Schoenmakers, 2012). Hence, the overall simplicity of this particular analytical process with its potential for (semi)-automatic performance, and the practicability of acquiring ready for analysis extracts, has led to the scientific acceptance and swift development of this environmentally friendly technique in various analytical chemistry research fields (Schoenmakers, 2012).

The time demanded to attain equilibrium conditions in SDME can vary from seconds to hours dependent upon a plethora of parameters from the degree of agitation and phase volumes to the equilibrium distribution constant, leading the procedure to be performed under non-equilibrium conditions most of the times (Jeannot et al., 2010). The extraction of the analytes is not completely exhaustive, as most of the time small

amounts of the target compounds still remain present in the sample solution at equilibrium, being the aftermath of the small volume ratio between the organic drop and the aqueous sample (Jeannot et al., 2010; Kailasa et al., 2021).

Jeannot and Cantwell proposed a model for equilibrium and mass transfer in a two-phase-liquid-liquid microextraction system (A. F. Cantwell et al., 1996; Jeannot & Cantwell, 1996). The equilibrium concentration of analyte in the organic phase ($C_{o,eq}$) can be expressed as follows:

$$C_{o,eq} = KC_{w,eq} = \frac{KC_w^o}{1+KV_o/V_w} \quad (1.1)$$

where K is the equilibrium distribution constant, $C_{w,eq}$ is the equilibrium concentration in the aqueous phase, C_w^o the initial concentration in the aqueous phase and V_o and V_w are the organic and aqueous volumes correspondingly (A. F. Cantwell et al., 1996; Jeannot & Cantwell, 1996).

Accordingly, at equilibrium the distribution coefficient D, is expressed by the following equation:

$$D = \frac{C_{org,eq}V_w}{C_{aq,eq}V_w - C_{org,eq}V_o} \quad (1.2)$$

where $C_{org,eq}$ is the concentration of the organic phase at equilibrium, $C_{aq,eq}$ the concentration of the analyte in the aqueous phase at equilibrium and V_o and V_w are the organic and aqueous volumes accordingly (A. F. Cantwell et al., 1996; Jeannot & Cantwell, 1996).

The slow diffusion rates renders the transport of analyte molecules from the aqueous bulk solution to the microdrop of organic phase, difficult (Jeannot et al., 2010). The goal is to eliminate as much as possible the distance over which the diffusion occurs. In that case, magnetic stirring or mechanical vibration in order to increase the interfacial contact area and the diffusion distance could help (Jeannot et al., 2010).

Direct-immersion SDME (DI-SDME) is founded on the exposure of a microdrop of a water-immiscible extractant, which is suspended on the tip of a microsyringe needle, to an aqueous sample (Pena-Pereira et al., 2009). Upon the conclusion of the extraction the microdrop is withdrawn back to the microsyringe and injected into the appropriate detector for analysis. The key factor in this type of extraction procedure is use of target

analytes that are more soluble in the extractant phase than the aqueous one (Pena-Pereira et al., 2009). DI-SDME has been rendered beneficial for the extraction of non-polar and semivolatile analytes from water samples with limited amounts of particulate or dissolved matter (Ma & Cantwell, 1999). Polar analytes extraction has been accomplished with the devise of a modification called liquid-liquid-liquid micro-extraction (LLLME) (Ma & Cantwell, 1999). Some of the disadvantages of this particular method is primarily the instability of the microdrop in the case of high agitation rates and high temperatures, and secondly the unsuitability of usage of solvents with low boiling points due to their elevated rate of evaporation (Pena-Pereira et al., 2009).

Headspace SDME (HS-SDME) was firstly introduced by Theis et al. as a sample preparation technique allowing the preconcentration of compounds of volatile and semi-volatile nature into a microdrop which is exposed to the headspace above the sample of interest (Pena-Pereira et al., 2009). HS-SDME is recommended mainly as a means of preconcentration of volatile and non-polar analytes with appliance to aqueous, gaseous and solid sample matrices. Various techniques like the agitation of the sample solution to improve mass transfer in the aqueous phase can be recruited, accelerating thus the attainment of thermodynamic equilibrium between the aqueous and vapor phases drastically (Pena-Pereira et al., 2009; Theis et al., 2001).

In order to reduce the equilibrium times needed during headspace microextraction, approaches such as heating the sample have been employed, which unfortunately could lead to decomposition of the sample as well as favoring of the gas phase over the extracting one (Psillakis, 2020). An alternative technique is the sampling under reduced atmospheric pressure condition called which accelerates significantly the extraction kinetics effectuating faster equilibration times. This particular technique is called vacuum-assisted HS-SDME (Vac-HS-SDME) and was introduced for the first time by by Trujillo-Rodríguez et al., managing to accomplish faster equilibration times for short-chain free fatty acids when in comparison with regular atmospheric pressure (Trujillo-Rodríguez, Pino, & Anderson, 2017). Psillakis et. al, later brought into fruition a quantification numerical model of the pressure dependance of extraction yields, applying the theory on experimental data using polycyclic aromatic hydrocarbons as the target analytes (Psillakis et al., 2019).

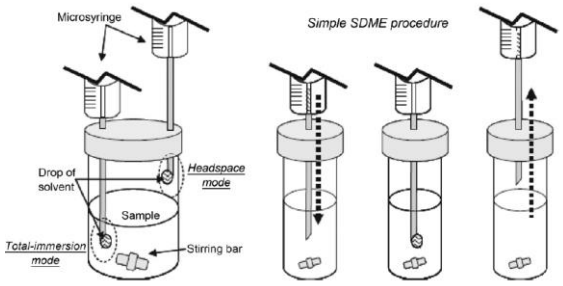

Figure 1.2. Basic configurations for SDME and steps in the SDME immersion mode (Schoenmakers, 2012).

Amongst other techniques developed was the hollow fiber-protected two-phase solvent microextraction (HF(2)ME), which was presented for the first time by He and Lee in 1997 (Y. He & Lee, 1997). This particular technique includes a small-diameter polypropylene tube which is the "hollow fiber" and in which the extracting solvent is enclosed while the tube remains sealed at one end. The open end of the hollow fiber is affixed to a micro-syringe needle which would have been previously used to load the fiber with the extracting organic solvent (Kokosa et al., 2009). The fiber then with the extracting solvent would be immersed to the aqueous sample matrix under investigation for a preset period time so as to allow the target analytes to migrate through its walls. After the passage of the preselected extraction time, the solvent enriched with the target analytes would be withdrawn back into the syringe and finally transferred to the analytical instrument for analysis (Kokosa et al., 2009). Thus, it can be concluded that HF(2)ME, is a liquid-liquid membrane extraction (Kokosa et al., 2009).

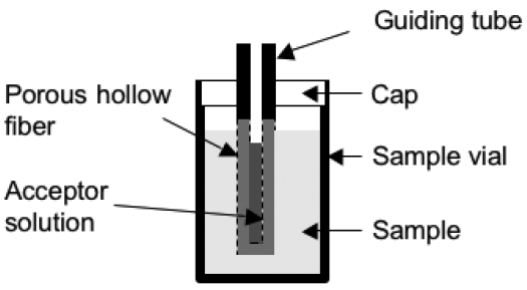

Figure 1.3. Schematic illustration of set-up for hollow fiber LPME (Pawliszyn & Pedersen-Bjergaard, 2006).

In 2006 Assadi and his group introduced the dispersive liquid-liquid microextraction (DLLME) (Rezaee et al., 2006) which is considered an alteration of miniaturized LLE. In this technique, 10-50μL of a water immiscible solvent are dissolved in 0.5-2mL of

water soluble solvent and then swiftly injected with a syringe to the aqueous sample of interest (Rezaee et al., 2006). Small micro-drops of the water immiscible solvent are formed and dispersed inside the aqueous sample as a product of the rapid injection of the mixture of organic solvents. The target analytes are rapidly extracted by the micro-drops formulated (Rezaee et al., 2006). The enriched organic phase is then separated from the aqueous mass through centrifugation and transferred to the analytical instrument for analysis. The technique was initially focused on the determination of non-polar analytes (Rezaee et al., 2006), but later it was used also for the determination of polar analytes (Fattahi et al., 2007; J. Liu et al., 2011).

Other approaches of modes of LPME involve liquid phase microextraction based on solidification of floating organic drop (LPME-SFO) (Khalili Zanjani et al., 2007), supported liquid membrane (SLM) (Audunsson, 1986; A. Jonsson & Mathiasson, 2000), microporous membrane liquid-liquid extraction (MMLLE) (J. A. Jonsson & Mathiasson, 2001, 1999), microextraction using immiscible liquid films including liquid – liquid microextraction (two-phase system) (Y. He & Lee, 1997), and liquid – liquid – liquid microextraction using back-extraction (three-phase system) (Ma & Cantwell, 1998, 1999) and vortex – assisted liquid – liquid microextraction (VALLME) (Yiantzi et al., 2016).

1.2.3. Solvent-free sample preparation techniques

1.2.3.1. Gas-phase sample preparation methods

Analysis of compounds with the use of gas chromatography from the sample's headspace is an effective approach in order to evade problems connected with liquid sample handling and injection, such as contamination (Aguinaga et al., 2008; Kolb & Ettre, 2006; Kremser et al., 2016). At its core, this sampling technique revolves around the fact that substances in an aqueous or generally a liquid matrix equilibrate in relation to the concentrations between the sample solution and the gaseous phase above it (Kremser et al., 2016). Upon the effectuation of phase equilibrium, the deliverance of an aliquot of the headspace gas is effectuated with the use of a gastight syringe straight to the gas chromatography injector. This specific approach of sampling is called static headspace sampling as it is occuring under static conditions in the sampler (Kolb & Ettre, 2006; Kremser et al., 2016). Numerous analytical instruments have applied its

automated approach through the years since its first appearance in 1958 (Bovijn et al., 1958). The principal drawback of the static headspace-GC approach however is its limited sensitivity in comparison with other dynamic headspace techniques (Snow & Slack, 2002). On the other side of the spectrum, dynamic headspace purge-and-trap sampling, entails the passing of carrier gas through a liquid sample, whose volatile analytes are trapped on a sorbent material and finally desorbed onto GC (Snow & Slack, 2002). In this case, exhaustive extraction is actually manageable, as the sample headspace is being depleted of analytes continuously, and ideally, both the sample solution's and the headspace's analytes are subsequently transferred to the sorbent phase (Kremser et al., 2016). Dynamic headspace purge-and-trap sampling is performed regularly and its one of the easiest methods for the analysis of low concentrations of volatile organic analytes in aqueous matrices, since its introduction in 1970's after the launching of Tenax as a commercial adsorbent (Snow & Slack, 2002; Zlatkis et al., 1973).

A technique that is capable of removing semi-volatile analytes at ambient temperatures is supercritical fluid extraction (SFE). In this particular gas-phase sample preparation approach, a liquid such as compressed carbon dioxide is acting as an extractant in order to retract the aforementioned compounds (Chester et al., 1994; Hawthorne, 1990; Pawliszyn, 1993). The most significant parameter of a supercritical fluid is the combination of both gas like mass transfer and liquid like solvating characteristics. It is beneficial for the analysis of thermally unstable analytes as it has the innate capacity to extract non-volatile compounds at room temperature (Chester et al., 1994; Hawthorne, 1990; Pawliszyn, 1993). Unfortunately, it is its impractical heavy equipment that makes SFE challenging on instances such as in situ field analysis (Chester et al., 1994; Hawthorne, 1990; Pawliszyn, 1993).

1.2.3.2. Membrane extraction methods

Microporous, highly hydrophobic flat or tubular-shaped membranes are commonly used in a technique called "gas diffusion" which has been introduced in flow-through systems and which is rooted in the separation of volatile compounds from a sample solution through an aforementioned gas-permeable membrane into a receiver liquid solution (Miró & Frenzel, 2004). Another technique is membrane based passive sampling that is widely implemented in a pre-valve position intending to supply the

analytical column of a liquid or a gas chromatograph with an interference-free permeate plug or performed within a continuous flow configuration with direct hyphenation to a flow through detector (Miró & Frenzel, 2004). In gas-to-gas transfer, transfer of gaseous compounds through a semi-permeable membrane into a gaseous receiver has been utilized to effectuate separation of gases from one another on the basis of their different permeability. In this instance, the distribution of the gaseous compounds between the air sample and the membrane relies upon the chemical composition of the membrane used (Miró & Frenzel, 2004). In gas-to-liquid transfer, soluble trace gases permeate a polymeric membrane and get trapped into a recipient aqueous stream as compact species, which could be chemically derivatized and the liquid then injected to an appropriate flow-through detection unit (Miró & Frenzel, 2004).

Non-porous membrane extraction provides an overall increased degree of selectivity and high influence on enrichment along with the conveniency of possible automation in chromatographic and other analytical instruments (J. A. Jonsson & Mathiasson, 2000).

In supported liquid membrane extraction (SLM), initially introduced by Audunsson in 1986 (Audunsson, 1986), an organic solvent is held in the pores of a hydrophobic porous membrane utilizing capillary forces. The liquid membrane proper is the liquid in these pores, between and in contact with the two aqueous phases (J. A. Jonsson & Mathiasson, 1999). In microporous membrane liquid-liquid extraction (MLLE), which is more appropriate than SLM for hydrophobic analytes, the acceptor is an organic solvent which shapes the liquid membrane by packing the pores in the porous hydrophobic membrane (J. A. Jonsson & Mathiasson, 1999). In polymeric membrane extraction a plethora of implementation has been performed so far. One of the most routinely used materials of membrane is that of the durable silicon rubber. In an aqueous-polymer-organic approach, the organic solvent normally permeates the polymeric material resulting in its substantial swelling, comparably to MMLE (J. A. Jonsson & Mathiasson, 2000). In the membrane extraction with a sorbent interface approach (MESI), a gaseous acceptor phase is used which is more suitable and appropriate for gas chromatography analysis (Handley, 1999; J. A. Jonsson & Mathiasson, 2000; Pratt & Pawliszyn, 1992). This particular technique can be used for both gaseous and aqueous samples. The set-up is composed of a membrane component

(typically a silicon rubber hollow fiber), into which the target compounds are extracted from the given sample. Subsequently, gas flows through the fiber and carries the compound molecules from the membrane into a cooled cold trap. Through thermal desorption from the sorbent trap the analytes are then transferred to GC for analysis (Handley, 1999; J. A. Jonsson & Mathiasson, 2000; Pratt & Pawliszyn, 1992). A hybrid technique inspired by LPME and electrophoresis called electromembrane microextraction (EME) was also introduced utilizing both passive diffusion and electro-migration (Ocaña-González et al., 2016). Essentially, EME, which was firstly introduced in 2006 (Pedersen-Bjergaard, S., Rasmussen, K. E., 2006) , is a liquid-phase microextraction concept designed to meet the needs of selective extraction and pre-concentration of target analytes from aqueous samples, where charged analytes are typically drug substances and the aqueous sample is a biological fluid such as blood or urine (Pedersen-Bjergaard, S. et al., 2017). Under the influence of an electric field, charged compound molecules from the sample migrate towards the opposite charged electrode residing in the acceptor solution, crossing a supported liquid membrane, and then they are consequently trapped in an acceptor solution as a result of ionization and direction of the electric field (Ocaña-González et al., 2016). This specific approach, is a selective and green analytical chemistry membrane extraction technique widely studied the last few years particularly in the sector of pharmaceuticals, but also in environmental and food applications as well. (Huang et al., 2015, Pedersen-Bjergaard, S. et al., 2017). A chip format which is essentially a downscaling of EME was introduced in 2010, recording a variety of advantages such as selective extraction removing the high ionic strength of biological samples and fast kinetics with exact control of the beginning (Petersen, N.J., Jensen, H., Hansen, S.H. et al., 2010). Lastly, parallel artificial liquid membrane extraction (PALME), a new approach in the direction of liquid-liquid-liquid membrane extraction was presented in 2013, where a donor plate and acceptor plate create a sandwich, in which each sample (in this case human plasma) and acceptor solution is spaced apart by an artificial liquid membrane (Gjelstad, A. et al., 2013). PALME is a modification of hollow-fiber liquid-phase microextraction, where the hollow fibers are replaced by flat membranes in a 96-well plate format (Gjelstad, A. et al., 2013).

1.2.3.3. Sorption-based extraction methods

Solid phase extraction (SPE), has been mentioned for about 35-40 years. However, the aforementioned duration of time is only referring to the flourish of this groundbreaking method, whose origins of conception and first experimental implementations are extending back to seven decades ago (Liská, 2000). The basic principle of SPE is that the target compounds to be extracted are partitioned between a solid phase (adsorbent material) and a sample matrix (Berrueta et al., 1995). The analytes in question should have a higher affinity for the solid phase than for the liquid, proving the effectiveness of the adsorbent material. Initially, the sample matrix is placed in an appropriate vessel combined with the solid phase, where shaking of the mixture occurs for a preset period of time (Berrueta et al., 1995). Then, filtration or elutriation of the two phases is performed following the attainment of the distribution equilibrium between the solid and liquid phase. In that case, if the adsorbent material was effectual the compound of interest will be mainly in the solid phase, having being extracted from the sample matrix (Berrueta et al., 1995). The analyte can then be desorbed by the solid phase with the utilization of an effective solvent (Berrueta et al., 1995). SPE is generally considered one of the most broadly acknowledged techniques regarding pre-concentration and clean-up of compounds from aqueous samples. The broad range of sorbents available at a commercial level as well as the introduction of novel sorbent materials exhibiting significant retention of polar compounds, higher loading capacities and overall selectivity (e.g. ISPEs and MIPs), renders this method of extraction quite popular for compounds with diverse polarities and chemical structures (Fontanals et al., 2007; Schoenmakers, 2012; Tamayo et al., 2007). In on-line SPE, the sorbent material is packed in a short stainless-steel column, integrated as part of the analytical instrument commonly as part of the sample loop (Berrueta et al., 1995; Hyotylainen, 2007; Pichon, 2000). The cleanup and analyte retention are succeeded through the injection of the sample in the solid phase cartridge, from where the target analytes are washed out from the SPE column to the column of the analytical instrument with the use of the appropriate mobile phase solvent with the aim of separation and detection (Camel, 2003; C. He et al., 2007; Pichon, 2000).

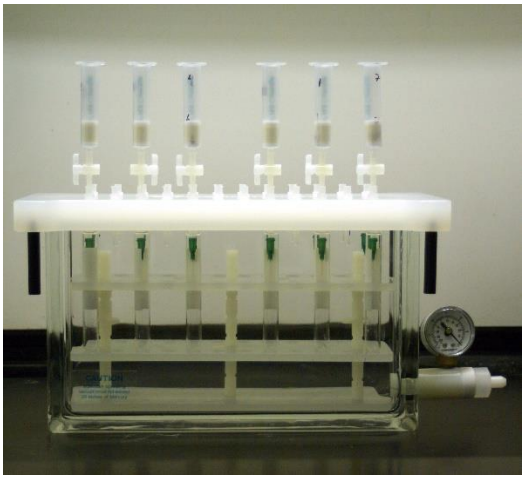

Figure 1.4. A typical solid phase extraction manifold. The cartridges drip into the chamber below, where tubes collect the effluent. A vacuum port with gauge is used to control the vacuum applied to the chamber.

The microextraction by packed sorbent (MEPS), which is essentially a miniaturized sample preparation method and an automated version of SPE, was developed in 2004 by Abdel-Rehim (Abdel-Rehim, 2011; Liská, 2000). In this specific technique, the sorbent packing material is arranged at the top of a syringe needle, while a small volume of an aqueous sample is ejected and withdrawn so preconcentration of the target compounds on the sorbent could be achieved successfully (Schoenmakers, 2012). After a subsequent elution of the analytes to a specific solvent, transfer of the liquid sample to the GC injection port could be effectuated (Schoenmakers, 2012).

Anastassiades et al. presented in 2003 a novel advancement in the sphere of SPE, called QuEChERS (Anastassiades et al., 2003). The aforementioned method is considered to be a very straightforward sample preparation technique predicated on liquid partition with organic solvent succeeded by a cleanup step of dispersive solid extraction (dSPE) (C. Ribeiro et al., 2014). Its relative cheap procedure in combination with a substantially good recovery and reproducibility render it as a widely utilized methods used in analytical chemistry laboratories on a global basis, analyzing a broad spectrum of compounds and matrices (C. Ribeiro et al., 2014).

In dispersive solid phase (dSPE), a fraction of the sample extracted is placed in a tube which contains a limited amount of the SPE sorbent and a drying agent. Following mixing of this particular mixture, the sorbent material is separated commonly by the utilization of centrifugation (C. Ribeiro et al., 2014). The main role of the sorbent used

is to withhold the matrix molecules and interference, and not the target analytes (C. Ribeiro et al., 2014).

1.2.3.4. Solid-phase microextraction (SPME)

Solid-phase microextraction is a groundbreaking approach based on sorptive extraction that was primarily presented by Pawliszyn's group in 1990 (Arthur & Pawliszyn, 1990). The main objective of the formation of SPME was the ever increasing demand for accelerated sample preparation, both in laboratory and on-site (Pawliszyn & Pedersen-Bjergaard, 2006). The successful pairing of SPME with GC, lead to the research and analysis of various groups of organic pollutants in aqueous matrices, while maintaining a remarkable sensitivity (Liská, 2000). Amongst the different groups of compounds of interest analyzed are pesticides (Eisert & Levsen, 1995), nitroaromatics (Horng & Huang, 1994), phenols (Buchholz & Pawliszyn, 1994) and volatile organic compounds (Page & Lacroix, 1993; Potter & Pawliszyn, 1992). Despite SPME being an equilibrium and non-exhaustive approach, the scientific community has established it as a fast, reproducible, miniaturized and green technique (Schoenmakers, 2012).

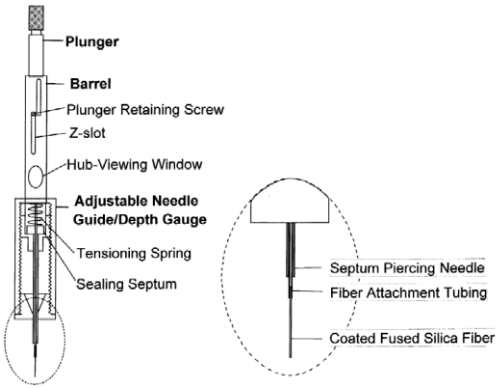

Figure 1.5. Commercial SPME device (Lord & Pawliszyn, 2000).

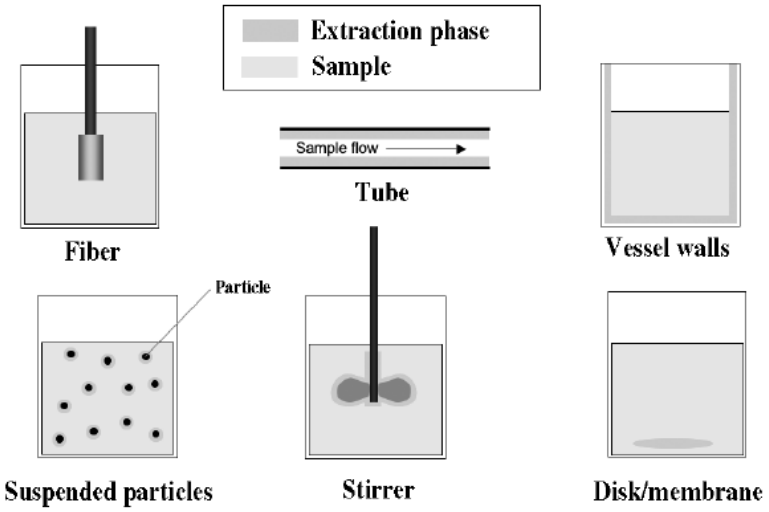

Figure 1.6. Configurations of SPME (Lord & Pawliszyn, 2000).

In SPME, a small amount of extracting phase (fiber) disseminated on a solid support is subject to the sample under investigation for a preset period of time (Pawliszyn & Pedersen-Bjergaard, 2006). The fiber's relative small size and shape of the fiber enables it to fit easily inside the needle of a syringe-like apparatus. In that case, the fiber can be readily exposed (as it is attached to the syringe plunger) for extraction or retraction for storage (Baltussen et al., 2002). The sampling procedure could be effectuated in two modes, depended upon the nature of the target analytes, their polarities and volatility: the direct immersion (DI-SPME) and the headspace (HS-SPME) (C. Ribeiro et al., 2014). In DI-SPME the fiber is immersed within the sample matrix. It is commonly applied to polar or nonvolatile analytes with subsequent GC or LC analysis (Malik et al., 2006; A. Ribeiro et al., 2002; C. Ribeiro et al., 2014). In HS-SPME, the fiber is exposed to the vapor phase of each target sample, being thus a more suitable option used for the research of volatile compounds accompanied by GC or GC-MS analysis (C. Ribeiro et al., 2014).

The small amount of the extracting phase is set in contact with the sample for a fixed period of time, within which if significant, a concentration equilibrium between the extractant and the sample matrix is actualized (Lord & Pawliszyn, 2000). It is important to note, that this procedure is a non-exhaustive one, thus, prolonged exposure of the fiber would not give rise to the accumulation of more of the target analytes. SPME as a matter of fact is a multiphase equilibrium process. A two phase system consists of the sample (homogeneous matrix) and the extracting fiber phase while a three phase

system is composed of the sample matrix, the extracting phase and the gaseous headspace of the sample (Lord & Pawliszyn, 2000). As a rule, SPME extraction is deemed as complete when the analyte concentration has attained distribution equilibrium between the sample matrix and the fiber coating (Lord & Pawliszyn, 2000). In simpler terms, this can be translated as the point when no matter of the prolongation of the extraction time the extracted amount of target analytes is steady (Lord & Pawliszyn, 2000). The equilibrium conditions can be expressed as:

$$\frac{K_{fs}V_sC_o}{K_{fs}V_f+V_s} \quad (1.3)$$

where n is the number of moles extracted by the fiber coating, K_{fs} is the fiber coating/sample matrix distribution constant, V_f is the fiber coating volume, V_s is the sample volume and C_o is the initial concentration of the target analyte in the sample each time (Louch et al., 1992).

In case of a big sample volume (such a case is a field analysis) the aforementioned equation is modified to:

$$n = K_{fs}V_fC_o \ (1.4)$$

(Lord & Pawliszyn, 2000).

The distribution coefficients and the **thickness of the fiber coating** are responsible for the partition of the compounds between the sample solution and the sorbent material. More bulky fiber coatings can lead to the extraction of larger amounts of the target analytes in comparison with thin coatings and thus are preferrable for volatile compounds facilitating transfer of these analytes without any loss chromatographically (Wardencki et al., 2007). A thinner layer of fiber coating is recommended in the case of preconcentration of target compounds with high boiling points, succeeding a much faster chromatographic analysis (Wardencki et al., 2007).

On the other hand, the **fiber type** is impactful upon the amount and nature of the sorbed analytes (Górecki et al., 1999). The key aspect in the selection of the most effectual fiber coating is that “like attracts like”. In that case, nonpolar and polar analytes are sorbed on nonpolar and polar fiber coatings, accordingly (Wardencki et al., 2007).

The most commonly used fiber material, especially for environmental analysis is polydimethylsiloxane (PDMS) (sub-ppm detection limits). PDMS is thermally stable,

with well-known physicochemical properties while requiring smaller extraction times (Wardencki et al., 2007).

Other commercially available coatings include polyacrylate (PA), divinylbenzene (DVB), Carboxen (CAR), and Carbowax (CW), in addition to fibers with a variety of different thicknesses and combinations of coatings.

While working on enhancing the extraction efficiencies apart from the fiber's material and thickness of coating, other parameters should be considered as well.

The **sample volume** should be significantly limited when higher extraction yields are aimed (Pawliszyn, 1997). The transfer of the analyte molecules from the solution to the headspace can be assisted in an elevated **temperature**, as the distribution constant (K_{hs}), depends on temperature and accordingly increases in the case of a rising temperature, even though caution must be given to excessive increases in temperature as decomposition of the fiber might occur (Wardencki et al., 2007). **Extraction time** has also been proven a powerful tool to enhance extraction efficiency as prolonged times of exposure can result in more analyte molecules attaching to the fiber coating (Z. Zhang & Pawliszyn, 1993). A reduction in solubility of the target analytes with the addition of an appropriate **salting out agent** in the sample can also affect positively the yielded extraction performance (Wu et al., 2000).

Regarding the use of the operational modes in order to boost the extraction efficiency of the SPME method, emphasis has been given to the headspace mode. More particularly, Pawliszyn and his team actualized the idea of warming up the sample at elevated temperatures while simultaneously maintaining the fiber at low temperatures (Carasek et al., 2007; Z. Zhang & Pawliszyn, 1995). In this innovative way, faster transfer of the analytes from the sample to the headspace is effectuated by the heating of the sample enhancing thus the partition coefficient (Trujillo-Rodríguez et al., 2020). Psillakis et. al proposed in 2012 a novel sampling method in order to improve the mass transfer from the sample solution to the headspace by reducing the atmospheric pressure conditions by adding a step of air evacuation of the sample's vial prior to HS-SPME (Psillakis, Yiantzi, et al., 2012). Although the amount of analytes extracted in the equilibrium state with the use of reduced pressure conditions they were proven to be the same as in regular atmospheric pressure, for those analytes whole Henry's rate constant was low, the reduced pressure was proven to be beneficial as it assisted them

to transfer from the sample to the headspace faster (Psillakis, 2017; Trujillo-Rodríguez et al., 2020; Trujillo-Rodríguez, Pino, Psillakis, et al., 2017). This effect leads to significantly faster times of reaching equilibrium conditions under mild temperatures. One of the most important aspects of this method is that the enhanced extraction yields are appearing already in the pre-equilibrium state (Psillakis, 2017; Trujillo-Rodríguez et al., 2020; Trujillo-Rodríguez, Pino, Psillakis, et al., 2017).

1.3. STIR BAR SORPTIVE EXTRACTION (SBSE)

Stir bar sorptive extraction (SBSE) was primarily introduced in 1999 by Baltussen and his team as a novel technique in an attempt to develop an extraction method that is both a solventless sample preparation method and in accordance with the principles already established by green analytical chemistry (Baltussen, Sandra, David, & Cramers, 1999; Florêncio Nogueira, 2017). The final product of their work offered extraction and enrichment of organic compounds by aqueous matrices, in one single step (David & Sandra, 2007). Aside from its others assets, this technique displays fast and relatively easy manipulation combined with low sample volume requirements, reutilization and easy synergistic combination with modern analytic chemistry instrumentation (Nogueira, 2015).

In spite of the fact that SBSE is established upon the same principles with SPME, as opposed to its predecessor, it demonstrates a higher sensitivity, robustness, capacity for sorbent phase and capability for the detection of trace and even ultra-trace organic compounds in real water matrices (Nogueira, 2015) . In actuality, the volume of extraction phase in SBSE is up to 50-250 times larger compared with the equivalent one of typical SPME fibers (David & Sandra, 2007). The degradation of the fiber, the low specificity demanding the use of different fiber materials and displacement effects due to matrix effects and other limitations imposed by SPME are finally partially overcome with the higher amount of solid phase extractant used in SBSE (Camino-Sánchez et al., 2014).

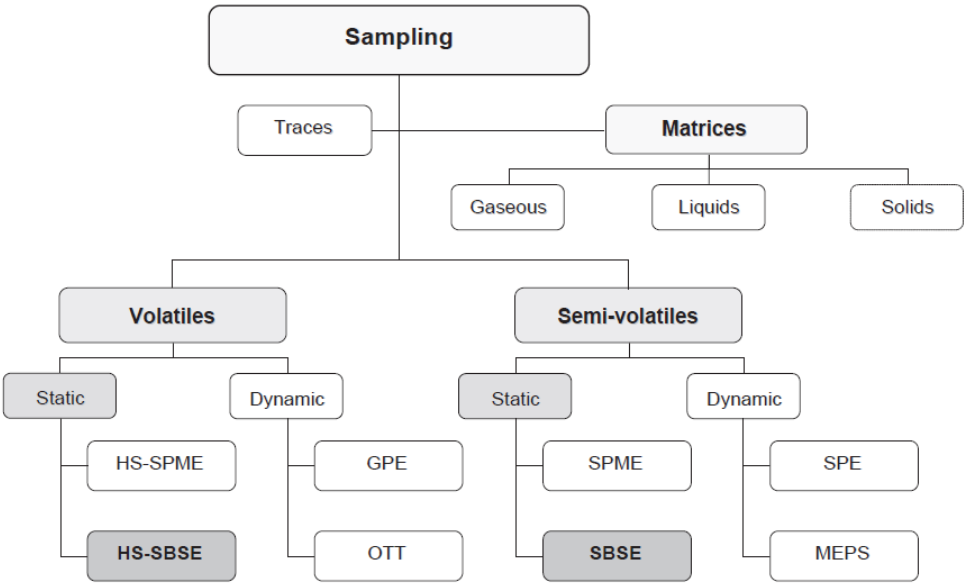

Figure 1.7. Diagram summarizing the most currently used sorption-based methods for trace analysis of volatile and semi-volatile compounds from all types of matrices (Nogueira, 2012).

SBSE has been trademarked worldwide under the commercial name of Twister. Essentially, its structure consists of a magnetic stir bar incorporated into a glass jacket (10-20mm in length), with typical PDMS coating volumes ranging from 24 to 126 µL (Nogueira, 2015). Its original conception and development was derived from an observation of a significant deviation between theory and the yielded experimental data in SPME on PDMS, pointing towards a scientific argument on sorption vs. adsorption phenomena (Yang et al., 1998). Further investigation shed light to the fact that during SPME extraction of highly non-polar solutes adsorption phenomena were taking place on the Teflon stir bar used for agitating the sample while sorption on the PDMS was simultaneously occurring (Baltussen, Sandra, David, Janssen, et al., 1999). Thus, the development of SBSE was implemented (Baltussen, Sandra, David, & Cramers, 1999).

1.3.1. Principles of SBSE

Polydimethylsiloxane (PDMS), the sorbent used, is a non-polar polymeric phase that fosters hydrophobic interactions with the target molecules. The retention mechanism is effectuated mainly through van der Waals forces even though hydrogen bonds can be established as well with the oxygen atoms present in the PDMS, whose diffusion and thermostable properties render it suitable to operate under a wide range of temperatures (Nogueira, 2015; Seethapathy & Górecki, 2012).

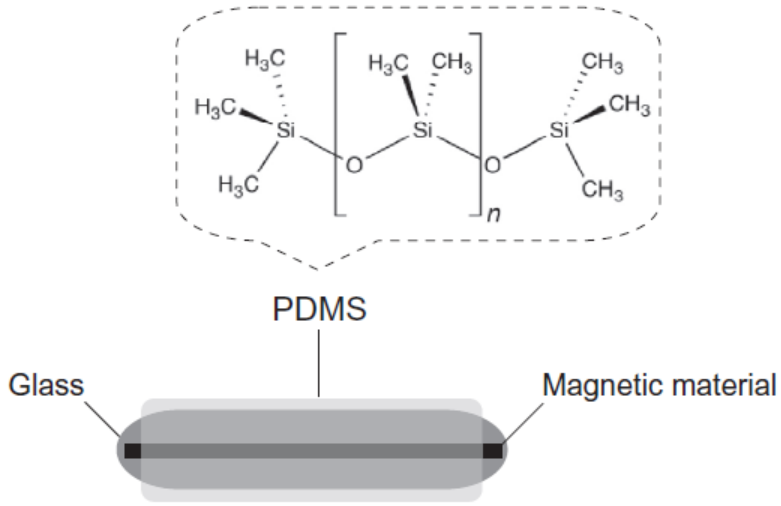

Figure 1.8. Analytical device used for stir-bar sorptive extraction [SBSE(PDMS)] (Nogueira, 2015).

The partitioning coefficient between the PDMS and the aqueous phase is the basic premise under which SBSE is operating, being known that it is an equilibrium extraction technique (David & Sandra, 2007). Several past studies have associated the partitioning coefficient with the octanol-water distribution coefficients ($K_{o/w}$) and the phase ratio β (David & Sandra, 2007).

The equations that govern the partition between the liquid and stationary phases are:

$$\frac{m_{SBSE}}{m_o} = \frac{K_{O/W}/\beta}{1+(K_{O/W}/\beta)} \quad (1.5)$$

$$Recovery(\%) = (K_{O/W}/\beta)/(1 + K_{O/W}/\beta)\, x100\% \quad (1.6)$$

$$\beta = \frac{volume\ of\ sample}{volume\ of\ stationary\ phase} = \frac{V_W}{V_{PDMS}} \quad (1.7)$$

Where m_{SBSE} is the mass of the target analyte in the sorbent phase and m_o is the mass of the target analyte in the aqueous solution (Camino-Sánchez et al., 2014).

The lower phase ratio β explained by the considerable volume of the stationary phase, leads to high capacity and quantitative recoveries mainly in target analytes of hydrophobic nature (Florêncio Nogueira, 2017). Thus, the volume of stationary phase employed in an SBSE device is responsible for achieving higher extraction yields over SPME (Camino-Sánchez et al., 2014).

On the basis of a constant $K_{o/w}$ for a target solute, the phase ratio could therefore be optimized each time. Figure 1.9 represents the theoretical efficiency of SBSE against log $K_{o/w}$ (Nogueira, 2015). As the sample volume becomes lower, higher extraction

yields are being noticed. A similar pattern is evident in the case of higher hydrophobicity (Nogueira, 2015).

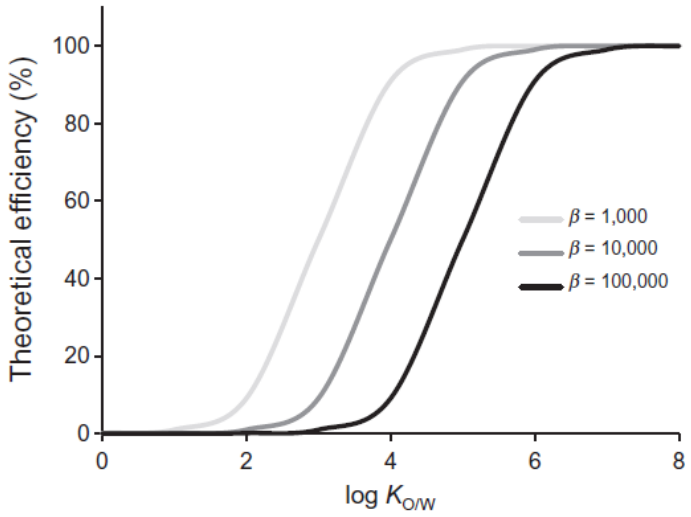

Figure 1.9. Influence of the phase ratio (β) on the theoretical efficiency of SBSE(PDMS) against log $K_{o/w}$ (Nogueira, 2015).

1.3.2. Extraction Modes for coated stir bars of PDMS and different materials

SBSE sampling can be performed in two basic modes, where the coated stir bar can get in contact with the target analytes in question, either by direct extraction (immersion) or by headspace extraction, depending on the hydrophobicity and volatility of the aforementioned solutes. Other less used modes, depending on the material of the stationary phase of the stir bar, should be discussed as well.

Firstly, enrichment or extraction of the target analytes is effectuated from the sample bulk to the stationary phase through an adsorption process (Nogueira, 2015). Secondly, back-extraction of the analytes from the stationary phase is achieved through thermal or liquid desorption. In this context SBSE is a static microextraction technique (Nogueira, 2015).

In the **direct extraction (immersion) mode**, more commonly known as SBSE, the polymer coated stir bar is added inside a headspace vial filled with the aqueous sample under investigation and it is stirred under steady state conditions for a preset period of time (Prieto et al., 2010). Upon the conclusion of extraction, the stir bar is removed, rinsed with distilled water and wiped with a lint-free tissue. After sorption the stir bar can be desorbed either chemically in a liquid or thermally in a gas chromatography

inlet (Prieto et al., 2010). The importance of the rinsing step is paramount, especially on the grounds of complex matrices where non-volatile compounds can block the desorption process (Prieto et al., 2010).

In the **headspace extraction mode**, commonly known as headspace solvent extraction or HSSE, the sampling and simultaneous extraction process is materialized by suspending the stir bar on the top of the vial, while the sorbent is in static contact with the vapor phase of the sample in question (Nogueira, 2015). It is preferred for volatile analytes and by circumventing the contact with the sample, potential contamination can be eliminated (Nogueira, 2015). It was firstly introduced by Bicchi et. al in their work of analysis of roasted arabica coffee and coffee brew (Bicchi et al., 2002).

Another approach used in order to overcome the problems aroused where different classes of target analytes are being investigated, is multi-mode assays. The first technique involves the extraction of a matrix with the utilization of different assays with one stir bar per sample, under the same or different experimental conditions (Nogueira, 2012). In another scenario, more than one stir bars can be used while being subsequently simultaneously desorbed (Nogueira, 2012).

As mentioned above, after extraction, the target compounds can be inserted into the analytical instrument quantitatively by thermal desorption (TD) or back extraction with the use of an appropriate organic solvent (liquid desorption, LD). TD is considered an on-line approach and it restricted to thermally stable and semi-volatile analytes. TD can be manifested with the usage of a glass tube in a separate unit for bake-out purposes (~350^{o}C), paired with a GC analytical system (Nogueira, 2012). One of its many advantages is the achievement of high sensitivity since the entire sample can be channeled into the GC instrument, rendering automation quite applicable (Nogueira, 2012) . On the other hand, LD is an off-line approach, where after the extraction the stir bar can be completely immersed inside a glass insert filled with an organic solvent (e.g., methanol, acetonitrile etc.) for a preset period of time so desorption can be successfully effectuated. LD is more suitable for semi-volatile to non-volatile analytes, and it can be coupled with a plethora of analytical instruments such as liquid chromatography (LC), capillary electrophoresis (CE), gas chromatography (GC) etc (Nogueira, 2012). One of its many advantages is the possibility of multiple reanalysis of the same sample (Nogueira, 2012).

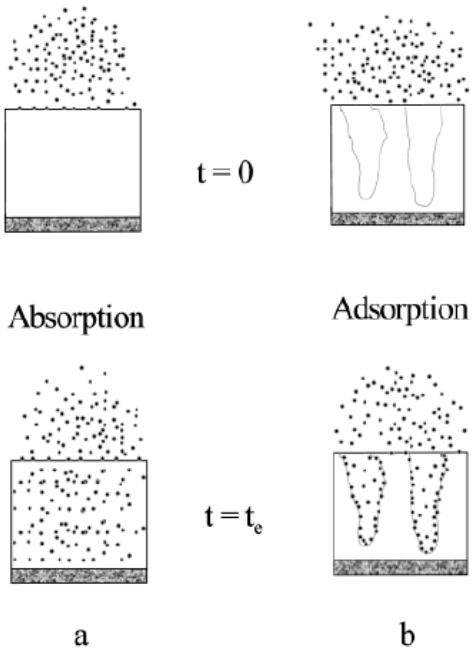

Figure 1.10. Extraction using absorptive (a) and adsorptive (b) extraction phases immediately after exposure of the phase to the sample t =0 and after completion of the extraction t= te (Pawliszyn, 2003).

While PDMS is the stationary phase of choice by researchers worldwide, other phases have been developed and promoted through a significant amount of works. The use of sol-gel technology was utilized for the development of thin 30μm layers of PDMS on stirring rods (W. Liu et al., 2004, 2005). Efforts for the extraction of caffeine and metabolites in biological fluids were made using a coated restricted access material (RAM) on stir bars (Lambert et al., 2005). Bicchi et. al, (Bicchi et al., 2005), introduced in another of their works the use of a dual phase stir bar in both of the aforementioned SBSE and HSSE modes. The composition of these stir bars was comprised of an outer PDMS coating and a carbon adsorbent material in the inner part (David & Sandra, 2007). Increased extraction yields and much better recoveries were recorded with the use of this particular stir bar for polar solutes in water as well as for significantly volatile compounds (David & Sandra, 2007). Polypropylene (PP) microporous membranes and PDMS rods have been used as well for the concentration from medium to low polarity analytes (Nogueira, 2012). As of recently, PDMS/ethylene glycol (EG) stir bards have been available commercially albeit with a lack of applications proposed (Nogueira, 2012).

1.3.3. Optimization parameters for SBSE

There are multiple ways to boost and assist in the improvement of recoveries in SBSE. Some of the most studied variables with respect to the extraction steps that should be followed for the ultimate optimization of an SBSE technique are the amount of sorbent, the sample volume and equilibrium time, extraction time, pH, temperature, stirring rate, ionic strength, matrix effect and addition of organic modifiers.

In SBSE the extraction efficiency depends on a considerable degree on the **amount of sorbent** material used. More specifically, in cases where there are non-qualitative conditions of extraction a higher amount of stationary phase assists in the extraction of the target analytes and facilitating higher extraction yields as an overall outcome (Vállez-Gomis et al., 2021). Attention must be paid though, as larger sorbent volumes can lead to proportionally larger stir bars which could ultimately affect the extraction efficiency negatively as bigger desorption volumes will be needed in the case of LD (Vállez-Gomis et al., 2021). Representatively, Leon et. al in their study of 35 priority semi-volatile compounds recorded a higher number of extracted analytes for the 20mm×0.5mm, 47μL PDMS coated stir-bars in comparison with the 10mm×0.5mm, 24μL ones, as it should be expected (León et al., 2003). An interesting observation was disclosed by the scientific team of Franc et. al with an increase in sensitivity of more polar compounds with the use of higher PDMS volumes (Franc et al., 2009).

One of the most versatile ways to achieve improvement in recoveries in SBSE is a corresponding increase in the **sample volume**. The aforementioned idea can be applied to the point where the loss of extraction efficiency subdues the gain of mass analyte, in accordance with eq. (1.5) (Camino-Sánchez et al., 2014). The equilibrium constant (K_c) (ratio between the concentration of the analyte in the stationary phase and in the sample) is closely interconnected with $K_{o/w}$. It should be noted that the eq. (1.5) is applicable only under conditions when equilibrium is reached (Camino-Sánchez et al., 2014). Under these circumstances, the higher the volumes of both the sample and the stationary phase are, the longer are the equilibration times that are demanded. This observation is setting SBSE apart from SPME where the volumes of the sorbent are vastly lower (Camino-Sánchez et al., 2014).

For analytes with acidic or basic properties, **sample pH** is a significant parameter to be taken into consideration. The goal is for the pH to be adjusted in such a way so that the solute can be obtained in its non-ionic form, thus giving rise to higher extraction efficiencies (Prieto et al., 2010). It should be noted though that an extremely acidic (pH<2) or basic (pH>9) environment degrade faster the stationary PDMS phase, ultimately reducing the number of extraction cycles a stir bar can perform (Franc et al., 2009; Melo et al., 2009).

A key element for manipulating the extraction kinetics in order to achieve higher extraction yields is the **stirring rate**. This process is explained by the fact that thinning the boundary layer between the stir bar and the sample solution can be proven a key factor for faster extraction kinetics (W. Liu et al., 2005; Prieto et al., 2010). Caution should be given in the case of substantially high stirring rates as they can physical damage to the stir bar due to a constant contact with the bottom of the sampling vial (W. Liu et al., 2005; Prieto et al., 2010). According to many researchers, the effect of the stirring rate to the extraction yields is prominent mostly at values 500-750 rpm, as in higher values no effect is mostly recorded as poor homogeneity can be one of the main causes (Quintana et al., 2007; Serôdio & Nogueira, 2005; Yu & Hu, 2009).

Ionic strength is yet another worth mentioning parameter affecting the solubility of the analytes and accordingly the extraction efficiency. Based on the salting-out effect, with an increase of the ionic strength, the solubility of less polar analytes of interest decreases, leading to a higher partitioning of these particular analytes onto the sorbent (Ochiai et al., 2002, 2006; Quintana et al., 2007). Nonetheless, a significant increase in the salt addition could lead to a hindering of the mass transfer process as viscosity also increases within the sample bulk (Quintana et al., 2007; Vállez-Gomis et al., 2021). In the case of non-polar analytes ($\log_{ko,w}$>3.5) addition of salt lead to reduction in the extraction efficiency (Chaves et al., 2007; Rodil & Moeder, 2008; Zuin et al., 2005).

Matrix effect could be regarded as one of the principal constraints of SBSE. This happens because the adsorption of the compounds of interest onto the organic matter surface competes with the sorption of the same analytes in the stir bar. Matrix effect can be presented not only as organic or suspended soils but as any substance present in the sample matrix that can cause a three-phase partitioning of the analyte amongst the solvent, sorbent and the competitor (Camino-Sánchez et al., 2014). Two solutions to

the problem of matrix could be implemented. A dilution of the sample in question, until the matrix effects are unsignificant as well as the implementation of a matrix-matched calibration that can also leave LOQ and LOD unaffected (Camino-Sánchez et al., 2014).

Extraction time is another critical parameter to be considered when aiming to achieve higher extraction efficiencies and one of the most documented variables. As a general rule, this parameter is studied after the determination of the other fixed parameters discussed earlier. In that case, the time profiles are investigated so that an equilibration time could be obtained. It is critical that the contact time between the donor phase and the sorbent is sufficient enough for the equilibration time to be reached whether quantitation extraction is the aim or not (Vállez-Gomis et al., 2021). Working under equilibrium conditions can be a guarantee for maximum sensitivity and precision. Nevertheless many researches choose to sacrifice these conditions so as to lessen the overall analysis time (Guan et al., 2008; Melo et al., 2009; Popp et al., 2005; Quintana et al., 2007).

1.4. THE EFFECT OF VACUUM IN HEADSPACE MICROEXTRACTION SAMPLING

1.4.1. Background and history

During headspace microextraction sampling, the uptake of analytes from the sorbent material used, was always favored in the case of volatiles, in comparison with semivolatiles (Pawliszyn, 2011). For this particular category of compounds, several optimization techniques such as prolonged extraction times, heating and stirring of the sample were applied, but to no dramatic effect (Pawliszyn, 2011). An alternative way of accelerating the kinetics and attaining therefore faster equilibration times, is headspace sampling under reduced pressure conditions (Psillakis, 2020). Brunton et. al applied for the first time low pressure conditions in their sampling studies, while Darouzes et. al validated the procedure (Brunton et al., 2001; Darrouzès et al., 2005) . In 2012 Psillakis et. al introduced water samples in pre-evacuated sample vials, forming a new sampling technique named vacuum-assisted HSSPME (Vac-HSSPME), while also developing a theoretical model, that was corroborated experimentally, to support their claims of a positively affected pre-equilibrium HSSPME sampling for

target analytes with low affinity for the headspace (Psillakis, 2017; Psillakis, Mousouraki, et al., 2012; Psillakis, Yiantzi, et al., 2012). Vac-HSSPME was later applied in the sampling of solid matrices (Yiantzi et al., 2015), as well as significant range of other types of matrices (Capetti et al., 2020; Orazbayeva et al., 2018), and food matrices like wine (Vakinti et al., 2019), dairy products (Sýkora et al., 2020; Trujillo-Rodríguez, Pino, Psillakis, et al., 2017), extra virgin olive oil (Mascrez et al., 2020), and fish (Delbecque et al., 2022). The effectiveness of the sampling under low pressure conditions was tested as well for other types of sorptive microextraction techniques. Notably, Trujillo-Rodríguez et al. tested the vacuum conditions of sampling in SDME, developing a method termed vacuum-assisted HS-SDME (Vac-HS-SDME), which proved that free fatty acids can be extracted in significantly faster equilibration times than in regular atmospheric conditions (Trujillo-Rodríguez, Pino, & Anderson, 2017). Psillakis et. al then, brought into fruition a quantification numerical model of the pressure dependance of extraction yields, applying the theory on experimental data using polycyclic aromatic hydrocarbons as the target analytes (Psillakis et al., 2019). Solomou et. al proposed in 2020 a procedure of headspace sampling employing SBSE, called vacuum-assisted headspace sorptive extraction (Vac-HSSE) (Solomou et al., 2020). Lastly, in 2022 Yiantzi et. al proposed a headspace sampling technique using TFME, termed vacuum-assisted headspace thin-film microextraction (Vac-HS-TFME) (Yiantzi et al., 2022).

1.4.2. Theoretical considerations

At this point it is crucial to state that the theory underlying the kinetics of the evaporation step in HSSE is similar to that formulated for HS-SPME (Nogueira, 2015; Tienpont et al., 2000), while also HSSE's pressure dependence has been demonstrated and experimentally verified (Psillakis, 2017; Psillakis, Yiantzi, et al., 2012; Yiantzi et al., 2015). Therefore, the theoretical aspects concerning the headspace/PDMS interfacial system are the matter of concern here.

1.4.2.1. Pressure (in)dependence at equilibrium and pressure dependence at pre-equilibrium conditions of headspace sampling from water samples

Headspace microextraction in its pre-equilibrium stage is characterized by two significant steps: (i) the volatilization/evaporation step and (ii) the absorption of the analyte in question by the extracting phase (Psillakis, 2020). The first step occurs in the sample/headspace system while the second one in the headspace/extractant system (Psillakis, 2020). Depending on the nature of the studied analytes, the sample matrix, the extracting phase etc. each of the aforementioned steps can be a limiting or boosting parameter to determine the extraction process (Psillakis, 2020).

At this point, it is imperative to mention that partial pressures and equilibrium concentrations are independent of the total pressure in equilibrium, based on the grounds that, partition coefficients and Henry law's constants are only affected at extremely high pressures only (Psillakis, 2017). In that case, the amount of analyte molecules extracted under regular or vacuum conditions is the same, and hence, independent of the total pressure at the equilibrium phase (Psillakis, 2017; Psillakis, Yiantzi, et al., 2012). On the contrary, it was proven in past research, that HSSPME sampling under low pressure conditions in nonequilibrium, could result in higher extraction yields as evaporation rates can be highly boosted in an air-evacuated headspace (Psillakis, Yiantzi, et al., 2012). A theoretical model was also developed as part of the aforementioned research which established for the very first time the pressure dependence of HSSPME sampling under nonequilibrium conditions (Psillakis, Yiantzi, et al., 2012):

$$V_s \frac{dC_s}{dt} = -K_L A(C_s - C_i) \quad (1.8),$$

where:

C_i (mol m^{-3}) is the concentration of the analyte at the water/air interface,

A is the interfacial contact area between the sample and the gas phase and

K_L (m h^{-1}) is the overall mass transfer coefficient at the gas phase–sample interface related to the evaporation rate constant (k; h^{-1}) (Psillakis, Yiantzi, et al., 2012).

1.4.2.2. The K_H criterion: A way to predict the effect of vacuum on headspace/PDMS sampling from water or water-containing samples

Headspace sampling, such as HSSPME or HSSE, is a multi-stage process involving mass transfer in three stages (sample, headspace and fiber) and across two interfaces (sample/headspace and headspace/fiber) (David & Sandra, 2007). The sample is initially left to come to equilibration conditions with the headspace prior to the introduction of the SPME fiber or coated stir bar (Psillakis, 2017). Following that, the fiber is exposed to the headspace in order to sorb the molecules of the analyte from the already enriched gaseous phase (Psillakis, 2017). In the case of analytes with high affinity for the vapor phase, that are characterized by high K_H value, the extracted amount of analyte, during that stage, is relatively small, which results in a fast equilibration process between the three phases described above (Psillakis, 2017). For analytes having a low predisposition to escape the headspace (low K_H value), a rapid uptake of analytes by the fiber is followed by low headspace concentrations that fall below the equilibrium level, rendering this particular equilibration process to be rather slow, as more analyte molecules have to be transferred from the sample to the headspace (Gorecki et al., 1998; Psillakis, 2017).

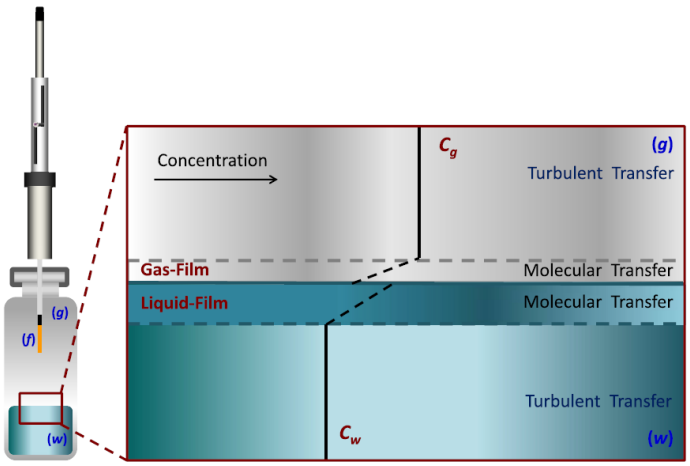

Fig. 1.11. Representation of the HSSPME experimental setup and the two-film model of the gas-liquid interface where: (w), (g) and (f) are the water, gas and SPME fiber phases; Cg and Cw are the concentrations in the bulk gas- and water-phases respectively (Psillakis, 2017).

In order to prefigure the effect of vacuum in both the volatilization/evaporation step but also in the efficiency of the whole extraction procedure the paradigm that was proposed by Psillakis et. al in 2012 was the K_H criterion which is essentially based on

the Henry's Law of the target analytes that are under investigation each time (Psillakis, 2020; Psillakis, Mousouraki, et al., 2012). In accordance with this criterion, the analytes' in question values of K_H are being compared with experimental threshold values. These threshold values stem from the two-film hypothesis, which was initially used to explain the pressure dependence during the evaporation stage from liquid samples, and thoroughly presented in Fig. 1.11 (Mascrez et al., 2020; Psillakis, 2017; Psillakis, Mousouraki, et al., 2012; Psillakis, Yiantzi, et al., 2012).

The overall mass transfer coefficient at the gas phase–sample interface related to the evaporation rate constant, used in function (1.8), was described for the first time with the use of the two-film hypothesis taking into consideration that the overall resistance to mass transfer is a byproduct of resistances through the gas and liquid thin films contiguous to the gas – liquid interface (Liss & Slater, 1974; Mackay & Wolkoff, 1973):

$$K_L = \left[\frac{1}{k_L} + \frac{RT}{K_H k_g}\right]^{-1} \quad (1.9),$$

where:

k_L and k_g (m h^{-1}) are the liquid-film and gas-film mass-transfer coefficients respectively,

K_H (atm m^3 mol^{-1};1 atm = 1.01 × 10^5 Pa) is the Henry's law constant defined as the ratio of partial pressure to aqueous concentration,

T is the absolute temperature (K) and

R is the gas constant (8.2 × 10^{-5} m^3 atm mol^{-1} K^{-1}).

According to this model, the aqueous sample and the headspace are well mixed and only the liquid and gas thin stagnant films which are adjacent to the air/water interface contain a concentration gradient (Liss & Slater, 1974; Mackay & Wolkoff, 1973). Additionally, the mass transfer resistance stems from resistances between the aforementioned thin films (Liss & Slater, 1974; Mackay & Wolkoff, 1973; Psillakis, 2017). The properties of the analytes have a significant impact on whether the resistance will be pinpointed in the liquid-film, gas-film, or both. All assumptions considered above, lowering the sampling pressure during the pre-equilibrium stage is bound to limit the gas-phase resistance, for analytes with low K_H values, leading to

faster mass transfer of the analytes while the diffusion and mass transfer coefficients are being increased (Psillakis, 2017). On the other side, for analytes characterized by liquid-phase resistance, which is not affected by the headspace pressure conditions, the effect of vacuum is not able to affect the headspace extraction process (Psillakis, 2017; Psillakis, Mousouraki, et al., 2012; Psillakis, Yiantzi, et al., 2012).

The K_H criterion therefore is an aftermath of the extensive past Vac-HSSPME investigations with an applicability of predicting the impact of the vacuum effect on HSSPME sampling of water samples as well as soil-water mixtures (Glykioti et al., 2016; Psillakis, Mousouraki, et al., 2012; Trujillo-Rodríguez, Pino, Psillakis, et al., 2017; Yiantzi et al., 2015, 2016). Fig. 1.12 links the different ranges of K_H values with the location the phase resistance is being noticed and the predicted effect of vacuum sampling on HSSPME which could apply as noted before also in the case of HSSE (Psillakis, 2017).

More specifically:

- Analytes with Henry's Law constant $\mathbf{K_H \leq 1.6\times10^{-4}\ atm\ m^3\ mol^{-1}}$ and especially $\mathbf{K_H \leq 1.2\times10^{-4}\ atm\ m^3\ mol^{-1}}$ showed higher extraction yields under low pressure conditions, indicating that sampling under vacuum can potentially be beneficial for semi-volatile and volatile analytes (Psillakis, 2020, 2017; Psillakis, Mousouraki, et al., 2012). This hypothesis can be verified from the fact that for analytes with the aforementioned K_H values, gas-phase resistance is responsible for dominating more than 50-95% of the evaporation rate (Lee et al., 2004; Mackay & Wolkoff, 1973; Psillakis, 2017; Smith et al., 1980).
- Analytes with $\mathbf{K_H \geq 1.6\times10^{-4}\ atm\ m^3\ mol^{-1}}$ and especially $\mathbf{K_H \geq 5\times10^{-4}\ atm\ m^3\ mol^{-1}}$, were proven to be unaffected by the vacuum sampling setting, as for these analytes liquid-phase resistance starts to control more than 50-95% of the overall evaporation rate (Mackay & Wolkoff, 1973; Smith et al., 1980).

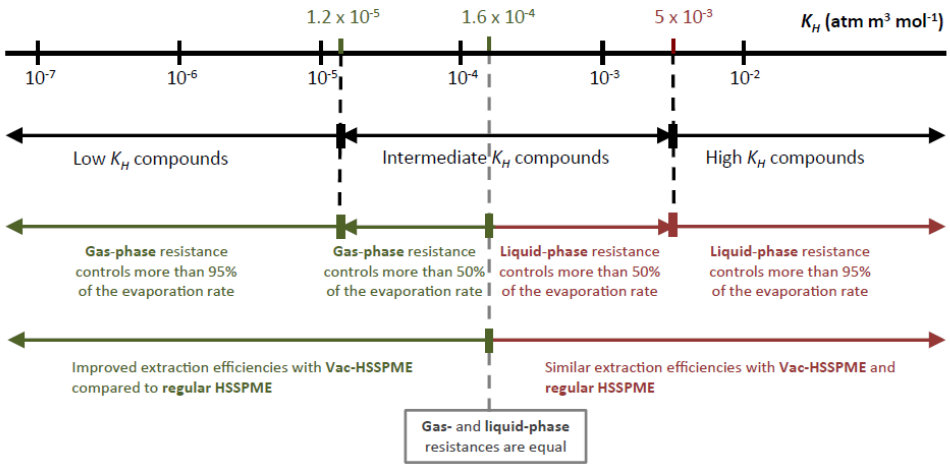

Fig. 1.12. Ranges of Henry's law constant associated with the location of the resistance on evaporation rates and the predicted effect of vacuum on HSSPME sampling of water and water-containing samples (Psillakis, 2017).

Nevertheless, the aforementioned above K_H criterion, should be considered with discretion in the step of analyte uptake by the extracting phase as it will not always work in the same manner as in the volatilization/evaporation step, meaning that even if the K_H criterion is not being fulfilled by the studied analytes, vacuum conditions could assist the overall analyte uptake (Psillakis, 2020). Such an instance could be the high uptake of naphthalene in the case of Vac-HS-SDME and Vac-HSSE sampling, even if this particular analyte is characterized by a relatively high K_H constant value (Psillakis, 2020; Psillakis et al., 2019; Solomou et al., 2020).

1.4.2.3. The effect of vacuum on headspace sampling of analytes with high affinity for the extracting phases or extracting phase of different volumes

For analytes with a high affinity for the extracting phase, or in the case of extracting phases of a specific geometry or high volume (Schnobrich & Jeannot, 2008) or slow mass transfer of the analytes inside the extracting phase (Kenessov et al., 2019; Psillakis et al., 2019), the second step of the analyte uptake by the extractant can be a time consuming process, leading to longer demanded time frames in order to achieve equilibrium conditions (Psillakis, 2020). For analytes with high affinity for the extractant or with extracting phases with high capacity, the prolonged equilibration times needed can be explained by the $t_{95\%}$, which is the time necessary so that the analyte's concentration can reach equilibrium in the PDMS extracting phase (Psillakis, 2020; Qin et al., 2008).

$$t_{95\%} = 3\frac{\delta K_{fs}(b-a)}{D_s} \quad (1.10)$$

where (b−a) is the thickness of PDMS extraction phase, D_s is the diffusion coefficient of the analyte in the sample, and K_{fs} is the analyte's distribution coefficient between extracting phase (in the case of HS-SPME is the fiber) and sample (Qin et al., 2008).

This function shows that large partition coefficients lead to large $t_{95\%}$, as well as the fact that high capacity sorbent phases can result in longer equilibration times. In that case, coated stir bars, which have significant PDMS volumes, can take longer times to reach equilibrium conditions in comparison with SPME fibers whose extracting phases are much smaller in capacity (Solomou et al., 2020).

In relation to the mass transfer of the analytes within the extracting phase during pre-equilibrium headspace conditions two cases were examined. In the case of HS-SDME, if hindrances related to diffusion inside the microdrop are insignificant, then low pressure conditions could be proven ideal for accelerating the analyte's adsorption by the microdrop (Psillakis, 2020; Psillakis et al., 2019). As regards HSSE, analyte uptake was proved to be faster when operating under vacuum conditions in comparison with regular atmospheric pressure (Solomou et al., 2020).

1.4.3. Parameters studied during method optimization

The effect of vacuum can be used in combination with some other specific parameters during the optimization stage in order to effectuate faster equilibration times and higher extraction yields. The assortment of different parameters to be tested alongside the effect of vacuum mostly depends on the nature of the compounds tested each time, the nature and properties of the extractant material used, as well as the nature of the matrix.

One of the most crucial points to examine is the **air-evacuation step**, which includes the suction of the air from the sample container before the initiation of the extraction process. The air-evacuation step is most commonly accomplished with the use of a vacuum pump where the air is suctioned out of the vial by piercing the septa attached to a specifically designed cap (Sýkora et al., 2020).

In the case of solid matrices the air evacuation is happening simultaneously and shortly after the introduction of the sample into the container (Orazbayeva et al., 2018; Yiantzi et al., 2015). The situation is different in the case of liquid samples where the air-

evacuation step can be performed prior or after the introduction of the sample into the container (Solomou et al., 2020; Yiantzi et al., 2016). In both cases of solid and liquid samples the volatility of the studied compounds can define the level under which there is loss of the more volatile compounds due to aspiration (Capetti et al., 2020; Psillakis, 2020; Yiantzi et al., 2015). This limitation can be eliminated by sufficiently reducing the air-evacuation time to the minimum, around 1 min, or by freezing the sample in question prior to air-evacuation to effectuated the reduction of analytes in the headspace or their aspiration during the whole air-suctioning process (Capetti et al., 2020; Orazbayeva et al., 2018; Psillakis, 2020). It was proven that the extracting phase was not affected negatively when exposed to the air-evacuation step in the case of VAC-HSSE (Solomou et al., 2020).

The **temperature of the sample** during extraction is another crucial factor to consider when optimizing under vacuum conditions. Although in the case of volatile compounds warming up the sample is not necessary as room temperature can be applied and yield satisfactory results, the situation is not the same for semi-volatile analytes that need an extra boost to be effectively transported to the headspace. In the case of semi-volatile compounds heating up the sample can lead to significant reductions of the equilibration times and to an overall speeding up of the extraction process (Psillakis, Yiantzi, et al., 2012). Unfortunately, on an experimental basis this was not always the case as extracting under high temperatures has many times led to low extraction efficiencies, explained by the affect produced humidity has in combination with an absorbent type of extractant such as PDMS (Psillakis, 2020). Additionally, it has been scientifically proven that heating up the sample leads to high vapor pressure which increases the total pressure inside the vial and therefore cancels the effect of vacuum (Psillakis, 2020; Vakinti et al., 2019).

Despite the aforementioned considerations extracting under vacuum conditions favors the application of milder temperatures as it has been proven to effectively yield similar extraction efficiencies with those under regular atmospheric conditions and much higher temperatures, as well as prolonging the longevity of the extractant material used each time (Solomou et al., 2020).

Extraction time is another parameter to be considered when coupled with extracting under vacuum conditions. Sampling under vacuum conditions was proven to yield

impressively higher extraction efficiencies at half the time needed under atmospheric conditions. This is an important observation to consider as it works not only in the case of analytes with a low affinity for the headspace but also for extractants constituted with a high capacity sorbent material as in the case of a coated stir bar in HSSE whose surface area to volume ratio leads to long equilibration times (Solomou et al., 2020). On the other hand, when dealing with absorbent type of materials as the extractant phase it is advisable to eliminate the extraction time so as to avoid the development of the effect of competitive adsorption (Trujillo-Rodríguez, Pino, Psillakis, et al., 2017). In those cases, a fast analyte uptake can succeed to a faster effectuation of an absorbent maximum which will be progressively lower to that documented under regular atmospheric conditions (Psillakis, 2020).

An important, last parameter to consider is the **effect of matrix**, when sampling under vacuum. The challenges scientifically faced here, in the case of complex matrices, are similar to those recorded when sampling under regular conditions. Nevertheless, a larger number of analytes can be extracted from complex samples compared with the standard methodology (Psillakis, 2020). In the case of complex oil samples, the richer volatile profile obtained under vacuum compared with regular pressure resulted in partial co-elution of analytes, giving thus the opportunity for a more detailed future two - dimensional GCMS analysis to explore untargeted analytes (Mascrez et al., 2020; Psillakis, 2020). Another worth mentioning application is the Vac-HS-SPME sampling of haloanisoles from wine samples (Vakinti et al., 2019). Despite wine's high content in ethanol and a plethora of other volatile compounds that could both stimulate changes in the solubilities of analytes in the headspace and compete with the haloanisoles for binding sites on the porous material of PDMS, plus the possible increase of the total pressure within the sample vial due to the ethanol which could inhibit the positive effect of sampling under vacuum conditions (Trujillo-Rodríguez, Pino, Psillakis, et al., 2017), results from the study showed that sampling for 30 min at 25 °C could yield lower detection limits than those with regular HS-SPME sampling for 30 min at 55 °C (Vakinti et al., 2019). Lastly, soil samples were notably the first type of complex matrix to be successfully investigated with Vac-HS-SPME (Orazbayeva et al., 2018; Yiantzi et al., 2015). The addition of water to the soil samples created a slurry consistency and enhanced significantly the release of analytes into the headspace (Yiantzi et al., 2015).

1.5. HISORB SORPTIVE EXTRACTION

The HiSorb Sorptive Extraction technique, a solid phase microextraction technique, emerged in 2018 by Markes International alongside with the Centri, an entirely automated multimode platform orchestrated to sample and concentrate for GC-MS (Dugheri et al., 2020, 2022). The Centri autosampler presented a customized injection port for their thermal desorption (Dugheri et al., 2020, 2022).

HiSorb Extraction Technique is a non-exhaustive approach, launched by Markes International Inc. in 2016. Its launching established the commercialization of a new extraction medium, that of the HiSorb. A HiSorb, is essentially a PDMS extraction probe. The probes are constituted by a thin rod of inert material around of which a short sleeve of polydimethyloxane rubber is wrapped, serving as a sorbent phase (Dugheri et al., 2020). Two lengths of probes are readily available commercially, to allow immersive or headspace sampling in 10 or 20 mL vials (MARKES International, n.d.). The HiSorb Agitator, an extraction medium is designed to facilitate the stirring and heating of the sample, concurrently (MARKES International, n.d.). The probes are then washed with deionized water to rinse off the presence of any matrix residue (MARKES International, n.d.). The probe is then inserted into a standard TD tube for analysis by a TD-GC-MS (MARKES International, n.d.). The combination of a larger volume of PDMS sorbent phase fixed on a more robust metal probe than SPME provides high sensitivity and protection from matrix interferences, simultaneously (Dugheri et al., 2022). Furthermore, its adaptability for using both for headspace or immersive sampling of liquids and solid samples while being also compatible with TD-GC-MS by the use of standard industry tubes makes it a very flexible analytical tool in the sample preparation field (MARKES International, n.d.).

The coupling of the HiSorb probes by TD analysis is offering quite a few key advantages. A wide analyte range of compounds of interest can be samples and analyzed as backflush operation permits the tubes to be packed with sorbents of a broad spectrum of strengths without the heavier analytes being bound to the stronger sorbent materials (MARKES International, n.d.). The two – stage desorption process offers a higher sensitivity as it allows concentration enhancements of the HiSorb tubes up to 10^6, while leading to a cleaner chromatographic system with the avoidance of solvent artifacts and thus a greater analytical quality as the narrow – bore focusing trap permits

a highly concentrated band of vapour to be introduced to the GC system as a part of the splitless operation (MARKES International, n.d.). A disadvantage that could be noted is that with the higher sorbent phase capacity and the concurrent slow thermal desorption process, the development of broader chromatographic peaks is a commonly occurring problem, which fortunately can be solved with a band focusing interface (Paiva et al., 2021).

The sorbent phase has the ability to pre-concentrate volatile and semi-volatile analytes from gaseous and aqueous samples when coupled with thermal desorption, rendering HiSorb extraction an excellent sorbent extraction technique with high analytical potential (Brown et al., 2021). Various research projects have conducted over the last few years by authors mainly concentrating on food and aroma analysis such as flavor profiling of milk and premium tea as well as volatile analysis of milk powder (Cheng et al., 2021; Roberts, 2016), flavor profiling of beverages (Barden & Lara, 2017) , brewed coffee volatiles (Eggermont et al., 2022) and sampling volatiles from fragranced consumer products (Kelly & Barden, 2018) among many.

1.6. PHOTODEGRADATION

1.6.1. Degradation mechanisms

Pharmaceuticals and organic pollutants in general, are a diverse group of chemical compounds that have been considered an emerging pollutant, especially when in combination with their metabolites and corresponding degradation products. The main sources of pharmaceutical products can be classified as domestic (through improper disposal of sewage) and medical wastewater discharge, where the aforementioned compounds in their unmetabolized state or with their active metabolites, are excreted through human urine or feces (Bavumiragira et al., 2022). The issue is often amplified by the inability of WWTPs to effectively eradicate them from their influents (Bavumiragira et al., 2022).

Upon their release into the environment through treated or unprocessed wastewater, organic pollutants, are contingent on various transport and degradation processes, where they end up accumulating or bioaccumulating in the natural ecosystems causing

a series of complications to many non-target organisms (Arnold & McNeill, 2007; Bavumiragira et al., 2022).

The physical processes include mainly transport processes (volatilization, wet deposition, dispersion, sedimentation, resuspension, soil or sediment mixing and diffusion) (Holt, 2000). These processes that are based on transport, define the variation in spatial and temporal distribution of a chemical in the environment. The chemical and biological processes include transformation reactions (biodegradation, hydrolysis, photolysis, speciation) (Holt, 2000). Photolysis and biodegradation are amongst the most important degradation processes as they can cleanse the environment in an organic and physical manner (Holt, 2000) .

The various degradation techniques can be effectuated in different rates which are dependent upon the type of the compound, the matrix in which the compound is present, as well as the characteristic environmental factors affecting a specific matrix. The byproducts of the original compound can be more or less harmful for the environment (Dabrowska et al., 2005; Holt, 2000).

1.6.2. Photolysis processes

One of the most important features of photochemical processes is the use of light hydrolysable (Bavumiragira et al., 2022). Photodegradation is an essential abiotic degradation process of organic compounds in the aquatic environment. The whole process is led by solar radiation, where a parent compound is transformed into other molecules by breaking covalent bonds. The byproducts formed are usually biodegradable and hydrolysable (Bavumiragira et al., 2022). The use of these processes for organic pollutant degradation and disinfection has been well documented for many decades now, and although energy absorption leads to photo-degradation, some compounds are still resistant and are not able to photolyze (Gmurek et al., 2017). In these cases, photochemical processes are applied in the presence of additional oxidants and/or catalysts. The efficiency of photochemical processes lies in the fact that they are premised on the generation of reactive and short-lived oxygen intermediates, such as hydroxyl radicals or sulfate radicals (Gmurek et al., 2017). The photodegradation mechanism proceeds until the total mineralization of pollutants, with the release of carbon dioxide, water and inorganic acids (Gmurek et al., 2017).

In the process of photodegradation, various parameters such as pH, temperature, type of matrix and various impurities (salts, soils etc.) are crucial in the formation of stable or toxic compounds (Gothwal & Shashidhar, 2015). Photodegradation processes achieve mineralization and concurrent disinfection of the waste with two possible reactions, including: a) photodegradation based on the effect of UV radiation, excitation and degradation of the molecules of organic compounds and b) the indirect oxidation of organics of pollutants under UV radiation, in the presence of various oxidizing reagents, such as O_3, H_2O_2, HSO^{5-} and $S_2O_8^{2-}$ (Oturan & Aaron, 2014; Parsons, 2004).

In direct photolysis an organic compound absorbs light directly and undergoes disintegration, meaning that the target compound absorbs a solar photon for the procedure to initiate (Arnold & McNeill, 2007; Rivera-Utrilla et al., 2013). The action and solar spectrum are primarily responsible for the rate of photon absorption (Arnold & McNeill, 2007; Rivera-Utrilla et al., 2013). The rate of direct photolysis is heavily influenced by the compound structure, as the molecule's capability to absorb a type of radiation can increase its energy to reach an excited state and thus lead to bond rapture (Arnold & McNeill, 2007; Rivera-Utrilla et al., 2013). The degradation depends on the radiation wavelength (λ), compound molar capacity (ε) and quantum yield (Φ) based on the following equation (1.11):

$$\Phi_\lambda = \frac{k_\lambda}{2.303 E_\lambda \varepsilon_\lambda} \text{ (1.11),}$$

where k_λ is the degradation kinetic constant at a given λ (s^{-1}), E_λ is the energy emitted by the source (Eistein $s^{-1}m^{-2}$), ε_λ is the absorption coefficient od the compound at the given λ (m^2mol^{-1}) and Φ_λ is the quantum yield at a given λ (mol $Einsten^{-1}$) (Rivera-Utrilla et al., 2013).

The quantum efficiency of the reaction can also be defined as the rate of photochemical conversion to the rate of absorption of photons by the system as follows:

$$\Phi_\lambda = \frac{-\frac{dc}{dt}}{I_a(\lambda)} \text{ (1.12)}$$

where,

$-\frac{dc}{dt}$: the rate of the photochemical reaction ($mol \cdot L^{-1} \cdot s^{-1}$)

$I_a(\lambda)$: the rate of absorption of photons by the organic compound at wavelength λ, in $mol \cdot L^{-1} \cdot s^{-1}$ (Parsons, 2004).

The value of the quantum efficiency depends on several factors, such as the wavelength of the radiation, the pH of the solution, the concentration of the pollutant, the temperature, the type of solvent as well as the concentration of dissolved oxygen (Parsons, 2004).

The second law of photochemistry or Starck-Einstein law states that each molecule participating in a chemical reaction induced by radiation absorbs only one photon of incident radiation (Parsons, 2004). According to this law, the value of the quantum efficiency usually does not exceed 1 (Parsons, 2004). However, its value can be bigger than 1 when photochemical reactions occur involving thermal chain reactions between photochemically generated free radicals (Parsons, 2004).

As a rule, the concentrations of organic pollutants in water and waste are very small and this leads to low radiation absorption (Parsons, 2004). In addition, most organic pollutants have a low quantum yield (Parsons, 2004). Because of the aforementioned limitations, the application of direct photolysis in industrial applications is therefore limited (Parsons, 2004).

Various scientific investigations have been focused over the years in direct photolysis including, UV-induced transformation of 2, 3-dibromo-5, 6-dimethyl-1, 4-benzoquinone in water and treated wastewater (Kourounioti et al., 2019), of 2, 4-dinitrotoluene in various water solutions analyzing further the effect of dissolved species (Mihas et al., 2007), of estrogens in aqueous solutions (B. Liu & Liu, 2004), of sulfamethoxazole and ibuprofen (Luo et al., 2018), among others.

On the other hand, in indirect photolysis the target compound cannot absorb light as another chromophore such as dissolved organic matter (DOM) which is present in natural waters and acts as a sensitizing species. In this instance, in a typical indirect photodegradation mechanism, the majority of the times, the sensitizer absorbs light and as a consequence it reacts in a direct manner with the substrate (Arnold & McNeill, 2007). The importance of the indirect photolysis in the photochemical fate of a specific compound can be decided via the addition of dissolved organic matter (Arnold & McNeill, 2007). A speedup of the degradation process can denote the significance of dissolved organic matter and the positive contribution of indirect photolysis (Arnold &

McNeill, 2007). The indirect photolysis is based on the production of various strong oxidizing chemical species, such as hydroxyl free radicals ($HO^{\bullet}$) and sulfate radicals ($SO_4^{\bullet -}$), the first formed by the effect of ultraviolet radiation in the presence of H_2O_2 while the second ones by the presence of persulfate anions, such as the monopersulfate anion (HSO^{5-}) and the persulfate anion ($S_2O_8^{2-}$) (Dewil et al., 2017; Parsons, 2004). The sulfate radicals aim to oxidize the organic pollutants dissolved in the aqueous phase, so at to achieve their complete mineralization, i.e conversion to water, carbon dioxide and inorganic ions (Dewil et al., 2017; Parsons, 2004).

1.6.3. Basic principles of photolysis

According to the wave-particle theory, which was developed in 1905 by Albert Einstein, electromagnetic radiation can behave both as a wave and a particle. The relationship that connects the wavelength of electromagnetic radiation **λ** (in m) and the frequency **f** (in s^{-1}), also known as the basic wave equation, is the following:

$$c = \lambda \cdot f \quad (1.13)$$

where c = 3 x 10^8 m/s which signifies the speed of light in vacuum.

The photoelectric effect and photochemical reactions are founded upon Planck's quantum theory of radiation, which are explained by the fact that a particle's properties of electromagnetic radiation include emission and absorption of radiation (Serway et al., 2004). The Planck relation is used to describe the quantity of spectral radiance at a specific wavelength radiated by a black body in equilibrium (Serway et al., 2004). According to this formula, the energy of a particle of light (E), known as a photon, is proportional to its frequency (v), by a continuing factor (h), h=6.625×10^{-34}J·s (Serway et al., 2004):

$$E = h \cdot v \quad (1.14)$$

By combining relations (1.13) and (1.14) the equation (1.15) is derived, which combines the wave and particle properties of radiation. Thus, it is deduced that radiation is not continuous but it is propagated in discrete units, called photons or particles of light, which explains the particle nature of radiation, while also having a frequency and therefore a wavelength, which explains the wave nature of radiation (Serway et al., 2004):

$$E = \frac{h \cdot c}{\lambda} \quad (1.15)$$

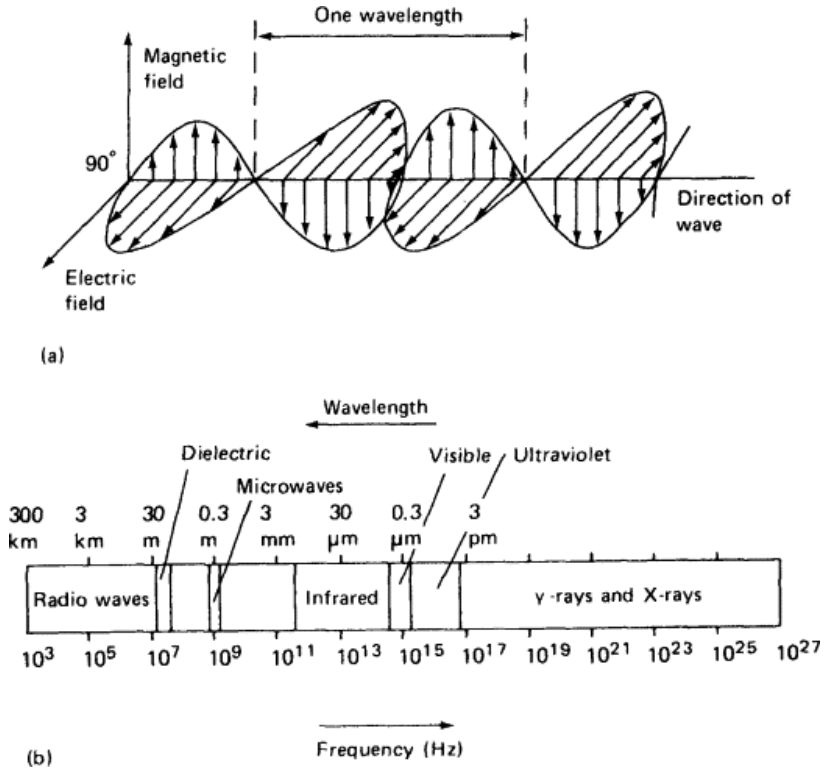

Fig. 1.13. (a) Electromagnetic radiation considered as a waveform; (b) types of electromagnetic radiation (Lewis, 1990).

Ultraviolet radiation is defined as a portion of electromagnetic radiation with a wavelength shorter than that of visible light and longer than that of X-rays that ranges from 100nm to 400nm (750THz) (Rivera-Utrilla et al., 2013).

UV radiation is divided into 4 sub-regions:

- Vacuum UV (VUV): 100-200 nm
- UV-C: 200-280 nm
- UV-B: 280-315 nm
- UV-A: 315-400 nm

The most common radiation for photolysis resides in the ultraviolet spectrum region (λ=200-400nm) (Rivera-Utrilla et al., 2013).

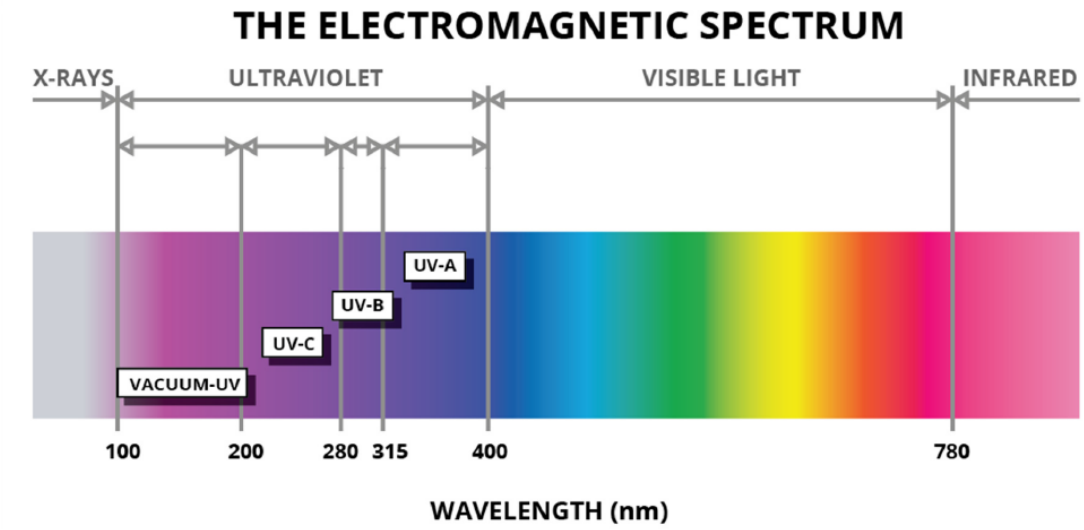

Fig 1.14. Color spectrum highlighting UV-A, UV-B, and UV-C.

Organic pollutants as well as other water components, such as dissolved organic and inorganic compounds, absorb ultraviolet radiation from 200 nm to 280 nm, i.e. part of UV-C radiation. In this value range the water molecules absorb at a minimum degree. Thus, this spectral region is the most interesting in the photolysis of water and wastewater, where degradation of organic and inorganic pollutants is achieved as well as water disinfection (Parsons, 2004).

The Beer-Lambert law quantitatively relates the absorption of radiation by the components of a solution. According to the Beer-Lambert law the fraction of electromagnetic radiation absorbed by the solvent-solute system is proportional to the number of molecules of the various components of the solution that absorb the radiation (Parsons, 2004):

$$P_\lambda = P_\lambda^0 \times 10^{-[\alpha(\lambda)+\varepsilon(\lambda)c]l} \quad (1.16)$$

where:

P_λ^0 is the spectral power of the incident radiation, measured in $W \cdot m^{-1}$,

P_λ is the spectral power of the transmitted radiation, measured in $W \cdot m^{-1}$,

$\alpha(\lambda)$ is the attenuation coefficient of the medium at wavelength λ, measured in cm^{-1},

$\varepsilon(\lambda)$ is the molar absorption coefficient of the solute, measured in $L \cdot mol^{-1} \cdot cm^{-1}$,

c is the concentration of the substance, measured in $mol \cdot L^{-1}$ and

l is the optical path length, measured in cm.

When the medium, i.e. the solvent, does not absorb electromagnetic radiation (applies to aqueous solutions), then α(λ) = 0, so the Beer–Lambert law is written as:

$$P_\lambda = P_\lambda^0 \times 10^{-\varepsilon(\lambda)cl} \quad (1.17)$$

The Beer-Lambert law assumes that interactions between solute molecules are negligible. According to this assumption, the concentrations of organic pollutants are extremely low explained by the fact that the pollutant molecules absorb radiation individually as well as that their degradation can also be examined individually (Parsons, 2004). In the case of concentrated solutions the interactions of the molecules are important and there is the possibility of formation of dimers or other inerts, rendering the relationship between absorption and concentration non-linear (Parsons, 2004).

1.6.4. Kinetics of degradation processes

The knowledge of the kinetic parameters of the reactions of the organic pollutant being studied each time, is crucial in order to choose the optimal applicable photochemical process for that specific pollutant each time (Parsons, 2004). Through the kinetics, the degradation of the pollutant can be predicted, in a reactor of specific geometry, knowing the type of radiation, the quality and the volume of the solvent (Parsons, 2004). Thus, the desired removal of the organic pollutant can be effectuated (Parsons, 2004).

The rate of direct photolysis of a pollutant (reaction rate) depends on:

a) the absorption of radiation by the organic compound
b) the efficiency with which the absorbed radiation leads to a chemical reaction (Parsons, 2004)

Thus the rate of a photochemical reaction under monochromatic radiation of wavelength λ, expressed in mol/(L·s) is given by the equation (1.18) (Parsons, 2004) :

$$r(\lambda) = (-\frac{dc}{dt})_\lambda = I_a(\lambda)\Phi(\lambda) \quad (1.18)$$

where,

$r(\lambda)$: the rate of the photochemical reaction, in mol·L^{-1}·s^{-1}

c : the concentration of the substance, in mol·L^{-1}

$I_a(\lambda)$: the rate of absorption of photons by the organic compound at wavelength λ, in mol·L^{-1}·s^{-1}

and,

$\Phi(\lambda)$: the quantum yield at wavelength λ, (dimensionless quantity).

The absorption rate of photons $I_a(\lambda)$ is written as follows in equation (1.19):

$$I_a(\lambda) = E^0_{p,o}(\frac{S}{V})F_s(\lambda)F_c(\lambda) \quad (1.19)$$

where,

$E^0_{p,o}$: the incident photon fluence rate, in mol/(dm^2·s),

$\frac{S}{V}$: the ratio of the reactor surface area exposed to radiation to the reactor volume, in dm^{-1},

$F_s(\lambda)$: the fraction of radiation absorbed by the solvent-solute system (dimensionless quantity),

and,

$F_c(\lambda)$: the fraction of radiation absorbed by the solute (dimensionless quantity).

Combining the equations (1.18) and (1.19) and given the fact that $E^0_{p,o}(\frac{S}{V}) = I_o$, where I_o is the flow of incident radiation in the photochemical reactor in mol·L^{-1}·s^{-1} the reaction rate is expressed as:

$$r(\lambda) = (-\frac{dc}{dt})_\lambda = I_o F_s(\lambda)F_c(\lambda)\Phi(\lambda) \quad (1.20)$$

According to Beer-Lambert law:

$$F_s(\lambda) = 1 - 10^{-[a(\lambda)+\varepsilon(\lambda)c]\cdot l} = 1 - e^x \quad (1.21)$$

$$F_c(\lambda) = \frac{\varepsilon(\lambda)c}{a(\lambda)+\varepsilon(\lambda)c} \quad (1.22)$$

thus, by replacing equation (1.21) and (1.22) to equation (1.20):

$$r(\lambda) = (-\frac{dc}{dt})_\lambda = E_{p,o}^0(\frac{S}{V})(1 - 10^{-[a(\lambda)+\varepsilon(\lambda)c]\cdot l})(\frac{\varepsilon(\lambda)c}{a(\lambda)+\varepsilon(\lambda)c})\Phi(\lambda) \text{ (1.23)}$$

The exponential term $10^{-[a(\lambda)+\varepsilon(\lambda)c]\cdot l} = e^{-(ln10)[a(\lambda)+\varepsilon(\lambda)c]\cdot l} = e^{-2.303[a(\lambda)+\varepsilon(\lambda)c]\cdot l} = e^x$ so, eq. (1.21) is transformed as follows:

$$F_s(\lambda) = 1 - e^x \text{ (1.24)}$$

According to Taylor series e^{-x} is written as follows:

$$e^{-x} = 1 - x + \frac{x^2}{2!} - \frac{x^3}{3!} + \cdots$$

When the absorption of electromagnetic radiation by the organic compound is small $A(\lambda)<0.1$, i.e. $x<0.1$ the terms $x^2/2!$, $x^3/3!$,... are much smaller than x and can be omitted.

Thus, eq. (1.21) is simplified as follows:

$$F_s(\lambda) = 1 - e^x \simeq 1 - (1 - x) = x = 2.303[a(\lambda) + \varepsilon(\lambda)c]l \text{ (1.25)}$$

By replacing the eq. (1.25) to eq. (1.23):

$$r(\lambda) = 2.303E_{p,o}^0(\frac{S}{V})l\Phi(\lambda)\varepsilon(\lambda)c \text{ (1.26)}$$

By setting, $k_1(\lambda) = 2.303E_{p,o}^0(\frac{S}{V})l\Phi(\lambda)\varepsilon(\lambda)$, eq. (1.26) is transformed as follows:

$$r(\lambda) = -\frac{dc}{dt} = k_1(\lambda)c \text{ (1.27)}$$

Eq. (1.27) corresponds to a first-order kinetic equation.

The degradation processes are usually described by first order reactions, even in the case of persistent organic contaminants that record a high degree of durability (Dabrowska et al., 2005).

The degradation kinetic of a first order reaction from eq. (1.27) could be expressed as follows in equation (1.22):

$$\frac{d_C}{d_t} = -kC \qquad (1.28)$$

where,

C : the concentration of the target compound that degrades at a given time t

and,

k : the degradation rate constant.

The integration of the eq. (1.23) with initial conditions: t=0 and C=C_0 results in eq. (1.29):

$$C(t) = C_0 e^{-kt} \quad (1.29)$$

where,

C_0 : denotes the initial concentration of the studied compound.

From eq. (1.29) it can be deduced that the concentration of a compound is an exponential function of the degradation time and thus can be expressed as follows in eq. (1.30):

$$lnC(t) = lnC_0 - kt \quad (1.30)$$

hence, the logarithm of the concentration is a linear function of the degradation time in a first order kinetic reaction.

The use of the half-time life ($t_{1/2}$) is a useful parameter, defined as the time needed for the reduction of the reactant compounds to the half of their initial concentrations and hence is expressed as follows in eq. (1.31):

$$t_{1/2} = \frac{ln2}{k} \quad (1.31)$$

For first order reactions the half life time is independent of the reactant's initial concentration and it is inversely related with the degradation rate constant (Dabrowska et al., 2005).

An interesting note to highlight is that when the absorption of electromagnetic radiation of the solution is high, then $F_c(\lambda) = 1$. Additionally, the exponential term $10^{-[a(\lambda)+\varepsilon(\lambda)c]\cdot l}$ becomes very small, thus $F_s(\lambda) = 1$, as well. In that case, equation (1.25) could be simplified as follows:

$$r(\lambda) = (-\frac{dc}{dt})_\lambda = I_o \Phi(\lambda) \quad (1.32)$$

from where it is concluded that the rate of the reaction is independent of the concentration of the studied substance and follows zero-order kinetics.

1.6.5. Reaction mechanisms during photolysis

The electronically excited molecules of a substance RX*, reach this state through the reaction:

$$RX + h\nu \rightarrow RX^* \text{ (1.33)}$$

$$RX^* \rightarrow (R^{\cdot} \ldots X^{\cdot})_{cage} \rightarrow R^{\cdot} + X^{\cdot} \text{ (1.34)}$$

$$(R^{\cdot} \ldots X^{\cdot})_{cage} \rightarrow RX \text{ (1.35)}$$

$$RX^* \rightarrow (R^+ \ldots X^-)_{cage} \rightarrow R^+ + X^- \text{ (1.36)}$$

$$RX^* + O_2 \rightarrow RX^{\cdot +} + O_2^{\cdot -} \text{ (1.37)}$$

$$RX^* + {}^3O_2 \rightarrow RX + {}^1O_2 \text{ (1.38)}$$

The excited molecules of the substance RX* result from the absorption of UV radiation by molecules of the substance RX. Equation (1.34) presents the homolytic fission of the covalent bond of the RX compound which happens in the solvent cage (Oturan & Aaron, 2014; Parsons, 2004). Free radicals that escape from the cage can undergo further redox reactions, depending on their structure (Oturan & Aaron, 2014; Parsons, 2004).

1.7. Scope

The uncontrolled occurrence of significant amounts of organic compounds in the aquatic element, due to their constant discharge through numerous sources of production, use and disposal of a wide variety of chemicals frequently utilized in medicine, industry, agriculture, tobacco, and household appliances, has led to the development of novel technologies in the field of analytical instrumentation and methods for analysis of trace organic compounds. The immoderate release of such substances into water ecosystems through urban wastewater, even at trace concentration levels of ng L^{-1}-μg L^{-1}, has been pivotal to their accumulation in the aquatic element with arguably disastrous effects to both ecosystems and human health. Taking into consideration the need of the scientific community to orientate towards a sustainable and environmentally friendly perspective Green Analytical Chemistry (GAC) has been introduced the last decades as an initiative to investigate for practical

alternatives to the off-line treatment of wastes to substitute methodologies with high load of pollutants (toxic reagents, solvents etc.) with clean ones.

Additionally, the need to thoroughly understand the behavior and fate of emerging pollutants after their introduction in the aquatic environment and especially surface waters, has induced the study of the role of photodegradation to investigate the impact of the aforesaid pollutants in the environment.

The present doctoral research is orientated towards the broad topic of advanced studies of detection and monitoring of the fate of organic pollutants in the aquatic environment using various scientific means, ranging from the establishment of novel microextraction techniques under atmospheric pressure as well as vacuum conditions regarding the presence of aromatic hydrocarbons in water and tobacco product leachates, to the UVC-induced degradation of a prominent pharmaceutical substance, cilastatin, and nicotine, a basic tobacco constituent, in natural water and treated waste water.

1.8. REFERENCES

Abdel-Rehim, M. (2011). Microextraction by packed sorbent (MEPS): A tutorial. *Analytica Chimica Acta*, *701*(2), 119–128. https://doi.org/10.1016/j.aca.2011.05.037.

Aguinaga, N., Campillo, N., Viñas, P., & Hernández-Córdoba, M. (2008). A headspace solid phase microextraction procedure coupled with gas chromatography-mass spectrometry for the analysis of volatile polycyclic aromatic hydrocarbons in milk samples. *Analytical and Bioanalytical Chemistry*, *391*(3), 753–758. https://doi.org/10.1007/s00216-008-1841-2.

Anastassiades, M., Scherbaum, E., & Bertsch, D. (2003). Validation of a Simple and Rapid Multiresidue Method (QuEChERS) and its Implementation in Routine Pesticide Analysis. *MGPR Symposium: Aix En Provence, France*, *7*.

Arnold, W. A., & McNeill, K. (2007). Chapter 3.2 Transformation of pharmaceuticals in the environment: Photolysis and other abiotic processes. *Comprehensive Analytical Chemistry*, *50*. https://doi.org/10.1016/S0166-526X(07)50011-5.

Arthur, C. L., & Pawliszyn, J. (1990). Solid phase microextraction with thermal desorption using fused silica optical fibers. *Analytical Chemistry*, *62*(19), 2145–2148. https://doi.org/10.1021/ac00218a019.

Audunsson, G. (1986). Aqueous/ Aqueous Extraction by Means of a Liquid Membrane for Sample Cleanup and Preconcentration of Amines in a Flow System. *Analytical Chemistry*, *58*(13), 2714–2723. https://doi.org/10.1021/ac00126a030.

Baltussen, E., Cramers, C. A., & Sandra, P. J. F. (2002). Sorptive sample preparation - A review. *Analytical and Bioanalytical Chemistry*, *373*(1–2), 3–22. https://doi.org/10.1007/s00216-002-1266-2.

Baltussen, E., Sandra, P., David, F., & Cramers, C. (1999). Stir Bar Sorptive Extraction (SBSE), a Novel Extraction Technique for Aqueous Samples: Theory and Principles. *Journal of Microcolumn Separations*, *11*(10), 737–747. https://doi.org/10.1002/(SICI)1520-667X(1999)11:10<737::AID-MCS7>3.0.CO;2-4.

Baltussen, E., Sandra, P., David, F., Janssen, H. G., & Cramers, C. (1999). Study into the equilibrium mechanism between water and poly(dimethylsiloxane) for very apolar solutes: Adsorption or sorption? *Analytical Chemistry*, *71*(22), 5213–5216. https://doi.org/10.1021/ac990313g.

Bao, L., & Dasgupta, P. K. (1992). Membrane Interfaces for Sample Introduction in Capillary Zone Electrophoresis. *Analytical Chemistry*, *64*(9), 991–996. https://doi.org/10.1021/ac00033a006.

Barden, D., & Lara, K. (2017). Flavour Profiling of Beverages Using Probe Based Sorptive Extraction and Thermal Desorption-GC-MS.

Bavumiragira, J. P., Ge, J., & Yin, H. (2022). Fate and transport of pharmaceuticals in water systems: A processes review. *Science of the Total Environment*, *823*. Elsevier B.V. https://doi.org/10.1016/j.scitotenv.2022.153635.

Berrueta, L. A., Gallo, B., & Vicente, F. (1995). A Review of Solid Phase Extraction: Basic Principles and New Developments. *Chromatographia*, *40*(7), 474–483. https://doi.org/10.1007/BF02269916.

Bicchi, C., Cordero, C., Liberto, E., Rubiolo, P., Sgorbini, B., David, F., & Sandra, P. (2005). Dual-phase twisters: A new approach to headspace sorptive extraction and stir bar sorptive extraction. *Journal of Chromatography A*, *1094*(1–2), 9–16. https://doi.org/10.1016/j.chroma.2005.07.099.

Bicchi, C., Iori, C., Rubiolo, P., & Sandra, P. (2002). Headspace sorptive extraction (HSSE), stir bar sorptive extraction (SBSE), and solid phase microextraction (SPME) applied to the analysis of roasted Arabica coffee and coffee brew. *Journal of Agricultural and Food Chemistry*, *50*(3), 449–459. https://doi.org/10.1021/jf010877x.

Bovijn, L., Pirotte, J., & Berger, A. (1958). Determination of hydrogen in water by means of gas chromatography. *Gas Chromatography*.

Brown, R. W., Mayser, J. P., Widdowson, C., Chadwick, D. R., & Jones, D. L. (2021). Dependence of thermal desorption method for profiling volatile organic compound (VOC) emissions from soil. *Soil Biology and Biochemistry*. https://doi.org/10.1016/j.soilbio.2021.108313.

Brunton, N. P., Cronin, D. A., & Monahan, F. J. (2001). The effects of temperature and pressure on the performance of Carboxen/PDMS fibres during solid phase microextraction (SPME) of headspace volatiles from cooked and raw turkey breast. *Flavour and Fragrance Journal*, *16*(4), 294–302. https://doi.org/10.1002/ffj.1000.

Buchholz, K. D., & Pawliszyn, J. (1994). Optimization of solid-phase mixroextraction conditions for determination of phenols. *Analytical Chemistry*, *66*(1), 160–167. https://doi.org/10.1021/ac00073a027.

Camel, V. (2003). Solid-phase extraction. *Comprehensive Analytical Chemistry*, *41*, 393–457. https://doi.org/10.1016/S0166-526X(03)41014-3.

Camino-Sánchez, F. J., Rodríguez-Gómez, R., Zafra-Gómez, A., Santos-Fandila, A., & Vílchez, J. L. (2014). Stir bar sorptive extraction: Recent applications, limitations and future trends. *Talanta*, *130*, 388–399. Elsevier B.V. https://doi.org/10.1016/j.talanta.2014.07.022.

Cantwell, A. F., Nernst, F. F., Lewis, W., Whitman, W. K., Cussler, W. G., & Danckwerts, E. L. (1996). Diffusion: Mass Transfer in Fluid Systems. In *Higbie, R. Trans. AIChE* (Vol. 68, Issue 2). Cambridge University Press.

Cantwell, F. F., & Losier, M. (2002). Liquid-liquid extraction. *Comprehensive Analytical Chemistry*, *37*, 297–340. https://doi.org/10.1016/S0166-526X(02)80048-4.

Capetti, F., Rubiolo, P., Bicchi, C., Marengo, A., Sgorbini, B., & Cagliero, C. (2020). Exploiting the versatility of vacuum-assisted headspace solid-phase microextraction in combination with the selectivity of ionic liquid-based GC stationary phases to discriminate Boswellia spp. resins through their volatile and semivolatile fractions. *Journal of Separation Science*, *43*(9–10), 1879–1889. https://doi.org/10.1002/jssc.202000084.

Carasek, E., Cudjoe, E., & Pawliszyn, J. (2007). Fast and sensitive method to determine chloroanisoles in cork using an internally cooled solid-phase microextraction fiber. *Journal of Chromatography A*, *1138*(1–2), 10–17. https://doi.org/10.1016/j.chroma.2006.10.092.

Chaves, A. R., Silva, S. M., Queiroz, R. H. C., Lanças, F. M., & Queiroz, M. E. C. (2007). Stir bar sorptive extraction and liquid chromatography with UV detection for determination of antidepressants in plasma samples. *Journal of Chromatography B: Analytical Technologies in the Biomedical and Life Sciences*, *850*(1–2), 295–302. https://doi.org/10.1016/j.jchromb.2006.11.042.

Cheng, Z., Mannion, D. T., O'sullivan, M. G., Miao, S., Kerry, J. P., & Kilcawley, K. N. (2021). Comparison of automated extraction techniques for volatile analysis of whole milk powder. *Foods*, *10*(9). https://doi.org/10.3390/foods10092061.

Chester, T. L., Pinkston, J. D., & Raynie, D. E. (1994). Supercritical fluid chromatography and extraction. *Analytical Chemistry*, *66*(12), 106–130. https://doi.org/10.1021/ac00084a006.

Craig, L. C., & Craig, D. (1956). *Techniques of Organic Chemistry: Vol. III* (A. Weissberger, Ed.; 2nd ed.). Interscience Publishers. https://doi.org/10.1007/978-94-011-0599-6_1.

Dabrowska, D., Kot-Wasik, A., & Namieśnik, J. (2005). Pathways and analytical tools in degradation studies of organic pollutants. *Critical Reviews in Analytical Chemistry*, *35 (2)*, 155–176. https://doi.org/10.1080/10408340500207565.

Darrouzès, J., Bueno, M., Pécheyran, C., Holeman, M., & Potin-Gautier, M. (2005). New approach of solid-phase microextraction improving the extraction yield of butyl and phenyltin compounds by combining the effects of pressure and type of agitation. *Journal of Chromatography A*, *1072*(1), 19–27. https://doi.org/10.1016/j.chroma.2005.02.026.

David, F., & Sandra, P. (2007). Stir bar sorptive extraction for trace analysis. *Journal of Chromatography A*, *1152(1–2)*, 54–69. https://doi.org/10.1016/j.chroma.2007.01.032.

Dean, J. (1998). *Extraction Methods for Environmental Analysis*. John Wiley.

Delbecque, N., Mascrez, S., Psillakis, E., & Purcaro, G. (2022). Sub-ambient temperature sampling of fish volatiles using vacuum-assisted headspace solid phase microextraction: Theoretical considerations and proof of concept. *Analytica Chimica Acta*, *1192*. https://doi.org/10.1016/j.aca.2021.339365.

Dewil, R., Mantzavinos, D., Poulios, I., & Rodrigo, M. A. (2017). New perspectives for Advanced Oxidation Processes. *Journal of Environmental Management*, *195*, 93–99. Academic Press. https://doi.org/10.1016/j.jenvman.2017.04.010.

Dugheri, S., Mucci, N., Bonari, A., Marrubini, G., Cappelli, G., Ubiali, D., Campagna, M., Montalti, M., & Arcangeli, G. (2020). Solid phase microextraction techniques used for gas chromatography: A review. *Acta Chromatographica*, *32(1)*. Akademiai Kiado Rt. https://doi.org/10.1556/1326.2018.00579.

Dugheri, S., Mucci, N., Cappelli, G., Trevisani, L., Bonari, A., Bucaletti, E., Squillaci, D., & Arcangeli, G. (2022). Advanced Solid-Phase Microextraction Techniques and Related Automation: A Review of Commercially Available Technologies. *Journal of Analytical Methods in Chemistry*, *2022*. Hindawi Limited. https://doi.org/10.1155/2022/8690569.

Eggermont, D., Mascrez, S., & Purcaro, G. (2022, February). HISORB-GCxGC-QMS A POWERFUL MARRIAGE TO EXPLORE BREWED COFFEE VOLATILES. *Multidimensional Chromatography Workshop*. https://hdl.handle.net/2268/268099.

Eisert, R., & Levsen, K. (1995). Determination of organophosphorus, triazine and 2,6-dinitroaniline pesticides in aqueous samples via solid-phase microextraction (SPME) and gas chromatography with nitrogen-phosphorus detection. *Fresenius' Journal of Analytical Chemistry*, *351*(6), 555–562. https://doi.org/10.1007/BF00322732.

Fattahi, N., Samadi, S., Assadi, Y., & Hosseini, M. R. M. (2007). Solid-phase extraction combined with dispersive liquid-liquid microextraction-ultra preconcentration of chlorophenols in aqueous samples. *Journal of Chromatography A*, *1169*(1–2), 63–69. https://doi.org/10.1016/j.chroma.2007.09.002.

Florêncio Nogueira, J. M. (2017). Stir Bar Sorptive Extraction. *Comprehensive Analytical Chemistry*, *76*, 463–481. https://doi.org/10.1016/bs.coac.2017.01.006.

Fontanals, N., Marcé, R. M., & Borrull, F. (2007). New materials in sorptive extraction techniques for polar compounds. *Journal of Chromatography A*, *1152*(1–2), 14–31. https://doi.org/10.1016/j.chroma.2006.11.077.

Franc, C., David, F., & de Revel, G. (2009). Multi-residue off-flavour profiling in wine using stir bar sorptive extraction-thermal desorption-gas chromatography-mass spectrometry. *Journal of Chromatography A*, *1216*(15), 3318–3327. https://doi.org/10.1016/j.chroma.2009.01.103.

Gjelstad A., Rasmussen K.E., Parmer M.P., Pedersen-Bjergaard S. (2013). Parallel artificial liquid membrane extraction: micro-scale liquid-liquid-liquid extraction in the 96-well format. *Bioanalysis, 5(11),* 1377-1385. https://doi: 10.4155/bio.13.59. PMID: 23742307.

Glykioti, M. L., Yiantzi, E., & Psillakis, E. (2016). Room temperature determination of earthy-musty odor compounds in water using vacuum-assisted headspace solid-

phase microextraction. *Analytical Methods*, *8*(45), 8065–8071. https://doi.org/10.1039/C6AY02210C.

Gmurek, M., Olak-Kucharczyk, M., & Ledakowicz, S. (2017). Photochemical decomposition of endocrine disrupting compounds - A review. *Chemical Engineering Journal*, *310*, 437–456. https://doi.org/10.1016/j.cej.2016.05.014.

Gorecki, T., Khaled, A., & Pawliszyn, J. (1998). The effect of sample volume on quantitative analysis by solid phase microextraction Part 2 Experimental verification. *Analyst*, *123*(12), 2819–2824. https://doi.org/10.1039/A806788K.

Górecki, T., Yu, X., & Pawliszyn, J. (1999). Theory of analyte extraction by selected porous polymer SPME fibres †. *Analyst*, *124*(5), 643–649. https://doi.org/10.1039/A808487D.

Gothwal, R., & Shashidhar, T. (2015). Antibiotic Pollution in the Environment: A Review. *Clean - Soil, Air, Water*, *43(4)*, 479–489. Wiley-VCH Verlag. https://doi.org/10.1002/clen.201300989.

Guan, W., Wang, Y., Xu, F., & Guan, Y. (2008). Poly(phthalazine ether sulfone ketone) as novel stationary phase for stir bar sorptive extraction of organochlorine compounds and organophosphorus pesticides. *Journal of Chromatography A*, *1177*(1), 28–35. https://doi.org/10.1016/j.chroma.2007.10.077.

Handley, A. , Ed. (1999). *Extraction Methods in Organic Analysis*. Sheffield Academic Press. https://doi.org/10.1021/ja995767+.

Hawthorne, S. B. (1990). Analytical-Scale Supercritical Fluid Extraction. *Analytical Chemistry*, *62*(11), 633A-642A. https://doi.org/10.1021/ac00210a001.

He, C., Long, Y., Pan, J., Li, K., & Liu, F. (2007). Application of molecularly imprinted polymers to solid-phase extraction of analytes from real samples. *Journal of Biochemicals and Biophysical Methods*, *70*(2), 133–150. https://doi.org/10.1016/j.jbbm.2006.07.005.

He, Y., & Lee, H. K. (1997). *Liquid-Phase Microextraction in a Single Drop of Organic Solvent by Using a Conventional Microsyringe*. https://doi.org/10.1021/ac970242q.

Holt, M. S. (2000). Sources of Chemical Contaminants and Routes into the Freshwater Environment. *Food and Chemical Toxicology*, *38*, S21–S27. https://doi.org/10.1016/S0278-6915(99)00136-2.

Horng, J. Y., & Huang, S. D. (1994). Determination of the semi-volatile compounds nitrobenzene, isophorone, 2, 4-dinitrotoluene and 2, 6-dinitrotoluene in water using

solid-phase microextraction with a polydimethylsiloxane-coated fibre. *Journal of Chromatography A, 678*(2), 313–318. https://doi.org/10.1016/0021-9673(94)80478-8.

Huang, C., Seip, K. F., Gjelstad, A., & Pedersen-Bjergaard, S. (2015). Electromembrane extraction for pharmaceutical and biomedical analysis - Quo vadis. *Journal of Pharmaceutical and Biomedical Analysis*, *113*, 97–107. https://doi.org/10.1016/j.jpba.2015.01.038.

Hyotylainen, T. (2007). Principles, developments and applications of on-line coupling of extraction with chromatography. *Journal of Chromatography A*, *1153*(1–2), 14–28. https://doi.org/10.1016/j.chroma.2006.11.102.

Irving, H., & Williams, R. J. P. (1961). *Treatise on Analytical Chemistry* (I. M. Kolthoff & P. J. Elving, Eds.; Vol. 3). Interscience Publishers.

Jeannot, M. A., & Cantwell, F. F. (1996). Solvent microextraction into a single drop. *Analytical Chemistry*, *68*(2), 2236–2240. https://doi.org/10.1021/ac960042z.

Jeannot, M. A., Przyjazny, A., & Kokosa, J. M. (2010). Single drop microextraction-Development, applications and future trends. In *Journal of Chromatography A* (Vol. 1217, Issue 16, pp. 2326–2336). https://doi.org/10.1016/j.chroma.2009.10.089.

Jonsson, A., & Mathiasson, L. (2000). Membrane-based techniques for sample enrichment. *Journal of Chromatography A*, *902*(1), 205–225. https://doi.org/10.1016/S0021-9673(00)00922-5.

Jonsson, J. A., & Mathiasson, A. (2001). Membrane extraction in analytical chemistry. *Journal of Separation Science*, *24*(7), 495–507. https://doi.org/10.1002/1615-9314(20010801)24:7<495::AID-JSSC495>3.0.CO;2-B.

Jonsson, J. A., & Mathiasson, L. (1999). Liquid membrane extraction in analytical sample preparation: II. Applications. *TrAC Trends in Analytical Chemistry*, *18*(5), 325–334. https://doi.org/10.1016/S0165-9936(99)00103-X.

Jonsson, J. A., & Mathiasson, L. (2000). Membrane-based techniques for sample enrichment. *Journal of Chromatography A*, *902*(1), 205–225. https://doi.org/10.1016/S0021-9673(00)00922-5.

Kailasa, S. K., Koduru, J. R., Park, T. J., Singhal, R. K., & Wu, H. F. (2021). Applications of single-drop microextraction in analytical chemistry: A review. In *Trends in Environmental Analytical Chemistry* (Vol. 29). Elsevier B.V. https://doi.org/10.1016/j.teac.2020.e00113.

Kelly, L., & Barden, D. (2018). Sampling Volatiles From Fragranced Consumer Products Using High-Capacity Sorptive Extraction. *The Column*, *14*(1), 14–19.

Kenessov, B., Derbissalin, M., Koziel, J. A., & Kosyakov, D. S. (2019). Modeling solid-phase microextraction of volatile organic compounds by porous coatings using finite element analysis. *Analytica Chimica Acta*, *1076*, 73–81. https://doi.org/10.1016/j.aca.2019.05.042.

Khalili Zanjani, M. R., Yamini, Y., Shariati, S., & Jönsson, J. Å. (2007). A new liquid-phase microextraction method based on solidification of floating organic drop. *Analytica Chimica Acta*, *585*(2), 286–293. https://doi.org/10.1016/j.aca.2006.12.049.

Kokosa, J. M., Przyjazny, A., & Jeannot, M. (2009). *Solvent microextraction: theory and practice*. John Wiley & Sons.

Kolb, B., & Ettre, L. S. (2006). *Static headspace-gas chromatography: theory and practice*. John Wiley & Sons.

Kourounioti, E., Psillakis, E., & Vione, D. (2019). UV-induced transformation of 2,3-dibromo-5,6-dimethyl-1,4-benzoquinone in water and treated wastewater. *Environmental Research*, *175*, 343–350. https://doi.org/10.1016/j.envres.2019.05.018.

Kremser, A., Jochmann, M. A., & Schmidt, T. C. (2016). Systematic comparison of static and dynamic headspace sampling techniques for gas chromatography. *Analytical and Bioanalytical Chemistry*, *408*(24), 6567–6579. https://doi.org/10.1007/s00216-016-9843-y.

Lambert, J. P., Mullett, W. M., Kwong, E., & Lubda, D. (2005). Stir bar sorptive extraction based on restricted access material for the direct extraction of caffeine and metabolites in biological fluids. *Journal of Chromatography A*, *1075*(1–2), 43–49. https://doi.org/10.1016/j.chroma.2005.03.119.

Lee, C. K., Chao, H. P., & Lee, J. F. (2004). Effects of organic solutes properties on the volatilization processes from water solutions. *Water Research*, *38*(2), 365–374. https://doi.org/10.1016/j.watres.2003.10.009.

León, V. M., Álvarez, B., Cobollo, M. A., Muñoz, S., & Valor, I. (2003). Analysis of 35 priority semivolatile compounds in water by stir bar sorptive extraction-thermal desorption-gas chromatography-mass spectrometry: I. Method optimisation. *Journal of Chromatography A*, *999*(1–2), 91–101. https://doi.org/10.1016/S0021-9673(03)00600-9.

Lewis, M. J. (1990). *Physical properties of foods and food processing systems*.Elsevier.

Liská, I. (2000). Fifty years of solid-phase extraction in water analysis-historical development and overview. *Journal of Chromatography A*, *885*(1–2), 3–16. https://doi.org/10.1016/S0021-9673(99)01144-9.

Liss, P. S., & Slater, P. G. (1974). Flux of gases across the air-sea interface. *Nature*, *247*(5438), 181–184. https://doi.org/10.1038/247181a0.

Liu, B., & Liu, X. (2004). Direct photolysis of estrogens in aqueous solutions. *Science of the Total Environment*, *320*(2–3), 269–274. https://doi.org/10.1016/j.scitotenv.2003.08.005.

Liu, H., & Dasgupta, P. K. (1996). Analytical Chemistry in a Drop. Solvent Extraction in a Microdrop. *Analytical Chemistry*, *68*(11), 1817–1821. https://doi.org/10.1021/ac960145h.

Liu, J., Zhang, C., Lei, Y., Gao, Q., & Li, Y. (2011). Determination of estrogenic hormones in water samples using high performance liquid chromatography combined with dispersive liquid-liquid micro-extraction method based on solidification of floating organic drop and pre-column derivatization. *Fresenius Environmental Bulletin*, *20*(4a), 1075–1083.

Liu, W., Hu, Y., Zhao, J., Xu, Y., & Guan, Y. (2005). Determination of organophosphorus pesticides in cucumber and potato by stir bar sorptive extraction. *Journal of Chromatography A*, *1095*(1–2), 1–7. https://doi.org/10.1016/j.chroma.2005.07.107.

Liu, W., Wang, H., & Guan, Y. (2004). Preparation of stir bars for sorptive extraction using sol-gel technology. *Journal of Chromatography A*, *1045*(1–2), 15–22. https://doi.org/10.1016/j.chroma.2004.06.036.

Lord, H., & Pawliszyn, J. (2000). Evolution of solid-phase microextraction technology. *Journal of Chromatography A*, *885*(1–2), 153–193. https://doi.org/10.1016/S0021-9673(00)00535-5.

Louch, D., Motlagh, S., & Pawliszyn, J. (1992). Dynamics of organic compound extraction from water using liquid-coated fused silica fibers. *Analytical Chemistry*, *64*(10), 1187–1199. https://doi.org/10.1021/ac00034a020.

Luo, S., Wei, Z., Spinney, R., Zhang, Z., Dionysiou, D. D., Gao, L., & Xiao, R. (2018). UV direct photolysis of sulfamethoxazole and ibuprofen: an experimental and modelling study. *Journal of Hazardous Materials*, *343*, 132–139. https://doi.org/10.1016/j.jhazmat.2017.09.019.

Ma, M., & Cantwell, F. F. (1998). Solvent Microextraction with Simultaneous Back-Extraction for Sample Cleanup and Preconcentration: Quantitative Extraction. *Analytical Chemistry*, *70*(18), 3912–3919. https://doi.org/10.1021/ac980174n.

Ma, M., & Cantwell, F. F. (1999). Solvent microextraction with simultaneous back-extraction for sample cleanup and preconcentration: Preconcentration into a single microdrop. *Analytical Chemistry*, *71*(2), 388–393. https://doi.org/10.1021/ac9805899.

Mackay, D., & Wolkoff, A. W. (1973). Rate of evaporation of low-solubility contaminants from water bodies to atmosphere. *Environmental Science & Technology*, *7*(7), 611–614. https://doi.org/10.1021/es60079a001.

Malik, A. K., Kaur, V., & Verma, N. (2006). A review on solid phase microextraction - High performance liquid chromatography as a novel tool for the analysis of toxic metal ions. *Talanta*, *68*(3), 842–849. https://doi.org/10.1016/j.talanta.2005.06.005.

MARKES International. (n.d.). *HiSorb Sorptive Extraction - Rapid, versatile analysis of VOCs & SVOCs in liquids and solids by TD-GC-MS*. https://markes.com/media/frfj4ptp/hisorb-sorptive-extraction-brochure.pdf.

Mascrez, S., Psillakis, E., & Purcaro, G. (2020). A multifaceted investigation on the effect of vacuum on the headspace solid-phase microextraction of extra-virgin olive oil. *Analytica Chimica Acta*, *1103*, 106–114. https://doi.org/10.1016/j.aca.2019.12.053.

Melo, L. P., Nogueira, A. M., Lanças, F. M., & Queiroz, M. E. C. (2009). Polydimethylsiloxane/polypyrrole stir bar sorptive extraction and liquid chromatography (SBSE/LC-UV) analysis of antidepressants in plasma samples. *Analytica Chimica Acta*, *633*(1), 57–64. https://doi.org/10.1016/j.aca.2008.11.042.

Mihas, O., Kalogerakis, N., & Psillakis, E. (2007). Photolysis of 2,4-dinitrotoluene in various water solutions: effect of dissolved species. *Journal of Hazardous Materials*, *146*(3), 535–539. https://doi.org/10.1016/j.jhazmat.2007.04.054.

Miró, M., & Frenzel, W. (2004). Automated membrane-based sampling and sample preparation exploiting flow-injection analysis. *TrAC - Trends in Analytical Chemistry*, *23*(9), 624–636. https://doi.org/10.1016/j.trac.2004.07.006.

Noble, R. D., & Stern, S. A. (1995). *Membrane separations technology: principles and applications*. Elsevier.

Nogueira, J. M. F. (2012). Novel sorption-based methodologies for static microextraction analysis: A review on SBSE and related techniques. In *Analytica Chimica Acta* (Vol. 757, pp. 1–10). https://doi.org/10.1016/j.aca.2012.10.033.

Nogueira, J. M. F. (2015). Stir-bar sorptive extraction: 15 years making sample preparation more environment-friendly. *TrAC - Trends in Analytical Chemistry*, *71*, 214–223. https://doi.org/10.1016/j.trac.2015.05.002.

Ocaña-González, J. A., Fernández-Torres, R., Bello-López, M. Á., & Ramos-Payán, M. (2016). New developments in microextraction techniques in bioanalysis. A review. *Analytica Chimica Acta*, *905*, 8–23. https://doi.org/10.1016/j.aca.2015.10.041.

Ochiai, N., Sasamoto, K., Kanda, H., & Nakamura, S. (2006). Fast screening of pesticide multiresidues in aqueous samples by dual stir bar sorptive extraction-thermal desorption-low thermal mass gas chromatography-mass spectrometry. *Journal of Chromatography A*, *1130*(1 SPEC. ISS.), 83–90. https://doi.org/10.1016/j.chroma.2006.06.032.

Ochiai, N., Sasamoto, K., Takino, M., Yamashita, S., Daishima, S., Heiden, A. C., & Hoffmann, A. (2002). Simultaneous determination of preservatives in beverages, vinegar, aqueous sauces, and quasi-drug drinks by stir-bar sorptive extraction (SBSE) and thermal desorption gc-MS. *Analytical and Bioanalytical Chemistry*, *373*(1–2), 56–63. https://doi.org/10.1007/s00216-002-1257-3.

Orazbayeva, D., Kenessov, B., & Zhakupbekova, A. (2018). Quantification of transformation products of unsymmetrical dimethylhydrazine in aqueous extracts from soil based on vacuum-assisted headspace solid-phase microextraction. *Chemical Bulletin of Kazakh National University*, *2*, 4–11. https://doi.org/10.15328/cb1014.

Oturan, M. A., & Aaron, J. J. (2014). Advanced oxidation processes in water/wastewater treatment: Principles and applications. A review. *Critical Reviews in Environmental Science and Technology*, *44(23)*, 2577–2641. https://doi.org/10.1080/10643389.2013.829765.

Page, B. D., & Lacroix, G. (1993). Application of solid-phase microextraction to the headspace gas chromatographic analysis of halogenated volatiles in selected foods. *Journal of Chromatography A*, *648*(1), 199–211. https://doi.org/10.1016/0021-9673(93)83303-A.

Paiva, A. C., Crucello, J., de Aguiar Porto, N., & Hantao, L. W. (2021). Fundamentals of and recent advances in sorbent-based headspace extractions. *TrAC - Trends in Analytical Chemistry*, *139*. Elsevier B.V. https://doi.org/10.1016/j.trac.2021.116252.

Parsons, S. (2004). *Advanced oxidation processes for water and wastewater treatment*. IWA publishing. https://doi.org/10.2166/9781780403076.

Pawliszyn, J. (1993). Kinetic model of supercritical fluid extraction. *Journal of Chromatographic Science*, *31*(1), 31–37. https://doi.org/10.1093/chromsci/31.1.31.

Pawliszyn, J. (1997). *Solid phase microextraction: theory and practice*. John Wiley & Sons.

Pawliszyn, J. (2003). Sample preparation: Quo vadis?. *Analytical Chemistry*, *75*(11), 2543–2558. https://doi.org/10.1021/ac034094h.

Pawliszyn, J. (2011). *Handbook of solid phase microextraction*. Elsevier. https://doi.org/10.1016/C2011-0-04297-7.

Pawliszyn, J., & Pedersen-Bjergaard, S. (2006). Analytical microextraction: current status and future trends. *Journal of Chromatographic Science*, *44*(6), 291–307. https://doi.org/10.1093/chromsci/44.6.291.

Pedersen-Bjergaard, S., Huang, C., Gjelstad, A. (2017). Electromembrane extraction–Recent trends and where to go. *Journal of Pharmaceutical Analysis, 7(3),* 141-147. https://doi.org/10.1016/j.jpha.2017.04.002.

Pedersen-Bjergaard, S., Rasmussen K. E. (2006). Electrokinetic migration across artificial liquid membranes: New concept for rapid sample preparation of biological fluids. *Journal of Chromatography A, 1109(2),* 183-190. https://doi.org/10.1016/j.chroma.2006.01.025.

Pena-Pereira, F., Lavilla, I., & Bendicho, C. (2009). Miniaturized preconcentration methods based on liquid-liquid extraction and their application in inorganic ultratrace analysis and speciation: A review. *Spectrochimica Acta - Part B Atomic Spectroscopy*, *64(1),* 1–15. https://doi.org/10.1016/j.sab.2008.10.042.

Petersen, N.J., Jensen, H., Hansen, S. H., Foss, S. T., Snakenborg, D. & Pedersen-Bjergaard, S. (2010). On-chip electro membrane extraction. *Microfluid Nanofluid, 9,* 881-888. https://doi.org/10.1007/s10404-010-0603-6.

Pichon, V. (2000). Solid-phase extraction for multiresidue analysis of organic contaminants in water. *Journal of Chromatography A, 885*(1–2), 195–215. https://doi.org/10.1016/S0021-9673(00)00456-8.

Popp, P., Keil, P., Montero, L., & Rückert, M. (2005). Optimized method for the determination of 25 polychlorinated biphenyls in water samples using stir bar sorptive extraction followed by thermodesorption-gas chromatography/mass spectrometry. *Journal of Chromatography A, 1071*(1–2), 155–162. https://doi.org/10.1016/j.chroma.2005.01.066.

Potter, D. W., & Pawliszyn, J. (1992). Detection of substituted benzenes in water at the pg/ml level using solid-phase microextraction and gas chromatography-ion trap mass spectrometry. *Journal of Chromatography A, 625*(2), 244–257. https://doi.org/10.1016/0021-9673(92)85209-C.

Pratt, K. F., & Pawliszyn, J. (1992). Gas extraction kinetics of volatile organic species from water with a hollow fiber membrane. *Analytical Chemistry*, *64*(18), 2101–2106.

Prieto, A., Basauri, O., Rodil, R., Usobiaga, A., Fernández, L. A., Etxebarria, N., & Zuloaga, O. (2010). Stir-bar sorptive extraction: A view on method optimisation, novel applications, limitations and potential solutions. *Journal of Chromatography A*, *1217(16)*, 2642–2666. https://doi.org/10.1016/j.chroma.2009.12.051.

Psillakis, E. (2020). *The effect of vacuum: an emerging experimental parameter to consider during headspace microextraction sampling*. https://doi.org/10.1007/s00216-020-02738-x.

Psillakis, E. (2017). Vacuum-assisted headspace solid-phase microextraction: A tutorial review. *Analytica Chimica Acta*, *986*, 12–24. Elsevier B.V. https://doi.org/10.1016/j.aca.2017.06.033.

Psillakis, E., Koutela, N., & Colussi, A. J. (2019). Vacuum-assisted headspace single-drop microextraction: Eliminating interfacial gas-phase limitations. *Analytica Chimica Acta*, *1092*, 9–16. https://doi.org/10.1016/j.aca.2019.09.056.

Psillakis, E., Mousouraki, A., Yiantzi, E., & Kalogerakis, N. (2012). Effect of Henry's law constant and operating parameters on vacuum-assisted headspace solid phase microextraction. *Journal of Chromatography A*, *1244*, 55–60. https://doi.org/10.1016/j.chroma.2012.05.006.

Psillakis, E., Yiantzi, E., Sanchez-Prado, L., & Kalogerakis, N. (2012). Vacuum-assisted headspace solid phase microextraction: Improved extraction of semivolatiles by non-equilibrium headspace sampling under reduced pressure conditions. *Analytica Chimica Acta*, *742*, 30–36. https://doi.org/10.1016/j.aca.2012.01.019.

Qin, Z., Bragg, L., Ouyang, G., & Pawliszyn, J. (2008). Comparison of thin-film microextraction and stir bar sorptive extraction for the analysis of polycyclic aromatic hydrocarbons in aqueous samples with controlled agitation conditions. *Journal of Chromatography A*, *1196–1197*(1–2), 89–95. https://doi.org/10.1016/j.chroma.2008.03.063.

Quintana, J. B., Rodil, R., Muniategui-Lorenzo, S., López-Mahía, P., & Prada-Rodríguez, D. (2007). Multiresidue analysis of acidic and polar organic contaminants in water samples by stir-bar sorptive extraction-liquid desorption-gas chromatography-mass spectrometry. *Journal of Chromatography A*, *1174*(1–2), 27–39. https://doi.org/10.1016/j.chroma.2007.07.088.

Rezaee, M., Assadi, Y., Milani Hosseini, M. R., Aghaee, E., Ahmadi, F., & Berijani, S. (2006). Determination of organic compounds in water using dispersive liquid-liquid

microextraction. *Journal of Chromatography A*, *1116*(1–2), 1–9. https://doi.org/10.1016/j.chroma.2006.03.007.

Ribeiro, A., Neves, M. H., Almeida, M. F., Alves, A., & Santos, L. (2002). Direct determination of chlorophenols in landfill leachates by solid-q phase micro-extraction-gas chromatography-mass spectrometry. *Journal of Chromatography A*, *975*(2), 267–274. https://doi.org/10.1016/S0021-9673(02)01280-3.

Ribeiro, C., Ribeiro, A. R., Maia, A. S., Gonçalves, V. M. F., & Tiritan, M. E. (2014). New Trends in Sample Preparation Techniques for Environmental Analysis. *Critical Reviews in Analytical Chemistry*, *44*(2), 142–185. https://doi.org/10.1080/10408347.2013.833850.

Rivera-Utrilla, J., Sánchez-Polo, M., Ferro-García, M. Á., Prados-Joya, G., & Ocampo-Pérez, R. (2013). Pharmaceuticals as emerging contaminants and their removal from water. A review. *Chemosphere*, *93(7)*, 1268–1287. Elsevier Ltd. https://doi.org/10.1016/j.chemosphere.2013.07.059.

Roberts, G. et. al. (2016). Flavor profiling of milk and premium teas by HiSorb sorptive extraction with thermal desorption GC-MS analysis. *LC-GC North America*, *34*(12), S66.

Rodil, R., & Moeder, M. (2008). Development of a method for the determination of UV filters in water samples using stir bar sorptive extraction and thermal desorption-gas chromatography-mass spectrometry. *Journal of Chromatography A*, *1179*(2), 81–88. https://doi.org/10.1016/j.chroma.2007.11.090.

Schnobrich, C. R., & Jeannot, M. A. (2008). Steady-state kinetic model for headspace solvent microextraction. *Journal of Chromatography A*, *1215*(1–2), 30–36. https://doi.org/10.1016/j.chroma.2008.11.011.

Schoenmakers, P. J. (2012). Editorial on "Critical overview of selected contemporary sample preparation techniques" by L. Ramos. *Journal of Chromatography A*, *1221*, 83. https://doi.org/10.1016/j.chroma.2011.12.026.

Seethapathy, S., & Górecki, T. (2012). Applications of polydimethylsiloxane in analytical chemistry: A review. *Analytica Chimica Acta*, *750*, 48–62. https://doi.org/10.1016/j.aca.2012.05.004.

Serôdio, P., & Nogueira, J. M. F. (2005). Development of a stir-bar-sorptive extraction-liquid desorption-large- volume injection capillary gas chromatographic-mass spectrometric method for pyrethroid pesticides in water samples. *Analytical and Bioanalytical Chemistry*, *382*(4), 1141–1151. https://doi.org/10.1007/s00216-005-3210-8.

Serway, R. A., Moses, C. J., & Moyer, C. A. (2004). *Modern physics*. Cengage Learning.

Smith, J. H., Bomberger, D. C., & Haynes, D. L. (1980). Prediction of the volatilization rates of high-volatility chemicals from natural water bodies. *Environmental Science & Technology*, *14*(11), 1332–1337. https://doi.org/10.1021/es60171a004.

Snow, N. H., & Slack, G. C. (2002). Head-space analysis in modern gas chromatography. *TrAC Trends in Analytical Chemistry*, *21*(9–10), 608–617. https://doi.org/10.1016/s0165-9936(02)00802-6.

Solomou, N., Bicchi, C., Sgorbini, B., & Psillakis, E. (2020). Vacuum-assisted headspace sorptive extraction: Theoretical considerations and proof-of-concept extraction of polycyclic aromatic hydrocarbons from water samples. *Analytica Chimica Acta*, *1096*, 100–107. https://doi.org/10.1016/j.aca.2019.10.050.

Sýkora, M., Vítová, E., & Jeleń, H. H. (2020). Application of vacuum solid-phase microextraction for the analysis of semi-hard cheese volatiles. *European Food Research and Technology*, *246*(3), 573–580. https://doi.org/10.1007/s00217-020-03426-x.

Tamayo, F. G., Turiel, E., & Martín-Esteban, A. (2007). Molecularly imprinted polymers for solid-phase extraction and solid-phase microextraction: Recent developments and future trends. *Journal of Chromatography A*, *1152*(1–2), 32–40. https://doi.org/10.1016/j.chroma.2006.08.095.

Theis, A. L., Waldack, A. J., Hansen, S. M., & Jeannot, M. A. (2001). Headspace solvent microextraction. *Analytical Chemistry*, *73*(23), 5651–5654. https://doi.org/10.1021/ac015569c.

Thurman, E. M., & Mills, M. S. (1998). *Solid-Phase Extraction Principles and Practice*. Wiley and Sons.

Trujillo-Rodríguez, M. J., Pacheco-Fernández, I., Taima-Mancera, I., Díaz, J. H. A., & Pino, V. (2020). Evolution and current advances in sorbent-based microextraction configurations. *Journal of Chromatography A*, *1634*, 461670. https://doi.org/10.1016/j.chroma.2020.461670.

Trujillo-Rodríguez, M. J., Pino, V., & Anderson, J. L. (2017). Magnetic ionic liquids as extraction solvents in vacuum headspace single-drop microextraction. *Talanta*, *172*, 86–94. https://doi.org/10.1016/j.talanta.2017.05.021.

Trujillo-Rodríguez, M. J., Pino, V., Psillakis, E., Anderson, J. L., Ayala, J. H., Yiantzi, E., & Afonso, A. M. (2017). Vacuum-assisted headspace-solid phase microextraction

for determining volatile free fatty acids and phenols. Investigations on the effect of pressure on competitive adsorption phenomena in a multicomponent system. *Analytica Chimica Acta*, *962*, 41–51. https://doi.org/10.1016/j.aca.2017.01.056.

Vakinti, M., Mela, S. M., Fernández, E., & Psillakis, E. (2019). Room temperature and sensitive determination of haloanisoles in wine using vacuum-assisted headspace solid-phase microextraction. *Journal of Chromatography A*, *1602*, 142–149. https://doi.org/10.1016/j.chroma.2019.03.047.

Vállez-Gomis, V., Grau, J., Benedé, J. L., Giokas, D. L., Chisvert, A., & Salvador, A. (2021). Fundamentals and applications of stir bar sorptive dispersive microextraction: A tutorial review. *Analytica Chimica Acta*, *1153*. https://doi.org/10.1016/j.aca.2021.338271.

Vitenberg, A. G., Kostkina, I., & Ioffe, B. v. (1984). Preparation of Standard Vapor-Gas Mixtures for Gas Chromatography: Continuous Gas Extraction. *Trans. Faraday Soc*, *56*(26), 103–111. https://doi.org/10.1021/ac00277a052.

Wardencki, W., Curyło, J., & Namieśnik, J. (2007). Trends in solventless sample preparation techniques for environmental analysis. *Journal of Biochemical and Biophysical Methods*, *70*(2), 275–288. https://doi.org/10.1016/j.jbbm.2006.07.004.

Wu, J., Xie, W., & Pawliszyn, J. (2000). Automated in-tube solid phase microextraction coupled with HPLC-ES-MS for the determination of catechins and caffeine in tea. *Analyst*, *125*(12), 2216–2222. https://doi.org/10.1039/b006211l.

Xia, L., Yang, J., Su, R., Zhou, W., Zhang, Y., Zhong, Y., Huang, S., Chen, Y., & Li, G. (2020). Recent Progress in Fast Sample Preparation Techniques. *Analytical Chemistry*, *92*(1), 34–48. https://doi.org/10.1021/acs.analchem.9b04735.

Yang, Yu., Hawthorne, S. B., & Miller, D. J. (1998). Adsorption versus Absorption of Polychlorinated Biphenyls onto Solid-Phase Microextraction Coatings. *Analytical Chemistry*, *70*, 1866–1869. https://doi.org/10.1021/ac970823f.

Yiantzi, E., Kalogerakis, N., & Psillakis, E. (2015). Vacuum-assisted headspace solid phase microextraction of polycyclic aromatic hydrocarbons in solid samples. *Analytica Chimica Acta*, *890*, 108–116. https://doi.org/10.1016/j.aca.2015.05.047.

Yiantzi, E., Kalogerakis, N., & Psillakis, E. (2016). Design and testing of a new sampler for simplified vacuum-assisted headspace solid-phase microextraction. *Analytica Chimica Acta*, *927*, 46–54. https://doi.org/10.1016/j.aca.2016.05.001.

Yiantzi, E., Murtada, K., Terzidis, K., Pawliszyn, J., & Psillakis, E. (2022). Vacuum-assisted headspace thin-film microextraction: Theoretical formulation and method

optimization for the extraction of polycyclic aromatic hydrocarbons from water samples. *Analytica Chimica Acta*, *1189*. https://doi.org/10.1016/j.aca.2021.339217.

Yu, C., & Hu, B. (2009). Sol-gel polydimethylsiloxane/poly(vinylalcohol)-coated stir bar sorptive extraction of organophosphorus pesticides in honey and their determination by large volume injection GC. *Journal of Separation Science*, *32*(1), 147–153. https://doi.org/10.1002/jssc.200800486.

Zhang, J., & Hu, B. (2013). Liquid-Liquid Extraction (LLE). *Separation and Purification Technologies in Biorefineries*, 61–78. https://doi.org/10.1002/9781118493441.ch3.

Zhang, Z., & Pawliszyn, J. (1993). Headspace Solid-Phase Microextraction. In *Anal. Chem* (Vol. 65). https://doi.org/10.1021/ac00062a008.

Zhang, Z., & Pawliszyn, J. (1995). Quantitative Extraction Using an Internally Cooled Solid Phase Microextraction Device. *J. /. High Resolut. Chromatogr*, *67*(2), 1477–1483. https://doi.org/10.1021/ac00097a007.

Zlatkis, A., Lichtenstein, H. A., & Tishbee, / A. (1973). Concentration and Analysis of Trace Volatile Organics in Gases and Biological Fluids with a New Solid Adsorbent. *Chromatographia*, *6*(2), 67–70. https://doi.org/10.1007/BF02270540.

Zuin, V. G., Montero, L., Bauer, C., & Popp, P. (2005). Stir bar sorptive extraction and high-performance liquid chromatography-fluorescence detection for the determination of polycyclic aromatic hydrocarbons in Mate teas. *Journal of Chromatography A*, *1091*(1–2), 2–10. https://doi.org/10.1016/j.chroma.2005.07.057.

CHAPTER 2: VACUUM-ASSISTED HEADSPACE SORPTIVE EXTRACTION: THEORETICAL CONSIDERATIONS AND PROOF-OF-CONCEPT EXTRACTION OF POLYCYCLIC AROMATIC HYDROCARBONS FROM WATER SAMPLES

Solomou, N., Bicchi, C., Sgorbini, B., & Psillakis, E. (2020). Vacuum-assisted headspace sorptive extraction: Theoretical considerations and proof-of-concept extraction of polycyclic aromatic hydrocarbons from water samples. Analytica Chimica Acta, 1096, 100–107.

Credit author statement

N. Solomou: Investigation. C. Bicchi: Writing. B. Sgorbini: Writing. E. Psillakis: Conceptualization, Writing - Review & Editing, Visualization.

2.1. ABSTRACT

The use of a thick sorbent coating in headspace sorptive extraction (HSSE) increases the amount of analytes extracted at equilibrium as well as the time needed to reach it. In this work we propose HSSE sampling under vacuum conditions to reduce equilibration times. A theoretical model is presented that describes the pressure dependence of the so-called vacuum-assisted HSSE (Vac-HSSE) method, and predicts the reduction in equilibration times when lowering the sampling pressure. We take advantage of the theoretical formulation to reach some general conclusions for HSSE on the relationship between the physical characteristics of the stir bar, uptake rates and equilibration times. The theoretical predictions were experimentally verified using water solutions spiked with naphthalene, acenaphthene and fluoranthene as model compounds. The effects of sampling temperature and extraction time under vacuum and regular pressure conditions were thoroughly investigated. The positive combined effect of heating the sample under low sampling pressure pointed that high humidity did not affect the performance of the extraction phase; an effect commonly recorded in headspace solid-phase microextraction. The extraction time profiles built at 25 and 55^{o}C visualized the substantial improvement in extraction kinetics with Vac-HSSE compared to the regular HSSE method. The results on naphthalene (assumed to evaporate relatively fast from the water sample) provided evidence that at 1 atm gas-sided resistance limited analyte uptake by the stir-bar and that this limitation could be effectively reduced by adopting the vacuum sampling approach. The accelerations of acenaphthene and fluoranthene suggested that gas phase constraints limited both the evaporation and analyte uptake processes. Independent method optimization of HSSE under each pressure condition yielded a shorter sampling time for Vac-HSSE compared to the regular HSSE procedure (30 min vs. 60 min respectively). The analytical performances of the two optimized methods were evaluated and it was concluded that Vac-HSSE was performing similar (naphthalene and acenaphthene) or better (fluoranthene) than regular HSSE in half the sampling time needed.

2.2. INTRODUCTION

Stir bar sorptive extraction (SBSE) was introduced in 1999 as a novel configuration for sorptive sampling (Baltussen et al., 1999). The method used polydimethylsiloxane (PDMS) coated stir bars and consisted of a two-step procedure where target analytes were initially absorbed into the PDMS coating and then desorbed following a liquid or thermal desorption step. The stir bars were marketed under the name Twister™ (Gerstel, Mülheim a/d Ruhr, Germany), and the method was successfully applied to the analysis of organic compounds and elemental speciation in a variety of samples including environmental, food and biological (Camino-Sánchez et al., 2014; David & Sandra, 2007; He et al., 2014; Lucena, 2012; Nogueira, 2015) .

The headspace sampling mode was reported in 2001 by Tienpont et al. (Tienpont et al., 2000) and Bicchi et al. (Bicchi et al., 2000). The procedure was termed headspace sorptive extraction (HSSE), and has mainly been used for studying the headspace composition of flavors and fragrances (Bicchi et al., 2004; He et al., 2014; Prieto et al., 2010). In HSSE, the stir bar was placed in the gas-phase with analytes transferring from the sample to the headspace and then into the sorbent phase. The use of a high PDMS volume as coating for the stir bar resulted in higher extraction capacities and recoveries than those obtained with other PDMS-based methods, e.g. headspace solid-phase microextraction (HS-SPME) using a 100-mm PDMS fiber (Bicchi et al., 2004). At the same time, HSSE needed longer times to reach equilibrium (Nogueira, 2015); an effect also reported for the immersion sampling mode (SBSE) that was related to the thickness of the PDMS coating (Qin et al., 2008). The theoretical principles of HSSE at equilibrium have been discussed at different occasions and were analogous to those applied in HS-SPME (Bicchi et al., 2003, 2005; David & Sandra, 2007; He et al., 2014). Next to these thermodynamic considerations, the kinetic aspects of the extraction process are equally important, especially because HSSE is mainly operated under non-equilibrium conditions. Nonetheless, to the best of our knowledge, a detailed discussion on the theoretical aspects of pre-equilibrium HSSE sampling has not yet been reported (David & Sandra, 2007).

Different approaches are available to accelerate extraction kinetics in headspace sorbent-based methods, including e.g. stirring and/or heating the sample (Bicchi et al., 2003; Prieto et al., 2010). An alternative approach used to improve the extraction rates

of analytes with a low affinity for the headspace, suggests headspace sampling under reduced pressure conditions. The approach was first applied to HS-SPME by Brunton et al. (Brunton et al., 2001) and the effect was later confirmed by Darouzes et al. (Darrouzès et al., 2005). In 2012, Psillakis et al. presented the theoretical model describing the pressure dependence of the so-called vacuum-assisted HSSPME (Vac-HS-SPME) for water (Psillakis, Yiantzi, et al., 2012) and (later) for solid matrices (Yiantzi et al., 2015), and successfully applied the method to a variety of analytes and matrices (Psillakis, 2017; Vakinti et al., 2019; Zhakupbekova et al., 2019). Recently, Trujillo-Rodríguez et al. expanded the applicability of the vacuum-based sampling approach to headspace single drop microextraction and reported shorter equilibration times for short chain free fatty acids (Trujillo-Rodríguez, Pino, & Anderson, 2017). In a subsequent report, Psillakis et al. (Psillakis et al., 2019) formulated the pressure dependence of the analyte evaporation and uptake processes taking place during this procedure.

This study aims to investigate for the first time the applicability of the vacuum sampling approach to HSSE as a viable tool to accelerate extraction kinetics and reduce equilibration times. The resulting procedurewas termed vacuum-assisted HSSE (Vac-HSSE). The theoretical model describing the HSSE pressure dependence under non-equilibrium conditions is here discussed. A comparative study between Vac-HSSE and regular HSSE (under atmospheric pressure) was carried out to demonstrate the benefits of adopting the vacuum approach. The use of three model polycyclic aromatic hydrocarbons (PAHs) as target analytes enabled exploring some new and important insights on HSSE. The effects of temperature and sampling time were thoroughly investigated and discussed under each pressure condition. Finally, the two methods were independently optimized and their analytical performance was assessed and compared.

2.3. THEORETICAL CONSIDERATIONS

During HSSE sampling from water samples, analytes transfer in three phases (water, headspace and PDMS coating) and across two interfaces (water/headspace and headspace/PDMS coating) until equilibrium between the three phases is reached (David & Sandra, 2007). Initially and as soon as the coated stir bar is exposed to the

headspace above the aqueous sample, analyte uptake by the PDMS coating is linear with time. This is followed by a curvilinear region that finally moves to a constant phase, representing equilibrium conditions between all phases involved (Bartkow et al., 2004; Goirecki & Pawliszyn, 1997; Harner et al., 2003). Current knowledge concludes that the amount of analyte extracted at equilibrium is independent on the total pressure in the sample vial, as partition coefficients and equilibrium concentrations are only affected at high operating pressures (Psillakis, 2017; Psillakis, Yiantzi, et al., 2012).

The pre-equilibrium aspects of the HSSE analytical system can be better understood by decoupling the system into two interfacial ones: (i) the evaporation step (water/headspace system), and (ii) the analyte uptake by the PDMS coating of the stir bar (headspace/PDMS system). The theory underlying the kinetics of the evaporation step is similar to that formulated for HS-SPME (Nogueira, 2015; Tienpont et al., 2000), and its pressure dependence has been demonstrated and experimentally verified (Psillakis, 2017; Psillakis, Yiantzi, et al., 2012). For this reason, the theoretical aspects concerning the headspace/PDMS interfacial system are only dealt with here.

The PDMS coating of the stir bar is considered as a single uniform phase. Accordingly, the overall mass transfer coefficient, k_o, controlling analyte uptake can be described using the two-film approach. The approach assumes uniformly mixed liquid and gas bulk phases, separated by two thin films of air and PDMS adjacent to the interface where analyte mass transfer is by molecular diffusion alone (Schwarzenback et al., 2003). The two films are modeled as follows

$$\frac{1}{k_o} = \frac{1}{k_g} + \frac{1}{K_{eg} k_e} \quad (2.1)$$

where K_{eg} is the PDMS/headspace partition coefficient and k_g and k_e are the mass transfer coefficients for the gas- and PDMS-side boundary layers. In Eq. (2.1) the two films are modeled as two resistances in series where the overall resistance to analyte uptake ($1/k_o$) equals the sum of resistances of the gas-phase boundary layer ($1/k_g$) and the PDMS boundary layer ($1/(K_{eg}k_e)$) (Harner et al., 2003; Reyes-Garcés et al., 2018). In general, the net rate of analyte accumulation in the PDMS coating can be represented by the following flux equation (Bartkow et al., 2005; Tuduri et al., 2012).

$$V_e \frac{dC_e}{dt} = k_o A_e (C_g - \frac{C_e}{K_{eg}} \quad (2.2)$$

with t denoting time, V_e the volume of PDMS coating, C_g and C_e the analyte's concentrations in the gas-phase and PDMS respectively, and A_e the surface area of the PDMS coating. During the initial stage of linear uptake by the coated stir bar, C_e is very small and K_{eg} is large, resulting in a small analyte loss from the PDMS coating (C_e/K_{eg} term) (Harner et al., 2003; Tuduri et al., 2012). The change in analyte concentration in the PDMS coating can then be simplified to

$$V_e \frac{dC_e}{dt} = k_o A_e C_g \quad (2.3)$$

Assuming constant values for C_g during this initial stage, then Eq. (2.3) can be integrated and expressed on a mass basis (Bartkow et al., 2004; Harner et al., 2003).

$$N_e = k_o A_e C_g t \quad (2.4)$$

which shows that in the linear region, the amount of extracted analyte, N_e, is directly proportional to the overall mass transfer coefficient and the area of the sampler. The latter relationship suggests that at an early stage of extraction, the large surface area of the PDMS coating will ensure high analyte uptake over time. It also suggests that during this stage, any other PDMS-based configuration having the same surface area with the PDMS coated stir bar will extract the same amount of analytes over time regardless of the coating volume (Bartkow et al., 2004).

As the analyte concentration in the PDMS coating increases, the loss from the PDMS coating becomes more important and uptake will become curvilinear (Tuduri et al., 2012). At equilibrium, the net uptake will approach zero and rearrangement of Eq. (2.2) gives

$$N_{e(eq)} = K_{eg} V_e C_g \quad (2.5)$$

which shows that the final amount of analyte extracted at equilibrium, $N_{e(eq)}$, is directly proportional to the volume of the coating (and independent of A_e).

The complete uptake profile can be described by integrating Eq. (2.2) to yield

$$C_e = K_{eg} C_g \left(1 - e^{-\left(\frac{A_e}{V_e} x \frac{k_e}{K_{eg}} x\, t\right)}\right) \quad (2.6)$$

Eq. (2.6) is a form of a first order reaction where the time taken to attain equilibrium will be influenced by the coating, analyte properties and gas-phase characteristics

(Bartkow et al., 2005). In particular, the time to effective equilibrium, $t_{95\%}$, defined as when reaches 95% of its true equilibrium value can be estimated as

$$t_{95\%} = \frac{3V_e}{A_e k_o} K_{eg} \quad (2.7)$$

From this equation, the relationship between the physical characteristics of the sorbent and the time to equilibrium is now clear: decreasing the surface area to volume ratio of the sorbent coating will increase the time needed to approach equilibrium. This explains the extended equilibration times recorded with SBSE compared to SPME (headspace and direct sampling modes). The 0.5-mm thick and 1-cm long PDMS coating of the stir bar has a 1 cm^2 surface area and a 24 mL coating volume (Qin et al., 2008). These values yield a A_e/V_e ratio that is four times lower than that of a 100-mm thick and 1-cm long PDMS SPME fiber (surface area 0.1 cm^2 and 0.612 mL coating volume (Pawliszyn, 2011)). Hence, when a coated stir bar is used for extraction, the larger PDMS volume will extract a larger amount of analyte at equilibrium, but the time needed to achieve the equilibrium will increase. It is also interesting to consider the case of thin film microextraction (TFME) where thin sheets of PDMS are used for extraction (e.g. the thin film considered in the past with a 5-cm^2 surface area on each side and a 63.5 mL volume (Qin et al., 2008)). In this configuration, the PDMS volume is increased compared to the conventional SPME fiber and coated stir bar approaches. However, the maximization of the surface area when using a thin PDMS sheet yields a surface area to volume ratio that is comparable to that in SPME and close to four times larger than that in SBSE. For this reason, equilibration times recorded with TFME should (and were found to) be similar to those with SPME (Bruheim et al., 2003), and shorter than those recorded with SBSE (headspace and direct sampling modes) (Qin et al., 2008).

According to Eq. (2.1), K_{eg} is an important parameter to consider for predicting the gas- or PDMS-sided limitations on uptake for a given analyte. For nonpolar organics, K_{eg} was assumed to be similar in magnitude to the octanol-air partition coefficient (K_{OA}) (Harner et al., 2003). In particular, past reports discussing the theoretical aspects of passive air sampling suggested gas-sided limitations during uptake of semivolatiles such as polycyclic aromatic hydrocarbons (PAHs) and polychlorinated biphenyls (Bartkow et al., 2005; Harner et al., 2003), as for these analytes K_{OA} values were sufficiently large (K_{OA} > 106) to yield a negligible PDMS-sided resistance (i.e. the

$1/(K_{eg}\ k_e)$ term in Eq. (2.1)) (Harner et al., 2003). This implies that for gas-side limited analytes (where $k_o = k_g$) changes in the value of k_g will induce changes in the uptake rates throughout the preequilibrium stage (Eqs. (2.2), (2.4) and (2.6)) and as such in the equilibration times (Eq. (2.7)). Conversely, for analytes with a small K_{eg}, extraction will be limited by diffusion in the PDMS phase (the $1/ (K_{eg}\ k_e)$ term in Eq. (2.1) dominates) and any changes in k_g will not affect uptake rates by the PDMS. It is reminded however, that analytes with small K_{eg} value will not have a high affinity for the extracting phase, and that the use of PDMS coated stir bar might not be a sensitive tool for their detection and quantification.

In general, k_g is proportional to the diffusion coefficient in air (D_g) raised to some power, the value of which depends on the model assumed (Psillakis, Yiantzi, et al., 2012). Among the different representations used for expressing D_g, the Fuller-Schettler-Giddings diffusivity correlation for binary mixtures of gases at low pressures shows that the value of D_g is inversely proportional to the total pressure in the gas phase (Psillakis, Yiantzi, et al., 2012). This implies that reducing the total pressure will increase D_g and consequently kg, leading to a reduced gas-sided resistance (expressed as $1/k_g$ in Eq. (2.1)). Accordingly, for analytes where gas phase resistance controls analyte uptake (i.e. $k_o = k_g$), applying a low sampling pressure will accelerate the extraction kinetics during both the linear and curvilinear stages of the process. Moreover, Eq. (2.7) shows that for these analytes any enhancements in k_g upon lowering the sampling pressure will also induce improvements in $t_{95\%}$, leading to shorter equilibration times between the headspace and the PDMS phases.

The following general conclusions can be reached by combining the theoretical aspects of the evaporation step (as discussed in Refs. (Psillakis, 2017; Psillakis, Yiantzi, et al., 2012)) and those applied during analyte uptake by the PDMS coated stir bar (as discussed here): (i) for analytes where gas-phase resistance controls analyte uptake (headspace/PDMS system) and/ or evaporation (water/headspace system), reducing the sampling pressure will accelerate mass transfer in the thin gas film involved and reduce equilibration times, compared to atmospheric pressure, (ii) for analytes where liquid-sided resistance controls the step(s) of analyte uptake (headspace/PDMS system) and/or evaporation (water/headspace system), reducing the sampling pressure will not affect the extraction kinetics (and as such the equilibration times) of the step(s) compared to standard pressure, and (ii) in cases where only one of the two steps is

accelerated, then the magnitude of the effect of sampling under vacuum will depend on the relative importance of the step involved i.e. accelerations will be recorded if the step involved is controlling the overall extraction kinetics.

2.4. MATERIALS AND METHODS

2.4.1. CHEMICALS, MATERIALS AND SAMPLES

Naphthalene (Nap) and Acenaphthene (Ace) were purchased from Sigma-Aldrich (Steinheim, Germany) at a purity > 99% and Fluoranthene (Flu) from Riedel-de-Haen (Seelze, Germany) at a purity of 98.4%. A 100 mg L^{-1} acetone stock solution of the three model analytes was prepared and used for preparing spiked water samples. The acetone stock solution containing the three target analytes was stored in an amber vial at -18 ^{o}C when not in use. Acetone (ACS Reagent grade) and acetonitrile (HPLC grade) was provided by Honeywell (New Jersey, USA). Deionized water was prepared on a Barnstead EASYpure II water purification system purchased by Thermo Scientific (Dubuque, USA). The 10-mm long stir bars (Twister™) were coated with a 0.5-mm thickness PDMS layer (24 mL) and were obtained from Gerstel (Mülheim an der Ruhr, Germany). New and used stir bars were conditioned by sonicating them in 1ml of acetonitrile. The effect of matrix was studied using tap water collected from the University campus (Technical University of Crete, Greece) and secondary treated wastewater effluent (WWTP effluent) from the municipal wastewater treatment plant of Chania, Greece, serving approximately 70,000 inhabitants.

2.4.2. VAC-HSSE AND REGULAR HSSE PROCEDURES

20mL screw top vial (Restek, Bellefonte, USA) containing a magnetic polytetrafluoroethylene (PTFE) stir bar (15mm x 5 mm; Sigma Aldrich) was placed on top of a magnetic and heating stir bath plate (Heidolph MR-Standard, Germany). The stir bar was then fixed on the inner top part of the vial wall with the help of two external magnets hooked on metallic binder clips. A tailor-made closure designed and constructed by the Laboratory of Aquatic Chemistry (Technical University of Crete) was used for all experiments. The closure was equipped with a cylindrical Thermogreen®LB-1 septum (Supelco) with half-hole (6mm diameter x 9mm length).

Alternatively, the previously reported modified crimp-top Mininert®valve (Sigma-Aldrich) can be used to ensure gastight conditions inside the sampler (Tuduri et al., 2012). VP 2 Autovac pumping unit (7 mbar = 0.007 atm ultimate vacuum without gas ballast) manufactured by Vacuubrand (Wertheim, Germany), was used to evacuate the air inside the sample container (Trujillo-Rodríguez, Pino, Psillakis, et al., 2017). A 10ml aqueous sample containing a known concentration of target analytes was introduced inside the vial through the septa using a gastight syringe (SGE, Australia). Agitation at 500 rpm was applied, initiating HSSE sampling for a preset period time and temperature. The effect of agitation was investigated during a preliminary set of experiments (tested values: 0, 500 and 1000 rpm). The results, shown in Fig. S.1 in the Appendix 1 in the Supporting Information showed that agitating the sample improved extraction efficiencies compared to the stagnant (standing) mode. Moreover, increasing the stirring speed from 500 rpm to 1000 rpm did not improve extraction efficiencies. However, the error associated to the measurements increased at 1000 rpm, most probably due to inconsistent agitation at high stirring speeds (García-Falcón et al., 2004). For this reason a stirring speed at 500 rpm was applied. When extraction was completed, the septum was pierced with an open-end disposable needle allowing pressure equilibration and easy opening of the closure. The stir bar was then removed with the help clean tweezers, dried with a lint-free tissue and transferred to a 350 μL-glass insert vessel containing 150 μL acetonitrile. The stir bar and solvent were sonicated for 15 min. Note that the glass inserts were placed in 2mL vials containing a minimum amount of deionized water to afford successful propagation of ultrasound waves. Upon completion of the liquid desorption step, 40 μL of the acetonitrile extract were used for analysis. It is noted that the liquid desorption step was optimized here during a preliminary study and the results are given in Fig. S.2 of Supporting Information (García-Falcón et al., 2004; Popp et al., 2001). The parameters controlled in this set of experiments were: desorption solvent volume (tested values: 150, 200 and 300 μL), sonication time (tested values: 1-20min), and number of liquid desorption steps (1-3). The optimum conditions found were: one liquid desorption step, 150 μL of acetonitrile and 15 min sonication time. These were similar to the optimum liquid desorption conditions reported in the past after immersion SBSE sampling of PAHs from water samples: (i) one desorption step sonication, 150 μL of acetonitrile and 10 min sonication time (García-Falcón et al., 2004) and (ii) one liquid desorption step, 200 μL of acetonitrile and leaving the mixture for 15 min unattended (Popp et al., 2001).

For regular HSSE extraction the air-evacuation step was omitted and all extractions were performed under regular atmospheric conditions.

For both Vac- and regular HSSE, the closure's septum was replaced on a daily basis. Blanks were also run periodically to ensure the absence of carry over between runs. All extractions were run in triplicate.

2.4.3. HIGH-PERFORMANCE LIQUID CHROMATOGRAPHY (HPLC) COUPLED TO FLUORESCENCE DETECTION

Separation and detection was performed on a HPLC (Shimadzu Corporation, Kyoto, Japan), equipped with two solvent delivery pumps (LC 10AD VP), a fluorescence detector (RF 10A XL), a Rheodyne manual sample injector valve with a 20-mL loop (Chrom Tech Inc., MN, USA) and a Macherey-Nagel C18 (250mm x 3.0mm i.d., with 5 mm particles size) (Macherey-Nagel, Duren; Germany). The mobile phase was acetonitrile: water 85:15 v/v and flow rate 1.0mL min^{-1}. The selection of the excitation/emission pairs for detection were: 280/355 for Nap and Ace and 260/460 for Flu.

2.5. RESULTS AND DISCUSSION

2.5.1. EFFECTS OF TEMPERATURE AND EXTRACTION TIME ON VAC-HSSE

Temperature is one of the most important experimental parameters to consider during HSSE method optimization (Prieto et al., 2010). Heating the sample will increase Henry's Law volatility constants, K_H, leading to higher headspace concentrations and shorter equilibration times. However, high sample temperatures may also reduce the PDMS-headspace partition coefficients and, as such, decrease the final amount of analyte accumulated at equilibrium (Camino-Sánchez et al., 2014). Here, the effect of sample temperature was investigated from 25 to 65 ^oC under vacuum and atmospheric pressure (30 min extraction time) and the results are given in Fig. 2.1. The spiking concentration was set at 5 $\mu g\ L^{-1}$, so as to ensure detection of all target analytes with regular HSSE at lower sampling temperatures. As can be seen, at each sampling temperature, Vac-HSSE greatly improved extraction efficiencies compared to regular HSSE and the effect was more important for Ace and Flu. A more accurate evaluation

of the Vac- HSSE results, revealed an optimum temperature at 45 ºC for Ace, whereas for Flu, heating the sample gradually increased the amount extracted. For Nap, no substantial changes in extraction efficiencies were recorded with increasing sample temperature. With regular HSSE, the amount of Nap extracted seems to increase slightly when heating the sample at 55 ºC. On the contrary, the beneficial effect of heating the sample at 1 atm was evident for Ace and Flu.

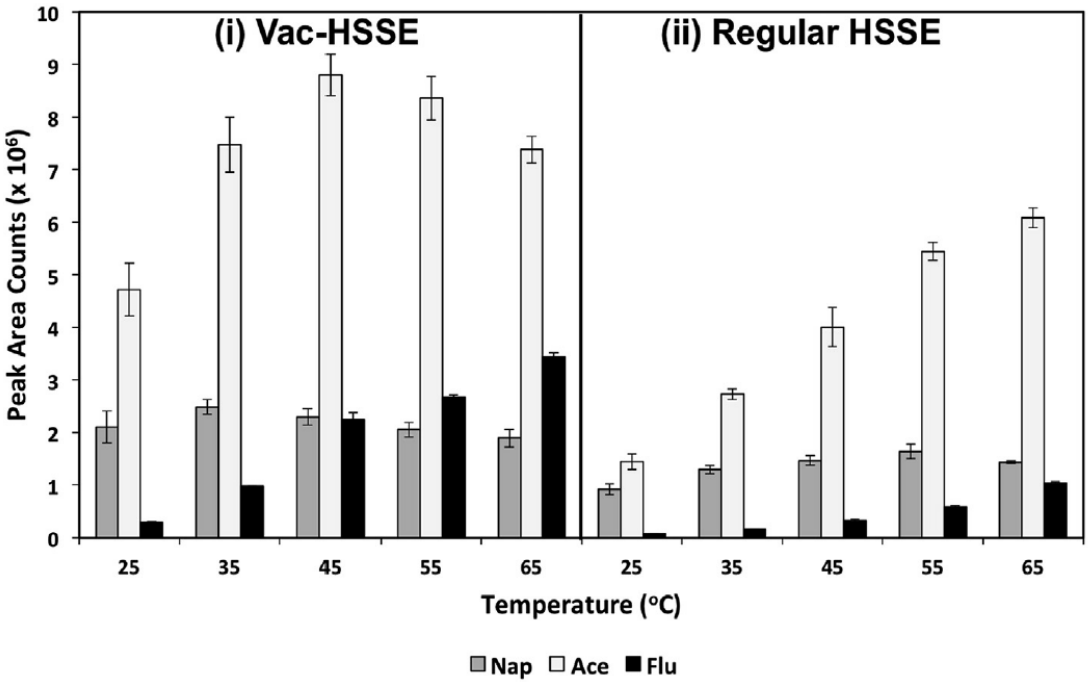

Fig. 2.1 Effect of temperature on (i) Vac-HSSE and (ii) regular HSSE. Experimental conditions: 10 mL aqueous samples spiked at 5 μg L^{-1}; 30 min sampling time; 500 rpm agitation speed. Some error bars are too small to be visible as compared with the physical size of the symbol.

An important point to consider in Vac-HSSE is the successful combination of the effects of sample temperature and low sampling pressure. This was not the case when a low pressure was applied during HS-SPME sampling of PAHs from aqueous solutions (Psillakis et al., 2013), and higher sampling temperatures were unexpectedly found to affect mass loading of PAHs into the SPME fiber. At the time, it was assumed that the high amount of water molecules interacted with the PDMS coating of the SPME fiber and changed its properties. It is noted however, that the use of PDMS as a material in permeation type passive air samplers resulted in a low permeability towards water vapor and a low energy of activation of permeation towards gas phase organic compounds (Prieto et al., 2010, Bicchi et al., 2003), rendering water uptake and the possibility of sorbent saturation with water very small. In this connection, no

significant variations in the analyte uptake rate from the gas-phase were observed when high humidity (Seethapathy & Górecki, 2012) or temperatures were applied (Park et al., 2014; Seethapathy & Górecki, 2012) to PDMS acting as a coating or membrane material. It therefore appears that the non-ideal performance of the PDMS fiber during Vac-HS-SPME at elevated temperatures is related to the small thickness of the fiber coating compared to that of a PDMS coated stir bar. At high humidity conditions, any surface irregularities/uncoated sites of the SPME fiber (due, for instance, to its repeated use) might act as a spot for water adsorption and suppress analyte uptake (Seethapathy & Górecki, 2010). Here, the relatively high PDMS volume and layer thickness of the stir bar, prevented water molecules interfering with analyte uptake during Vac-HSSE sampling, and afforded effective coupling of the effects of temperature and low pressure.

The effect of sampling time was initially investigated at 25 ^{o}C under vacuum and atmospheric pressure conditions. The spiking concentration was again set at 5 μg L^{-1}, so as to allow detection of Flu with regular HSSE at short sampling times. The results, depicted in Fig. 2.2(ia) and (ib), verified our theoretical predictions and a remarkable improvement when sampling under vacuum vs. atmospheric pressure was recorded during both the linear and curvilinear stages of extraction. With Vac-HSSE, Nap reached equilibrium after only 30 min of sampling, whereas with regular HSSE equilibrium was assumed to be between 90 and 120 min, since the Vac-HSSE/HSSE peak area ratios were close to unity (at equilibrium Vac- and regular HSSE have the same extraction efficiencies and this peak area ratio takes the value of 1). The long HSSE equilibration time required for Nap at 1 atm was in agreement with a past report aiming at the determination of PDMS-air partition coefficients using regular HSSE (Park et al., 2014). This study monitored concentrations in air and the PDMS coating of a stir bar and reported a 90 min equilibration time for naphthalene at temperatures between 20 and 30 ^{o}C.

Fig. 2 (ia) and (ib) also showed that the extracted amount of Ace under vacuum gradually increased with time, and the extraction rate appeared to slow down close to 120 min, i.e. as Ace slowly approached equilibrium. On the contrary, with regular HSSE, Ace was still away from equilibrium even after 120 min (Vac-HSSE/ HSSE peak area ratio was 1.5 at this time point). The extraction time profiles obtained for Flu, the most hydrophobic and least volatile analyte tested here, were away from

equilibrium at both investigated pressures. However, the improvement in extraction efficiency with Vac-over regular HSSE was important at each sampling time tested (e.g. at 120 min the Vac-HSSE/HSSE peak area ratio for Flu was 4).

Comparison of the present results to those obtained with HSSPME can give some important insights into the HSSE process. Past studies reported a rather fast equilibration for HS-SPME sampling of Nap from water solutions under regular and low pressure conditions (Psillakis et al., 2013; Psillakis, Mousouraki, et al., 2012). These short equilibration times were associated to the relatively fast evaporation rate of Nap from the water sample (Psillakis, Mousouraki, et al., 2012), taken that equilibration between the headspace and the SPME fiber polymer interface during HS-SPME is assumed to be fast for semi-volatiles (Górecki et al., 1997). This conclusion was in agreement with a past report stating that for Nap, evaporation from water was largely controlled by liquid-phase resistance (82.2%) (Mackay & Wolkoff, 1973), and was therefore, expected to be relatively independent of the total pressure in the sampling vial (Psillakis, Mousouraki, et al., 2012). Here, the extraction time profiles under each pressure were substantially different: Nap reached equilibrium at about 30 min with Vac-HSSE, whereas equilibrium with regular HSSE was assumed to be between 90 and 120 min. Assuming that Nap evaporates relatively fast from the water sample, this finding suggested that the rate-limiting step in HSSE was located in the headspace/PDMS system. Moreover, the acceleration in extraction rates recorded when lowering the sampling pressure highlighted that mass transfer from the headspace to the PDMS coating of the stir bar was pressure-dependent (i.e. the major resistance was gas-sided where $k_o = k_g$) and that these gas-phase constrains could effectively be reduced by lowering the total pressure. The latter effect was predicted by the theory presented here, as for this gas-side limited analyte reducing the value of k_g was expected to increase analyte uptake by the PDMS phase rate throughout the pre-equilibrium stage (Eqs. (2.2), (2.4) and (2.6)) and as such, reduce its equilibration time (Eq. (2.7)). It is noted that air-sided resistance to diffusion into passive samplers has been demonstrated for PAHs in general (Bartkow et al., 2004; Müller et al., 2000). This implies that gas-phase limitations were also present during Ace and Flu uptake by the PDMS coated stir bar and that they could be effectively reduced when sampling under vacuum. However (and as will be discussed in the following paragraph), for Ace and

Flu, evaporation is also expected to be a slow step in extraction and reducing the sampling pressure will contribute to accelerations in the overall extraction kinetics.

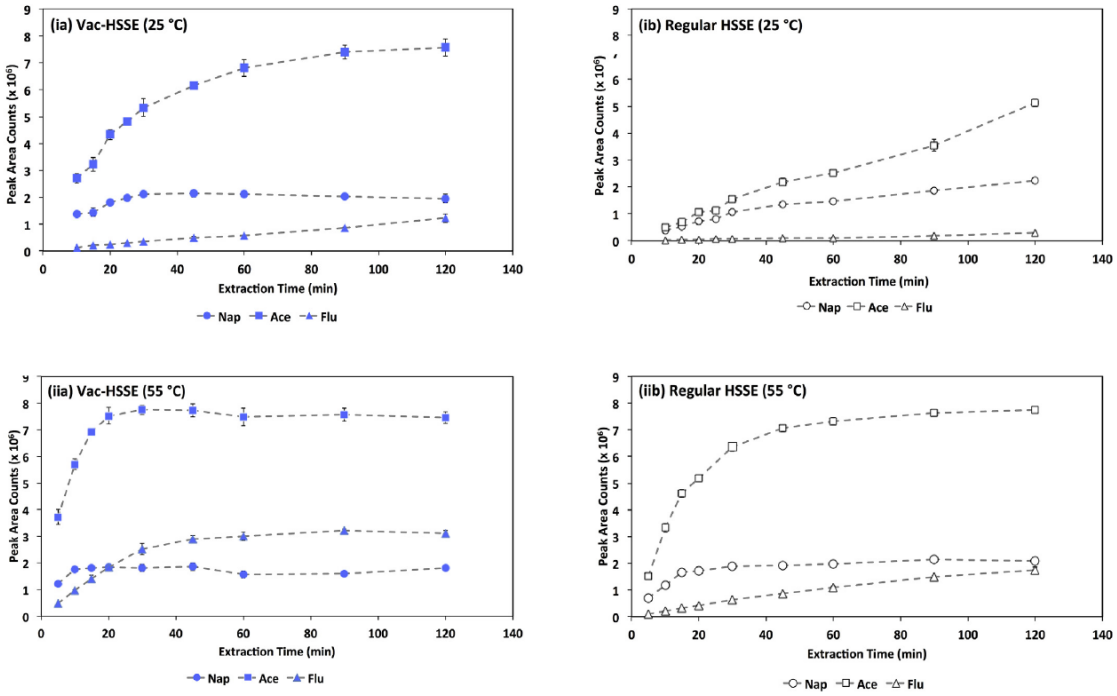

Fig. 2.2 Extraction time profiles for the three model PAHs obtained at 25ºC (ia) under vacuum (filled symbols) and (ib) regular (open symbols) pressure conditions and at 55ºC (iia) under vacuum (filled symbols) and (iib) regular (open symbols) pressure conditions. Experimental conditions: 10 mL aqueous samples spiked at 5 μg L^{-1}; 500 rpm agitation speed. Some error bars are too small to be visible as compared with the physical size of the symbol.

HS-SPME enables to predict the effect of low sampling pressure on extraction rates using the so-called K_H criterion, where the K_H values of target analytes are compared to some threshold values (Psillakis, 2017 ,Psillakis, Mousouraki, et al., 2012). This type of evaluation should be used with caution with the HSSE sampling approach. According to the K_H criterion, the extraction kinetics of Nap was not expected to be affected when lowering the sampling pressure, since its K_H value suggested a liquid-sided resistance to evaporation, which is independent of the total pressure (Psillakis, 2017). Nonetheless, a significant improvement in the extraction rate of Nap was recorded with Vac-HSSE, as gas-sided resistance controlled analyte uptake in the headspace/PDMS system. For Ace and Flu (low K_H compounds), the K_H criterion predicted gas-sided control of the evaporation step (Psillakis, 2017) and low evaporation rates from water samples. Taken that Ace and Flu have K_{OA} values sufficiently large (K_{OA} > 106) to yield a negligible PDMS sided resistance (i.e. the $1/(K_{eg}\, k_e)$ term in Eq. (2.1)) (Psillakis et al., 2019, Bartkow et al., 2004, Muller et al.,

2000) the gas-phase limitations to diffusion into the PDMS coated stir bar should also be effectively removed by lowering the sampling pressure. Accordingly, for Ace and Flu, lowering the sampling pressure was expected to accelerate both the evaporation (water/ headspace system) and analyte uptake (headspace/PDMS system) HSSE steps.

The extraction time profiles where then constructed at 55 ºC and the results are reported in Fig. 2(iia) and (iib). As expected, heating the aqueous sample accelerated the extraction process under each pressure condition and the effect was more pronounced with sampling under vacuum. In particular, an important enhancement in extraction rates was recorded with Vac-HSSE, where all target analytes reached equilibrium within the sampling times tested (15 min for Nap, 30 min for Ace and 90 min for Flu). Under regular pressure conditions, Nap reached equilibrium at about 20 min and Ace was approaching equilibrium close to 120 min of sampling (Vac-HSSE/HSSE peak area ratio was close to 1). Flu was away from equilibrium under each pressure condition and the positive effect of sampling under vacuum was important at each sampling time tested (e.g. at 120 min the Vac-HSSE/HSSE peak area ratio was 1.8).

In order to evaluate the analytical performances Vac-HSSE and regular HSSE, the sampling temperature was set as a compromise at 55 ºC for both sampling pressures and the sampling times were set at 30 min for Vac-HSSE and 60 min for regular HSSE.

Table 2.1 Analytical performances of the optimized Vac-HSSE and regular HSSE procedures.

Analyte	Vac-HSSE						Regular HSSE					
	Linear range (ng L^{-1})	r^2 (n=5)[a]	LOD (ng L^{-1})	Precision (%)[b]	Relative Recovery (RSD,%)[c]		Linear range (ng L^{-1})	r^2 (n=5)[a]	LOD (ng L^{-1})	Precision (%)[b]	Relative Recovery (RSD,%)[c]	
					Tap water	WWTP effluent					Tap water	WWTP effluent
Nap	100-5000	0.9999	43	1.2	102(3)	99.9 (3)	100-5000	0.9997	44	1.2	102(3)	98 (6)
Ace	100-5000	0.9998	6	2.5	101(3)	101 (3)	100-5000	0.9997	5	2.4	102(1)	105 (4)
Flu	100-5000	0.9995	3.1	3.1	99.8(5)	99.4 (7)	250-5000	0.9992	101	6.5	95.8(7)	97.0 (8)

[a] Correlation coefficient, number of calibration points (n) in parenthesis.

[b] Intra-day precision expressed as relative standard deviation (n = 5).

[c] Spiking level 1000 ng L^{-1}; % RSD values given in parentheses; n = 3.

2.5.2. ANALYTICAL PERFORMANCE OF THE OPTIMIZED VAC-HSSE AND REGULAR HSSE PROCEDURES

The performances of Vac-HSSE and regular HSSE methods were evaluated after extracting samples for 30 and 60 min, respectively, at 55 ^{o}C. Selected quality analytical parameters are given in Table 2.1. The results show that the linearity ranges of Vac- and regular HSSE for Nap and Ace were between 100 and 5000 ng L^{-1}. For Flu, a wider linearity range was found with Vac-HSSE compared to regular HSSE, reflecting the improvement in extraction rates discussed above. The determination coefficients (r^2) ranged from 0.9995 to 0.9999 with Vac-HSSE and from 0.9992 to 0.9997 with regular HSSE. The limits of detection (LODs) were estimated as three times the signal-to-noise ratio, and were verified by performing extractions at those levels. Table 2.1 shows that LOD values with the proposed Vac-HSSE procedure were similar for Nap and Ace or lower for Flu to those obtained with regular HSSE in half of the sampling time needed for regular HSSE. Similar conclusions could be reached for the estimated limits of quantification (LOQ) defined as ten times the signal-to-noise ratio (estimated values not given in Table 2.1). Intra-day precision for both methods, estimated as the relative regular deviation (RSD) at 1000 ng L^{-1} (Table 2.1) ranged from 1.2% to 3.1% with Vac-HSSE sampling, and between 1.2% and 6.5% for regular HSSE. Initial Vac-HSSE analyses of tap and wastewater effluent samples did not show detectable amounts of the target analytes and were therefore used for recovery studies. The relative recoveries, defined as the ratio of the concentrations found in real and deionized water samples spiked with the same amount of analytes, were then determined and the results are given in Table 2.1. For both types of real world water samples, matrix did not affect extraction, also reflecting the relatively simple nature of matrices examined here.

2.6. CONCLUSION

The effect of low pressure is a new experimental parameter to consider during method optimization in headspace (micro)extraction. For the first time, this work extended the applicability of the vacuum-based sampling approach to HSSE. The theoretical model describing the pressure dependence of Vac-HSSE was here discussed and the reduction in equilibration times was predicted. Inducing accelerations in HSSE is important, since the low surface area to volume ratio typically results in long equilibration times

at 1 atm compared to other PDMS-based methods (e.g. SPME). The relatively high PDMS volume and layer thickness used for coating the stir bars, prevented water molecules interfering with analyte uptake during Vac-HSSE sampling, and allowed effective coupling of the effects of temperature and low pressure. Moreover, the extraction time profiles demonstrated the substantial improvement in kinetics when adopting the Vac-HSSE sampling approach.

Target analytes could more rapidly reach equilibrium, and the optimum sampling time with Vac-HSSE was half of that found with regular HSSE. The analytical performance of Vac-HSSE was similar or better than that of regular HSSE in a shorter sampling time. The results on naphthalene revealed for the first time that gas-phase limitations can control extraction kinetics and that this type of constrains can effectively be reduced with sampling at a low pressure. For Ace and Flu, gas-sided limitations were assumed to control both the evaporation and analyte uptake processes and sampling under vacuum was found to accelerate the overall extraction kinetics.

2.7. REFERENCES

Baltussen, E., Sandra, P., David, F., & Cramers, C. (1999). Stir Bar Sorptive Extraction (SBSE), a Novel Extraction Technique for Aqueous Samples: Theory and Principles. *Journal of Microcolumn Separations*, *11*(10), 737–747. https://doi.org/10.1002/(SICI)1520-667X(1999)11:10<737::AID-MCS7>3.0.CO;2-4.

Bartkow, M. E., Booij, K., Kennedy, K. E., Müller, J. F., & Hawker, D. W. (2005). Passive air sampling theory for semivolatile organic compounds. *Chemosphere*, *60*(2), 170–176. https://doi.org/10.1016/j.chemosphere.2004.12.033.

Bartkow, M. E., Hawker, D. W., Kennedy, K. E., & Müller, J. F. (2004). Characterizing Uptake Kinetics of PAHs from the Air Using Polyethylene-Based Passive Air Samplers of Multiple Surface Area-to-Volume Ratios. *Environmental Science and Technology*, *38*(9), 2701–2706. https://doi.org/10.1021/es0348849.

Bicchi, C., Cordero, C., Iori, C., Rubiolo, P., & Sandra, P. (2000). Headspace Sorptive Extraction (HSSE) in the headspace analysis of aromatic and medicinal plants. *Journal of High Resolution Chromatography*, *23*(9), 539–546. https://doi.org/10.1002/1521-4168(20000901)23:9<539::AID-JHRC539>3.0.CO;2-3.

Bicchi, C., Cordero, C., Liberto, E., Rubiolo, P., Sgorbini, B., & Sandra, P. (2005). Impact of phase ratio, polydimethylsiloxane volume and size, and sampling

temperature and time on headspace sorptive extraction recovery of some volatile compounds in the essential oil field. *Journal of Chromatography A*, *1071*(1–2), 111–118. https://doi.org/10.1016/j.chroma.2004.09.054.

Bicchi, C., Cordero, C., & Rubiolo, P. (2004). A survey on high-concentration-capability headspace sampling techniques in the analysis of flavors and fragrances. *Journal of Chromatographic Science*, *42*(8), 402–409. https://doi.org/10.1093/chromsci/42.8.402.

Bicchi, C., Cordero, C., Rubiolo, P., & Sandra, P. (2003). Impact of water/PDMS phase ratio, volume of PDMS, and sampling time on Stir Bar Sorptive Extraction (SBSE) recovery of some pesticides with different KO/W. *Journal of Separation Science*, *26*(18), 1650–1656. https://doi.org/10.1002/jssc.200301613.

Bruheim, I., Liu, X., & Pawliszyn, J. (2003). Thin-film microextraction. *Analytical Chemistry*, *75*(4), 1002–1010. http://www.ncbi.nlm.nih.gov/pubmed/23039367.

Brunton, N. P., Cronin, D. A., & Monahan, F. J. (2001). The effects of temperature and pressure on the performance of Carboxen/PDMS fibres during solid phase microextraction (SPME) of headspace volatiles from cooked and raw turkey breast. *Flavour and Fragrance Journal*, *16*(4), 294–302. https://doi.org/10.1002/ffj.1000.

Camino-Sánchez, F. J., Rodríguez-Gómez, R., Zafra-Gómez, A., Santos-Fandila, A., & Vílchez, J. L. (2014). Stir bar sorptive extraction: Recent applications, limitations and future trends. *Talanta*, *130*, 388–399. Elsevier B.V. https://doi.org/10.1016/j.talanta.2014.07.022.

Darrouzès, J., Bueno, M., Pécheyran, C., Holeman, M., & Potin-Gautier, M. (2005). New approach of solid-phase microextraction improving the extraction yield of butyl and phenyltin compounds by combining the effects of pressure and type of agitation. *Journal of Chromatography A*, *1072*(1), 19–27. https://doi.org/10.1016/j.chroma.2005.02.026.

David, F., & Sandra, P. (2007). Stir bar sorptive extraction for trace analysis. *Journal of Chromatography A*, *1152(1–2)*, 54–69. https://doi.org/10.1016/j.chroma.2007.01.032.

García-Falcón, M. S., Cancho-Grande, B., & Simal-Gándara, J. (2004). Stirring bar sorptive extraction in the determination of PAHs in drinking waters. *Water Research*, *38*(7), 1679–1684. https://doi.org/10.1016/j.watres.2003.12.034.

Goirecki, T., & Pawliszyn, J. (1997). The effect of sample volume on quantitative analysis by SPME. Part I: theoretical considerations. *Analyst*, *122*, 1079–1086. https://doi.org/10.1039/a701303e.

Harner, T., Farrar, N. J., Shoeib, M., Jones, K. C., & Gobas, F. A. P. C. (2003). Characterization of polymer-coated glass as a passive air sampler for persistent organic pollutants. *Environmental Science and Technology*, *37*(11), 2486–2493. https://doi.org/10.1021/es0209215.

He, M., Chen, B., & Hu, B. (2014). Recent developments in stir bar sorptive extraction Microextraction Techniques. *Analytical and Bioanalytical Chemistry*, *406(8),* 2001–2026. Springer Verlag. https://doi.org/10.1007/s00216-013-7395-y.

Lucena, R. (2012). Extraction and stirring integrated techniques: examples and recent advances. *Analytical and Bioanalytical Chemistry*, *403*(8), 2213–2223. https://doi.org/10.1007/s00216-012-5826-9.

Mackay, D., & Wolkoff, A. W. (1973). Rate of evaporation of low-solubility contaminants from water bodies to atmosphere. *Environmental Science & Technology*, *7*(7), 611–614. https://doi.org/10.1021/es60111a012.

Müller, J.F., Hawker, D.W., Connell, D.W., Komp, P., McLachlan, M.S. (2000). Passive sampling of atmospheric SOCs using tristearin-coated fibreglass sheets. *Atmospheric Environment, 34*, 3525-3534. https://doi.org/10.1016/S1352-2310(00)00097-2.

Nogueira, J. M. F. (2015). Stir-bar sorptive extraction: 15 years making sample preparation more environment-friendly. *TrAC - Trends in Analytical Chemistry*, *71*, 214–223. https://doi.org/10.1016/j.trac.2015.05.002.

Park, E. J., Cho, Y. K., Kim, D. H., Jeong, M. G., Kim, Y. H., & Kim, Y. D. (2014). Hydrophobic polydimethylsiloxane (PDMS) coating of mesoporous silica and its use as a preconcentrating agent of gas analytes. *Langmuir*, *30*(34), 10256–10262. https://doi.org/10.1021/la502915r.

Pawliszyn, J. (2011). *Handbook of solid phase microextraction*. Elsevier.

Popp, P., Bauer, C., & Wennrich, L. (2001). Application of stir bar sorptive extraction in combination with column liquid chromatography for the determination of polycyclic aromatic hydrocarbons in water samples. *Analytica Chimica Acta*, *436*, 1-9. https://doi.org/10.1016/S0003-2670(01)00895-9.

Prieto, A., Basauri, O., Rodil, R., Usobiaga, A., Fernández, L. A., Etxebarria, N., & Zuloaga, O. (2010). Stir-bar sorptive extraction: A view on method optimisation, novel applications, limitations and potential solutions. *Journal of Chromatography A, 1217(16),* 2642–2666. https://doi.org/10.1016/j.chroma.2009.12.051.

Psillakis, E. (2017). Vacuum-assisted headspace solid-phase microextraction: A tutorial review. *Analytica Chimica Acta*, *98*, 12–24. Elsevier B.V. https://doi.org/10.1016/j.aca.2017.06.033.

Psillakis, E., Koutela, N., & Colussi, A. J. (2019). Vacuum-assisted headspace single-drop microextraction: Eliminating interfacial gas-phase limitations. *Analytica Chimica Acta*, *1092*, 9–16. https://doi.org/10.1016/j.aca.2019.09.056.

Psillakis, E., Mousouraki, A., Yiantzi, E., & Kalogerakis, N. (2012). Effect of Henry's law constant and operating parameters on vacuum-assisted headspace solid phase microextraction. *Journal of Chromatography A*, *1244*, 55–60. https://doi.org/10.1016/j.chroma.2012.05.006.

Psillakis, E., Yiantzi, E., & Kalogerakis, N. (2013). Downsizing vacuum-assisted headspace solid phase microextraction. *Journal of Chromatography A*, *1300*, 119–126. https://doi.org/10.1016/j.chroma.2013.02.009.

Psillakis, E., Yiantzi, E., Sanchez-Prado, L., & Kalogerakis, N. (2012). Vacuum-assisted headspace solid phase microextraction: Improved extraction of semivolatiles by non-equilibrium headspace sampling under reduced pressure conditions. *Analytica Chimica Acta*, *742*, 30–36. https://doi.org/10.1016/j.aca.2012.01.019.

Qin, Z., Bragg, L., Ouyang, G., & Pawliszyn, J. (2008). Comparison of thin-film microextraction and stir bar sorptive extraction for the analysis of polycyclic aromatic hydrocarbons in aqueous samples with controlled agitation conditions. *Journal of Chromatography A*, *1196–1197*(1–2), 89–95. https://doi.org/10.1016/j.chroma.2008.03.063.

Reyes-Garcés, N., Gionfriddo, E., Gómez-Ríos, G. A., Alam, M. N., Boyacl, E., Bojko, B., Singh, V., Grandy, J., & Pawliszyn, J. (2018). Advances in Solid Phase Microextraction and Perspective on Future Directions. *Analytical Chemistry, 90(1),* 302–360. American Chemical Society. https://doi.org/10.1021/acs.analchem.7b04502.

R.P. Schwarzenbach, P.M. Gschwend, D.M. Imboden (2003). Environmental Organic Chemistry, second ed., John Wiley & Sons Inc, Hoboken, New Jersey.

Seethapathy, S., & Górecki, T. (2012). Applications of polydimethylsiloxane in analytical chemistry: A review. *Analytica Chimica Acta*, *750*, 48–62. https://doi.org/10.1016/j.aca.2012.05.004.

Tienpont, B., David, F., Bicchi, C., & Sandra, P. (2000). High capacity headspace sorptive extraction. *Journal of Microcolumn Separations*, *12*(11), 577–584. https://doi.org/10.1002/1520-667X(2000)12:11<577::AID-MCS30>3.0.CO;2-Q.

Trujillo-Rodríguez, M. J., Pino, V., & Anderson, J. L. (2017). Magnetic ionic liquids as extraction solvents in vacuum headspace single-drop microextraction. *Talanta*, *172*, 86–94. https://doi.org/10.1016/j.talanta.2017.05.021.

Trujillo-Rodríguez, M. J., Pino, V., Psillakis, E., Anderson, J. L., Ayala, J. H., Yiantzi, E., & Afonso, A. M. (2017). Vacuum-assisted headspace-solid phase microextraction for determining volatile free fatty acids and phenols. Investigations on the effect of pressure on competitive adsorption phenomena in a multicomponent system. *Analytica Chimica Acta*, *962*, 41–51. https://doi.org/10.1016/j.aca.2017.01.056.

Tuduri, L., Millet, M., Briand, O., & Montury, M. (2012). Passive air sampling of semi-volatile organic compounds. *TrAC - Trends in Analytical Chemistry*, *31*, 38–49. https://doi.org/10.1016/j.trac.2011.08.007.

Vakinti, M., Mela, S. M., Fernández, E., & Psillakis, E. (2019). Room temperature and sensitive determination of haloanisoles in wine using vacuum-assisted headspace solid-phase microextraction. *Journal of Chromatography A*, *1602*, 142–149. https://doi.org/10.1016/j.chroma.2019.03.047

Yiantzi, E., Kalogerakis, N., & Psillakis, E. (2015). Vacuum-assisted headspace solid phase microextraction of polycyclic aromatic hydrocarbons in solid samples. *Analytica Chimica Acta*, *890*, 108–116. https://doi.org/10.1016/j.aca.2015.05.047

Zhakupbekova, A., Baimatova, N., & Kenessov, B. (2019). A critical review of vacuum-assisted headspace solid-phase microextraction for environmental analysis. *Trends in Environmental Analytical Chemistry*, *22*. Elsevier B.V. https://doi.org/10.1016/j.teac.2019.e00065.

CHAPTER 3: TOTAL AND BIOAVAILABLE POLYCYCLIC AROMATICA HYDROCARBONS IN UNUSED AND OPERATED HEAT-NOT-BURN TOBACCO PRODUCTS AND CONVENTIONAL CIGARETTES

Solomou, N., Fernández, E., Szafnauer, R., Psillakis, E. (2023). Total and bioavailable polycyclic aromatic hydrocarbons in unused and operated heat-not-burn tobacco products and conventional cigarettes. Chemosphere, 139050.

Credit author statement

N. Solomou: Investigation, Formal analysis, Writing – Original Draft. E. Fernández: Investigation, Formal analysis. R. Szafnauer: Resources, Formal analysis. E. Psillakis: Conceptualization, Writing - Review & Editing, Visualization, Supervision, Project administration, Funding acquisition.

3.1. ABSTRACT

Tobacco product waste poses a global environmental issue, affecting urban and coastal areas alike. The present studies report, for the first time, the total and bioavailable polycyclic aromatic hydrocarbons (PAHs) concentrations in unused and operated heat-not-burn (HnBs) tobacco products. To enable direct comparisons, identical sets of studies were conducted using conventional cigarettes (CCs). Five low-molecular PAHs were determined in HnBs at total concentrations that were of the same order before and after operation (Σ_5PAH = 47.37 ± 3.44 ng unit^{-1} and Σ_5PAH = 69.36 ± 5.78 ng unit^{-1} in unused and used HnBs, respectively). The incomplete combustion of organics during smoking of CCs, yielded substantially higher amounts of PAHs with their sum (Σ_{10}PAHs = 1449 ± 113 ng unit^{-1}) being >20 times larger than those in HnBs. The tobacco and filter were the most contaminated parts in HnBs. In unused CCs, tobacco had the highest PAHs load and after smoking, the spent filter was the most contaminated part, containing ∼80% of the total amount of PAHs. Naphthalene was the most abundant PAH detected in all tobacco products. Despite the high total PAH concentrations found in smoked CCs, the sums of the bioavailable PAH concentrations were of the same order in all tested tobacco products (Σ_5PAH = 61.38 ± 1.79 ng unit^{-1} in unused HnBs, Σ_5PAH = 70.87 ± 7.67 ng unit^{-1} in used HnBs, Σ_4PAH = 66.92 ± 5.95 ng unit^{-1} in unused CCs, and Σ_6PAH = 47.94 ± 1.26 ng unit^{-1} in smoked CCs). This finding was related to smoking affecting PAHs' leachability from CCs and delaying their desorption from the solid matrix. Adjusting the pH, salt and humic acids content at environmentally relevant values did not affect PAHs leaching at 24 h of soaking. Finally, the leaching behavior of PAHs in natural waters (river water, rainwater, and seawater) was found similar to that in ultrapure water, experimentally verifying the ability of tobacco product waste to leach PAHs into the aquatic environment.

3.2. INTRODUCTION

An estimated 5.8 trillion cigarettes are consumed every year, with ~4.5 trillion of them being improperly discarded in the environment (Zafeiridou et al., 2018). As a result, tobacco product waste is now widely recognized as a significant problem in urban sites, with the highest concentrations being recorded near points of purchase and consumption (Marah and Novotny, 2011). Cigarette butts are also the most collected item of litter in International Coastal Cleanups (Ocean conservancy-International Coastal Cleanup, 2021) and the second most commonly found item on beaches in the European Union (European Commission, 2019). The accumulation of tobacco product waste in urban and coastal sites is a significant ongoing environmental problem, with cigarette filters reported to release microplastic fibers into the aquatic environment at an estimated annual rate of 300,000 tons (Shen et al., 2021). Additionally, cigarette butts contain thousands of chemicals that can be released after exposure to water, for example, during rainfall or flood events (Araújo and Costa, 2019; Soleimani et al., 2023). In this regard, the toxicity of cigarette butt leachates to various aquatic and terrestrial species has been reported on multiple occasions (Beutel et al., 2021; Booth et al., 2015; Koutela et al., 2020; Lee and Lee, 2015; Micevska et al., 2006; Parker and Rayburn, 2017; Slaughter et al., 2011; Soleimani et al., 2023).

The pollutants known to leach from smoked cigarettes were recently reviewed (Beutel et al., 2021; Soleimani et al., 2022) and they included metals, nicotine, aromatic amines, nitrosamines, polycyclic aromatic hydrocarbons (PAHs), phenols, and BTEX (benzene, toluene, ethylbenzene and xylene). In particular, PAHs are ubiquitous environmental pollutants that attract much attention because of their ability to bioaccumulate, potential carcinogenic, mutagenic and teratogenic properties, and persistence in the environment (Dobaradaran et al., 2020; Kumar et al., 2021). The total amounts of PAHs bound in freshly smoked cigarettes (Dobaradaran et al., 2019; King et al., 2021) and cigarette butts collected from roads and riversides (Dobaradaran et al., 2019; Moriwaki et al., 2009) have been reported in the past, along with the total PAHs present in the filter and tobacco plug before and after operation (Bentley and Burgan, 1960; Shimazu, 2016; Shimazu et al., 2018; Vu et al., 2015). Moreover, the amounts of PAHs leached from cigarette butts were recently determined (Dobaradaran et al.,

2020; Soleimani et al., 2023), although not directly related to the total PAHs originally present in the solid tobacco product.

Heat-not-burn products (HnBs) were recently introduced as an alternative to conventional cigarettes (CCs). HnBs use a device to heat specially prepared and blended tobacco sticks, producing an inhalable nicotine-containing aerosol. A key difference between HnBs and CCs is that HnBs heat tobacco to temperatures up to 350 °C, whereas CCs burn tobacco at temperatures above 600 °C to generate smoke and ash. Although the use of HnBs has rapidly increased, limited information exists regarding the impact of improperly discarded HnBs on the aquatic environment. In this connection, leachates produced from HnBs have been reported to have a strong ecotoxic effect on the growth of microorganisms (Baran et al., 2020). Another study, reported that several metals may leach from unused and used HnBs into water with varying composition, and provided additional evidence that improperly discarded tobacco products can serve as point sources of long-term metal contamination in the aquatic environment (Koutela et al., 2020).

The present studies aimed to fill the gap in scientific evidence regarding the total and bioavailable PAHs concentrations in HnBs before and after operation. Furthermore, laboratory leaching experiments were conducted to quantify the relative rates and magnitudes of PAHs released from HnBs as a function of time and the composition of the leaching solution. To enhance the current understanding and enable direct comparisons, identical sets of studies were conducted using both unused and smoked CCs.

3.3. MATERIALS AND METHODS

3.3.1. CHEMICALS

The 16 PAHs investigated in this study were: naphthalene (Nap), acenaphthylene (Acy), acenaphthene, (Ace), Flu (Flu), phenanthrene (Phe), anthracene (Ant), fluoranthene (Flt), pyrene (Py), benzo [a]anthracene (B [a]Ant), chrysene (Chry), benzo [b]fluoranthene (B [b]Flt), benzo [k]fluoranthene (B [k]Flt), benzo [a]pyrene (B [a]Py), indeno [1,2,3-cd]pyrene (IcdPy), dibenzo [a,h]anthracene (DB [ah]Ant) and benzo [ghi]perylene (B [ghi]Pe). For calibration purposes, the following solutions were

used: the EPA 525 PAH Mix B analytical standard containing 500 μg mL^{-1} of the 13 priority PAHs in acetone (Sigma-Aldrich, Steinheim, Germany) and a 100 μg mL^{-1} acetone solution of Nap (Sigma-Aldrich; ≥99%), Ace (Sigma-Aldrich; ≥99%) and Flt (Riedel-de-Haën, Seelze, Germany; 98.4%). A 500 μg mL^{-1} acetone solution of acenaphthene-d10, phenanthrene-d10, and chrysene-d12 was purchased from Sigma-Aldrich and used as the internal standard solution. Table S.1 in the Appendix 2 summarizes the 16 targeted PAHs and their main physicochemical properties.

Humic acids sodium salt was purchased from Fluka (Buchs, Switzerland), sodium chloride (≥99.9%) from Penta (Radiova, Praha), sodium hydroxide (≥98%, pellets) from Honeywell (Morris Plains, New Jersey, USA) and hydrochloric acid 37 wt% from Sigma-Aldrich. Milli-Q water was obtained from a Barnstead EASYpure II water purification system supplied by Thermo Scientific (Dubuque, USA). All organic solvents were of pesticide grade, and together with aluminum oxide 90 active neutral (activity stage I) for column chromatography were provided by Merck KGaA (Darmstadt, Germany). A Crison basic 20+ pH meter (Alella, Spain) was used to measure the pH.

River water samples were collected from Koiliaris river (Chania, Crete, Greece) and sea water from Koum Kapi beach in Chania, Crete, Greece. Rainwater was collected at the University Campus by placing amber bottles in open air. The chemical compositions of the natural water samples can be found in Table S.2 in the Appendix 2. All samples were collected in clean containers, filtered, and analyzed to ensure that they were free of PAHs. They were then stored in the dark at 4 °C until use.

3.3.2. UNUSED AND OPERATED TOBACCO PRODUCTS

Marlboro Red cigarettes were used as CCs and HEETS Sienna Selection as HnBs. They were all purchased from the local distributor of Philip Morris Products SA. Tobacco products were freshly operated before being used in experiments. Operation proceeded using a single port machine-smoking from Burghart (Wedel, Germany) that was programmed based on published smoking regimens (Koutela et al., 2020). For HnBs, the IQOS™ 2.4 Plus tobacco heating device and charger (Philip Morris Products S.A., Neuchâtel, Switzerland) were used for operation. The CCs were ignited using a flameless lighter and they were operated until a predefined butt length, which was the

length of the filter plus ~3 mm of the tobacco plug. Table S.3 in the Appendix 2 summarizes the mean masses of the used and unused tobacco products and their parts (Koutela et al., 2020). HnBs, CCs and their components displayed distinct characteristics before and after operation. For this reason, concentrations were expressed as ng unit^{-1} of solid tobacco product rather than ng g^{-1}. Table S.3 can be utilized for converting concentrations to μg g^{-1}.

3.3.3. TOTAL PAHS CONCENTRATIONS IN UNUSED AND OPERATED TOBACCO PRODUCTS

For the determination of the total PAHs concentrations, a modified ultrasound-assisted liquid-solid extraction method was used (Dobaradaran et al., 2019; Moriwaki et al., 2009), which offered faster extraction and consumed less energy and solvents compared to Soxhlet extraction (King et al., 2021). The number of tobacco products used for extraction varied based on the mass of the corresponding units. Accordingly, two units of HnBs or smoked CCs were placed in 4 mL glass vials together with 3.5 mL of hexane. In the case of unused CCs, only one unit was immersed in the same solvent volume. The solid-liquid mixtures were then sonicated for 30 min in a Branson 2510 E-MTH Bransonic Ultrasonic Cleaner (Danbury, USA). After extraction, the yellow supernatant was transferred using a glass pipette to a Falcon tube containing 0.250 g of Alumina for cleaning purposes. The mixture was manually shaken for 3 min and after centrifugation for 5 min at 3000 rpm using a Haraeus Labofuge 400 centrifuge from ThermoFisher Scientific (Waltham, USA), the clean supernatant was collected. A 500 μL aliquot of this purified extract was evaporated to near-dryness under a gentle N_2 flow, and then reconstituted using 25 μL of hexane containing 1 mg L^{-1} of the internal standard mixture. After this step, 1 μL was withdrawn and analyzed using a gas chromatograph-ion trap mass spectrometer (GC/ITMS). The contribution of the different components of the unused and operated tobacco products to the total concentration of PAHs was carried out following the same procedure. All experiments were run in triplicate, and average concentrations were reported in ng unit^{-1} of solid tobacco product.

3.3.4. LEACHING OF PAHS FROM UNUSED AND OPERATED TOBACCO PRODUCTS

The leachates were prepared following a published procedure (Koutela et al., 2020) using a 10 L kg^{-1} liquid to solid ratio (L/S), which is in accordance with the European regulatory batch tests (European Commission, 2013). The applied L/S ratio corresponded to either 4 unused HnBs, 4 used HnBs or 4 unused CCs soaked in 31 mL of water or 10 smoked CCs immersed in 25 mL of water. The pH in leachates obtained with deionized water varied from 6.6 to 7.1. The PAHs leaching from the filter, tobacco, or paper could not be determined due to the resulting dissolved concentrations being low. Table S.4 in the Appendix 2 summarizes the number of tobacco product units and water volumes used for leaching. Leaching was conducted in 40 mL amber screw-cap glass vials covered with aluminum foil for a preset period, and at 180 rpm using an Unimax 1010 shaker from Heidolph (Essex, UK). Soaking times of 1, 24, 72 and 192 h were examined. After leaching, the solid-water mixture was filtered under vacuum using a mixed cellulose ester gridded membrane filter (0.45 μm pore-size, 47 mm diameter) supplied by Membrane Solutions, LLC (Auburn, Washington, United States). The leaching behavior of PAHs from the studied tobacco products was investigated in natural water samples and water solutions of varying pH, ionic strength, or humic acids content, following the same procedure for a 24 h exposure time. All leachates were analyzed immediately after preparation, and experiments were conducted in triplicates. Average concentrations were reported as ng $unit^{-1}$ of solid tobacco product and Table S.3 can be used for converting them to μg g^{-1}.

3.3.5. EXTRACTION OF PAHS FROM LEACHATES USING HISORB

The analyses of tobacco product leachates included an initial sample preparation step that was a modification of published procedures (Alberti et al., 2021; Kremser et al., 2016). The HiSorb sorbent with a 63 μL polydimethylsiloxane (PDMS) coating (Markes International) was used for PAHs extraction. The procedure involved transferring 9 mL of the leachate into a 10 mL crimp-top glass vial followed by spiking with the internal standard solution, and capping the vial with a cap and septum supplied

by Markes International (Llantrisant, United Kingdom). The HiSorb unit was then introduced into the sampling vial through the septum and exposed to the leachate. Extraction proceeded for 60 min at 300 rpm using a HiSorb Agitator (Markes International). After extraction, the HiSorb unit was removed, washed with Milli-Q water to remove residual matrix components, and wiped gently with a lint-free tissue. Each HiSorb unit was then inserted in a stainless-steel thermal desorption tube (Markes International) and submitted for analysis using a thermodesorption-GC/ITMS (TD-GC/ITMS) analytical system. All HiSorb units were conditioned before use. Method blanks were frequently run to ensure that there was no carry-over between extractions.

3.3.6. GC/ITMS AND TD-GC/ITMS ANALYTICAL PROCEDURES

The hexane extracts prepared for the determination of the total PAHs concentrations, were directly analyzed using a Varian 450-GC gas chromatograph coupled with a Varian 240-MS IT mass spectrometer (Agilent Technologies Inc., Santa Clara, California, United States). Samples (1 μL) were injected in the split mode with the injector maintained at 290 °C.

For the determination of the bioavailable PAHs concentration, the HiSorb units were thermally desorbed using a TD100-xr Automated Thermal Desorber supplied by Markes International coupled to the same GC/ITMS used for the analysis of the hexane extracts. Each HiSorb unit was thermally desorbed at 280 °C for 20 min with a trap flow of 50 mL min^{-1} and the sample was collected on a 'General Purpose' cold trap at 30 °C. The cold trap was purged for 1 min at 50 mL min^{-1}, after which time it was desorbed for 3 min at 320 °C with a split flow of 10 mL min^{-1} (Alberti et al., 2021).

The GC/ITMS conditions were set based on a past report (Karkanorachaki et al., 2018). The chromatographic column was a MEGA-5 HT capillary column (30 m × 0.25 mm i. d., 0.25 μm film thickness; MEGA S. r.l., Legnano, Italy). The oven temperature was initially set at 50 °C for 5 min, followed by a ramp of 10 °C min^{-1} up to 160 °C for 13 min, followed by a second ramp of 5 °C min^{-1} up to 300 °C, to a final ramp of 25 °C min^{-1} up to 310 °C. Helium (99.999%) was used as the carrier gas at a constant flow rate of 1.1 mL min^{-1}. A solvent delay of 5 min was applied. Data was acquired in the selected ion storage detection mode and the masses are given in Table S.1 in the Appendix 2 together with the instrumental limits of detection. Separate calibration

curves were constructed for the determination of the total PAHs concentrations (using hexane PAHs solutions) and bioavailable PAHs concentrations (after extraction of water solutions spiked with PAHs standards).

At all times, QA/QC procedures were implemented to ensure the good quality of the data. These procedures included the use of instrumental blanks, frequent procedural blanks, conditioning of HiSorb units, and analysis of calibration standards every 10 samples as a calibration check. Additionally, recovery studies were carried out after every 20 samples, where tobacco products were fortified with approximately twice the concentrations of PAHs originally found in the sample. Relative recoveries varied between 90 and 110% (data not shown).

3.4. RESULTS AND DISCUSSION

3.4.1. TOTAL CONCENTRATIONS OF PAHS

The total PAHs concentrations found in the different types of tobacco products examined here are given in Fig. 3.1. As seen, five low molecular weight PAHs were detected in HnBs at concentrations ranging from 1.25 to 27.80 ng unit^{-1} and from 4.33 to 39.52 ng unit^{-1} for unused and used HnBs respectively (Fig. 3.1(a)). Nap was the most abundant PAH compound, accounting for ~60% of the total amount of PAHs detected in the solid product. The results also showed that after operation, the total average concentrations were of the same order (Σ_5PAH = 47.37 ± 3.44 ng unit^{-1} in unused HnBs and Σ_5PAH = 69.36 ± 5.78 ng unit^{-1} in used HnBs). In unused CCs, ten PAH compounds were detected at concentrations ranging from 6.66 to 47.74 ng unit^{-1} (Fig. 3.1(b)). After smoking, the same PAH compounds were detected in the solid waste, yet the sum of their average concentrations) was more than seven times larger than that found in unused CCs (Σ_{10}PAHs = 201.63 ± 14.27 ng unit^{-1} and Σ_{10}PAHs = 1449 ± 113 ng unit^{-1} in unused and smoked CCs respectively). The higher PAH concentrations observed in smoked CCs were likely due to the incomplete combustion of tobacco and other organic components during operation (Shimazu et al., 2018). Nap was again the most abundant PAH compound found, accounting for ~25% and 70% of the total PAHs detected in unused and smoked CCs, respectively. The concentrations of the 2- and most of the 3-rings PAHs were substantially higher in

smoked CCs compared to unused CCs. For the rest, total concentrations were similar or lower, either because additional amounts were not formed during operation or because the ash produced during CCs smoking retained them. It is important to note that the total PAH concentration found in smoked CCs was more than 20 times larger than the ones in unused and operated HnBs. This observation highlighted the importance of combustion over heating in generating PAHs during operation of tobacco products.

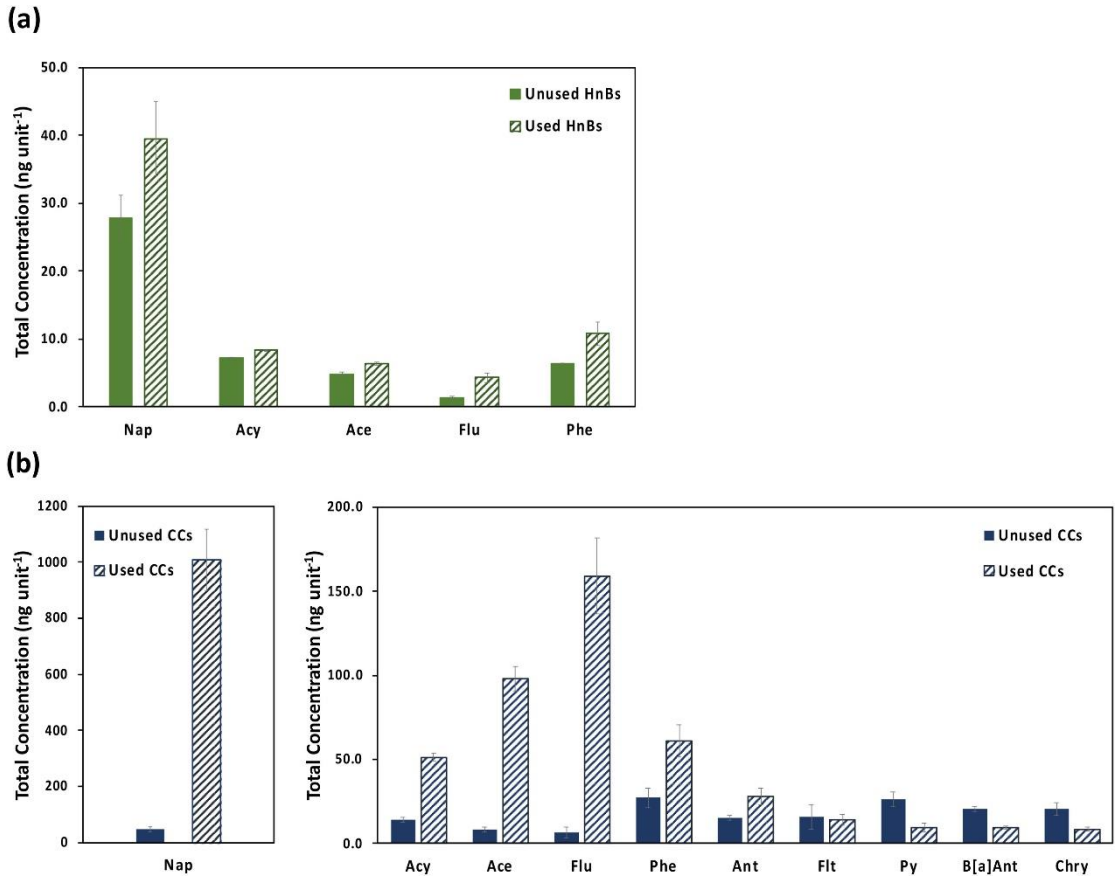

Fig. 3.1 Total concentrations of the PAHs found in unused and used (a) HnBs and (b) CCs.

To the best of our knowledge there are no published data on the total concentrations of PAHs in used and unused HnBs. Moreover, there is scarce information regarding the total PAHs in CCs, and these studies are limited to smoked CCs (Dobaradaran et al., 2019; King et al., 2021; Moriwaki et al., 2009). Table S.5 in the Appendix 2 summarizes representative published data on total PAHs concentrations in cigarette butts, and shows that the concentrations of most PAH compounds detected in the

present study were similar to those reported by King et al. (2021). Moreover, Dobaradaran et al. (2019) reported similar total concentrations for the lower molecular weight PAHs, but they also reported substantial amounts of 5- and 6-rings PAHs, presumably due to the different tobacco product brand used (Table S.5 – Appendix 2). The results presented here are also different to those reported by Moriwaki et al. (2009) where eleven 3- to 6-rings PAHs where detected at low total concentrations (Table S.5 – Appendix 2). However, in this report cigarette buts were not freshly prepared but were collected from roadsides with no information on their exposure time to outdoor conditions.

In general, tobacco contamination with PAHs is assumed to occur during fire curing of tobacco leaves (Vu et al., 2015). The filter and paper may also contain PAHs, as the result of the chemical additives used during manufacturing (Shimazu, 2016), emulsions used to attach the filter to the outer paper wrapper (De Fenzo et al., 2020), or from the inks used (Paschke et al., 2015). During the present studies, the contribution of the paper, filter, and tobacco to the total PAHs concentrations was investigated, and the results are given in Table 3.1. In accordance with a past report, the various cartons and packs of tobacco products used throughout the present studies, accounted for the small variations between the concentration found in the entire tobacco product and the combined concentrations in tobacco, filter and paper (Koutela et al., 2020). In HnBs, the results showed that tobacco and the filter were the most contaminated parts before and after operation. Not all PAHs detected in the whole product could be quantified in the different components of unused CCs. Trace amounts of the rest were detected in certain samples, but their presence could not be confirmed consistently across the triplicate runs. The results showed that in unused CCs, tobacco had the higher PAHs load. Conversely and in agreement with past reports (Shimazu, 2016; Shimazu et al., 2018), the filter was by far the most contaminated part of smoked CCs containing close to 80% of the total PAHs load.

Table 3.1 Total concentration of each PAH (given in ng unit^{-1}) in the different parts of used and unused HnBs and CCs. The error values correspond to the standard deviation of three-replicate samples.

HnBs (ng unit^{-1})

	UNUSED			USED		
	TOBACCO	**FILTER**	**PAPER**	**TOBACCO**	**FILTER**	**PAPER**
Nap	27.48 ± 1.72	15.23 ± 0.89	15.49 ± 0.89	22.63 ± 1.81	22.09 ± 1.19	16.41 ± 0.73
Acy	7.79 ± 0.83	5.54 ± 0.21	4.95 ± 0.19	4.78 ± 0.27	5.47 ± 0.99	2.39 ± 3.38
Ace	5.3 ± 1.42	1.76 ± 0.25	1.23 ± 0.35	1.52 ± 0.01	1.62 ± 0.57	0.59 ± 0.13
Flu	4.06 ± 1.97	1.46 ± 0.21	0.39 ± 0.09	0.46 ± 0.06	<LOD	0.47 ± 0.23
Phe	9.89 ± 2.84	7.61 ± 0.01	4.82 ± 0.03	4.77 ± 0.14	9.65 ± 6.3	4.31 ± 0.24
SUM	54.52 ± 41.97	31.59 ± 9.73	26.89 ± 9.81	34.15 ± 1.84	38.83 ± 6.52	24.18 ± 3.48

CCs (ng unit^{-1})

	UNUSED			USED		
	TOBACCO	**FILTER**	**PAPER**	**TOBACCO**	**FILTER**	**PAPER**
Nap	47.45 ± 4.72	33.02 ± 1.34	32.22 ± 0.07	156.25 ± 15.75	783.27 ± 21.09	40.72 ± 6.56
Acy	12.65 ± 0.15	11.61 ± 0.34	10.02 ± 0.31	12.82 ± 1.73	32.17 ± 0.98	6.06 ± 0.1
Ace	5.22 ± 1.08	3.01 ± 0.1	2.26 ± 0.53	22.65 ± 7.79	54.65 ± 6.29	3.76 ± 0.96
Flu	4.56 ± 0.34	2.42 ± 1.01	1.58 ± 0.02	19.43 ± 2.06	101.72 ± 19.9	3.86 ± 0.54
Phe	26.08 ± 3.36	11.4 ± 0.15	11.55 ± 1.7	16.49 ± 0.8	44.45 ± 0.42	7 ± 0.25
Ant	14.09 ± 0.43	61.47 ± 0	13.72 ± 0.51	10.59 ± 0.06	23.13 ± 0.15	6.97 ± 0.08
Flt	15.09 ± 1.47	<LOD	<LOD	7.18 ± 2.03	20.56 ± 1.96	<LOD
Py	11.96 ± 2.29	<LOD	<LOD	5.94 ± 1.65	26.4 ± 0.9	<LOD
B[a]Ant	<LOD	<LOD	<LOD	<LOD	8.86 ± 0.47	<LOD
Chry	<LOD	<LOD	<LOD	<LOD	7.79 ± 0.17	<LOD
SUM	137.12 ± 6.52	61.47 ± 1.72	71.35 ± 1.88	251.35 ± 17.98	1103.01 ± 29.77	68.37 ± 6.66

3.4.2. BIOAVAILABLE CONCENTRATIONS OF PAHS

Bioavailable concentrations (also known as free or dissolved concentrations) correspond to the fraction of the total concentrations that are available to be accumulated into an organism under a defined set of conditions (Yang et al., 2016). A typical procedure for determining bioavailable concentrations is to perform leaching studies, i.e., use water or another solvent to remove the soluble matter from a solid sample. The final amount of desorbed chemical will depend on the properties of the solid matrix and chemicals, the liquid to solid ratio applied and the composition of the water phase used for leaching (Koutela et al., 2020). During the present studies, the leaching behavior of PAHs from unused and operated tobacco products was investigated for soaking times up to 8 days, and the results are given in Figs. S.3 and S.4 in the Appendix 2. As seen, the dissolved concentrations of detected PAHs remained essentially the same for the soaking times tested, which is in agreement with a past study on leachates produced from smoked CCs (Dobaradaran et al., 2020). In this report, the authors found that the concentrations of PAHs with 2–4 rings (up to Py) could reach partition equilibrium fast, while the detection of heavier PAHs required 21 days of soaking, which is longer than the exposure times tested here. The findings from the analysis of the leachates from HnBs (Fig. S.3 – Appendix 2) confirmed the presence of the five low molecular weight PAHs previously detected in the solid waste. Conversely, not all PAHs could leach from CCs at detectable amounts (Fig. S.4 - Appendix 2). It was assumed that the low total concentrations, low solubility values and low affinity for the water phase restricted their release in the water phase. Ant was the only 3-ring PAH not detected in leachates from smoked CCs, most likely due to solubility limitations. Indeed, Ant has a water solubility value that is 25–90 times smaller than that of the rest 3-ring PAHs (Table S.1 – Appendix 2), and even fluoranthene, the only 4-ring PAH detected in leachates from used CCs, has a water solubility approximately 6 times higher.

A closer look on the bioavailable concentrations obtained at 24 h of soaking (Fig. 3.2) revealed some interesting findings. Firstly, dissolved concentrations and their sum remained practically the same for HnBs before and after operation (Σ_5PAH = 61.38 ± 1.79 ng unit^{-1} and Σ_5PAH = 70.87 ± 7.67 ng unit^{-1} in unused and used HnBs respectively). This indicates that the operation of HnBs did not generate

additional amounts of PAHs nor affect their leaching behavior. Among the detected PAHs, Nap was found to be the most abundant, which is consistent with the higher total Nap concentrations in the corresponding solid products, and its high water solubility value (Mulder et al., 2000). Calculations of the percentage ratios of dissolved Nap concentrations to the corresponding total concentrations in the solid product yielded values of ~210% and 170% for unused and used HnBs, respectively. For the rest of PAHs, the percentage ratios remained below 25%. The observed deviations for Nap were attributed to the use of HnBs from different packs purchased at different times and it was concluded that total amount of Nap present in the solid product became bioavailable.

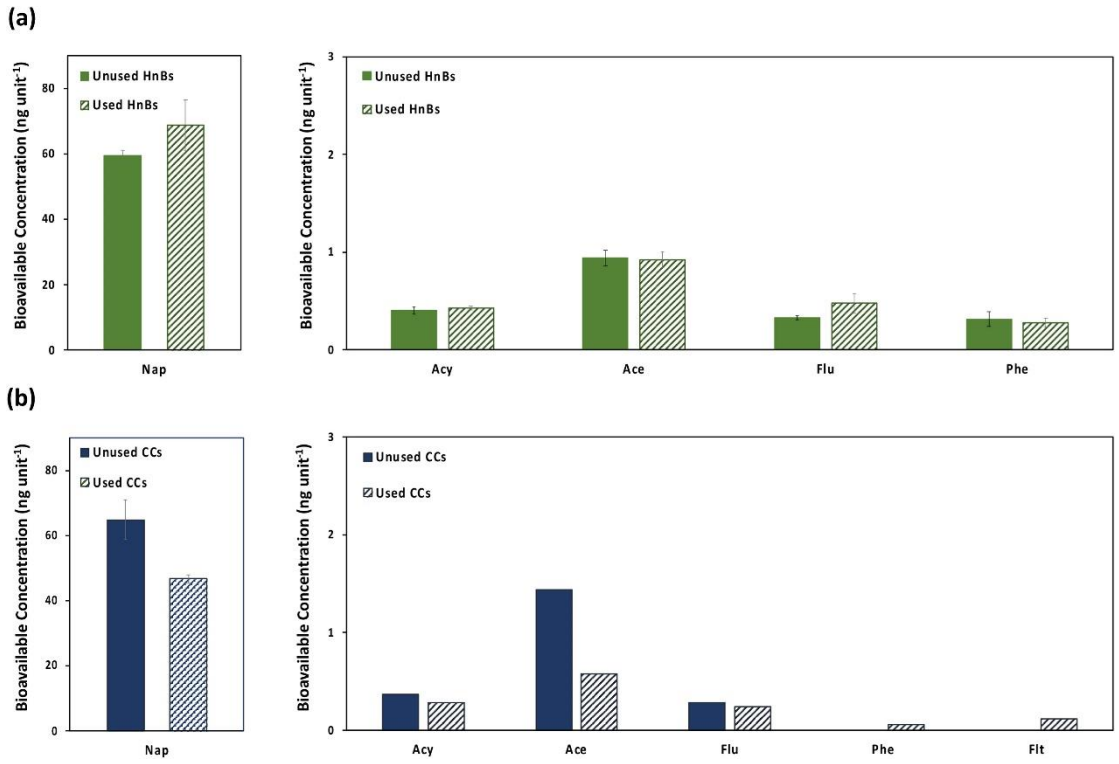

Fig. 3.2 Bioavailable PAH concentrations in leachates from unused and used (a) HnBs and (b) CCs.

The dissolved concentrations obtained from CCs are given in Fig. 3.2(b), and show that after smoking, CCs could leach a larger number of PAHs but the sum of their individual concentrations was of the same magnitude as the one from unused cigarettes (Σ_4PAH = 66.92 ± 5.95 ng unit^{-1} in unused CCs and Σ_6PAH = 47.94 ± 1.26 ng unit^{-1} in smoked CCs) and the ones from both unused and operated HnBs. Moreover, in

accordance with a past report by Dobaradaran et al. (2020), Nap was the most abundant PAH leaching into water from CCs. The percentage ratios of dissolved concentrations to the corresponding total concentration in unused CCs yielded a value close to 130% for Nap, and for the rest, calculated ratios were below 17%. In smoked CCs, the percentage ratio of Nap leaching into water dropped to ∼5% and for the remaining PAHs, it was below 1%. This drop in percentage ratios recorded after operating CCs suggested that under the tested conditions, smoking affected the leaching behavior of PAHs and potentially delayed their desorption. Considering the large total PAH concentrations found earlier in smoked CCs and the delayed desorption of heavier PAHs from cigarette butts reported in the literature (Dobaradaran et al., 2020), smoked CCs have the potential to act as a source of long-term PAHs contamination once exposed to water.

3.4.3. EFFECT OF PH, IONIC STRENGTH, HUMIC ACIDS AND LEACHING IN NATURAL WATER

The composition and properties of the solid waste and the water phase used for leaching may affect leachability of organics from a solid matrix (Kim and Osako, 2003). In the past, the leaching concentrations of Phe and Py from sandy soil was found to be independent of pH level of the solution (Kim and Osako, 2003). In another study using man-made soil spiked with PAHs among others, the slightly higher mobilization caused by elution at pH = 10 was assumed to be due to the activation of humic substances indigenous to the solid sample under alkaline conditions (Hirner et al., 1998). Similarly, PAHs sorbed on solids were found to be more mobile at high pH (pH = 12.4) than at neutral pH (Mulder et al., 2000) when a clay modifier was added. To study the effect of pH on the leaching behavior of PAHs, the pH level of the water phase used for leaching was adjusted to 4, 6 and 8 and the results are given in Tables S.6 and S.7 in the Appendix 2 for HnBs and for CCs, respectively. As seen, leaching concentrations were found to be practically independent of the pH level and any deviations were related to the use of different packs of tobacco products, and the error associated to the determination of these low concentrations.

In general, dissolved inorganic salts may affect aqueous solubilities and activity coefficients of organic compounds. To this end, it has been reported that the presence

of the predominant inorganic ionic species found in natural waters has the potential to decrease the aqueous solubility (or increase the aqueous activity coefficient) of nonpolar or weakly polar organic compounds, (Schwarzenbach et al., 2003). The effect of salt was investigated here by adjusting the ionic strength of the water solution to 3.5% w:v NaCl, a value representing the salt content of seawater. The results from these studies are also given in Table S.6 and S.7 in the Appendix 2 for HnBs and for CCs, respectively. As seen, increasing the ionic strength of the soaking solution did not affect considerably the leaching of PAHs from used and unused tobacco products. To the best of our knowledge there are no reports studying the effect of salt on the leachability of PAHs from tobacco products and any comparison can only be made to leaching tests from other solid matrices. In this connection, the distribution coefficients of Py in estuaries and coastal sediments were previously found to increase with increased salinity (Means, 1995; Oh et al., 2013; Turner, 2003). Moreover, in a study investigating partitioning of PAHs with coastal sediments, salinity was found to increase the sorbed capacity of PAHs and their desorption-resistance due to the "salting out effect" (Oh et al., 2013). Finally, investigations on the leaching behavior of Phe from sandy soil showed increased leaching concentrations with increasing ionic strength up to 0.005 M, and after this point leachability decreased (Kim and Osako, 2003).

Humic acids are considered to be a natural solubilizing agent that mobilize significant higher amounts than distilled water (Hirner et al., 1998). At the same time, humic acids exhibit a high affinity for PAHs and after association, PAHs bioavailability is minimized (Schwarzenbach et al., 2003). To investigate the effect of humic acids, unused and used tobacco products were soaked for 24 h in solutions containing 2.5 mg L^{-1} of humic acids, an environmentally relevant value for natural organic matter. The results from these studies (Table S.6 for HnBs and S.7 for CCs) showed practically no effect of humic acids on the leaching behavior of PAHs.

In a final set of experiments, sample of river water, seawater and rainwater were utilized for leaching. The results for HnBs are provided in Table 3.2, while Table S.8 in the Appendix 2 presents the results for CCs. It can be observed that the concentrations of dissolved PAHs in the various water types were not substantially different to those obtained with ultrapure water. This finding is consistent with a previous report studying PAHs leaching in tap and river water from smoked CCs

(Dobaradaran et al., 2020), where the authors also found no substantial differences in the dissolved concentrations of PAHs between the two water types when compared to the leaching behavior in deionized water.

Table 3.2 Dissolved concentrations in natural water samples (river water, rainwater, and seawater) from unused and used HnBs at 24 h of soaking time. Error values correspond to the standard deviation of three replicated analyses.

HnBs UNUSED (ng unit^{-1})

	RIVER WATER	RAINWATER	SEA WATER
Nap	103.08 ± 2.96	94.63 ± 10.67	73.76 ± 10.5
Acy	0.71 ± 0.1	0.64 ± 0	0.51 ± 0.23
Ace	2.19 ± 0.28	2.54 ± 0.29	2.49 ± 0.49
Flu	0.55 ± 0.12	0.44 ± 0.01	0.56 ± 0.03
Phe	1.4 ± 0.11	0.75 ± 0.08	0.84 ± 0.09
SUM	107.92 ± 2.98	99 ± 10.67	78.16 ± 10.52

HnBs USED (ng unit^{-1})

	RIVER WATER	RAINWATER	SEA WATER
Nap	73.29 ± 7.93	79.75 ± 0.8	51.09 ± 5.48
Acy	0.43 ± 0.1	0.48 ± 0.05	0.36 ± 0.02
Ace	1.94 ± 0.18	1.98 ± 0.13	1.69 ± 0.6
Flu	0.35 ± 0.03	0.89 ± 0.01	0.58 ± 0.06
Phe	1.19 ± 0.19	0.59 ± 0.04	0.57 ± 0.03
SUM	77.19 ± 7.94	83.69 ± 0.82	54.29 ± 5.51

3.5. CONCLUSION

The present studies addressed the knowledge gap on the total and bioavailable PAHs concentrations in HnBs tobacco products and compared the results to those obtained with CCs. It has been experimentally verified that the non-combustible HnBs have substantially lower total PAHs concentrations compared to smoked CCs. Tobacco and filter were the most contaminated parts in HnBs before after operation. In contrast, CCs operation generated substantial amounts of PAHs that mainly resided in the spent filter of the cigarette butts. Despite the high total PAH concentrations found in smoked CCs,

the sums of the bioavailable PAH concentrations were found practically the same in all tested tobacco products, presumably because smoking affected PAHs' leachability from CCs and delayed their desorption from the solid matrix. This finding is of concern as it may imply that improperly discarded CCs can act as point sources of long-term PAHs contamination. Furthermore, evidence was provided that the composition of the water phase does not affect the leaching of PAHs.

Numerous factors act together and impact the leachability of contaminants when a solid waste is exposed to water. It is challenging to encompass all possible scenarios in a laboratory-based experiment. In batch tests and depending on the L/S and leaching time applied, larger quantities of contaminants may be leached, which may not be a good approximation of the leaching process under real environmental settings. Therefore, extrapolating the present results to evaluate the annual release of PAHs based on the global number of CCs littered may not provide a realistic perspective of the problem. Instead, such an approach runs the risk to overlook the complexity of this problem and "connect" the critical issue of tobacco product waste to a single group of pollutants.

Applying targeted analysis may be a reasonable approach for risk assessment. However, in the case of complex samples, the presence of targeted organics does not always imply that these pollutants are the sole source of toxicity. Future research should consider utilizing comprehensive two-dimensional gas chromatography (GC × GC), an advanced analytical tool that enables enhanced separations of complex mixtures. Our ongoing and future investigations are focused on utilizing this approach with the aim of bringing new insights on this current global environmental issue.

One of the aims of the present studies was to increase the public perception of tobacco product waste as a significant global issue resulting from improper litter disposal. Insufficient attention has been given to tobacco product waste, perpetuating the false perception that discarded tobacco products are the end point of their lifecycle. Public education campaigns and raising of public awareness are urgently needed to promote proper disposal practices and change current attitudes and behaviors towards this waste. Tobacco product waste can leach toxic chemicals into aquatic ecosystems and the non-biodegradable filters are a known source of microplastic fibers (Shen et al., 2021). Therefore, it is crucial to intensify research efforts on characterizing, managing, recycling and disposing the tobacco product waste (Conradi and Sánchez-Moyano,

2022). Current solutions are still at early stages of development, limited in number, and lack sustainability (Conradi and Sánchez-Moyano, 2022; Marinello et al., 2020). Identifying the best methodological solutions and technologies for recycling this waste as well as testing applicability in real-life scenarios should be a priority. This will ensure ecosystem safety and support the transition towards a circular economy and sustainability.

3.6. REFERENCES

Alberti, S., Sotiropoulou, M., Fernández, E., Solomou, N., Ferretti, M., Psillakis, E., 2021. UV-254 degradation of nicotine in natural waters and leachates produced from cigarette butts and heat-not-burn tobacco products. *Environmental Research*, 194, 110695. https://doi.org/10.1016/j.envres.2020.110695.

Araújo, M.C.B., Costa, M.F., 2019. A critical review of the issue of cigarette butt pollution in coastal environments. *Environmental Research*, 172, 137–149. https://doi.org/10.1016/j.envres.2019.02.005.

Baran, W., Madej-Knysak, D., Sobczak, A., Adamek, E., 2020. The influence of waste from electronic cigarettes, conventional cigarettes and heat-not-burn tobacco products on microorganisms. *Journal of Hazardous Materials*, 385, 121591. https://doi.org/10.1016/j.jhazmat.2019.121591.

Bentley, H.R., Burgan, J.G., 1960. Polynuclear hydrocarbons in tobacco and tobacco smoke. Part II. The origin of 3:4-benzopyrene found in tobacco and tobacco smoke. *Analyst*, 85, 474 723–727. https://doi.org/10.1039/AN9608500723.

Beutel, M.W., Harmon, T.C., Novotny, T.E., Mock, J., Gilmore, M.E., Hart, S.C., Traina, S., Duttagupta, S., Brooks, A., Jerde, C.L., Hoh, E., Van De Werfhorst, L.C., Butsic, V., Wartenberg, A.C., Holden, P.A., 2021. A review of environmental pollution from the use and disposal of cigarettes and electronic cigarettes: Contaminants, sources, and impacts. *Sustainability*, 13, 1–25. https://doi.org/10.3390/su132312994.

Booth, D.J., Gribben, P., Parkinson, K., 2015. Impact of cigarette butt leachate on tidepool snails. *Marine Pollution Bulletin*, 95, 362–364. https://doi.org/10.1016/j.marpolbul.2015.04.004.

Conradi, M., Sánchez-Moyano, J.E., 2022. Toward a sustainable circular economy for cigarette butts, the most common waste worldwide on the coast. *Science of the Total Environment,* 847, 157634. https://doi.org/https://doi.org/10.1016/j.scitotenv.2022.157634.

De Fenzo, A., Giordano, M., Sansone, L., 2020. A clean process for obtaining high-quality cellulose acetate from cigarette butts. *Materials (Basel),* 13, 1–13. https://doi.org/10.3390/ma13214710.

Dobaradaran, S., Schmidt, T.C., Lorenzo-Parodi, N., Jochmann, M.A., Nabipour, I., Raeisi, A., Stojanović, N., Mahmoodi, M., 2019. Cigarette butts: An overlooked source of PAHs in the environment? *Environmental Pollution,* 249, 932–939. https://doi.org/10.1016/j.envpol.2019.03.097.

Dobaradaran, S., Schmidt, T.C., Lorenzo-Parodi, N., Kaziur-Cegla, W., Jochmann, M.A., Nabipour, I., Lutze, H. V., Telgheder, U., 2020. Polycyclic aromatic hydrocarbons (PAHs) leachates from cigarette butts into water. *Environmental Pollution*, 259, 113916. https://doi.org/10.1016/j.envpol.2020.113916.

European Commission, 2019. Directive (EU) 2019/904 of the European Parliament and the Council on the reduction of the impact of certain plastic products on the environment, O.J. L 155, 12 June 2019.

European Commission, 2013. Directive 2013/39/EU of the European Parliament and of the Council of 12 August 2013 Amending Directives 2000/60/EC and 2008/105/EC as Regards Priority Substances in the Field of Water Policy, O.J. L 226, 24 August 2013.

Hirner, A. V., Pestke, F.M., Busche, U., Eckelhoff, A., 1998. Testing contaminant mobility in soils and waste materials. *Journal of Geochemical Exploration*, 64, 127–132. https://doi.org/10.1016/S0375-6742(98)00025-9.

Karkanorachaki, K., Kiparissis, S., Kalogerakis, G.C., Yiantzi, E., Psillakis, E., Kalogerakis, N., 2018. Plastic pellets, meso- and microplastics on the coastline of Northern Crete: Distribution and organic pollution. *Marine Pollution Bulletin,* 133. https://doi.org/10.1016/j.marpolbul.2018.06.011.

Kim, Y., Osako, M., 2003. Leaching characteristics of polycyclic aromatic hydrocarbons (PAHs) from spiked sandy soil. *Chemosphere*, 51, 387–395. https://doi.org/10.1016/S0045-6535(02)00866-4.

King, I.C., Lorenzi, V., Blasius, M.E., Gossett, R., 2021. Leachates from Cigarette Butts Can Persist in Marine Sediment. *Water, Air, & Soil Pollution*, 232, 38. https://doi.org/10.1007/s11270-021-04999-3.

Koutela, N., Fernández, E., Saru, M.-L., Psillakis, E., 2020. A comprehensive study on the leaching of metals from heated tobacco sticks and cigarettes in water and natural waters. *Science of the Total Environment*, 714, 136700. https://doi.org/10.1016/j.scitotenv.2020.136700.

Kremser, A., Jochmann, M.A., Schmidt, T.C., 2016. PAL SPME Arrow—evaluation of a novel solid-phase microextraction device for freely dissolved PAHs in water. *Analytical and Bioanalytical Chemistry*, 408, 943–952. https://doi.org/10.1007/s00216-015-9187-z.

Kumar, M., Bolan, N.S., Hoang, S.A., Sawarkar, A.D., Jasemizad, T., Gao, B., Keerthanan, S., Padhye, L.P., Singh, L., Kumar, S., Vithanage, M., Li, Y., Zhang, M., Kirkham, M.B., Vinu, A., Rinklebe, J., 2021. Remediation of soils and sediments polluted with polycyclic aromatic hydrocarbons: To immobilize, mobilize, or degrade? *Journal of Hazardous Materials*, 420, 126534. https://doi.org/10.1016/j.jhazmat.2021.126534.

Lee, W., Lee, C.C., 2015. Developmental toxicity of cigarette butts – An underdeveloped issue. *Ecotoxicology and Environmental Safety*, 113, 362–368. https://doi.org/10.1016/j.ecoenv.2014.12.018.

Marah, M., Novotny, T.E., 2011. Geographic patterns of cigarette butt waste in the urban environment. *Tobacco Control*, 20, 42–44. https://doi.org/10.1136/tc.2010.042424.

Marinello, S., Lolli, F., Gamberini, R., Rimini, B., 2020. A second life for cigarette butts? A review of recycling solutions. *Journal of Hazardous Materials*, 384, 121245. https://doi.org/10.1016/j.jhazmat.2019.121245.

Means, J.C., 1995. Influence of salinity upon sediment-water partitioning of aromatic hydrocarbons. *Marine Chemistry*, 51, 3–16. https://doi.org/10.1016/0304-4203(95)00043-Q.

Micevska, T., Warne, M.S.J., Pablo, F., Patra, R., 2006. Variation in, and Causes of, Toxicity of Cigarette Butts to a Cladoceran and Microtox. *Archives of Environmental Contamination and Toxicology*, 50, 205–212. https://doi.org/10.1007/s00244-004-0132-y.

Moriwaki, H., Kitajima, S., Katahira, K., 2009. Waste on the roadside, "poi-sute" waste: Its distribution and elution potential of pollutants into environment. *Waste Management*, 29, 1192–1197. https://doi.org/10.1016/j.wasman.2008.08.017.

Mulder, E., Brouwer, J.P., Blaakmeer, J., Frénay, J.W., 2000. Immobilisation of PAH in waste materials. *Waste Management*, 1, 953–962. https://doi.org/10.1016/S0713-544 2743(00)80103-8.

Ocean conservancy-International Coastal Cleanup, 2021. Cleanup Report for 2021 (https://oceanconservancy.org/).

Oh, S., Wang, Q., Shin, W.S., Song, D.I., 2013. Effect of salting out on the desorption548 resistance of polycyclic aromatic hydrocarbons (PAHs) in coastal sediment. *Chemical Engineering Journal*, 225, 84–92. https://doi.org/10.1016/j.cej.2013.03.069.

Parker, T.T., Rayburn, J., 2017. A comparison of electronic and traditional cigarette butt leachate on the development of Xenopus laevis embryos. *Toxicology Reports*, 4, 77–82. https://doi.org/10.1016/j.toxrep.2017.01.003

Paschke, M., Hutzler, C., Brinkmann, J., Henkler, F., Luch, A., 2015. Polycyclic Aromatic Hydrocarbons in Newspaper Inks: Migration, Metabolism, and Genotoxicity in Human Skin. *Polycyclic Aromatic Compounds*, 35, 32–40. https://doi.org/10.1080/10406638.2014.900643.

Schwarzenbach, R.P., Gschwend, P.M., Imboden, D.M., 2003. Environmental Organic Chemistry, Second Edition. John Wiley & Sons Inc, Hoboken, New Jersey.

Shen, M., Li, Y., Song, B., Zhou, C., Gong, J., Zeng, G., 2021. Smoked cigarette butts: Unignorable source for environmental microplastic fibers. *Science of the Total*

Environment, 791, 148384. https://doi.org/https://doi.org/10.1016/j.scitotenv.2021.148384.

Shimazu, H., 2016. Determination of Polycyclic Aromatic Hydrocarbons in Cigarettes and Cigarette Smoke. *Environmental Pollution*, 5, 15. https://doi.org/10.5539/ep.v5n2p15.

Shimazu, H., Yata, T., Ozaki, N., 2018. Characteristics of polycyclic aromatic hydrocarbon formation during smoking. *International Journal of GEOMATE*, 14, 120–127. https://doi.org/10.21660/2018.42.88568.

Slaughter, E., Gersberg, R.M., Watanabe, K., Rudolph, J., Stransky, C., Novotny, T.E., 2011. Toxicity of cigarette butts, and their chemical components, to marine and freshwater fish. *Tobacco Control*, 20, 25–29. https://doi.org/10.1136/tc.2010.040170.

Soleimani, F., Dobaradaran, S., De-la-Torre, G.E., Schmidt, T.C., Saeedi, R., 2022. Content of toxic components of cigarette, cigarette smoke vs cigarette butts: A comprehensive systematic review. *Science of the Total Environment*, 813, 152667. https://doi.org/10.1016/j.scitotenv.2021.152667.

Soleimani, F., Dobaradaran, S., Vazirizadeh, A., Mohebbi, G., Ramavandi, B., De-la-Torre, G.E., Nabipour, I., Schmidt, T.C., Novotny, T.E., Maryamabadi, A., Kordrostami, Z., 2023. Chemical contents and toxicity of cigarette butts leachates in aquatic environment: A case study from the Persian Gulf region. *Chemosphere*, 311, 137049. https://doi.org/10.1016/j.chemosphere.2022.137049.

Turner, A., 2003. Salting out of chemicals in estuaries: Implications for contaminant partitioning and modelling. *Science of the Total Environment*, 314–316, 599–612. https://doi.org/10.1016/S0048-9697(03)00076-7.

Vu, A.T., Taylor, K.M., Holman, M.R., Ding, Y.S., Hearn, B., Watson, C.H., 2015. Polycyclic Aromatic Hydrocarbons in the Mainstream Smoke of Popular U.S. Cigarettes. *Chemical Research in Toxicology*, 28, 1616–1626. https://doi.org/10.1021/acs.chemrestox.5b00190.

Yang, X., Yu, L., Chen, Z., Xu, M., 2016. Bioavailability of Polycyclic Aromatic Hydrocarbons and their Potential Application in Eco-risk Assessment and Source

Apportionment in Urban River Sediment. *Scientific Reports*, 6, 1–9. https://doi.org/10.1038/srep23134.

Zafeiridou, M., Hopkinson, N.S., Voulvoulis, N., (2018). Cigarette Smoking: An Assessment of Tobacco's Global Environmental Footprint Across Its Entire Supply Chain. *Environmental Science & Technology*, 52, 8087–8094. https://doi.org/10.1021/acs.est.8b01533.

CHAPTER 4: UV-254 DEGRADATION OF NICOTINE IN NATURAL WATERS AND LEACHATES PRODUCED FROM CIGARETTE BUTTS AND HEAT-NOT-BURN TOBACCO PRODUCTS

Alberti, S., Sotiropoulou, M., Fernández, E., Solomou, N., Ferretti, M., Psillakis, E. (2021). UV-254 degradation of nicotine in natural waters and leachates produced from cigarette butts and heat-not-burn tobacco products. Environmental Research, 110695.

Credit author statement

S. Alberti: Investigation, Visualization, Writing – original draft. M. Sotiropoulou: Investigation. E. Fernández: Investigation, Visualization, Validation, N. Solomou: Formal analysis. M. Ferretti: Writing – review & editing. E. Psillakis: Conceptualization, Funding acquisition, Supervision, Visualization, Writing – review & editing

4.1. ABSTRACT

Nicotine is an important emerging contaminant widely detected in water resources. The main nicotine sources are human excretions from users and leaching from discarded tobacco product waste, which represents the most commonly littered item in urban areas and coasts. In this study, the UV_{254} photolytical fate of nicotine in natural water and leachates produced from conventional cigarettes (CCs) and the new generation heat-not-burn (HnBs) tobacco products is examined for the first time. The effect of UV_{254} irradiation on nicotine depletion in ultrapure water was initially studied. The reaction was pseudo first-order with respect to nicotine concentration at low concentrations and shifted to lower order at higher concentrations, an effect associated to absorption saturation. Although nicotine removal was fast, only 9.5% of the total organic carbon was removed after irradiation due to the formation of by-products. The chemical structures of six photo-products were derived by means of liquid and gas chromatography coupled to mass spectrometry. The photodegradation kinetics was found to depend on pH and faster kinetics were recorded when the monoprotonated form of nicotine was dominant (pH = 5–8). The presence of humic acids was found to slightly delay kinetics as they competed with nicotine for lamp irradiance, whereas the presence of salt had no effect on the direct photolysis of nicotine. Direct photolysis studies were also performed using natural waters. Compared to ultra-pure water, photodegradation was found to proceed slightly slower in river water, in similar kinetics in seawater, and relatively faster in rain water. The later was assumed to be due to the lower pH compared to the rest of the natural water tested. Leachates from used HnBs and smoked CCs were also submitted to UV_{254} irradiation and direct photolysis was found to proceed fast despite the high complexity of these matrices. Nonetheless, the total organic carbon in the system remained the same after irradiation due to the abundance of organics and photo-products formed. We take advantage of the present investigations and report the leaching behavior of nicotine from HnBs and CCs. Among others, we found that in HnBs ~70% of the total and bioavailable nicotine content remains in the tobacco sticks after operation and this percentage drops to 15% in CCs due to the reduction in mass after smoking. This finding demonstrated the importance of properly disposing tobacco product waste to prevent nicotine leaching in water bodies.

4.2. INTRODUCTION

Nicotine is a toxic alkaloid found in the tobacco plant (lethal dose for adults is 60 mg (Mayer, 2014)) and the most important component in tobacco products (Buerge et al., 2008). The vast consumption of tobacco products resulted in the widespread nicotine contamination in surface water, wastewater (Buerge et al., 2008; Gonzalez Alonso et al., 2012; Roder Green et al., 2014) and bottled mineral water (Gonzalez Alonso et al., 2012), and the classification of nicotine as an important emerging pollutant (de Granda-Orive et al., 2018; Oropesa et al., 2017). Once consumed, nicotine is extensively metabolized in the human liver by oxidative enzymatic transformations to a number of compounds, and excreted, mostly in the urine, as a complex mixture of the parent compound and its transformation products (Senta et al., 2015). In this connection, nicotine is frequently detected in wastewaters at a $\mu g\ L^{-1}$ concentration level, and together with its derivatives are used as anthropogenic markers for urban wastewater contamination and for the assessment of population size and dynamics (Buerge et al., 2008; Huerta-Fontela et al., 2008; Senta et al., 2015). Next to wastewater discharges, another important source of nicotine contamination is leaching from smoked cigarette butts (Oropesa et al., 2017; Roder Green et al., 2014). Indeed, the majority of the 16 billion cigarettes consumed daily are being thrown away rather than properly disposed in receptables (Roder Green et al., 2014). This makes cigarette butts the most widespread and numerous littered item found in urban areas and coasts (Araújo and Costa, 2019; Dobaradaran et al., 2020; Marah and Novotny, 2011; Roder Green et al., 2014; Torkashvand et al., 2020). Today, there is conclusive evidence that when this type of waste comes into contact with water, a number of inorganic (Cardoso et al., 2018; Chevalier et al., 2018; Koutela et al., 2020; Moerman and Potts, 2011; Moriwaki et al., 2009) and organic (Dobaradaran et al, 2019, 2020) compounds, including nicotine (Roder Green et al., 2014), are leached and become bioavailable to aquatic life (Cardoso et al., 2018; Chevalier et al., 2018; Dobaradaran et al., 2020; Koutela et al., 2020; Moerman and Potts, 2011; Moriwaki et al., 2009; Roder Green et al., 2014).

The heat-not-burn (HnBs) tobacco products were recently developed to provide the user with nicotine by heating specially designed tobacco sticks at 350 ◦C, well below the temperature required in conventional cigarettes (CCs) for initiating combustion (Schaller et al., 2016). Today, HnBs represent the new generation of tobacco products

and a fast-expanding market. However, there is a justified fear that improperly disposed HnBs may also have a negative environmental impact through leaching of its chemical components (Baran et al., 2020; Koutela et al., 2020). Although the release of nicotine from CCs has been reported in the past (Roder Green et al., 2014), there are no relevant studies for HnBs. This is of particular importance since in HnBs there is no mass reduction after operation (as seen in CCs where ash is produced during smoking) and as such, HnBs have the potential to release larger amounts of nicotine in water bodies when improperly discarded in the environment.

The transformation of organics (including nicotine) in water is a complex process, and includes biotic and abiotic transformation reactions (Lian et al., 2017; Medana et al., 2016; Passananti et al., 2014). In particular, photochemical reactions may be a major abiotic transformation pathway and can take place via direct and indirect photolysis mechanisms (Carena et al., 2020). Direct photolysis refers to the transformation of a molecule upon direct light absorption, i.e. the parent compound absorbs irradiation, reach excited molecular states and then undergo chemical transformation (Katagi, 2018). The direct photolysis of a molecule can be inhibited by competitive light-absorbing compounds, including the dissolved organic matter (DOM) that naturally occurs in surface waters (Carena et al., 2020). At the same time, DOM (and/or NO_3^-) may also act as photosensitizers and trigger the indirect photodegradation of water pollutants with photogenerated reactive oxygen species (Katagi, 2018). Nicotine was previously reported to undergo direct and indirect photolysis at different rates, depending on the conditions (Nienow et al., 2009; Passananti et al., 2014). In particular, indirect photodegradation was found to play a key role in sunlit surface waters (Passananti et al., 2014) and wastewaters (Lian et al., 2017). These studies concluded that nicotine transformation under simulated solar irradiation followed a pseudo-first-order rate reaction (Lian et al., 2017; Passananti et al., 2014), and showed that direct photolysis was non-significant due to the small overlap of the ultraviolet–visible spectrum between nicotine and solar irradiation. In another report, the indirect photolysis of nicotine was investigated in the presence of different naturally occurring photochemical sources of HO• and of nitrogen-centered radicals (Passananti et al., 2014). The second-order kinetic constants of nicotine with HO• and $^1O_2$ were determined, and allowed predicting environmental half-life times for such reactions as a function of the water chemistry and depth. In the same report, modelling studies

showed that the photochemical half-life of nicotine would vary in the month-year range depending on the environmental conditions. The indirect photolysis of aqueous nicotine in ultra-pure water at $\lambda = 254$ nm has also been reported within the frame of reporting a new H_2O_2-enhanced photodegradation process (Nienow et al., 2009). In this study, a preliminary set of experiments monitored the direct photolysis of nicotine in the absence of H_2O_2 and reported a fast nicotine degradation rate under UV_{254}. Based on the published results so far, there is no in-depth study on the direct photolysis of nicotine in aqueous solutions and natural waters; a knowledge indispensable for evaluating the basic photochemistry of nicotine in the aquatic environment. It is equally important that there are no reports studying the photolysis of nicotine in leachates produced from tobacco products, an important type of waste that represents a major nicotine source in the aquatic environment.

The aim of this work was to study for the first time the photolysis of nicotine in natural waters and water leachates produced from CCs and the new generation HnBs tobacco products. Initially, water samples spiked with nicotine were irradiated by UV_{254}, degradation rates were recorded and the reaction mechanisms were investigated. The effects of different experimental parameters (pH, effect of salt and humic acids) were then studied in separate sets of experiments. Building on this knowledge, the effect of matrix on nicotine photolysis fate was studied using natural water as leachant (rain, seawater and river water). Finally, the photodegradation of nicotine by UV_{254} was monitored in highly complex leachates produced from used HnBs and smoked CCs, yielding new knowledge on the fate of nicotine under a more realistic scenario.

4.3. MATERIALS AND METHODS

4.3.1. CHEMICALS AND NATURAL WATER SAMPLES

(-) Nicotine PESTANAL® was purchased from Supelco (Bellefonte, USA). Acetonitrile for LC/MS was obtained from Carlo Erba Reagents (Sabadell, Spain) and formic acid from Fluka Chemie GmbH (Bucks, Switzerland). Sodium chloride (99.9% purity), humic acid, ammonium acetate (≥90%; purity) and tert-butanol (≥99% purity) from Fisher Scientific UK Ltd (Loughborough, UK). Acetic acid (100% anhydrous GR for analysis) and boric acid (99.8% purity) were supplied by Merck KGaA (Darmstadt,

Germany), potassium phosphate dibasic trihydrate (≥99.0% purity) from Sigma-Aldrich (Steinheim, Germany), and sodium acetate trihydrate (≥99.5%) and potassium dihydrogen phosphate (≥99.5% purity) from Fluka Chemie GmbH. A basic 20+ pH meter from Crison (Alella, Spain) was used to measure the pH. A single-beam UV–visible spectrophotometer (UVmini-240, Shimadzu, Tokyo Japan), equipped with quartz cuvettes having a 1 cm optical path length was used to measure spectra. Ultra-pure water was prepared in an EASYpure RF water purification system (Barnstead/Thermolyne Corporation, Dubuque, IA, USA).

The natural samples used here were: (i) river water sampled from the river Koiliaris at Kyani Akti (Kalyves, Crete, Greece); (ii) seawater sampled near the beach of Koum Kapi in Chania, Crete, Greece, and (iii) rainwater collected at the campus of the Technical University of Crete in Chania. The compositions of the natural water samples are given in Table S.9 – Appendix 3 in the Supporting Information. All samples were initially filtered, analyzed to ensure that they were free of nicotine, and then stored in the dark at 4 ◦C until use.

4.3.2. TOBACCO PRODUCTS AND THEIR LEACHATES

The HEETS Sienna Selection tobacco units were used to study HnBs and the Marlboro Red Label brand for studying CCs. Both tobacco products were purchased from the local distributor in Chania-Crete, Greece. Tobacco products were operated in a programmable single port machine-smoking from Burghart (Wedel, Germany) and the puffing parameters were set according to a published procedure (Koutela et al., 2020). For HnBs, the IQOS™ 2.4 Plus tobacco heating device (Philip Morris Products S.A., Neuchatel, Switzerland) was used for operation. The CCs were ignited using a flameless lighter and were smoked until a predefined butt length (length of the filter plus approximately 3 mm of the tobacco plug).

For the preparation of leachates, tobacco products were submerged and allowed to soak in deionized water for 24 h at room temperature, unless otherwise stated in the text. Leaching proceeded in 40 mL clear glass vials equipped with caps. An approximate 10 L kg^{-1} liquid-to-solid ratio was used, which, depending on the experiment, corresponded to: 4 unused HnBs, 4 used HnBs or 4 unused CCs soaked in 31 mL water and 10 smoked CCs in 25 mL of the aqueous phase. Freshly made leachates were used

for each experiment. Leachates were diluted using ultrapure water to a final 10 mg L^{-1} nicotine concentration and used for photolysis experiments.

The total organic carbon (TOC) content of leachates was measured on filtered suspensions using a TOC-5000 analyzer (Shimadzu, Kyoto, Japan; catalytic oxidation on Pt at 680 ◦C). The calibration was performed using standards of potassium phthalate.

The determination of the total and bioavailable nicotine concentrations in unused and used tobacco products and their leachates was based on a standard procedure using solvent extraction followed by gas chromatography-flame ionization detection (GC-FID) (World Health Organization (WHO), 2014). The experimental procedure is discussed in details in Section S.1 – Appendix 3 in the Supporting Information.

4.3.3. PHOTOLYSIS EXPERIMENTS

All UV_{254} irradiation experiments were performed in a home-made laboratory photoreactor (28 cm × 28 cm × 28 cm). The photoreactor was equipped with two 8 W low-pressure mercury lamps (Osram HNS 8 W G8T5) having a strong emission line at 254 nm and mounted on opposing sidewalls of the photoreactor and each one. The distance between each lamp and the quartz vial used in the experiments was set to 13 cm. The quartz vial was placed on top of a magnetic stirrer that was switched on during photolysis. In all photolysis experiments, 10 mL aqueous solution or leachate having a known nicotine concentration was placed in a tailor-made quartz vial (2.4 cm outer diameter × 2.0 cm inner diameter × 5.2 cm height) and submitted to UV irradiation for a preset time. The incident photon flux entering the solution (Io, given in E L^{-1} s^{-1}, where E = Einstein) was determined using H_2O_2 as a chemical actinometer (Kourounioti et al., 2019), and was found equal to Io =$(6.11 \pm 0.22) \times 10^{-6}$ E L^{-1} s^{-1}. All experiments were run in triplicates.

During the photolysis of nicotine containing ultrapure or natural water samples, 50 μL samples were removed at preset exposure times and used for liquid chromatography/mass spectrometry analysis (LC/ MS). The remaining sample solution was UV-irradiated until complete conversion of nicotine. Tobacco product leachates could not be directly injected in an analytical instrumentation. The analytical procedure used for these samples included a sample preparation step that used HiSorb sorbent units for the extraction of nicotine followed by thermodesorption gas chromatography-

ion trap mass spectrometry analysis (TDGC/ ITMS). The sample preparation procedure is discussed in details in Section 4.3.5 that follows. For tobacco product leachates, fresh solutions had to be irradiated for studying each exposure time, as, each time, 9 mL of the 10 mL irradiated solution had to be extracted and used for analysis.

For each set of experiments, dark tests were run in parallel by placing the samples inside the photoreactor with the lamps switched off. These tests confirmed that changes in the analytical signal were due to the action of photons alone.

4.3.4. LC/MS ANALYTICAL PROCEDURE USED FOR ULTRAPURE AND NATURAL WATER SPIKED SAMPLES

All analyses of nicotine containing ultrapure or natural water samples were carried out using an Agilent 1200 Series high-performance liquid chromatography system equipped with a binary pump, autosampler, degasser and thermostated column compartment coupled to a diode array detector (DAD), and an Agilent 6110 single quadrupole LC/ MS system equipped with a multimode ionization source. For analysis, 50 μL of the irradiated sample were added in 250 μL glass inserts placed in 2 mL glass autosampler vials equipped with septum caps, all purchased from Agilent (Palo Alto, USA). The injection volume was 20 μL. A Thermo-Electron Betasil C18 column (Waltham, MA, USA) of dimensions 2.1 mm ID × 100 mm length and 5 μm particle size was used for separation. The mobile phase consisted of solvent (A) ultrapure water containing 0.1% formic acid (v:v) and (B) acetonitrile containing 0.1% formic acid (v:v). The LC gradient method used was 2% B for the first 1 min, then linearly increased to 100% B in 10 min, held for 2 min, followed by a 0.5 min ramp to 2% B where it was held for the rest of the analysis. Column temperature was set to 30 ◦C and the flow rate of the mobile phase was 300 μL min^{-1}, while the total analysis time was 20 min. The MS conditions were: drying gas flow, 8 L min^{-1}; drying gas temperature, 250 ◦C; nebulizer pressure, 30 psi; collector capillary voltage, 4.0 kV; fragmentor voltage, 70 V; scan range (m/z) of 100–1000 amu for signal 1 and the scan range 160–165 amu was used for nicotine. The mass spectrometry data were recorded using the positive electrospray ionization (ESI) mode.

4.3.5. TD-GC/ITMS ANALYTICAL PROCEDURE USED FOR TOBACCO PRODUCT LEACHATES

The analyses of tobacco product leachates included a sample preparation step, where 9 mL of the irradiated solution were placed in 10 mL vials and capped with a HiSorb cap and septum (Markes International). A HiSorb unit having a 63 μL polydimethylsiloxane (PDMS) coating (Markes International) was introduced through the septum and the PDMS coating was immersed into the leachate. Extraction occurred for 60 min at 40 ^{o}C and 300 rpm using a HiSorb Agitator from Markes International. Once extraction was completed, the HiSorb unit was removed, washed to remove residual matrix, dried with a lint-free tissue, and inserted in a stainless-steel thermal desorption tube (Markes International) for analysis using TD-GC/ITMS.

450-GC coupled with a Varian 240-MS ITMS (Varian, Walnut Creek, CA, U.S.A.) and fitted with a TD100-xr™ (Markes Inetrnaitonal). HiSorb units were thermally desorbed at 250 ^{o}C for 5 min with a trap flow of 50 mL min^{-1}. Following desorption, the sample was collected on a 'General Purpose' cold trap at 30 ^{o}C. The cold trap was purged for 1 min at 50 mL min^{-1} and was sequentially desorbed for 3 min at 320 ^{o}C with a split flow of 10 mL min^{-1}. The flow path temperature was set at 150 ^{o}C. Separation of desorbed analytes proceeded on a MEGA-5 HT capillary column (30 m × 0.25 mm i.d., 0.25 μm film thickness; MEGA S.r.l., Legnano, Italy). The column was held at 50 ^{o}C for 5 min, increased to 160 ^{o}C at 10 ^{o}C min^{-1} rate, held for 2 min, and again ramped to 310 ^{o}C at a rate of 5 ^{o}C min^{-1} where it was held for 5 min. Helium (>99.99% pure) was used as a carrier gas at 1.1 mL min^{-1} flow-rate. Manifold, ion trap, ion source and transfer line temperatures were maintained at 45, 180, 200 and 220 ^{o}C, respectively. The detection and quantification of nicotine proceeded using selected ion storage at m/z = 161.

The above analytical procedure was also used to monitor the formation of by-products during the photolysis of 10 mg L^{-1} nicotine ultrapure water solutions. In this case, irradiated samples were extracted according to the procedure described above, the only difference being that the MS was set in the full scan mode from 50 to 500 m/z.

4.4. RESULTS AND DISCUSSION

4.4.1. EFFECT OF CONCENTRATION ON THE DIRECT PHOTOLYSIS OF NICOTINE

A past report studying the elution of nicotine from average cigarette butts in a simulated rainfall experiment, estimated nicotine concentrations in the run-off water to reach 0.62 mg L^{-1} with local concentrations as high as 11.4 mg L^{-1} (Roder Green et al., 2014). In the same report, batch experiments were also run representing the elution dynamic when cigarette butts come into contact with standing water, such as a lake or a river, but also puddles in street or sidewalk depressions caused by precipitation. The authors concluded that the total releasable nicotine concentration from CCs was released after 24 h of cigarette exposure to water, and was measured 7.1 mg g^{-1}, which is equivalent to 2.13 mg L^{-1} according to the experimental conditions set (Roder Green et al., 2014).

A series of photodegradation experiments were carried out for initial nicotine concentration varying from 1 to 20 mg L^{-1}, and the resulting concentration time profiles are given in Fig. 4.1. In all cases, the direct photolysis of nicotine was recorded until complete conversion, reflecting the good overlap between the 254 nm emission peak of the low pressure mercury lamps used here and the maximum absorption band of nicotine (~261 nm). To quantify degradation rates, a pseudo-first order kinetic expression with respect to nicotine concentration was considered by applying equation (OECD, 2008)

$$[NIC]_t = [NIC]_0 e^{-k_{NIC}\ t} \qquad (4.1)$$

where $[NIC]_0$ is the initial concentration of nicotine, $[NIC]_t$ is the concentration of nicotine at time t, and k_{NIC} is the pseudo first-order reaction rate. The inset graph (i) in Fig. 4.1 depicts the computed rate constants k_{NIC}, which took values of 0.50 (r^2 = 0.9991), 0.18 (r^2 = 0.9999), 0.10 (r^2 = 0.9949) and 0.05 (r^2 = 0.9896) min^{-1} (r^2 is the regression coefficient) at respectively, 1, 5, 10 and 20 mg L^{-1} $[NIC]_0$. As seen, k_{NIC} decreased with increasing initial nicotine concentration, implying that the reaction kinetics did not follow a true first order (where the rate constant is independent of the nicotine concentration), and shifted towards zeroth order at higher $[NIC]_0$ due to absorption saturation (Kourounioti et al., 2019). The initial nicotine photodegradation

rates (R^0_{NIC}) were then calculated using the simple pseudo-first order approximation $R^0_{NIC} = k_{NIC}[NIC]_0$ (Braslavsky, 2007). The resulting R^0_{NIC} vs $[NIC]_0$ profile (inset graph (ii) in Fig. 4.1) showed an increase followed by a plateau. The cause of this plateau trend in direct photolysis is usually absorption saturation, confirming that nicotine absorbed radiation and became photolyzed up to saturation (Kourounioti et al., 2019).

In general, the photolytical degradation mechanism of nicotine is a complex process and past reports investigated the reactions involved during indirect photolysis of the parent compound (Lian et al., 2017; Medana et al., 2016; Passananti et al., 2014). Here, exposing aqueous solutions of nicotine to UV_{254} irradiation afforded the photo-transformation of the parent compound to different photoproducts. The amount of organics remaining in the system after treatment was evaluated by measuring the TOC of a 10 mg L^{-1} nicotine solution before and after 30 min of UV_{254} exposure. Although nicotine removal was almost complete after this irradiation time, only a 9.5% TOC removal was recorded.

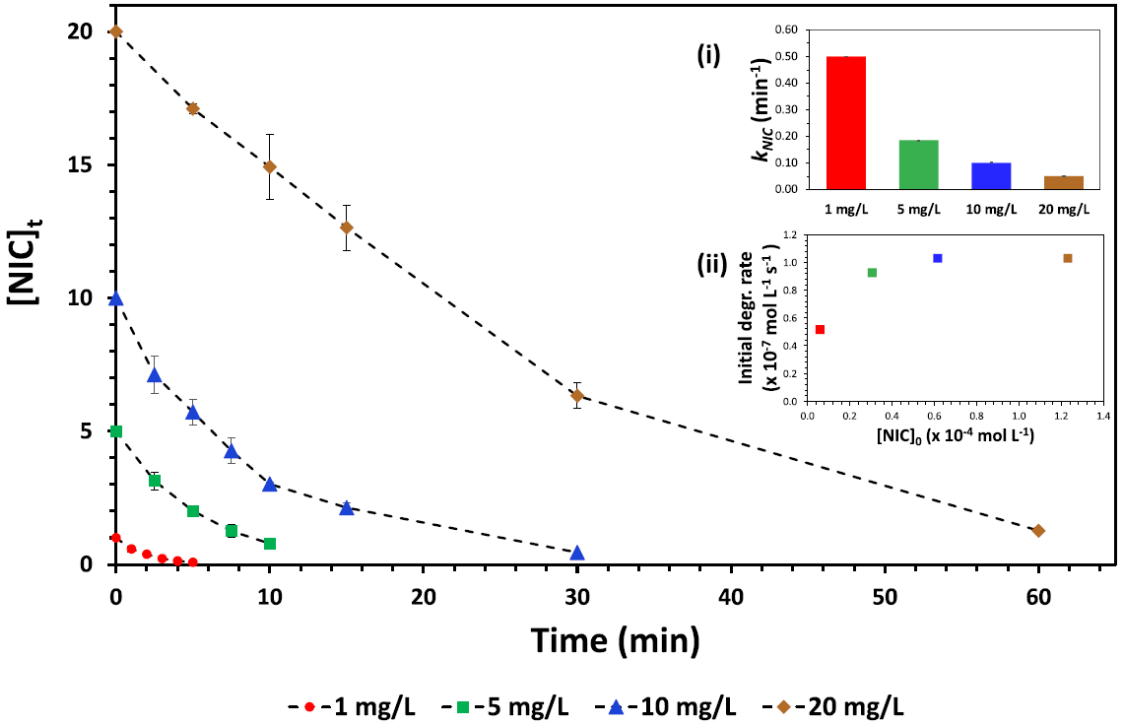

Fig. 4.1 Effect of concentration on the UV254-induced photolysis of nicotine in ultrapure water. Inset graphs: (i) apparent rate constants for each concentration tested and (ii) initial nicotine degradation rates as a function of concentration. Data points are linked with dashed lines to visualize trends. Some error bars are too small to be visible.

This observation pointed towards the formation of degradation products at different rates during irradiation that were more recalcitrant than the parent compound. Indeed, several photo-products eluted during LC/MS analysis, but not all of them could be identified either because they consisted of isomers or because they co-eluted with other by-products. To increase the number of identified photo-products, irradiated samples were also analyzed using the TD-GC/ITMS analytical procedure. The summary of these investigations is given in Table S.10 in the Appendix 3 of the Supporting Information. During TD-GC/ITMS analysis, the formation of 3-ethenylpyridine (P105 in Fig. 4.2) was confirmed at m/z = 105 and the MS spectrum had an excellent match with the MS library. The formation of P105 has been reported in the past during the photocatalytic degradation of cotinine at $\lambda = 360$ nm in the presence of TiO_2 (Medana et al., 2016). Cotinine is an important product of nicotine during ozonation, OH• oxidation, biodegradation, and during the indirect photolysis of nicotine in wastewater samples (Lian et al., 2017; Medana et al., 2016). It was therefore assumed that during direct photolysis, nicotine was oxidized to cotinine and further photo-transformed to P105. Here, the presence of cotinine (Fig. 4.2) was confirmed during LC/MS at [M-H]+ = 177 m/z. Other transformation by-products identified during LC/MS included P135, P181 and P208 at [M-H]+ = 136, 182 and 209 m/z respectively. The formation of these by-products has been proposed in the past during the indirect photolysis of nicotine together with their reaction pathways (Lian et al., 2017).

4.4.2. EFFECT OF PH ON THE DIRECT PHOTOLYSIS OF NICOTINE

In general, the relationship between photolysis and pH is linked to the protonation states of the molecule and the absorption spectrum of the substate (Boreen et al., 2004). Once dissolved in water, nicotine may be present in a neutral or ionic form, depending on the pH of the water solution. Fully protonated nicotine carries two protons and the reported acidity constants in water are $pKa_1 = 3.37$ and $pKa_2 = 8.07$ at 25°C (Nienow et al., 2009). At pH values below 4.0 the diprotonated nicotine is the principal species, between pH values 4–8 monoprotonated nicotine is dominant, and at higher pH values the neutral form of nicotine is dominant (Nienow et al., 2009).

To investigate the effect of pH at environmentally relevant values, nicotine containing water solutions having pH values between 5 and 9 were UV_{254} irradiated. All irradiated

water solutions were buffered and the pH was monitored before and after photolysis to confirm that there were no changes in the pH. Fig. 4.3 depicts the time trends in normalized nicotine concentration during irradiation at the pH values tested. As seen, at pH 4.9 and 6.9 (where the monoprotonated form of nicotine is the primary species present) decomposition was faster compared to that at pH 9.0. The apparent pseudo-first order rate constants (k_{NIC} was 0.16 (r^2 = 0.9937), 0.12 (r^2 = 0.9837) and 0.04 (r^2 = 0.9996) min^{-1} at pH 4.9, 6.9 and 9.0 respectively) confirmed the enhanced photodegradation rate of nicotine when the monoprotonated nicotine species is the most abundant. The present results were in agreement with some preliminary experiments performed whilst investigating the H_2O_2-enhanced photodegradation of nicotine (Nienow et al., 2009). In this report, UV_{254} irradiation of nicotine water solutions at pH = 1, 5.5, and 11.3 provided evidence that the direct photolysis of nicotine is faster when the monoprotonated nicotine is the primary species present in solution.

4.4.3. EFFECT OF DISSOLVED SPECIES ON THE DIRECT PHOTOLYSIS OF NICOTINE

Humic acids (HA) have a considerable light absorbing capacity and can act as photosensitizers by generating a range of reactive transient species (Kourounioti et al., 2019; Koutantou et al., 2013). During the present investigations, the presence of HA at an environmentally relevant concentration (2.5 mg L^{-1}), had a very small effect on the direct photolysis of a 10 mg L^{-1} nicotine water solution (Fig. S.5 – Appendix 3 in the Supporting Information) yielding $k_{NIC,HA}$ = 0.08 (r^2 = 0.903). It was assumed that this small delay in kinetics was due to competition for lamp irradiance between nicotine and HA (Kourounioti et al., 2019). In further experiments, the effect of salt was also investigated and the results from these studies are shown in Fig. S.5 – Appendix 3 in the Supporting Information. In general, salt can alter the ionic strength of the solution and lower the activity coefficient of the mono-protonated and especially the di-protonated species (Nienow et al., 2009; Schwarzenbach et al., 2003). The negatively charged chloride ions may thus result in a shielding effect of the positively charged nicotine ions, which in turn may decrease observed reaction rates of nicotine when free radicals are involved (Nienow et al., 2009). During the present investigations and as

expected, the presence of 3.5% w:v NaCl had practically no effect on the direct photolysis of 10 mg L^{-1} nicotine water solutions ($k_{NIC,\ NaCl}$ = 0.11 (r^2 = 0.9871)).

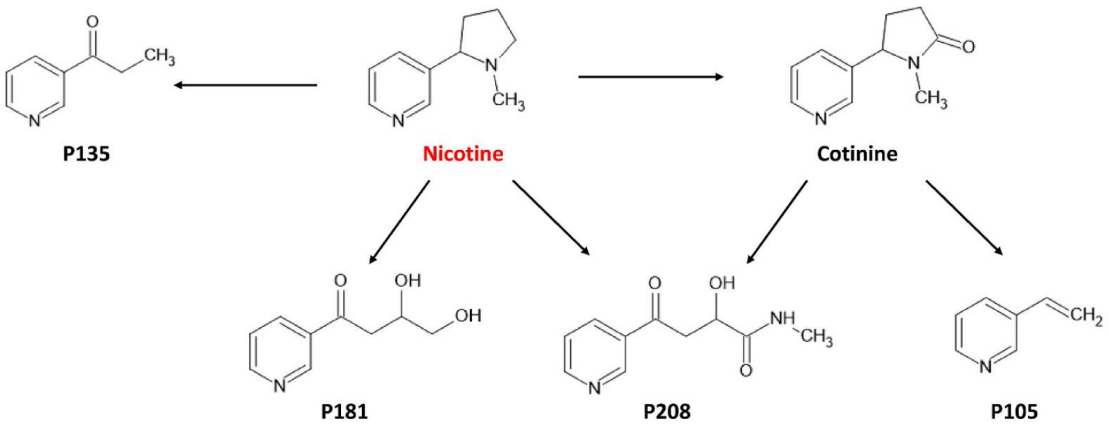

Fig. 4.2 Identified photoproducts during the direct photolysis of nicotine.

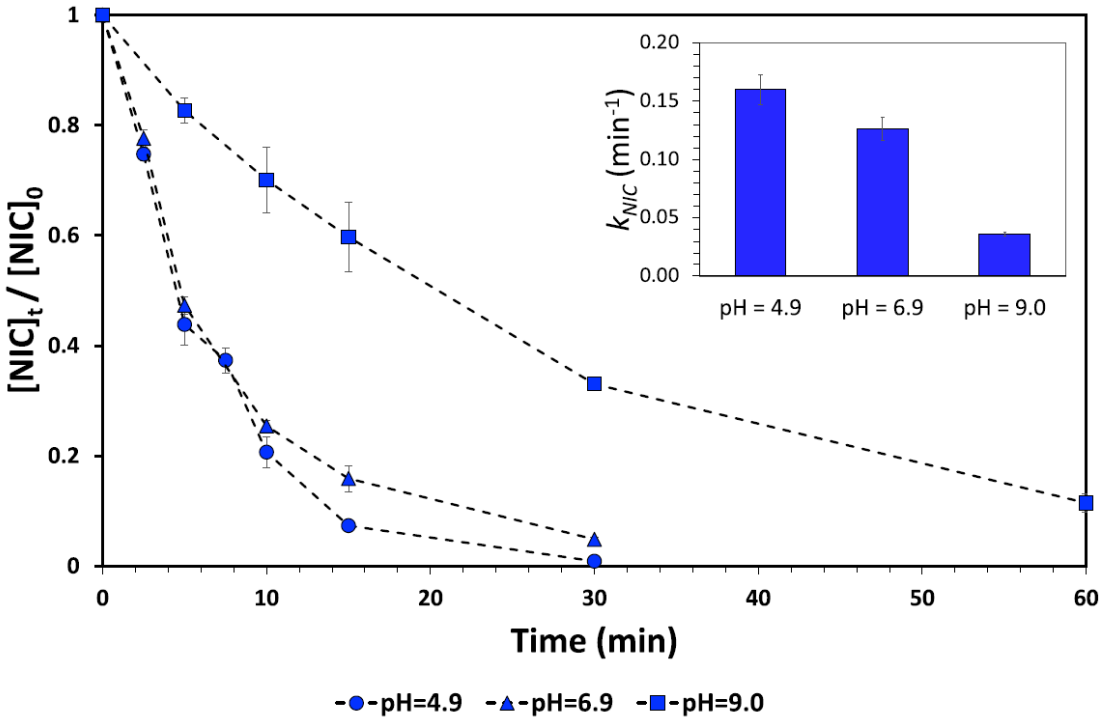

Fig. 4.3 The effect of pH on the direct photolysis of 10 mg L^{-1} nicotine solutions under UV_{254} irradiation. Inset graph: apparent rate constants for each pH tested. Data points are linked with dashed lines to visualize trends. Some error bars are too small to be visible.

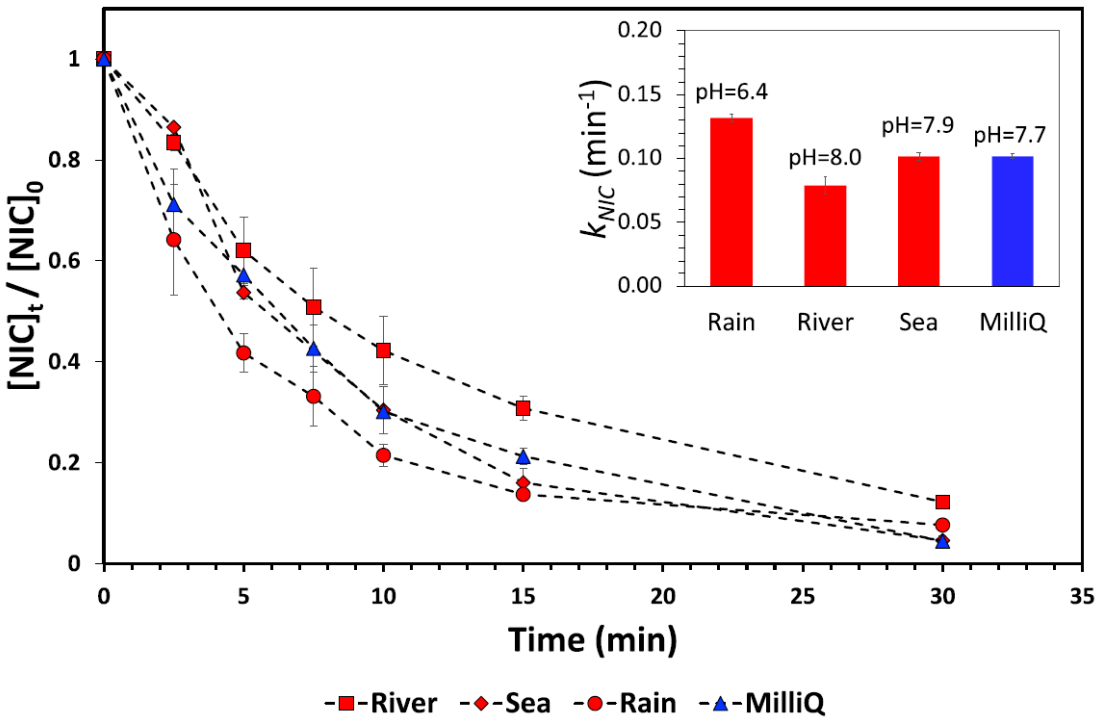

Fig. 4.4 Photolysis of 10 mg L^{-1} nicotine solutions in rain, river and sea water under UV_{254} irradiation. Inset graph: apparent rate constants for each natural water tested. The results in non-buffered ultrapure (MilliQ) water are also included. Data points are linked with dashed lines to visualize trends. Some error bars are too small to be visible.

4.4.4. THE PHOTODEGRADATION OF NICOTINE IN NATURAL WATERS

The photodegradation of nicotine was also studied in various natural water matrices (rain, river and sea water), and compared to the behavior of nicotine in ultrapure water (Fig. 4.4). In the case of sea water, the kinetics of nicotine photolysis were practically the same as in ultrapure water ($k_{NIC,sea}$ = 0.10 (r^2 = 0.9833)) and for this matrix type, the natural-water components could not alter the photolysis kinetics of nicotine. This conclusion was also supported by the no-effect of salt found earlier on the direct photolysis of nicotine. On the other hand the degradation of nicotine was slightly delayed in river water ($k_{NIC,\ river}$ = 0.08 (r^2 = 0.9880)). It was assumed that this was the result of light absorbing components present in this type of surface water that competed with nicotine for lamp irradiance and reduced the photon flux absorbed by nicotine, in agreement with our previous results on the effect of HA on the direct photolysis of nicotine. Finally, the direct photolysis kinetics of nicotine in rain water (Fig. 4.4) appeared to be somewhat enhanced compared to the rest of the natural water samples tested ($k_{NIC,\ rain}$ = 0.13 (r^2 = 0.9871)). This observation was assumed to be the result of

the pH of this matrix. Indeed, compared to the rest of the natural water samples tested, rain water sample was more acidic (pH = 6.4; pH values given in the inset of Fig. 4.4), and kinetics were closer to the one recorded for ultrapure water at pH = 6.9 where k_{NIC} = 0.12.

4.4.5. NICOTINE PHOTOLYSIS IN LEACHATES PRODUCED FROM USED TOBACCO PRODUCTS

4.4.5.1. PRELIMINARY STUDIES ON THE LEACHING BEHAVIOR OF NICOTINE FROM HnBs AND CCs

Tobacco consists of a very complex mixture having at least 4000 chemical constituents (Slaughter et al., 2011). Moreover, in a burning cigarette or a heated HnB many chemical reactions take place, that yield a number of new compounds (Baker and Bishop, 2004; Schaller et al., 2016). The leachates from tobacco product waste therefore consist of highly complex mixtures of compounds. In a preliminary set of experiments, leaching studies were performed using batch tests with unused or used HnBs and CCs soaked in ultrapure water for times ranging between 30 min to a maximum of 30 days, and the changes in TOC values were monitored. For each tobacco product, the results showed slower kinetics of organic content release from unused compared to operated units (Fig. S.6 – Appendix 3 in the Supporting Information). Moreover, a slower release was observed in leachates from HnBs compared to CCs regardless whether the product was operated or not (Fig. S.6 – Appendix 3 in the Supporting Information). This observation presumably reflected the differences in tobacco processing between the two products as well as the presence of a thin aluminum sheet to wrap the tobacco plug in HnBs, which also delayed the disintegration of tobacco sticks in water. In all cases, the TOC values after 24 h of leaching remained unchanged as the system was at equilibrium.

In tobacco product leachates, nicotine accounts only for a small amount of the carbon-containing compounds. Here, the nicotine contribution to the TOC values of leachates was ~5% for unused and operated HnBs, and 9% for unused and smoked CCs. Nonetheless, nicotine is a highly water-soluble compound, assumed to be released quickly to the water phase from tobacco products and become bioavailable to aquatic life (Roder Green et al., 2014). The total and bioavailable nicotine concentrations were

then measured for HnBs and CCs before and after being operated, since not all of these values are reported in the literature. For HnBs, the total nicotine content was 4.67 ± 0.09 mg unit^{-1} (past reported value was 4.7 mg unit^{-1} (Bekki et al., 2017)), and after operation the total nicotine content was reduced to 3.20 ± 0.09 mg unit^{-1} (Table S.11 – Appendix 3 in the Supporting Information). For CCs the total nicotine content was 9.46 ± 0.34 mg unit^{-1} (past reported value was 10.9 mg unit^{-1}; differences were accounted to tobacco variations in different countries and among CC packs (Kozlowski et al., 1998)), and after smoking CCs, this value was reduced to 1.55 ± 0.11 mg unit^{-1} (Table S.11 - Appendix 3). Moreover, for all types of tobacco product tested, the majority of the total nicotine content was bioavailable after 24 h (Table S.11 - Appendix 3). These results showed that ~70% of the total and bioavailable nicotine content remained in the HnBs units after operation and that this percentage dropped to ~15% for CCs (Table S.11 - Appendix 3). This drastic decrease in nicotine content for CCs was accounted to the reduction in length and mass after smoking (Koutela et al., 2020). This assumption was further supported by the similar TOC values in leachates from used CCs and unused CCs cut at an operated length i.e. length of the filter plus 3 mm of the tobacco plug (Fig. S.6 – Appendix 3 in the Supporting Information). Further studies on the contribution of the different parts of the tobacco product (filter, tobacco filler and paper) on the total and bioavailable nicotine content of HnBs and CCs showed that tobacco was the only source of nicotine from both types of unused tobacco products (Table S.11 – Appendix 3 in the Supporting Information). However, after operation, nicotine was evenly distributed in the remnant tobacco and filter and to a less extent in the paper used for tobacco wrapping (Table S.11 – Appendix 3). We also found that the bioavailable nicotine concentrations remained practically the same when varying the pH, salt and humic acid content at environmentally relevant values (Table S.12 – Appendix 3 in the Supporting Information) and when river water, rain water or seawater was used as leachant (Table S.13 – Appendix 3 in the Supporting Information).

4.4.5.2. NICOTINE PHOTOLYSIS IN LEACHATES PRODUCED FROM USED TOBACCO PRODUCTS

Leachates were prepared from used HnBs and smoked CCs at a 10 L g^{-1} liquid-to-solid ratio and further diluted to a 10 mg L^{-1} initial nicotine concentration (pH ~ 6.5 for the diluted solutions). Aliquots were then UV_{254} irradiated and the resulting normalized

concentration time profiles are given in Fig. 4.5. Despite the complexity of the matrix, the respective coefficients of linear regression after data fitting to Equation (4.1) were satisfactory and the resulting pseudo first-order reaction rates were: $k_{NIC,CC}$ = 0.11 (r^2 = 0.9812) and $k_{NIC,HnB}$ = 0.09 (r^2 = 0.9947). As seen, nicotine degradation in these leachates proceeded possibly in slightly slower kinetics compared to ultrapure water (at pH = 6.9 k_{NIC} = 0.12 (r^2 = 0.9837)). This was somewhat expected considering the increased complexity of the leachate compared to ultrapure water where nicotine accounted only for a small amount of the carbon-containing compounds. It was therefore assumed that the presence of other tobacco-derived leachate components absorbed UV_{254} light and decreased the irradiance available for the direct photolysis of nicotine (Kourounioti et al., 2019).

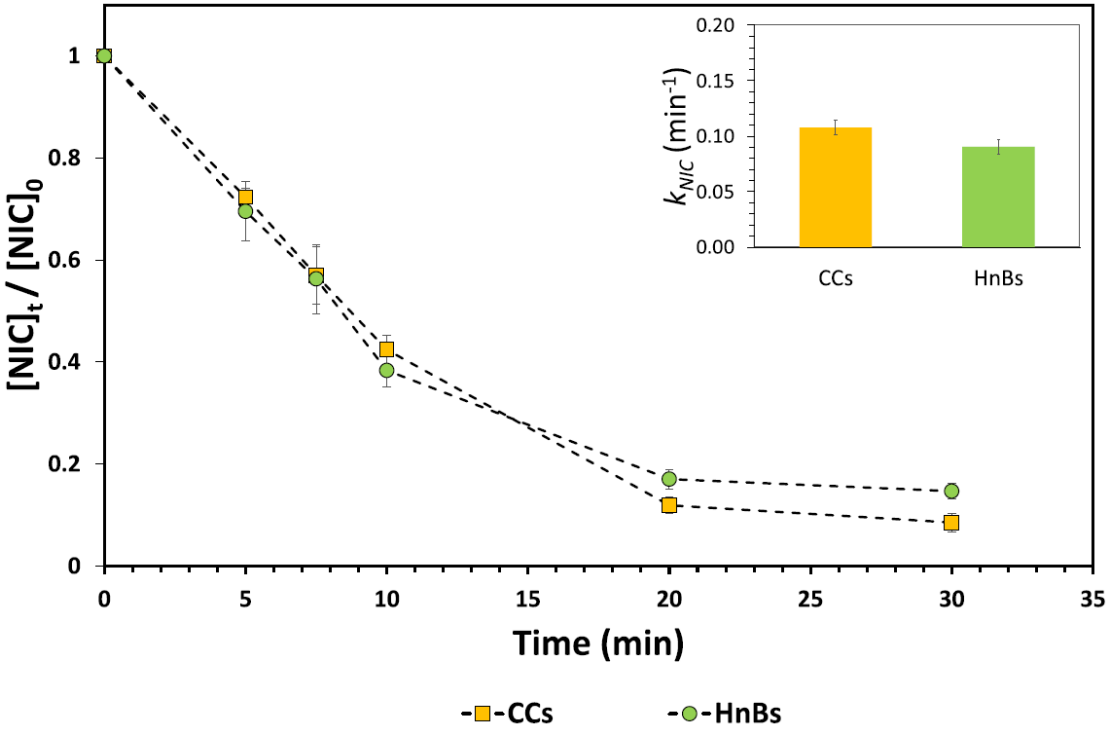

Fig. 4.5 UV_{254}-induced photolysis of nicotine in leachates from used HnBs and CCs. Inset graph: apparent rate constants for each tobacco product leachate tested. Leachates were diluted to a $[NIC]_0$ = 10 mg L^{-1}. Data points are linked with dashed lines to visualize trends.

Identification of the photo-transformation products formed under UV_{254} irradiation was not possible due to the large number of co-eluting extracted organics that impeded untargeted analysis when using one dimensional GC and the current type of mass spectrometry. To allow a better understanding of leachates, the organics remaining in the system after irradiation were evaluated in terms of TOC. The measured changes in

TOC values after irradiation were non-significant even after extending the exposure time to 180 min. It was concluded that despite the complete conversion of nicotine under UV_{254}, the mineralization degree of leachates in terms of TOC values was negligible due to the abundance of organics and the formation of new transformation products.

4.5. CONCLUSION

In this study, we report the direct photolytical degradation of nicotine in simple and highly complex matrices. The results showed that UV_{254}-induced photolysis is an efficient and fast process for the degradation of nicotine. Among the different photoproducts formed, only five were identified my means of LC/MS and TD-GC/ITMS. TOC removal was very low pointing towards the formation of photoproducts at different rates that were more recalcitrant than the parent compound. The photodegradation kinetics was found dependent on the pH and optimum conditions were found in the range where monoprotonated nicotine prevails. Humic acids slightly delay kinetics by screening light, whereas the presence of salt did not affect the reaction. From all the natural water tested, faster kinetics were recorded in rain water due to the lower pH value of this matrix. Leachates from operated CCs and the new generation HnBs were UV_{254} irradiated and photolysis proceeded fast despite the large amount of tobacco-derived components present in the solution. Nonetheless, TOC removal from both leachates was non-significant.

More information is needed to elucidate the photochemical fate of nicotine. The use of two-dimensional gas chromatography (GC × GC) will allow enhanced separations of the complex leachate mixtures through greater chromatographic peak capacity that will enable the identification to the maximum possible extent of the photoproducts formed in highly complex matrices like tobacco product leachates.

Finally, we take advantage of the present investigations and perform for the first time leaching studies on unused and operated HnBs and CCs. Slower kinetics of organic content release were recorded for HnBs products. After operation, ~70% of the total and bioavailable nicotine content remains in HnBs compared to the 15% in CCs. This finding confirms the importance of properly disposing tobacco product waste to prevent nicotine leaching in water bodies.

4.6. REFERENCES

Araújo, M.C.B., Costa, M.F., (2019). A critical review of the issue of cigarette butt pollution in coastal environments. *Environmental Research*, 172, 137–149. https://doi.org/10.1016/j.envres.2019.02.005.

Baker, R.R., Bishop, L.J., (2004). The pyrolysis of tobacco ingredients. *Journal of Analytical and Applied Pyrolysis*, 71, 223–311. https://doi.org/10.1016/S0165-2370(03)00090-1.

Baran, W., Madej-Knysak, D., Sobczak, A., Adamek, E., (2020). The influence of waste from electronic cigarettes, conventional cigarettes and heat-not-burn tobacco products on microorganisms. *Journal of Hazardous Materials*, 385, 121591. https://doi.org/10.1016/j.jhazmat.2019.121591.

Bekki, K., Inaba, Y., Uchiyama, S., Kunugita, N., (2017). Comparison of chemicals in mainstream smoke in heat-not-burn tobacco and combustion cigarettes. *Journal of UOEH*, 39, 201–207. https://doi.org/10.7888/juoeh.39.201.

Boreen, A.L., Arnold, W.A., McNeill, K., (2004). Photochemical fate of sulfa drugs in then aquatic environment: sulfa drugs containing five-membered heterocyclic groups. *Environmental Science & Technology*, 38, 3933–3940. https://doi.org/10.1021/es0353053.

Braslavsky, S.E., (2007). Glossary of terms used in photochemistry, 3rd edition (IUPAC Recommendations 2006). *Pure and Applied Chemistry*, 79, 293–465. https://doi.org/10.1351/pac200779030293.

Buerge, I.J., Kahle, M., Buser, H.R., Müller, M.D., Poiger, T., (2008). Nicotine derivatives in wastewater and surface waters: application as chemical markers for domestic wastewater. *Environmental Science & Technology*, 42, 6354–6360. https://doi.org/10.1021/es800455q.

Cardoso, L.S., Estrela, F.N., Chagas, T.Q., da Silva, W.A.M., Costa, D.R. de O., Pereira, I., Vaz, B.G., Rodrigues, A.S. de L., Malafaia, G., (2018). The exposure to water with cigarette residue changes the anti-predator response in female Swiss albino

mice. *Environmental Science and Pollution Research*, 25, 8592–8607. https://doi.org/10.1007/s11356-017-1150-4.

Carena, L., Fabbri, D., Passananti, M., Minella, M., Pazzi, M., Vione, D., (2020). The role of direct photolysis in the photodegradation of the herbicide bentazone in natural surface waters. *Chemosphere*, 246, 125705. https://doi.org/10.1016/j.chemosphere.2019.125705.

Chevalier, Q., El Hadri, H., Petitjean, P., Bouhnik-Le Coz, M., Reynaud, S., Grassl, B., Gigault, J., (2018). Nano-litter from cigarette butts: environmental implications and urgent consideration. *Chemosphere*, 194, 125–130. https://doi.org/10.1016/j.chemosphere.2017.11.158.

de Granda-Orive, J.I., de Granda-Beltr´an, C., Baz-Lomba, J.A., (2018). Contaminants of emerging concern: nicotine in wastewater as a public health analysis tool. *Archivos de Bronconeumologia*, 54, 495–496. https://doi.org/10.1016/j.arbres.2018.02.020.

Dobaradaran, S., Schmidt, T.C., Lorenzo-Parodi, N., Jochmann, M.A., Nabipour, I., Raeisi, A., Stojanovi´c, N., Mahmoodi, M., (2019). Cigarette butts: an overlooked source of PAHs in the environment? *Environmental Pollution*, 249, 932–939. https://doi.org/10.1016/j.envpol.2019.03.097.

Dobaradaran, S., Schmidt, T.C., Lorenzo-Parodi, N., Kaziur-Cegla, W., Jochmann, M.A., Nabipour, I., Lutze, H.V., Telgheder, U., (2020). Polycyclic aromatic hydrocarbons (PAHs) leachates from cigarette butts into water. *Environmental Pollution*, 259, 113916. https://doi.org/10.1016/j.envpol.2020.113916.

Gonzalez Alonso, S., Valcarcel, Y., Montero, J.C., Catala, M., (2012). Nicotine occurrence in bottled mineral water: analysis of 10 brands of water in Spain. *Science of the Total Environment*, 416, 527–531. https://doi.org/10.1016/j.scitotenv.2011.11.046.

Huerta-Fontela, M., Galceran, M.T., Martin-Alonso, J., Ventura, F., (2008). Occurrence of psychoactive stimulatory drugs in wastewaters in north-eastern Spain. *Science of the Total Environment*, 397, 31–40. https://doi.org/10.1016/j.scitotenv.2008.02.057.

Katagi, T., (2018). Direct photolysis mechanism of pesticides in water. *Journal of Pesticide Science*, 43, 57–72. https://doi.org/10.1584/jpestics.D17-081.

Kourounioti, E., Psillakis, E., Vione, D., (2019). UV-induced transformation of 2,3-dibromo-5,6-dimethyl-1,4-benzoquinone in water and treated wastewater. *Environmental Research*, 175, 343–350. https://doi.org/10.1016/j.envres.2019.05.018.

Koutantou, V., Kostadima, M., Chatzisymeon, E., Frontistis, Z., Binas, V., Venieri, D., Mantzavinos, D., (2013). Solar photocatalytic decomposition of estrogens over immobilized zinc oxide. *Catalysis Today*, 209, 66–73. https://doi.org/10.1016/j.cattod.2012.11.004.

Koutela, N., Fernandez, E., Saru, M.-L.L., Psillakis, E., (2020). A comprehensive study on the leaching of metals from heated tobacco sticks and cigarettes in water and natural waters. *Science of Total Environment*, 714, 136700. https://doi.org/10.1016/j.scitotenv.2020.136700.

Kozlowski, L.T., Mehta, N.Y., Sweeney, C.T., Schwartz, S.S., Vogler, G.P., Jarvis, M.J., West, R.J., (1998). Filter ventilation and nicotine content of tobacco in cigarettes from Canada, the United Kingdom, and the United States. *Tobacco Control*, 7, 369–375. https://doi.org/10.1136/tc.7.4.369.

Lian, L., Yan, S., Yao, B., Chan, S.A., Song, W., (2017). Photochemical transformation of nicotine in wastewater effluent. *Environmental Science & Technology*, 51, 11718–11730. https://doi.org/10.1021/acs.est.7b03223.

Marah, M., Novotny, T.E., (2011). Geographic patterns of cigarette butt waste in the urban environment. *Tobacco Control*, 20, 42–44. https://doi.org/10.1136/tc.2010.042424.

Mayer, B., (2014). How much nicotine kills a human? Tracing back the generally accepted lethal dose to dubious self-experiments in the nineteenth century. *Archives of Toxicology*, 88, 5–7. https://doi.org/10.1007/s00204-013-1127-0.

Medana, C., Santoro, V., Bello, F.D., Sala, C., Pazzi, M., Sarro, M., Calza, P., (2016). Mass spectrometric fragmentation and photocatalytic transformation of nicotine and

cotinine. *Rapid Communications in Mass Spectrometry*, 30, 2617–2627. https://doi.org/10.1002/rcm.7758.

Moerman, J.W., Potts, G.E., (2011). Analysis of metals leached from smoked cigarette litter. *Tobacco Control*, 20, i30–i35. https://doi.org/10.1136/tc.2010.040196.

Moriwaki, H., Kitajima, S., Katahira, K., (2009). Waste on the roadside, "poi-sute" waste: its distribution and elution potential of pollutants into environment. *Waste Management*, 29, 1192–1197. https://doi.org/10.1016/j.wasman.2008.08.017.

Nienow, A.M., Hua, I., Poyer, I.C., Bezares-Cruz, J.C., Jafvert, C.T., (2009). Multifactor statistical analysis of H2O2-enhanced photodegradation of nicotine and phosphamidon. *Industrial & Engineering Chemistry Research*, 48, 3955–3963. https://doi.org/10.1021/ie801311f.

OECD, (2008). Test No. 316: phototransformation of chemicals in water – direct photolysis. Test No 305 bioaccumulation fish aqueous diet. *Expo. Section*, 3, 1–72. https://doi.org/10.1787/9789264067585-en.

Oropesa, A.L., Floro, A.M., Palma, P., (2017). Toxic potential of the emerging contaminant nicotine to the aquatic ecosystem. *Environmental Science and Pollution Research*, 24, 16605–16616. https://doi.org/10.1007/s11356-017-9084-4.

Passananti, M., Temussi, F., Iesce, M.R., Previtera, L., Mailhot, G., Vione, D., Brigante, M., (2014). Photoenhanced transformation of nicotine in aquatic environments: involvement of naturally occurring radical sources. *Water Research*, 55, 106–114. https://doi.org/10.1016/j.watres.2014.02.016.

Roder Green, A.L., Putschew, A., Nehls, T., (2014). Littered cigarette butts as a source of nicotine in urban waters. *Journal of Hydrology*, 519, 3466–3474. https://doi.org/10.1016/j.jhydrol.2014.05.046.

Schaller, J., Keller, D., Poget, L., Pratte, P., Kaelin, E., Mchugh, D., Cudazzo, G., Smart, D., Tricker, A.R., Gautier, L., Yerly, M., Pires, R.R., Bouhellec, S. Le, Ghosh, D., Hofer, I., Garcia, E., Vanscheeuwijck, P., Maeder, S., Reis Pires, R., Le Bouhellec, S., Ghosh, D., Hofer, I., Garcia, E., Vanscheeuwijck, P., Maeder, S., (2016). Evaluation of the Tobacco Heating System 2.2. Part 2: chemical composition, genotoxicity,

cytotoxicity, and physical properties of the aerosol. *Regulatory Toxicology and Pharmacology*, 81, S27–S47. https://doi.org/10.1016/j.yrtph.2016.10.001.

Schwarzenbach, R.P., Gschwend, P.M., Imboden, D.M., (2003). Environmental Organic Chemistry, second ed. John Wiley & Sons Inc, Hoboken, New Jersey. Senta, I., Gracia-Lor, E., Borsotti, A., Zuccato, E., Castiglioni, S., 2015. Wastewater analysis to monitor use of caffeine and nicotine and evaluation of their metabolites as biomarkers for population size assessment. *Water Research*, 74, 23–33. https://doi.org/10.1016/j.watres.2015.02.002.

Slaughter, E., Gersberg, R.M., Watanabe, K., Rudolph, J., Stransky, C., Novotny, T.E., (2011). Toxicity of cigarette butts, and their chemical components, to marine and freshwater fish. *Tobacco Control*, 20, 25–29. https://doi.org/10.1136/tc.2010.040170.

Torkashvand, J., Farzadkia, M., Sobhi, H.R., Esrafili, A., (2020). Littered cigarette butt as a well-known hazardous waste: a comprehensive systematic review. *Journal of Hazardous Materials*, 383, 121242. https://doi.org/10.1016/j.jhazmat.2019.121242.

World Health Organization (WHO), 2014. WHO TobLabNet Official Method SOP 04 - Standard Operating Procedure for Determination of Nicotine in Cigarette Tobacco Filler 18.

CHAPTER 5: UVC-INDUCED DEGRADATION OF CILASTATIN IN NATURAL WATER AND TREATED WASTEWATER

Solomou, N., Minella, M., Vione, D., & Psillakis, E. (2021). UVC-induced degradation of cilastatin in natural water and treated wastewater. Chemosphere, 280, 130668.

Credit author statement

N. Solomou: Investigation. M. Minella: Data curation, Visualization, Writing - review & editing. D. Vione: Conceptualization, Data curation, Visualization, Writing - review & editing. E. Psillakis: Supervision, Visualization, Writing – review & editing

5.1. ABSTRACT

This work reports for the first time the UVC photodegradation of cilastatin, a renal dehydropeptidase inhibitor co-adminstered with the imipenem antibiotic. Initially, solutions of cilastatin at varying concentrations were prepared in ultra-pure water and the direct photolysis of cilastatin was monitored under 254-nm irradiation. Degradation was slower at higher initial cilastatin concentrations, due to absorption saturation. Of the different eluting photoproducts, only one was tentatively identified as oxidized cilastatin bearing a sulfoxide group. UV-254 photolysis occurred faster at lower pH values, because the protonated forms of the molecule (H_3A^+, H_2A) have both higher absorption coefficients and higher photolysis quantum yields than the non-protonated ones (HA^-, A^{2-}). The direct photolysis of cilastatin does not involve •OH, as excluded by experiments in which t-butanol was added as •OH scavenger, whereas the presence of humic acids inhibited photolysis due to competition for radiation absorption. The same explanation partially accounts for the observation that the photolysis kinetics of cilastatin was slower in tap water, river water and treated wastewater samples compared to ultra-pure water. Moreover, the direct photolysis quantum yield was also lower in water matrices compared to ultra-pure water. Similar findings reported for triclosan and the herbicide 2-methyl-4-chlorophenoxyacetic acid in previous studies might suggest that the water matrix components could carry out either physical quenching of cilastatin's excited states or back-reduction to cilastatin of the partially oxidized degradation intermediates. Overall, the present results demonstrate that UVC irradiation is a fast and efficient process for the degradation of cilastatin in natural water and treated wastewater.

5.2. INTRODUCTION

Antibiotics are frequently used in the treatment and prevention of infectious disease, as well as to treat humans and animals. Imipenem was the first member of the carbapenem class of antibiotics and an important broad-spectrum *β*-lactam antibiotic, often used as a "last-line antibiotic" when patients with infections became gravely ill or were suspected of harboring resistant bacteria (Proia et al., 2018; Reina et al., 2018; Briones et al., 2020). At early stages of development when imipenem was administered alone, low urinary recovery in animals and human volunteers were recorded, and further toxicological studies reported proximal tubular necrosis to rabbits (Drusano et al., 1984). The concept of coadministering imipenem together with a renal dehydropeptidase inhibitor to improve the urinary antibiotic profile resulted in the synthesis and use of cilastatin. The combination of imipenem and cilastatin in a ratio of 1:1 yielded high urinary concentrations of imipenem (recoveries increased from 12-42% to 70% of the dose when co-administered with cilastatin), and in addition, cilastatin prevented entry of imipenem into the proximal tubular epithelium (Hutt and O'Grady, 1996). At the same time, the urinary recoveries of cilastatin in the presence or absence of imipenem were reported to range between 70 and 80% after 6 h from administration (Norrby et al., 1984; Hsieh et al., 1985).

In recent years, the consumption of last-line antibiotics has been rapidly increasing across all income groups (Yılmaz and Özcengiz, 2017; Klein et al., 2018). In particular, the increased consumption of carbapenems such as imipenem, has resulted in their environmental release through various routes such as patients' excretions, hospital wastewater and the pharmaceutical industry (Cheng et al., 2015; Szekeres et al., 2017) and in their widespread occurrence in aquatic systems (Tran et al., 2016; Szekeres et al., 2017; Proia et al., 2018). The latter findings were assumed to account for the developed resistance of some Gram-negative bacteria to carbapenems (Kumarasamy et al., 2010), which is now spreading throughout the world and is threatening the efficiency of this essential class of lifesaving antibiotics (Papp-Wallace et al., 2011; Szekeres et al., 2017; Reina et al., 2018).

The increasing consumption of imipenem inevitably entails environmental release of cilastatin. Although, the photochemical fate (Reina et al., 2018) and treatment

(Cabrera-Reina et al., 2019) of imipenem have been the focus of past studies, very little is known on the photochemical fate of cilastatin in water, and its treatment was only recently proposed as part of an integrated advanced oxidation/reduction process for the degradation of imipenem/cilastatin antibiotic aqueous solutions (Godini et al., 2019). However, detailed data and discussion were not provided on the behavior/performance of cilastatin undergoing this process.

This contribution aims to explore for the first time the photolytic fate of cilastatin in water under 254-nm irradiation. Initially, ultrapure water was used as matrix to study the effects of concentration, pH, presence of t-butanol and humic acids on the cilastatin (photo) transformation rate. Building on this knowledge, the photolysis of cilastatin spiked to tap water, river water and wastewater effluent was monitored as a function of irradiation time. At all times, modeling results are presented to confirm suggested hypotheses and discussion on experimental data.

5.3. MATERIALS AND METHODS

5.3.1. CHEMICALS AND SAMPLES

Cilastatin sodium salt (purity grade >99.8%) was purchased from Sigma-Aldrich (Steinheim, Germany). All organic solvents used were LC/MS grade. t-Butanol (>99%) was supplied by Fisher Chemicals (Pittsburgh, Pennsylvania). Analytical grade formic acid and humic acid were supplied by Fluka Chemie GmbH (Bucks, Switzerland). Aqueous solutions of sodium hydroxide (Fluka Chemie GmbH) or buffer solutions were used to adjust the pH value of the irradiated solutions. The following chemicals were used to prepare the buffer solutions: glacial acetic acid and boric acid (99.8%) supplied by Merck, KGaA (Darmstadt, Germany), potassium phosphate dibasic trihydrate (>99.0%) from Sigma-Aldrich (Steinheim, Germany), sodium acetate trihydrate (>99.5%) and potassium dihydrogen phosphate (>99.5%), both supplied by Fluka Chemie GmbH (Germany).

An EASYpure RF water purification system supplied by Barnstead/Thermolyne Corporation (Dubuque, IA, USA) was used to prepare ultra-pure water. The matrix effect on cilastatin photolysis was studied using: (i) freshwater sampled from the river Koiliaris at Kyani Akti (Kalyves, Crete, Greece); (ii) tap water from the University

campus (Chania, Crete, Greece), and (iii) secondary treated wastewater effluent (WW) from the municipal wastewater treatment plant of Chania (Crete, Greece), serving approximately 70,000 inhabitants. See Table S.14 – Appendix 4 in the Supporting Information for the chemical composition of the three water types used in this work. Samples were collected the day before conducting the photo-experiments, and were stored in the dark at 4 ^{o}C. All samples were initially analyzed and found free of cilastatin.

5.3.2. PHOTOLYSIS EXPERIMENTS

For all photolysis experiments, a home-made laboratory photoreactor (28.0 cm height x 28.4 cm length x 28.0 cm width) was used. The photoreactor was equipped with two 8 W low-pressure mercury lamps having a strong emission line at 254 nm (Osram 8 W G8 T5), each mounted on an opposing sidewall of the photoreactor. The distance between each lamp and the quartz vial used in the experiments was 13 cm. The rate of the incident UV light intensity entering the solution (I_o, given in E L^{-1} s^{-1}, where E = Einstein) was determined using H_2O_2 as chemical actinometer, and was Io = (6.24 ± 0.19) x 10^{-6} E L^{-1} s^{-1}.

Aqueous solutions of cilastatin (CIL) were prepared daily by transferring the appropriate volume from a 7 g L^{-1} methanolic stock solution to a tailor-made quartz vial (2.4 cm outer diameter x 5.2 cm height). A gentle nitrogen stream was then applied to the headspace and, after complete evaporation of methanol, 9 mL of water were added (ultra-pure H_2O, H_2O with additives, tap water, natural water or WW effluent, depending on the experiment). The mixture was then sonicated for a short time to facilitate CIL solubilization. The quartz vial containing this aqueous solution was then capped and submitted to UV irradiation for the preset time under mild magnetic agitation. The inner diameter of the quartz vial (2.0 cm) was used as the optical path length of radiation. Blank experiments were also conducted by placing the water samples inside the photoreactor with the lamps switched off. CIL removal in the dark was below the error of the analytical method (varied between 0.1 and 2.6%) after 60 min, confirming that changes in the analytical signal after photolytic treatment were due to photochemical processes only. All experiments were run at least in duplicates.

5.3.3. ANALYTICAL METHODS

The absorbance of aqueous samples at 254 nm was measured using a single-beam UV-visible spectrophotometer (UVmini-240, Shimadzu, Tokyo Japan), equipped with quartz cuvettes having a 1 cm optical path length. The total organic carbon (TOC) content of water solutions was measured using a TOC-5000 analyzer (Shimadzu, Kyoto, Japan; catalytic oxidation on Pt at 680 ^{o}C). The calibration was performed using standards of potassium phthalate.

All liquid chromatography/mass spectrometry (LC/MS) analyses on CIL were carried out using an Agilent 1200 Series high performance liquid chromatography (HPLC) system equipped with a binary pump, autosampler, degasser and thermostated column compartment, coupled to a diode array detector (DAD; the CIL analytical wavelength was 200 nm), and to an Agilent 6110 single quadrupole MS system equipped with a multimode ionization source. A Thermo-Electron Betasil C18 column (Waltham, MA, USA) of dimensions 2.1 mm ID x 100 mm length with 5 mm particle size was used for separation. The mobile phase consisted of 85% of water containing 0.1% formic acid and of 15% of acetonitrile containing 0.1% formic acid. The flow rate of the mobile phase was 250 μL min^{-1}, and the total analysis time was 10 min. For analysis, 60 μL of the sample were added to 100 μL polypropylene inserts and placed in 2mL polypropylene autosampler vials equipped with caps, all purchased from Agilent (Palo Alto, USA). The injection volume was 20 μL. The MS conditions were: drying gas flow, 5 L min^{-1}; drying gas temperature, 350 ^{o}C; nebulizer pressure, 40 psi; collector capillary voltage, 2.0 kV; fragmentor voltage, 70 V; scan range (m/z),100-1000 amu. The mass spectrometry data were recorded using the positive electrospray ionization (ESI) mode. The linearity of the method was tested using five concentration levels ranging from 1 to 100 mg L^{-1} (correlation coefficient r^2 =0.9982). A 1.3 mg L^{-1} limit of quantification (LOQ) was estimated. This concentration level was not sufficiently to monitor the photolysis of 2.5 mg L x 1 CIL (i.e., 7 x 10^{-6} M). To increase sensitivity in these experiments, 100 μL of the irradiated sample were added to 250 μL vial inserts instead, the injection volume was set at 60 μL, and the 350-365 amu mass spectrometry signal was used to monitor changes in CIL concentration. The linearity of this method was assessed using a five-point calibration curve in the concentration range 0.5-5mg L^{-1} and the estimated LOQ was 0.36 mg L^{-1}, which was sufficient for monitoring close

to 85% CIL conversion. The linearity of the method was tested in each water matrix studied here and it was concluded that the matrix did not affect the analytical performance of the method.

5.4. RESULTS AND DISCUSSION

5.4.1. PHOTODEGRADATION KINETICS

CIL undergoes several acid-base equilibria, which are described by the acid dissociation constants pK_{a1} = 2.0, pK_{a2} = 4.4 and pK_{a3} = 9.2 (Drugbank, 2020). These data allow for the distribution of the different species to be derived as a function of pH (Nourmoradi et al., 2019). In particular, the species' fractions α can be obtained as follows from the deprotonation equilibria:

$$\alpha_{H_3A^+} = \frac{[H^+]^3}{[H^+]^3+K_{\alpha1}[H^+]^2+K_{\alpha1}K_{\alpha2}[H^+]+K_{\alpha1}K_{\alpha2}K_{\alpha3}} \quad (5.1)$$

$$\alpha_{H_2A} = \frac{K_{\alpha1}[H^+]^2}{[H^+]^3+K_{\alpha1}[H^+]^2+K_{\alpha1}K_{\alpha2}[H^+]+K_{\alpha1}K_{\alpha2}K_{\alpha3}} \quad (5.2)$$

$$\alpha_{HA^-} = \frac{K_{\alpha1}K_{\alpha2}[H^+]}{[H^+]^3+K_{\alpha1}[H^+]^2+K_{\alpha1}K_{\alpha2}[H^+]+K_{\alpha1}K_{\alpha2}K_{\alpha3}} \quad (5.3)$$

$$\alpha_{A^{2-}} = \frac{K_{\alpha1}K_{\alpha2}K_{\alpha3}}{[H^+]^3+K_{\alpha1}[H^+]^2+K_{\alpha1}K_{\alpha2}[H^+]+K_{\alpha1}K_{\alpha2}K_{\alpha3}} \quad (5.4)$$

Note that H_3A^+ is the form of CIL with the amino and the two carboxylic groups all protonated, and the progressive deprotonation of these groups yields H_2A, HA^- and A^2. The distribution of the different CIL forms as a function of pH is reported in Fig. S.7 – Appendix 4 in the Supporting Information. It can be observed that HA^- strongly prevails at pH 6-8, i.e., in the conditions around neutrality that are most often found in water treatment.

A first series of degradation experiments was carried out at pH 7, for concentration values of CIL ranging from 2.5 to 100mg L^{-1} (note that 100 mg L^{-1} correspond to 2.6 x 10^{-4} M). The 2.5 mg L^{-1} concentration represented the lowest concentration level where

conversion of up to 90% of the irradiated samples could be successfully monitored and quantified by the analytical instrumentation. The time evolution of CIL (Fig. 5.1) shows that degradation was more effective as the initial concentration was lower. Data fitting of the concentration profiles from Fig. 5.1 to $C_t = C_o\, e^{-kt}$ gave the k values used to compute the initial degradation rates R_0 (vide infra) shown in the inset graph, which increased with increasing C_o, from 2.2 x 10^{-8} Ms^{-1} at 2.5 mg L^{-1} to 2.5 x 10^{-7} M s^{-1} at 100 mg L^{-1}.

In a pseudo-first order approximation the initial degradation rate R_0 can be obtained as $R_0 = k\, C_0$, and the R_0 vs. C_0 trend is reported in the inset of Fig. 5.1. The observed increase with plateau may suggest that the substrate absorbs radiation and gets photolyzed as a consequence, up to saturation of absorption (Kourounioti et al., 2019; Alberti et al., 2021). The monochromatic irradiation set-up allows for a simple Lambert-Beer approach to be applied, where the initial degradation rate can be expressed as follows (Braslavsky, 2007):

$$R_o = \gamma[1 - 10^{-\varepsilon_{CIL} b C_o}] \qquad (5.5)$$

where γ is a constant proportionality factor, ε_{CIL} is the molar absorption coefficient of CIL at 254 nm, b = 2 cm the optical path length in solution, and C_o the initial CIL concentration. The experimental values of k and R_o in the different experiments conducted in this work are listed in Table S.15 – Appendix 4 in the Supporting Information.

Independent spectrophotometric measurements gave ε_{CIL}(254 nm) = 1660 L mol^{-1} cm^{-1} at pH 7 (molar absorption of the HA^- species, see Fig. S.7 in the Supporting Information). Therefore, by introducing in Eq. (5.5) all the known parameters it is possible to fit the experimental data of Fig. 5.1 (insert) with g as the only free-floating variable. The good fit results show that the phenomenon of absorption saturation indeed accounts for the plateau trend of R_0 vs. C_0.

In an attempt to identify the transformation products formed, the photolysis of 100 mg L^{-1} CIL solutions was monitored for 60 min, that is 15 min longer than the time required to remove CIL itself. During LC-MS analysis, the elution of several photoproducts was recorded. However, considering the parent compound, the use of a single quadrupole mass spectrometer could not provide a large amount of structural information, and specificity was limited compared to other more sophisticated types of mass

spectrometers such as tandem quadrupole mass spectrometers (Kourounioti et al., 2019; Petrovic et al., 2007).

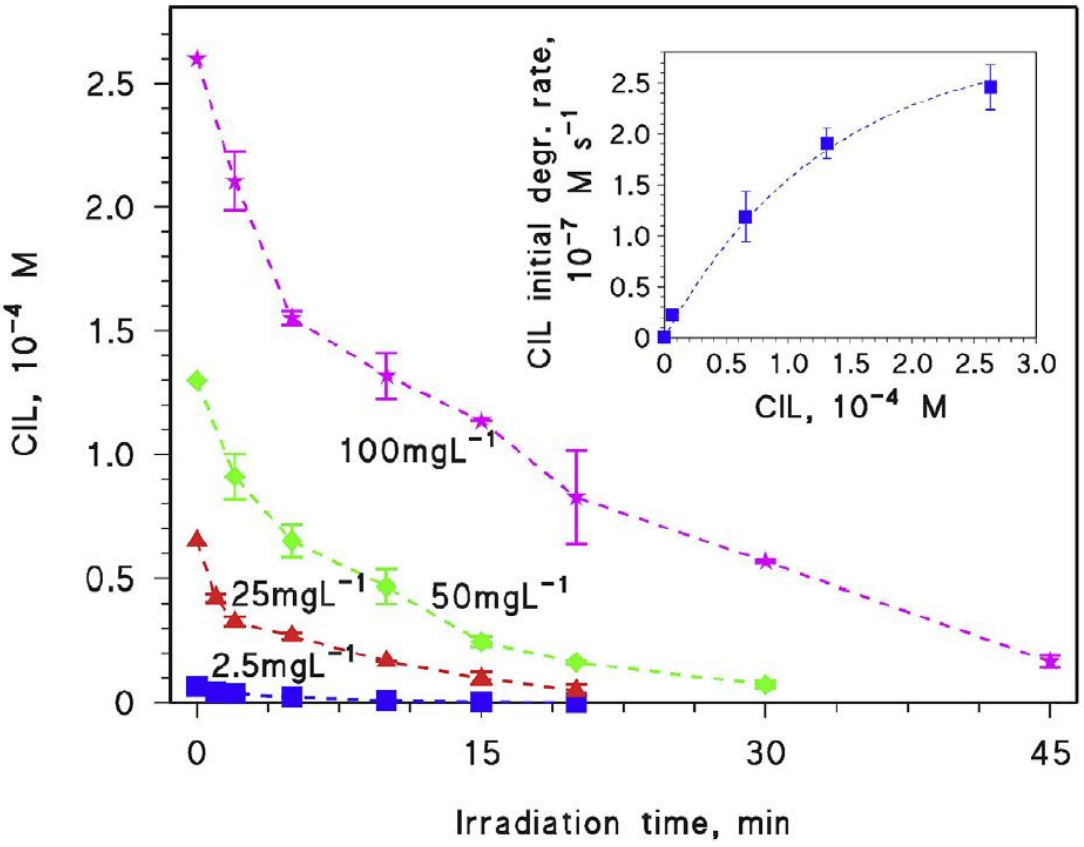

Fig. 5.1 Time trends of CIL concentration upon 254-nm irradiation at different initial concentration values, under ~ neutral conditions (pH ~ 7). Data points are linked with dashed lines to visualize trends. Inset: initial degradation rates (R_o = k C_o) for the different concentrations examined here (C_o). The dashed connecting curve represents data fit with Eq. (5.5). Some error bars are too small to be visible.

Moreover, co-elution of products formed further obstructed their identification. The only photoproduct that could be tentatively identified was P375 at $[M - H]^+$ = 375 m/z, where the sulfide moiety of CIL was oxidized to a sulfoxide group. In the Supporting Information, Fig. S.8 – Appendix 4 depicts the tentative mechanism and Table S.16 – Appendix 4 gives the summary of analytical characteristics. P375 appeared after exposing CIL to 254-nm radiation for 10 min and reached its maximum at 45 min. The amount of organics remaining in the system after complete conversion of CIL was also evaluated, by measuring the TOC of 15 mg L^{-1} CIL water solutions before irradiation and for up to 240 min of UV_{254} exposure, after which time only ~10% TOC removal was recorded. This observation pointed towards the formation and accumulation of

degradation products during irradiation, which were more recalcitrant than the parent compound (Yazdanbakhsh et al., 2018).

Another series of experiments studied the effect of pH on CIL degradation. The relevant time trends (see Fig. 5.2) suggest that degradation was faster at low pH and slowed down as the pH increased. A change in pH modifies the prevailing species that occur in solution, and the pH effect is most likely explained by different photochemical reactivity. The experimental degradation rate can be expressed as the sum of the contributions of the different species, each weighted for the relevant fraction, as follows:

$$R_o = \alpha_{H_3A^+} R_{H_3A^+} + \alpha_{H_2A} R_{H_2A} + \alpha_{HA^-} R_{HA^-} + \alpha_{A^{2-}} R_{A^{2-}} \quad (5.6)$$

where $\alpha_{H_3A^+}$, α_{H_2A}, α_{HA^-} and $\alpha_{A^{2-}}$ are expressed as per Eqs. (5.1)-(5.4) and are reported in Fig. S.7 – Appendix 4 in the Supporting Information.

The trend of R_0 vs. pH is shown in the inset of Fig. 5.2, and the experimental data (solid squares) were fitted with Eq. (5.6) using $R_{H_3A^+}$, R_{H_2A}, R_{HA^-} and $R_{A^{2-}}$ as floating parameters. The fit (see dashed curve in Fig. 5.2, inset) yielded $R_{H_3A^+} > R_{H_2A} > R_{HA^-} > R_{A^{2-}}$, which accounts for the observed pH trend. The contributions of the different CIL species to photodegradation (respectively, $\alpha_{H_3A^+} R_{H_3A^+}$, $\alpha_{H_2A} R_{H_2A}$, $\alpha_{HA^-} R_{HA^-}$ and $\alpha_{A^{2-}} R_{A^{2-}}$) are also reported in the inset of Fig. 5.2, as solid curves as a function of pH. Notably, degradation at pH 6-8 would mainly be accounted for by HA^-, and its kinetics is not expected to vary much in that pH interval.

The rate data derived for the different species ($R_{H_3A^+}$, R_{H_2A}, R_{HA^-} and $R_{A^{2-}}$) allow for the calculation of the relevant direct photolysis quantum yields. For a generic species x undergoing monochromatic 254-nm irradiation, the following relationship holds between the degradation rate R_x and the molar absorption coefficient at 254 nm, ε_x(254 nm):

$$R_x = \Phi_x I_o (1 - 10^{-\varepsilon_x(254nm) b C_o}) \quad (5.7)$$

where x = H_3A^+, H_2A, HA^- or A^{2-}, Φ_x is the direct photolysis quantum yield for the x species, $I_o = (6.24 \pm 0.19) \times 10^{-6}$ E L^{-1} s^{-1} the incident photon flux, b = 2 cm the optical path length, and the concentration $C_o = 2.6 \times 10^{-4}$ M (note that R_x is the contribution of the species x to the photodegradation of CIL when its molar fraction $\alpha_x = 1$, thus we

could use $C_x = C_o$). The absorbance of CIL was measured spectrophotometrically at 254 nm and at different pH values, and the experimental data of the molar absorption coefficients ε_{CIL}(254 nm) are reported in Fig. 5.3 as a function of pH (solid squares). The pH trend of ε_{CIL}(254 nm) is accounted for by fact that the different CIL species have different absorption coefficients ε_x(254 nm). Therefore, the experimental data can be fitted with the following equation:

$$\varepsilon_{CIL} = \alpha_{H_3A^+}\varepsilon_{H_3A^+} + \alpha_{H_2A}\varepsilon_{H_2A} + \alpha_{HA^-}\varepsilon_{HA^-} + \alpha_{A^{2-}}\varepsilon_{A^{2-}} \quad (5.8)$$

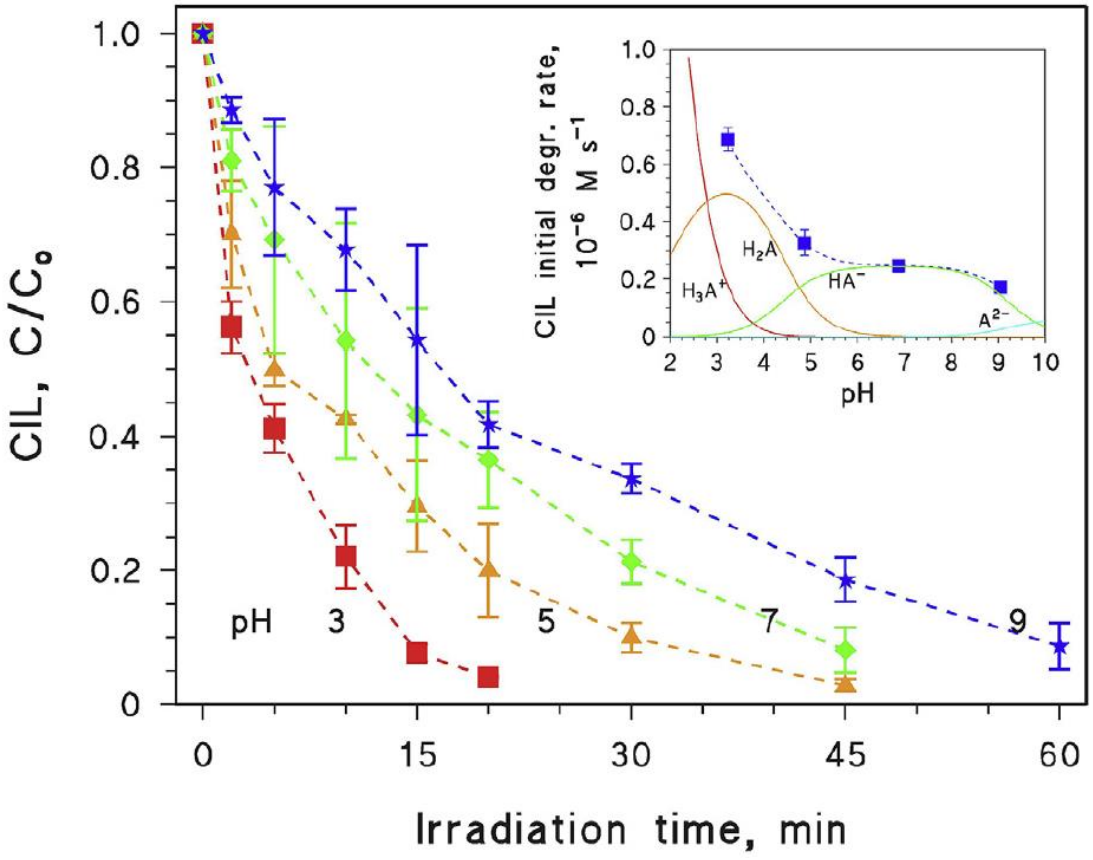

Fig. 5.2. Time trends of CIL (C_0 = 100 mg L^{-1} or 2.6 x 10^{-4} M) upon 254-nm irradiation, as a function of pH. Data points are linked with dashed lines to visualize trends. Inset: trend of R_0 (initial degradation rate of CIL) vs. pH. The solid blue squares are the experimental data, the dashed curve is the data fit with Eq. (5.6), using $R_{H_3A^+}$, R_{H_2A}, R_{HA^-} and $R_{A^{2-}}$ as free-floating parameters. The solid curves represent the contributions to photodegradation of the different CIL species. Some error bars are too small to be visible. (For interpretation of the references to colour in this figure legend, the reader is referred to the Web version of this article.)

where all the molar absorption coefficients are referred to 254 nm. The fit of the ε_{CIL} experimental data with Eq. (5.8), using $\varepsilon_{H_3A^+}$, ε_{H_2A}, ε_{HA^-} and $\varepsilon_{A^{2-}}$ as floating parameters, yielded the values of the 254- nm molar absorption coefficients of H_3A^+, H_2A, HA^- and A^{2-} that are reported in Table S.17 – Appendix 4 in the Supporting Information. With these values and those of R_x it is possible to obtain the direct photolysis quantum yields of the various species at 254 nm, using the relationship reported in Eq. (5.7). The quantum yield data thus calculated are reported in Table S.17 – Appendix 4 in the Supporting Information as well, and they follow the order $\Phi_{H_3A^+} > \Phi_{H_2A} > \Phi_{HA^-} > \Phi_{A^{2-}}$. The quantum yield value of H_3A^+ is remarkably high, which explains why H_3A^+ undergoes faster photodegradation compared to H_2A (Fig. 5.2), although it absorbs radiation at a somewhat lesser extent (Fig. 5.3).

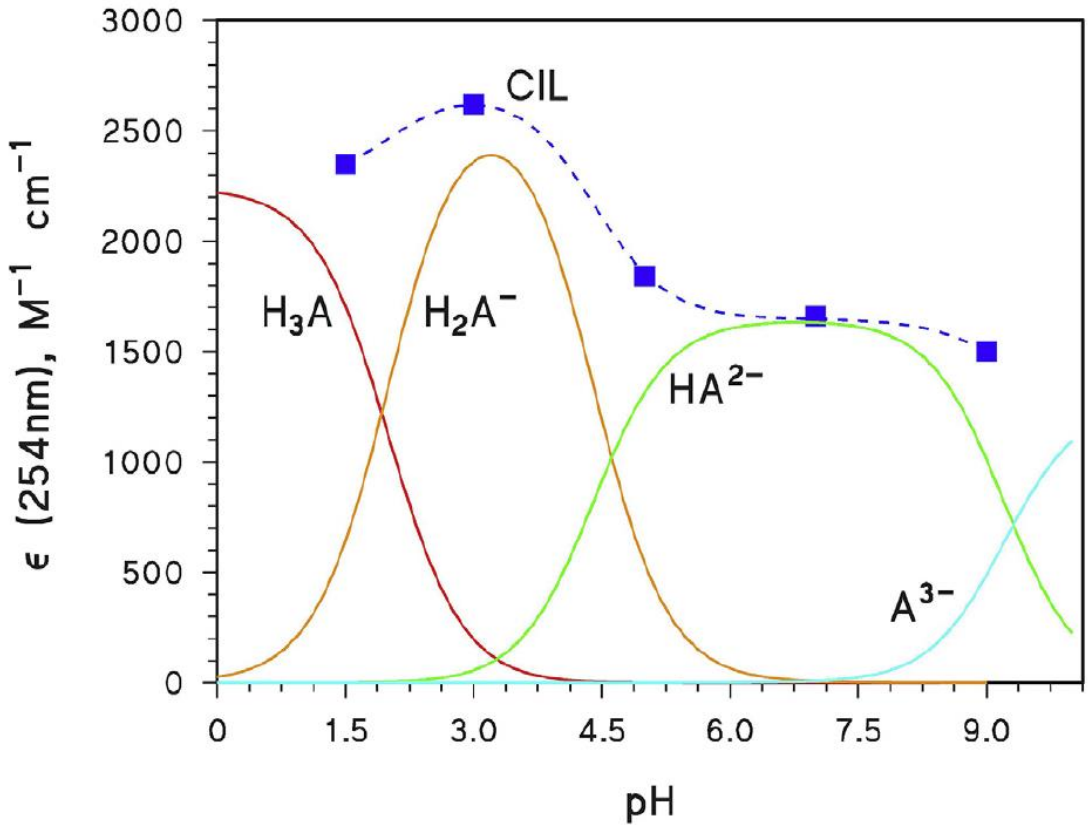

Fig. 5.3 Molar absorption coefficients (254 nm) of CIL and its different species, as a function of pH. The solid squares are the experimental data; the dashed curve is the data fit with Eq. (5.8), using $\varepsilon_{H_3A^+}$, ε_{H_2A}, ε_{HA^-} and $\varepsilon_{A^{2-}}$as floating parameters; the solid curves represent the contributions to radiation absorption of the different CIL species (given by the respective product $\alpha_{H_3A^+}\varepsilon_{H_3A^+}$, $\alpha_{H_2A}\varepsilon_{H_2A}$, $\alpha_{HA^-}\varepsilon_{HA^-}$, and $\alpha_{A^{2-}}\varepsilon_{A^{2-}}$).

5.4.2. EFFECT OF DISSOLVED SPECIES

In some cases, the direct photolysis of organic molecules follows a self-sensitized pathway where the excited state of a compound is involved in the degradation of the same compound in the ground-state. The occurrence of a bimolecular reaction between excited and ground states ensures that the process kinetics becomes faster as the concentration C_0 increases (Bedini et al., 2012). In such cases the trend of R_0 vs. C_0 would not follow absorption saturation, and the latter should underestimate the degradation kinetics at high C_0. The data reported in the inset of Fig. 5.1 show that degradation kinetics in our study strictly adhered to the absorption saturation model. Therefore, a self-sensitized process can be excluded. The same data rule out as well the opposite phenomenon, that ground state CIL quenches the excited states of the same molecule. Indeed, in such cases one expects R_0 to grow more slowly with C_0 compared to the case of absorption saturation, sometimes yielding a trend with a maximum (Minto et al., 1989). The experimental data of Fig. 5.1 rather suggest that CIL follows direct photolysis triggered by evolution of the excited state(s), excluding important interactions between these and the ground state.

In some relatively rare circumstances, the irradiation of a molecule in water can trigger $^{\bullet}$OH production. This happens for instance if the excited state is able to oxidize water (Sur et al., 2011), and in such cases photogenerated $^{\bullet}$OH could contribute to the degradation process. Such a hypothesis can be checked by addition of $^{\bullet}$OH scavengers to the irradiated system. t-butanol is a common and rather selective $^{\bullet}$OH scavenger that can be useful to this purpose (Buxton et al., 1988; Neta et al., 1988; Tsiampalis et al., 2019; Stathoulopoulos et al., 2020). As shown in Fig. S.9 – Appendix 4 in the Supporting Information, the addition of 100 mg L^{-1} t-butanol had very little effect on CIL degradation, thereby suggesting that the transformation process does not involve $^{\bullet}$OH to a significant degree. It is noted that the experimental data obtained with alcohols should be treated with caution, because sometimes alcohols scavenge reactive states rather than $^{\bullet}$OH (Vione et al., 2010). However, in the present case the alcohol had a minor effect that suggests a limited importance of both $^{\bullet}$OH production and the possible confounding process (in contrast, the finding that t-butanol inhibits photolysis would not necessarily prove that the process involves $^{\bullet}$OH).

Natural water components can affect photodegradation either by competing with the substrate for the incoming photons, or by sensitizing its transformation (Canonica and Freiburghaus, 2001). Differently from the case of self-sensitization, in this indirect photochemical path the excited state of another compound (i.e. the photosensitizer) triggers degradation by reacting with the ground-state substrate (McNeill and Canonica, 2016). Actually, while competition for lamp irradiance by other compounds inhibits degradation, the sensitization process favors it.

Humic substances are major light absorbers and photosensitizers in surface waters (Rosario-Ortiz and Canonica, 2016), thus they are very suitable compounds with which to test the inhibition/sensitization potential. The presence of humic compounds at environmental concentrations (2.5 mg L^{-1}) inhibited the photodegradation of CIL as shown in Fig. 5.4. This result suggests that humic acids can act as radiation absorbers, thereby inhibiting the direct photolysis of the substrate, and that this inhibition process prevails over photosensitization (*vide infra* for additional calculations over this issue).

5.4.3. CIL PHOTODEGRADATION IN REAL WATER MATRICES

In addition to humic substances, other components (organic and inorganic) that occur in natural waters might affect (either inhibit or enhance) the photodegradation kinetics of CIL. Therefore, photodegradation experiments were also carried out in the presence of natural water and treated wastewater samples spiked with CIL. The results of these experiments are shown in Fig. 5.5. Similar transformation rates were obtained in ultra-pure (Milli-Q quality) and tap water, while inhibition of CIL photodegradation was observed in river water and WW effluent. The recorded decrease in degradation kinetics with increasing matrix complexity, signified the importance of the organic and inorganic constituents typically found in natural waters and wastewaters.

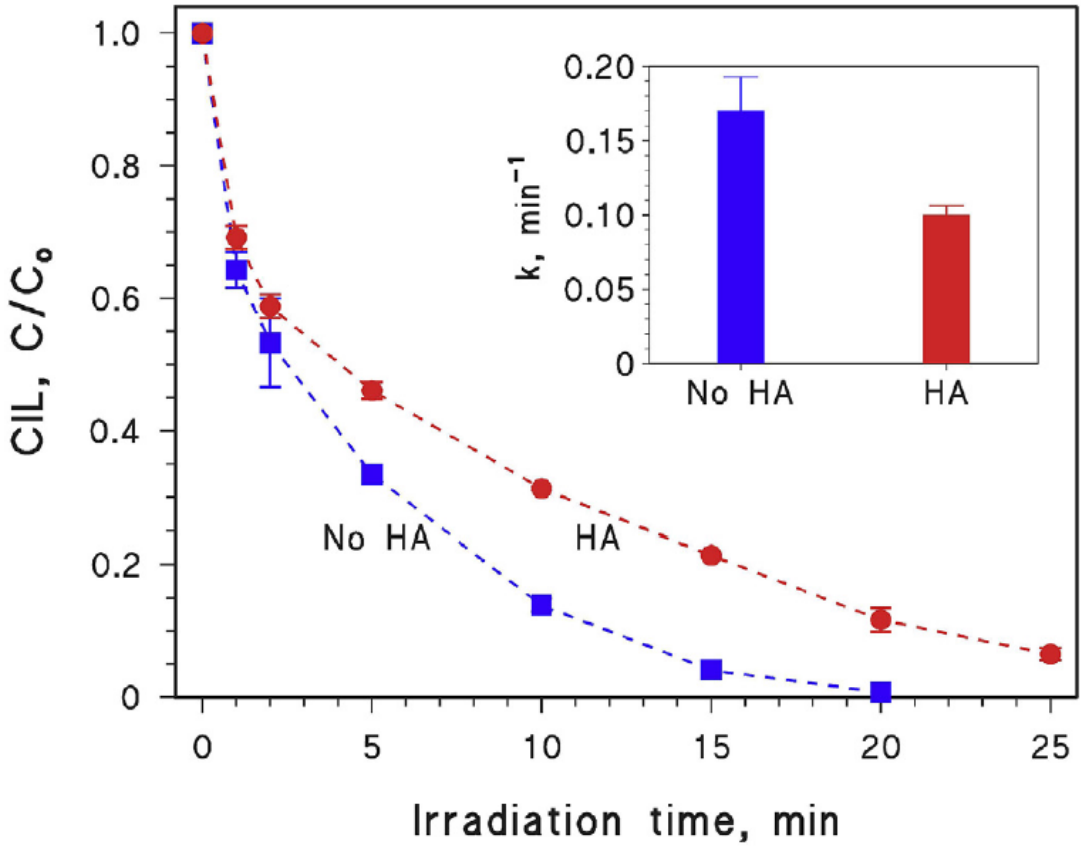

Fig. 5.4 Time trends of 2.5 mg L^{-1} CIL upon 254-nm irradiation at near-neutral pH, alone and upon addition of 2.5 mg L^{-1} humic acids (HA). Data points are linked with dashed lines to visualize trends. Inset: pseudo-first order photodegradation rate constants, together with their sigma-level error bounds. Some error bars are too small to be visible.

The absorption of radiation by CIL at concentration C_0 (in our case, C_0 = 2.5 mg L^{-1} that corresponds to 7 × 10^{-6} M) in solution can be expressed as the absorbed photon flux $P_{a,CIL}$ [E L^{-1} s^{-1}], which reads as follows according to the Lambert-Beer law (Braslavsky, 2007):

$$P_{\alpha,CIL} = I_0[1 - 10^{-\varepsilon_{CIL}(254nm)\times b\times C_0}] \quad (5.9)$$

where I_0 = 6.24 × 10^{-6} E L^{-1} s^{-1} is the incident photon flux from the lamp, ε_{CIL}(254 nm) =1660 L mol^{-1} cm^{-1} the molar absorption coefficient of CIL (HA^-) at the specified wavelength and pH 7, b = 2 cm the optical path length, and C_0 = 7 × 10^{-6} M the initial CIL concentration.

Eq. (5.9) holds if CIL is the only light-absorbing species in solution. In the presence of other light-absorbing compounds (Sheikhmohammadi et al., 2019), the photon flux absorbed by CIL gets modified as follows (Braslavsky, 2007):

$$P'_{\alpha,CIL} = I_0 \frac{\varepsilon_{CIL}(254nm)\times C_0}{A_W(254nm)}\left[1 - 10^{-A_W(254nm)\times b}\right] \quad (5.10)$$

where A_w(254 nm) [cm^{-1}] is the 254-nm absorbance of the water matrix spiked with CIL (in the present case, HA solution, tap water, river water or wastewater). In particular, it was A_w(254 nm) = 0.073 cm^{-1} for 2.5 mg L^{-1} HA, 0.034 cm^{-1} for tap water, 0.061 cm^{-1} for river water, and 0.240 cm^{-1} for wastewater.

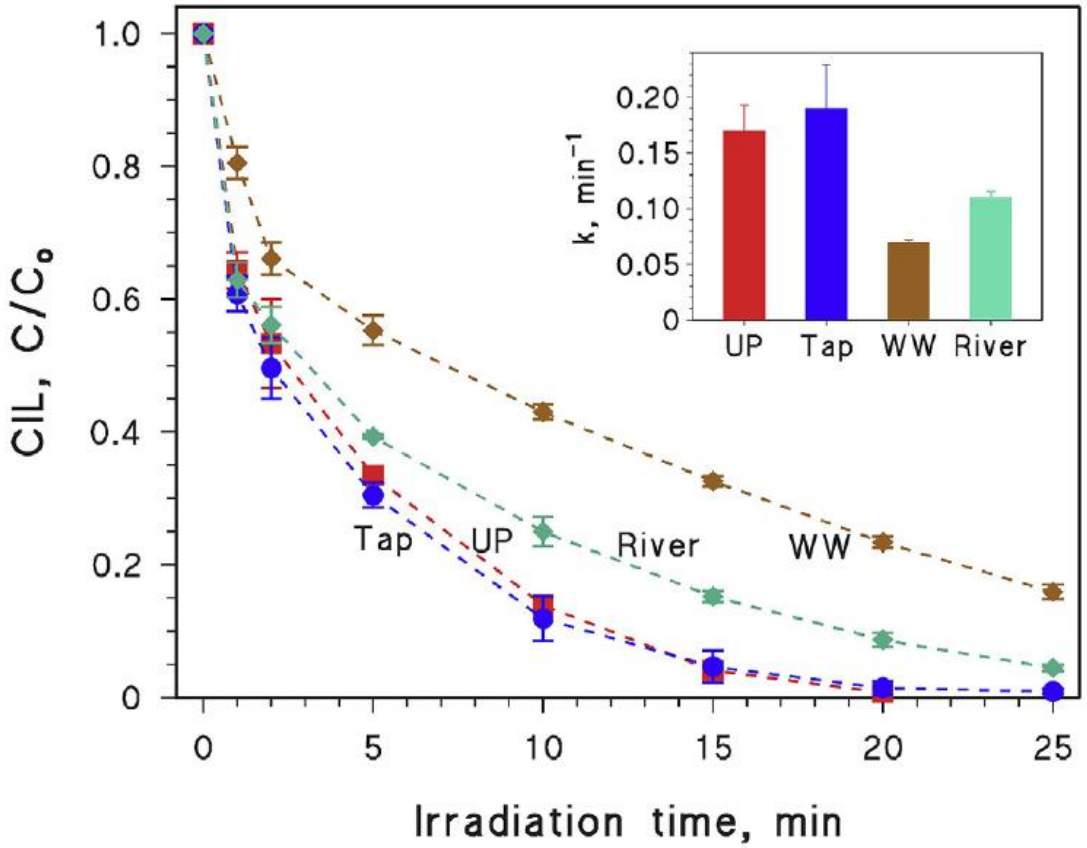

Fig. 5.5 Time trends of 2.5 mg L^{-1} CIL upon 254-nm irradiation in different water matrices: ultra-pure water (UP), tap water (Tap), treated wastewater (WW) and river water (River). Data points are linked with dashed lines to visualize trends. Inset: respective pseudo-first order photodegradation rate constants, together with their sigma-level error bounds. Some error bars are too small to be visible.

If the water matrix only affected radiation absorption by CIL, leaving its direct photolysis quantum yield unchanged, one would expect the CIL photolysis kinetics to be directly proportional to $P_{a,CIL}$. The trend of k (pseudo first-order photodegradation rate constant) as a function of $P_{a,CIL}$ is reported in Fig. 5.6 for the different samples, where the dashed line shows the trend that would be expected at constant photolysis quantum yield. It is clearly shown that only tap water follows a comparable trend as ultra-pure water, while the other water matrices and the sample containing HA feature

lower quantum yields for the direct photolysis of CIL (the relevant data points are unequivocally located below the dashed line, even when accounting for the experimental uncertainty). This finding suggests that the natural water components may on the one hand compete with CIL for the lamp irradiance; on the other hand, they do not behave as photosensitizers (in which case the relevant data points should be located above the dashed line) but rather inhibit the direct photolysis of CIL by lowering its quantum yield.

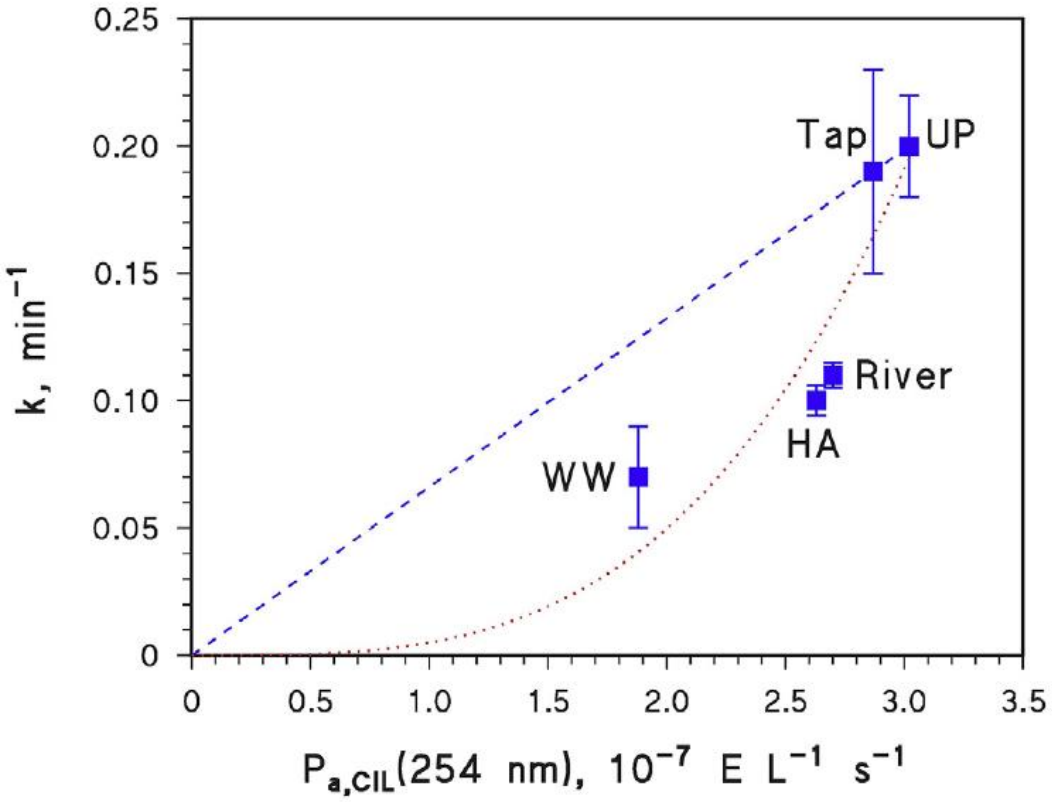

Fig. 5.6 Correlation between the pseudo-first order rate constant of CIL degradation (k) and the photon flux absorbed by CIL in solution ($P_{a,CIL}$). The dashed line shows the trend that would be expected if the water matrix (UP = ultra-pure water; Tap = tap water; HA = humic acids; River = river water; WW = wastewater) only acted as radiation absorber. The error bounds represent the sigma-level uncertainty deriving from the exponential fit of the time trend data, while the dotted curve is the result of data fit with a power function ($k = \alpha (P_{a,CIL})^{\beta}$).

Such a phenomenon of direct photolysis inhibition has already been observed in the presence of a range of natural organic compounds including humic substances (Vione et al., 2010; Liu et al., 2020), and might involve either the physical quenching of CIL excited states (which would be quenched back to the ground state, inhibiting photolysis), or the back-reduction to CIL of partially oxidized degradation

intermediates such as radicals or radical cations. The back-reduction effect could be triggered by the antioxidant (mostly phenolic) moieties that are ubiquitous in both HA and the natural organic matter (Wenk and Canonica, 2012).

5.5. CONCLUSION

The rising global consumption of antibiotics resulted in the widespread occurrence of antibiotic formulations in the aquatic environment. Although past investigations report the photolytic behavior of antibiotics, they overlook studying the entailed problem of co-administered agents released in water bodies. This is the first contribution studying in depth the direct photolysis of cilastatin, a co-administered agent for the antibiotic imipenem, under 254-nm irradiation. The experimental data showed fast depletion of cilastatin in water under UVC, and suggested that the direct photolysis of cilastatin is an efficient degradation technique. Our experimental and modelling data demonstrated that degradation proceeded faster at low pH values, thereby suggesting that altering the pH can synergistically accelerate degradation kinetics. Moreover, we showed that the transformation process does not involve $^{\bullet}OH$ to a significant degree, and that radiation absorbers may slow down degradation kinetics. Finally, degradation rates decreased with increasing matrix complexity (tap water ~ ultra-pure water > river water > wastewater effluent), suggesting that the natural water components may both compete with cilastatin for the 254 nm photon absorption and decrease its direct photolysis quantum yield. Nonetheless, cilastatin depletion in complex matrices can be completed within reasonable exposure times.

5.6. REFERENCES

Alberti, S., Sotiropoulou, M., Fernandez, E., Solomou, N., Ferretti, M., Psillakis, E., (2021). UV-254 degradation of nicotine in natural waters and leachates produced from cigarette butts and heat-not-burn tobacco products. *Environmental Research*, 110695 https://doi.org/10.1016/j.envres.2020.110695.

Bedini, A., De Laurentiis, E., Sur, B., Maurino, V., Minero, C., Brigante, M., Mailhot, G., Vione, D., (2012). Phototransformation of anthraquinone-2-sulphonate in aqueous solution. *Photochemical and Photobiological Sciences*, 11, 1445. https://doi.org/10.1039/c2pp25111f.

Braslavsky, S.E., (2007). Glossary of terms used in photochemistry, 3rd edition (IUPAC Recommendations 2006). *Pure and Applied Chemistry,* 79, 293-465. https://doi.org/10.1351/pac200779030293.

Briones, A.A., Guevara, I.C., Mena, D., Espinoza, I., Sandoval-Pauker, C., Guerrero, L.R., Jentzsch, P.V., Bisesti, F.M., (2020). Degradation of meropenem by heterogeneous photocatalysis using TiO2/fiberglass substrates. *Catalysts,* 10, 3-5. https://doi.org/10.3390/catal10030344.

Buxton, G.V., Greenstock, C.L., Helman, W.P., Ross, A.B., (1988). Critical Review of rate constants for reactions of hydrated electrons, hydrogen atoms and hydroxyl radicals ($^{\bullet}OH/^{\bullet}O^{-}$ in Aqueous Solution. *The Journal of Physical Chemistry,* Ref. Data 17, 513-886. https://doi.org/10.1063/1.555805.

Cabrera-Reina, A., Martínez-Piernas, A.B., Bertakis, Y., Xekoukoulotakis, N.P., Agüera, A., Sanchez Perez, J.A., (2019). TiO2 photocatalysis under natural solar radiation for the degradation of the carbapenem antibiotics imipenem and meropenem in aqueous solutions at pilot plant scale. *Water Research,* 166, 115037. https://doi.org/10.1016/j.watres.2019.115037.

Canonica, S., Freiburghaus, M., (2001). Electron-rich phenols for probing the photochemical reactivity of freshwaters. *Environmental Science & Technology,* 35, 690-695. https://doi.org/10.1021/es0011360.

Cheng, S.F., Lee, Y.C., Kuo, C.Y., Wu, T.N., (2015). A case study of antibiotic wastewater treatment by using a membrane biological reactor system. *International Biodeterioration & Biodegradation,* 102, 398-401. https://doi.org/10.1016/j.ibiod.2015.04.018.

Drugbank, (2020). last assessed: December 2020. https://go.drugbank.com/drugs/DB01597.

Drusano, G.L., Standiford, H.C., Bustamante, C., Forrest, A., Rivera, G., Leslie, J., Tatem, B., Delaportas, D., MacGregor, R.R., Schimpff, S.C., (1984). Multiple-dose pharmacokinetics of imipenem-cilastatin. *Antimicrobial Agents and Chemotherapy,* 26, 715-721. https://doi.org/10.1128/AAC.26.5.715.

Godini, H., Sheikhmohammadi, A., Abbaspour, L., Heydari, R., Khorramabadi, G.S., Sardar, M., Mahmoudi, Z., (2019). Energy consumption and photochemical degradation of Imipenem/Cilastatin antibiotic by process of UVC/Fe 2+/H 2 O 2 through response surface methodology. *Optik - International Journal for Light and Electron Optics*, 182, 1194-1203. https://doi.org/10.1016/j.ijleo.2019.01.071.

Hsieh, J.Y.K., Maglietto, B.K., Bayne, W.F., (1985). Separation identification, and quantification of n-acetyl cilastatin in human urine. *Journal of Liquid Chromatography*, 8, 513-520. https://doi.org/10.1080/01483918508067097.

Hutt, A.J., O'Grady, J., (1996). Drug chirality: a consideration of the significance of the stereochemistry of antimicrobial agents. *Journal of Antimicrobial Chemotherapy*, 37, 7-32. https://doi.org/10.1093/jac/37.1.7.

Klein, E.Y., Boeckel, T.P. Van, Martinez, E.M., Pant, S., Gandra, S., Levin, S.A., Goossens, H., Laxminarayan, R., (2018). Global increase and geographic convergence in antibiotic consumption between 2000 and 2015. *Proceedings of the National Academy of Sciences*, 115, E3463-E3470. https://doi.org/10.1073/PNAS.1717295115.

Kourounioti, E., Psillakis, E., Vione, D., (2019). UV-induced transformation of 2,3-dibromo-5,6-dimethyl-1,4-benzoquinone in water and treated wastewater. *Environmental Research*, 175, 343-350. https://doi.org/10.1016/j.envres.2019.05.018.

Kumarasamy, K.K., Toleman, M.A., Walsh, T.R., Bagaria, J., Butt, F., Balakrishnan, R., Chaudhary, U., Doumith, M., Giske, C.G., Irfan, S., Krishnan, P., Kumar, A.V., Maharjan, S., Mushtaq, S., Noorie, T., Paterson, D.L., Pearson, A., Perry, C., Pike, R., Rao, B., Ray, U., Sarma, J.B., Sharma, M., Sheridan, E., Thirunarayan, M.A., Turton, J., Upadhyay, S., Warner, M., Welfare, W., Livermore, D.M., Woodford, N., (2010). Emergence of a new antibiotic resistance mechanism in India, Pakistan, and the UK: a molecular, biological, and epidemiological study. *The Lancet Infectious Diseases*, 10, 597-602. https://doi.org/10.1016/S1473-3099(10)70143-2.

Liu, Y., Mekic, M., Carena, L., Vione, D., Gligorovski, S., Zhang, G., Jin, B., (2020). Tracking photodegradation products and bond-cleavage reaction pathways of triclosan using ultra-high resolution mass spectrometry and stable carbon isotope analysis. *Environmental Pollution*, 264, 114673. https://doi.org/10.1016/j.envpol.2020.114673.

McNeill, K., Canonica, S., (2016). Triplet state dissolved organic matter in aquatic photochemistry: reaction mechanisms, substrate scope, and photophysical properties. *Environmental Science: Processes & Impacts*, 18, 1381-1399. https://doi.org/10.1039/C6EM00408C.

Minto, R., Samanta, A., Das, P.K., (1989). Time-resolved nanosecond and picosecond absorption studies of excited-state properties of 1-thiobenzoylnaphthalene. *Canadian Journal of Chemistry*, 67, 967-972. https://doi.org/10.1139/v89-148.

Neta, P., Huie, R.E., Ross, A.B., (1988). Rate constants for reactions of inorganic radicals in aqueous solution. *The Journal of Physical Chemistry*, Ref. Data 17, 1027-1284. https://doi.org/10.1063/1.555808.

Norrby, S.R., Rogers, J.D., Ferber, F., Jones, K.H., Zacchei, A.G., Weidner, L.L., Demetriades, J.L., Gravallese, D.A., Hsieh, J.Y., (1984). Disposition of radiolabeled imipenem and cilastatin in normal human volunteers. *Antimicrobial Agents and Chemotherapy*, 26, 707-714. https://doi.org/10.1128/AAC.26.5.707.

Nourmoradi, H., Asgari, E., Sheikhmohammadi, A., Manshouri, M., (2019). Performance intensification of BzP photo-catalytic degradation through adding exogenous oxidant. *Optik - International Journal for Light and Electron Optics.* https://doi.org/10.1016/j.ijleo.2019.163571.

Papp-Wallace, K.M., Endimiani, A., Taracila, M.A., Bonomo, R.A., (2011). Carbapenems: past, present, and future. *Antimicrobial Agents and Chemotherapy*. https://doi.org/10.1128/AAC.00296-11.

Petrovic, M., Petrovic, M., Barcelo, D., (2007). LC-MS for identifying photodegradation products of pharmaceuticals in the environment. *TrAC Trends in Analytical Chemistry*, (Reference Ed.) 26, 486-493. https://doi.org/10.1016/j.trac.2007.02.010.

Proia, L., Anzil, A., Borrego, C., Farre, M., Llorca, M., Sanchis, J., Bogaerts, P., Balcazar, J.L., Servais, P., (2018). Occurrence and persistence of carbapenemases genes in hospital and wastewater treatment plants and propagation in the receiving river. *Journal of Hazardous Materials*, 358, 33-43. https://doi.org/10.1016/j.jhazmat.2018.06.058.

Reina, A.C., Martínez-Piernas, A.B., Bertakis, Y., Brebou, C., Xekoukoulotakis, N.P., Agüera, A., Sanchez Perez, J.A., (2018). Photochemical degradation of the carbapenem antibiotics imipenem and meropenem in aqueous solutions under solar radiation. *Water Research,* 128, 61-70. https://doi.org/10.1016/j.watres.2017.10.047.

Rosario-Ortiz, F.L., Canonica, S., (2016). Probe compounds to assess the photochemical activity of dissolved organic matter. *Environmental Science & Technology,* 50, 12532-12547. https://doi.org/10.1021/acs.est.6b02776.

Sheikhmohammadi, A., Yazdanbakhsh, A., Moussavi, G., Eslami, A., Rafiee, M., Sardar, M., Almasian, M., (2019). Degradation and COD removal of trichlorophenol from wastewater using sulfite anion radicals in a photochemical process combined with a biological reactor: mechanisms, degradation pathway, optimization and energy consumption. *Process Safety and Environmental Protection*, 123, 263-271. https://doi.org/10.1016/j.psep.2019.01.020.

Stathoulopoulos, A., Mantzavinos, D., Frontistis, Z., (2020). Coupling persulfate-based AOPs: a novel approach for piroxicam degradation in aqueous matrices. *Water,* 12. https://doi.org/10.3390/W12061530.

Sur, B., Rolle, M., Minero, C., Maurino, V., Vione, D., Brigante, M., Mailhot, G., (2011). Formation of hydroxyl radicals by irradiated 1-nitronaphthalene (1NN): oxidation of hydroxyl ions and water by the 1NN triplet state. *Photochemical & Photobiological Sciences*, 10, 1817. https://doi.org/10.1039/c1pp05216k.

Szekeres, E., Baricz, A., Chiriac, C.M., Farkas, A., Opris, O., Soran, M.L., Andrei, A.S., Rudi, K., Balcazar, J.L., Dragos, N., Coman, C., (2017). Abundance of antibiotics, antibiotic resistance genes and bacterial community composition in wastewater effluents from different Romanian hospitals. *Environmental Polluion,* 225, 304-315. https://doi.org/10.1016/j.envpol.2017.01.054.

Tran, N.H., Chen, H., Reinhard, M., Mao, F., Gin, K.Y.H., (2016). Occurrence and removal of multiple classes of antibiotics and antimicrobial agents in biological wastewater treatment processes. *Water Research,* 104, 461-472. https://doi.org/10.1016/j.watres.2016.08.040.

Tsiampalis, A., Frontistis, Z., Binas, V., Kiriakidis, G., Mantzavinos, D., (2019). Degradation of sulfamethoxazole using iron-doped titania and simulated solar radiation. *Catalysts*, 9, 612. https://doi.org/10.3390/catal9070612.

Vione, D., Khanra, S., Das, R., Minero, C., Maurino, V., Brigante, M., Mailhot, G., (2010). Effect of dissolved organic compounds on the photodegradation of the herbicide MCPA in aqueous solution. *Water Research*, 44, 6053-6062. https://doi.org/10.1016/j.watres.2010.07.079.

Wenk, J., Canonica, S., (2012). Phenolic antioxidants inhibit the triplet-induced transformation of anilines and sulfonamide antibiotics in aqueous solution. *Environmental Science & Technology*, 46, 5455-5462. https://doi.org/10.1021/es300485u.

Yazdanbakhsh, A., Eslami, A., Moussavi, G., Rafiee, M., Sheikhmohammadi, A., (2018). Photo-assisted degradation of 2, 4, 6-trichlorophenol by an advanced reduction process based on sulfite anion radical: degradation, dechlorination and mineralization. *Chemosphere*, 191, 156-165. https://doi.org/10.1016/j.chemosphere.2017.10.023.

Yılmaz, C., Ozcengiz, G., (2017). Antibiotics: pharmacokinetics, toxicity, resistance and multidrug efflux pumps. *Biochemical Pharmacology*, 133, 43-62. https://doi.org/10.1016/j.bcp.2016.10.005.

CHAPTER 6: CONCLUSIONS AND FUTURE WORK

6.1. CONCLUSIONS

The present doctoral thesis is centered on the theme of detection and fate of organic pollutants in water. The investigation was carried out through concentric scientific projects, in a way that enabled that their execution was able to be effectuated in a connective manner and produce interesting results.

At the outset, HSSE sampling under vacuum conditions (Vac-HSSE) was introduced within the context of the present thesis for the first time. Vac-HSSE was proven experimentally, with the extraction of polycyclic aromatic hydrocarbons (PAHs) from water samples, (and theoretically), to be a viable tool to accelerate extraction kinetics and reduce equilibration times, since the low surface area to volume ratio of the stir bar typically results in long equilibration times at 1 atm compared to other PDMS-based methods (e.g., SPME). An effort was made to comprehend the theoretical aspects of the extraction kinetics in the pre-equilibrium phase, as prior to that, research has been focused only on equilibrium conditions. Consequently, the theoretical model describing the pressure dependence of Vac-HSSE was here discussed and the reduction in equilibration times was predicted. The results underscored, for the first time, the fact that at 1 atm gas-sided resistance imposed significant limitations to the analyte uptake by the stir bar and subsequently to the extraction kinetics. This issue was successfully restricted by the utilization of the vacuum sampling approach. Correspondingly, the gas-sided limitations that could govern both the evaporation and analyte uptake stages were restrained by sampling under vacuum which assisted on the overall acceleration of the extraction kinetics. The positive combined effect of vacuum and temperature on HSSE was also proven to be possible due to the high PDMS volume and layer thickness of the stir bar coating, which essentially prevented water molecules from interfering with the overall analyte uptake. Additionally, lowering the sample pressure significantly reduced the time needed for the analytes to reach equilibrium, adding to an improvement of the yielded extraction kinetics and analytical performance of the Vac-HSSE in contrast with that recorded with regular HSSE.

Thenceforwards, within the framework of investigating PAHs, the research was oriented in the direction of the determination of total and bioavailable concentrations of PAHs in HnBs tobacco products and compared the results to those obtained with

CCs. Although in the past researchers, evaluated and compared the total concentration of PAH content from cigarette butts collected in cafeterias, near various urban sites and by a river (Dobaradaran et al., 2019), and studied the dissolved concentrations of PAHs in cigarette butts leachates in river, tap and deionized water in different leaching times (Dobaradaran et al., 2020), there was no interest in the impact of the exposure in the water element of novel 'heat-not-burn' tobacco products in comparison with the conventional cigarette butts. Our research demonstrated that total PAHs concentrations in smoked CCs are higher than in non-combustible HnBs tobacco products. It was also concluded that tobacco and filter were the most contaminated parts of HnBs products after operation as opposed to smoked CCs where the spent filter was the main part in which a substantial amount of PAHs resided in. Regardless the high total PAHs concentration detected in used CCs, similar sums of bioavailable PAHs concentrations were found in all leachates. This important finding can be seemingly explained by the fact that smoking affects the leachability of PAHs, rendering them highly absorbed to the solid matrix, thus delaying their desorption to the water element. In this instance, improperly discarded CCs can act as point sources of long-term PAHs contamination. Lastly, it was demonstrated that varying the composition of water did not affect the PAHs leaching.

Furthering our research into HnBs in correspondence with CCs, we investigated for the very first time the photolysis of nicotine in natural waters and water leachates produced by the aforementioned tobacco products. The results showed fast UV-254 degradation of nicotine in aqueous matrices, but low total organic carbon removal, due to the formation of photoproducts which were apparently more recalcitrant than the parent compound. At pH= 5-8 (where the monoprotonated form of nicotine is the primary species present) decomposition was faster compared to that at pH 9.0. The apparent pseudo-first order rate constants confirmed the enhanced photodegradation rate of nicotine when the monoprotonated nicotine species is the most abundant. The direct photolysis kinetics of nicotine in rain water appeared to be somewhat enhanced compared to the rest of the natural water samples (sea and river water) tested and it was assumed to be the result of the more acidic pH of this matrix. Nicotine degradation in the leachates proceeded in slightly slower kinetics compared to ultrapure water considering the increased complexity of the leachate compared to ultrapure water. Additionally, all total content of nicotine in used and unused tobacco products was

found to be released during leaching experiments. Overall, the findings demonstrate the importance of properly disposing tobacco product waste to prevent nicotine leaching in water bodies, as it was found that after operation, ~70% of the total and bioavailable nicotine content remains in HnBs compared to the 15% in CCs.

In closing, the research was steered towards a pharmaceutical compound's UVC-induced degradation in natural water and treated wastewater, a renal dehydropeptidase inhibitor called cilastatin, whose photochemical fate was little known up to this point. The experimental data showed fast UV-254 degradation of cilastatin in water, rendering photolysis of cilastatin an efficient process to deplete this compound from different water matrices. UV-254 photolysis of cilastatin occurred faster at lower pH values, which seems to indicate that pH modifications can coactively lead to significant acceleration of degradation kinetics. On the other hand, degradation was found to be slower at higher initial concentrations of the parent compound due to absorption saturation. It was verified that direct photolysis of cilastatin does not involve ·OH, as well as that radiation absorbers could decelerate the degradation kinetics. Last but not least, photolysis quantum yield was lower in water matrices compared to ultra-pure water, due to the presence of water components which can compete with cilastatin for the 254 nm photon absorption.

6.2. FUTURE WORK

The implementation of Vac-HSSE on other classes of organic pollutants (i.e., Polychlorinated biphenyls (PCBs), organophosphates (OPs), BTEX chemicals, organic pesticides etc.) should be explored further.

Concerning the issue risk assessment regarding the pollutants of tobacco product waste, the application of targeted analysis could be helpful in future studies, although in the case of complex matrices, such as the leachates produced by tobacco products, targeted organics cannot be solely considered as a source of toxicity. Therefore, it is advisable that future research should consider employing comprehensive two-dimensional gas chromatography (GC × GC), which is a progressive analytical tool that enables enhanced separations of complex mixtures. In that manner, novel ideas will be brought to surface in order to address the global environmental issue of disposing tobacco product waste properly. Likewise, the implementation of GC × GC will facilitate the

detection to the utmost possible degree of the photoproducts produced in complex matrices such as the tobacco product leachates.

Ultimately, one of the objectives of the present studies was to steer public awareness towards tobacco product waste as an alarming outcome of improper litter disposal. Therefore, it is crucial to align research efforts towards characterizing, managing, recycling and disposing the tobacco product waste which has been found not only to leach toxic chemicals in the aquatic ecosystems but also the non-biodegradable filters which are a ubiquitous source of microplastics.

Concerning the degradation of the compound of cilastatin, comprehensive two-dimensional gas chromatography (GC × GC) can be employed as well in future works for the identification of the formulated and accumulated degradation products.

PUBLICATIONS

- N. Solomou, E. Fernández, R. Szafnauer, E. Psillakis, Total and bioavailable polycyclic aromatic hydrocarbons in unused and operated heat-not-burn tobacco products and conventional cigarettes, Chemosphere, 335 (2023), 139050, https://doi.org/10.1016/j.chemosphere.2023.139050.
- N. Solomou, M. Minella, D. Vione, E. Psillakis, UVC-induced direct photolysis as an efficient process for the degradation of cilastatin in natural and waste water, Chemosphere, 280 (2021), 130668 https://doi.org/10.1016/j.chemosphere.2021.130668 .
- S. Alberti, M. Sotiropoulou, E. Fernández, N. Solomou, M. Ferretti, E. Psillakis, UV-254 degradation of nicotine in natural waters and leachates produced from cigarette butts and heat-not-burn tobacco products., Environ Res. (2021) 110695, https://doi.org/10.1016/j.envres.2020.110695.
- N. Solomou, C. Bicchi, B. Sgorbini, E. Psillakis, Vacuum-assisted headspace sorptive extraction: Theoretical considerations and proof-of-concept extraction of polycyclic aromatic hydrocarbons from water samples, Anal. Chim. Acta 1096 (2020) 100-107, https://doi.org/10.1016/j.aca.2019.10.050.

CHAPTER 7: SUPPORTING INFORMATION

7.1. APPENDIX 1: VACUUM-ASSISTED HEADSPACE SORPTIVE EXTRACTION: THEORETICAL CONSIDERATIONS AND PROOF-OF-CONCEPT EXTRACTION OF POLYCYCLIC AROMATIC HYDROCARBONS FROM WATER SAMPLES.

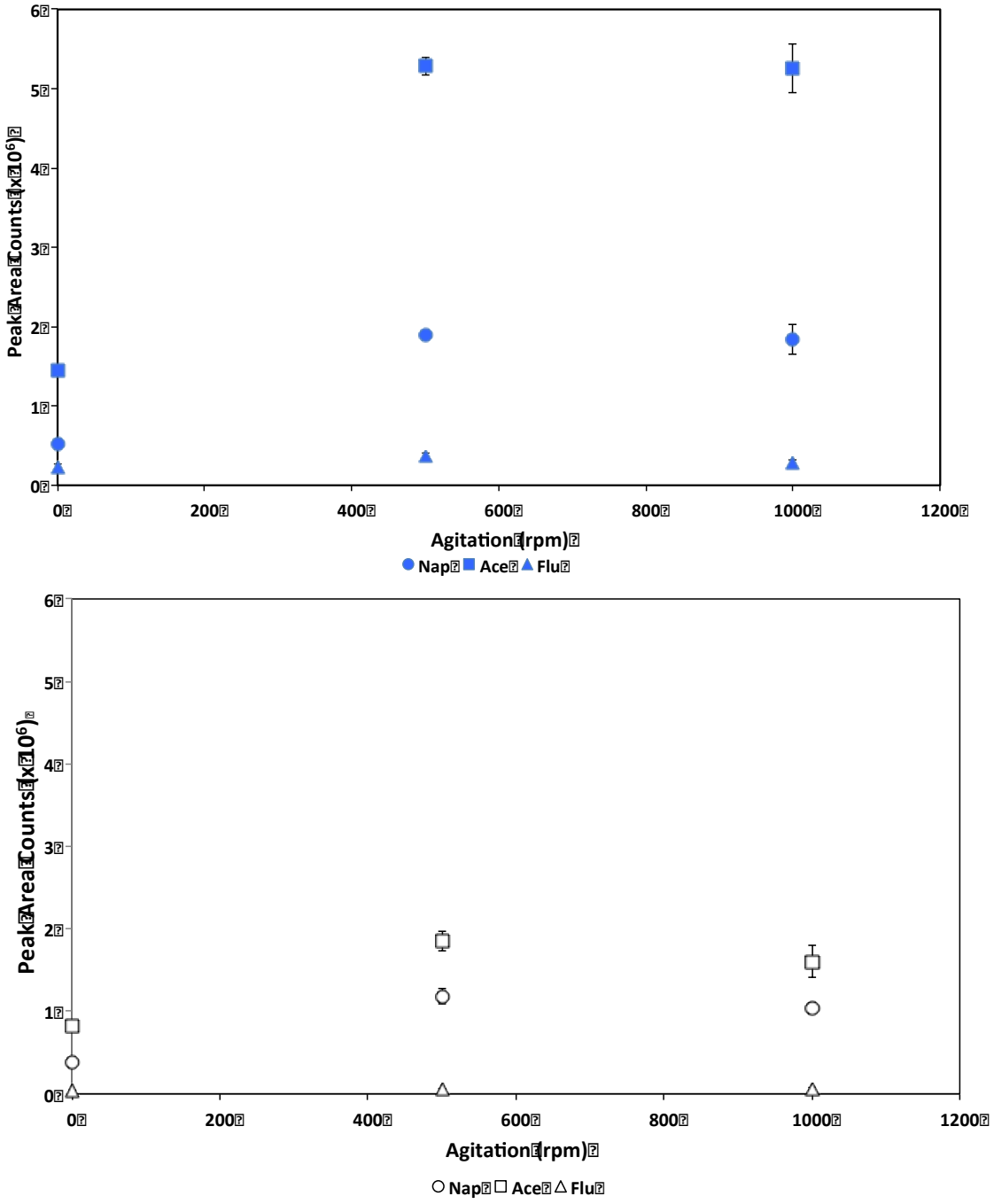

Fig. S.1 Effect of agitation on (i) Vac-HSSE and (ii) regular HSSE. Experimental conditions: 10 mL aqueous samples spiked at 5 μg L^{-1}; 30 min sampling time; 25 °C sampling temperature. Some error bars are too small to be visible as compared with the physical size of the symbol.

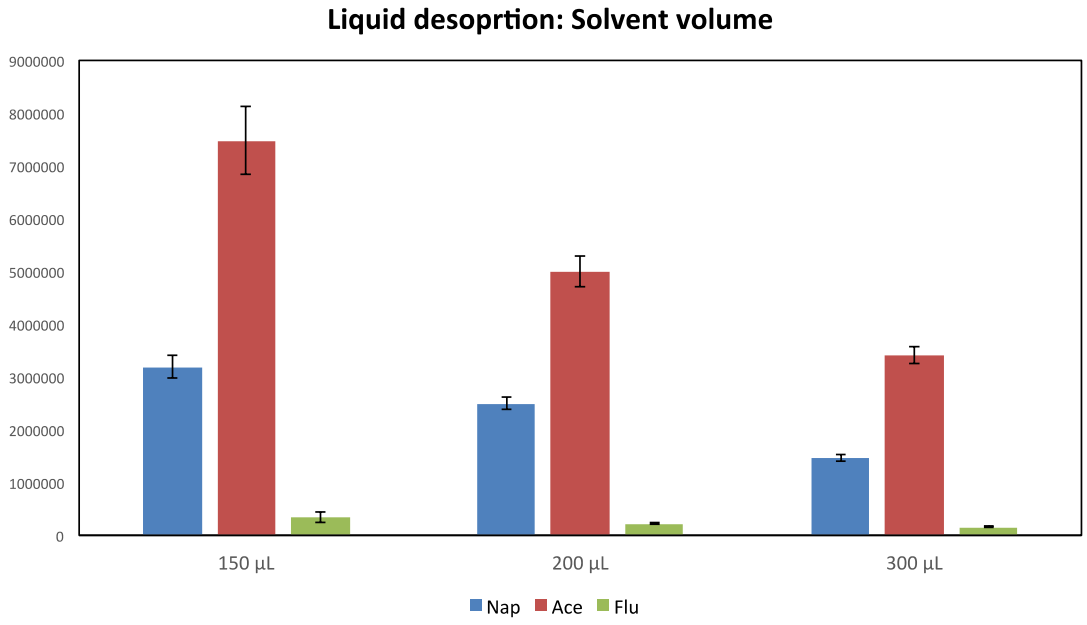

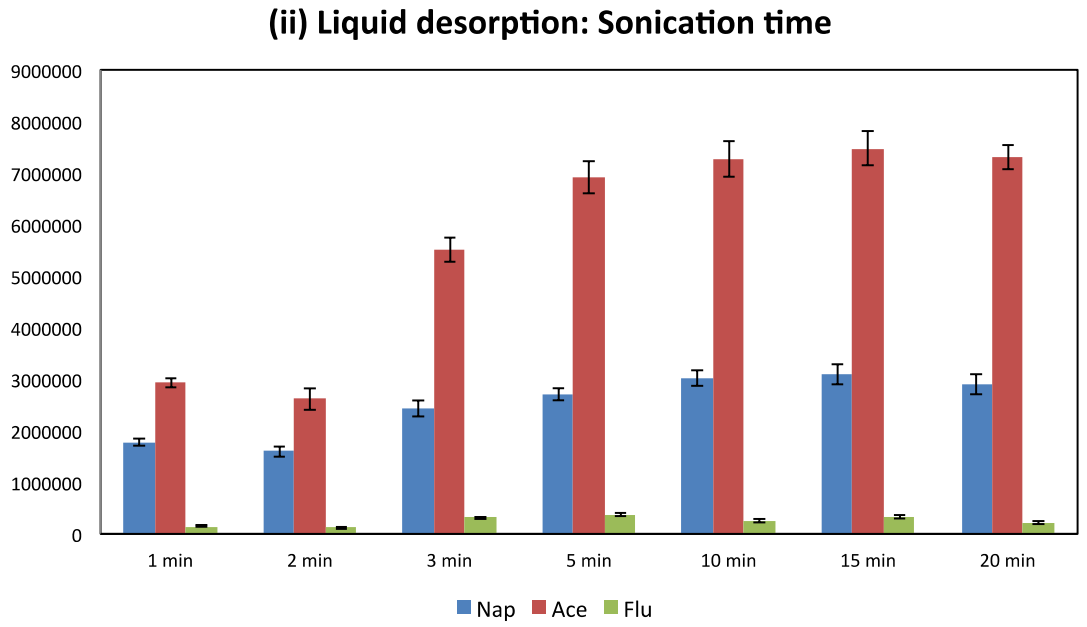

Fig. S.2 Optimization of the liquid desorption step using regular HSSE at 25 °C: (i) effect of solvent volume (sonication time 15 min) and (ii) effect of sonication time using 150 µL acetonitrile. Other experimental conditions: 10 mL aqueous samples spiked at 10 µg L^{-1}; 30 min sampling time; 25 °C sampling temperature.

7.2. APPENDIX 2: TOTAL AND BIOAVAILABLE POLYCYCLIC AROMATIC HYDROCARBONS IN UNUSED AND OPERATED HEAT-NOT-BURN TOBACCO PRODUCTS AND CONVENTIONAL CIGARETTES

Table S.1 The 16 priority PAHs investigated here, their acronym, main physicochemical properties and quantification ion used. The instrumental limits of detection (LOD) are also given and expressed as ng. The instrumental LODs were calculated as three times the standard deviation of the response divided by the slope of the eight-point calibration curve obtained for each PAH after injecting in 1 μL hexane solutions of PAHs in the concentration range 0.005 – 5.0 mg L^{-1}.

Name	Abbreviation	M.W.	Number of rings	Log K_{ow}	Water solubility (mg L^{-1})	Quant. Ion	LOD (ng)
Naphthalene	Nap	128.2	2	3.30	31.0	128	0.116
Acenaphthylene	Acy	152.2	2	3.94	2.49	152	0.055
Acenaphthene	Ace	154.2	3	3.92	3.90	153	0.059
Fluorene	Flu	166.2	3	4.18	1.89	165	0.061
Phenanthrene	Phe	178.2	3	4.46	1.15	178	0.066
Anthracene	Ant	178.2	3	4.45	0.0434	178	0.085
Fluoranthene	Flt	202.3	4	5.16	0.26	202	0.074
Pyrene	Py	202.3	4	4.88	0.135	202	0.082
Benzo(a)anthracene	B[a]Ant	228.3	4	5.76	0.0094	228	0.131
Chrysene	Chry	228.2	4	5.81	0.00345	228	0.124
Benzo(b)fluoranthrene	B[b]Flt	252.3	5	5.78	0.0012	252	0.098
Benzo(k)fluoranthrene	B[k]Flt	252.3	5	6.11	0.0008	252	0.123
Benzo(a)pyrene	B[a]Py	252.3	5	6.13	0.00162	252	0.198
Indeno(1,2,3-cd)pyrene	IcdPy	276.3	6	6.76	0.02786	276	0.477
Dibenzo(a,h)anthracene	DB[ah]Ant	278.3	6	6.75	0.00249	278	0.442
Benzo[ghi]perylene	B[ghi]Pe	276.3	6	6.70	0.002491	276	0.523

Table S.2 Composition of the natural water samples used in this work.

	River water	Rainwater	Sea water
Cl (mg L^{-1})	13	16	24990
N-NO_3(mg L^{-1})	0.53	0.53	2.12
SO_4 (mg L^{-1})	1.1	1.4	3329
P-PO_4 (mg L^{-1})	0.02	0.07	0.35
HCO_3(mg L^{-1})	103.8	19.2	965.8
N-NH_3(mg L^{-1})	0.06	0.05	0.15
N-NO_2 (mg L^{-1})	<0.002	<0.002	<0.002
F (mg L^{-1})	0.12	0.03	2.94
$CaCO_3$ (mg L^{-1})	84.7	15.6	788.6
IC (mg L^{-1})	21.4	3.8	209.0
TN (mg L^{-1})	0.64	0.58	2.5-3.0
EC (µS cm^{-1})	253	65.3	56600
pH	7.68	6.36	7.35

Table S.3 Mass weight of used and unused tobacco product units and their parts. All masses correspond to mean values obtained after weighting separately 3 different units of each product. Data taken from: Koutela N, Fernández E, Saru M-L, Psillakis E (2020), A comprehensive study on the leaching of metals from heated tobacco sticks and cigarettes in water and natural waters. Sci Total Environ 714, 136700. https://doi.org/10.1016/j.scitotenv.2020.136700.

		HnBs (g)	CCs (g)
UNUSED	WHOLE	0.7633	0.8386
	PAPER	0.1424	0.1109
	FILTER	0.3266	0.0970
	TOBACCO	0.2879	0.6077
USED	WHOLE	0.7099	0.2561
	PAPER	0.1464	0.0773
	FILTER	0.3609	0.1108
	TOBACCO	0.2163	0.0677

Table S.4 Number of units of heated tobacco sticks and cigarettes and volume of water used during leaching experiments.

	Tobacco product	Number of tobacco product units used	Water volume (mL)
UNUSED	HnBs	4	31
	CCs	4	31
USED	HnBs	4	31
	CCs	10	25

Table S.5 Total concentrations of PAHs for used CCs found in this work and those reported in three past reports[a-c]. Concentrations are expressed in µg unit^{-1} and µg g^{-1} to allow comparison between results.

	USED CCs				
	This work (µg unit^{-1})	**This work (µg g^{-1})**	**REF 1[a] (µg unit^{-1})**	**REF 2[b] (µg g^{-1})**	**REF 3[c] (µg g^{-1})**
Nap	1.0±0.1	3.9±0.6	0.404±0.063	2.87-11.6	-
Acy	0.051±0.002	0.19±0.02	0.177±0.025	0.79-1.62	-
Ace	0.098±0.007	0.38±0.04	0.092±0.014	1.01-4.04	-
Flu	0.16±0.02	0.6±0.1	0.401±0.030	0.99-3.70	0.028
Phe	0.06±0.01	0.24±0.05	0.277±0.019	0.29-0.66	0.0748
Ant	0.028±0.005	0.11±0.02	0.123±0.011	0.81-1.61	0.0071
Flt	0.014±0.003	0.05±0.01	0.113±0.011	0.73-1.6	-
Py	0.009±0.002	0.036±0.008	0.104±0.011	0.65-1.46	0.091
B[a]Ant	0.0094±0.0007	0.036±0.004	0.020±0.005	0.82-2.15	0.026
Chry	0.008±0.001	0.033±0.006	0.025±0.006	0.69-1.74	0.044
B[b]Flt	-	-	-	0.77-1.85	0.031
B[k]Flt	-	-	-	0.53-1.35	0.015
B[a]Py	-	-	-	0.70-1.84	0.031
IcdPy	-	-	-	1.00-2.60	-
DB[ah]Ant	-	-	-	0.4-1.02	0.0065
B[ghi]Pe	-	-	-	1.01-1.02	0.031

[a] Data taken from: King IC, Lorenzi V, Blasius ME, Gossett R (2021), Leachates from Cigarette Butts Can Persist in Marine Sediment. Water, Air, Soil Pollut 232:38. https://doi.org/10.1007/s11270-021-04999-3

[b] Data taken from: Dobaradaran S, Schmidt TC, Lorenzo-Parodi N, Jochmann MA, Nabipour I, Raeisi A, Stojanović N, Mahmoodi M (2019) Cigarette butts: An overlooked source of PAHs in the environment? Environ. Pollut. 249:932-939. doi: 10.1016/j.envpol.2019.03.097.

[c] Data taken from: Moriwaki, H, Kitajima, S., Katahira, K, (2009) Waste on the roadside, "poi-sute" waste: its distribution and elution potential of pollutants into environment. Waste Manag. 29, 11921197. https://doi.org/10.1016/j.wasman.2008.08.017.

Table S.6 Effect of pH, NaCl and humic acids content on the leaching of PAHs from unused and used HnBs at 24 h soaking time. The error values correspond to the standard deviation of three-replicate samples.

	HnBs				
	UNUSED (ng unit^{-1})				
	pH=4	**pH=6**	**pH=8**	**NaCl**	**Humic Acids**
Nap	76.24±1.52	82.06±9.78	80.92±34.87	70.76±2.99	87.59±3.15
Acy	0.31±0.01	0.31±0.02	0.38±0.02	1.82±0.25	0.93±0.02
Ace	1.9±0.25	1.9±0.2	2.05±0.33	2.15±0.18	2.53±0.47
Flu	0.3±0.01	0.3±0.02	0.32±0.05	0.7±0.01	0.44±0.04
Phe	0.61±0.02	0.63±0.06	1.1±0.32	1.21±0.32	1.6±0.09
SUM	**79.35±1.54**	**85.21±9.78**	**84.78±34.87**	**76.64±3.02**	**93.11±3.19**
	USED (ng unit^{-1})				
	pH=4	**pH=6**	**pH=8**	**NaCl**	**Humic Acids**
Nap	62.32±12.7	60.59±15.97	65.82±6.05	63.14±5.98	74.35±10.65
Acy	0.45±0.17	0.37±0.07	0.37±0.04	0.27±0.03	0.53±0.03
Ace	1.86±0.4	1.32±0.03	2.09±0.28	1.9±0.35	2.14±0.27
Flu	0.69±0.01	0.52±0.1	0.69±0.01	0.72±0.01	0.56±0.07
Phe	0.73±0.01	0.54±0.09	0.9±0.08	0.98±0.17	1.19±0.06
SUM	**66.05±12.71**	**63.34±15.97**	**69.87±6.05**	**67.01±5.99**	**78.78±10.66**

Table S.7 Effect of pH, NaCl and humic acids content on the leaching of PAHs from unused and used CCs at 24 h soaking time. The error values correspond to the standard deviation of three-replicate samples.

	CCs				
	UNUSED (ng unit^{-1})				
	pH=4	**pH=6**	**pH=8**	**NaCl**	**Humic Acids**
Nap	73.24±2.03	58.58±21.76	62.28±6.33	72.92±8.93	76.24±14.86
Acy	0.6±0.01	0.6±0.28	0.97±0.01	0.25±0.01	0.26±0.02
Ace	3.54±0.73	1.9±0.21	3.16±0.11	2.76±0.48	2.88±0.88
Flu	0.65±0.01	0.53±0.09	1.73±0.74	0.43±0.3	0.35±0.08
SUM	**78.02±2.16**	**61.61±21.76**	**68.14±6.38**	**76.36±8.95**	**79.73±14.89**
	USED (ng unit^{-1})				
	pH=4	**pH=6**	**pH=8**	**NaCl**	**Humic Acids**
Nap	42.75±4.34	42.27±0.74	35.86±6.61	41.76±4.38	48.58±3.3
Acy	0.71±0.01	0.67±0.08	0.87±0.05	0.41±0.07	0.55±0.04
Ace	0.92±0.05	1.03±0.13	1.11±0.13	1.11±0.28	0.94±0.12
Flu	0.59±0.19	0.7±0.11	0.91±0.16	0.54±0.05	0.45±0.04
Phe	0.36±0.01	0.41±0.01	0.51±0.11	0.35±0.02	0.47±0.04
Flt	0.19±0.01	0.18±0.02	0.17±0.01	0.25±0.01	0.33±0
SUM	**45.33±4.35**	**45.09±0.77**	**39.25±6.61**	**44.17±4.39**	**51±3.31**

Table S.8 Dissolved concentrations in natural water samples (river water, rainwater, and seawater) from unused and smoked CCs at 24 h soaking time. Error values correspond to the standard deviation of three replicated analyses.

	CCs		
	UNUSED (ng unit^{-1})		
	RIVER WATER	**RAINWATER**	**SEA WATER**
Nap	84.24±13.51	71.96±12.78	78.57±24.69
Acy	0.34±0.16	0.44±0.08	0.29±0.02
Ace	2.91±0.13	2.22±0.26	2.94±0.73
Flu	0.55±0.06	0.72±0.2	0.46±0.11
SUM	**88.04±13.51**	**75.34±12.34**	**82.26±24.7**
	USED (ng unit^{-1})		
	RIVER WATER	**RAINWATER**	**SEA WATER**
Nap	49.67±2.92	48.44±2.02	35.88±0.45
Acy	0.59±0.07	0.6±0.02	0.37±0.03
Ace	1.01±0.06	0.99±0.11	0.95±0.04
Flu	0.57±0.3	0.73±0.03	0.39±0.09
Phe	0.6±0.18	0.46±0.03	0.25±0.01
Flt	0.47±0.21	0.37±0	0.25±0.06
SUM	**52.44±2.95**	**51.22±2.02**	**37.85±0.47**

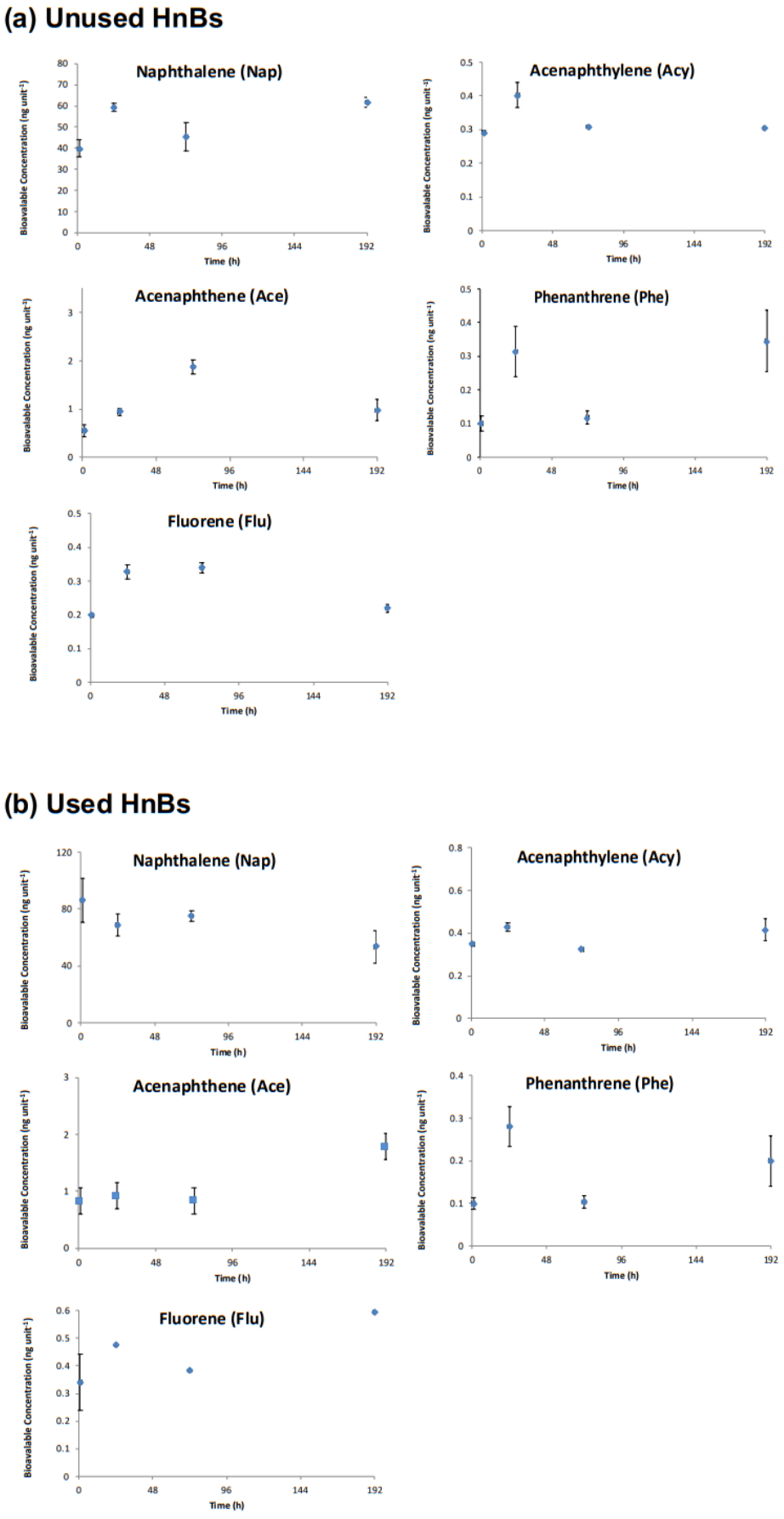

Fig. S.3 Leaching kinetics curves obtained for (a) unused and (b) used HnBs in ultrapure water.

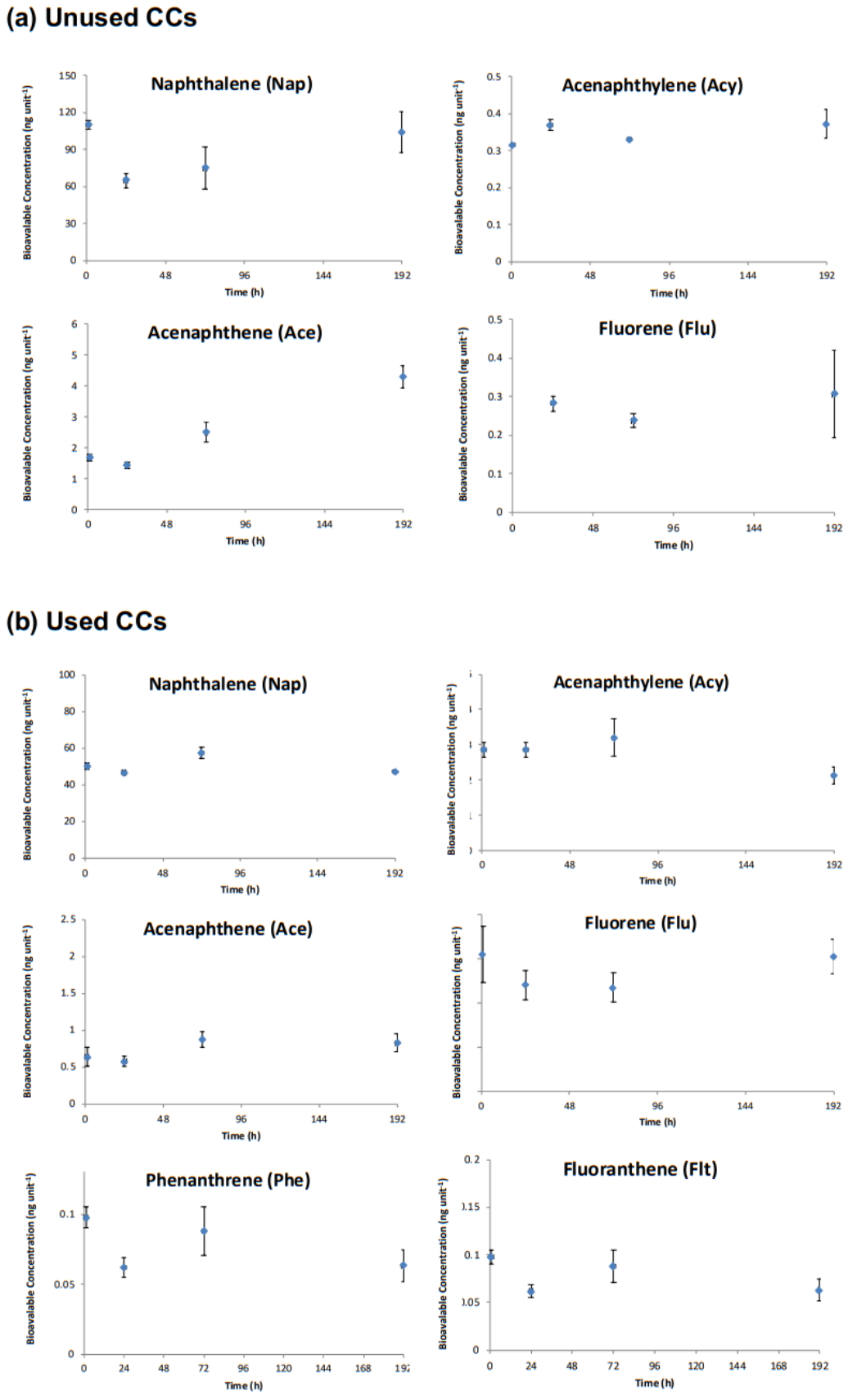

Fig. S.4 Leaching kinetics curves obtained for (a) unused and (b) unused CCs in ultrapure water.

7.3. APPENDIX 3: UV-254 DEGRADATION OF NICOTINE IN NATURAL WATERS AND LEACHATES PRODUCED CIGARETTE BUTTS AND HEAT-NOT-BURN TOBACCO PRODUCTS.

S.1 *Determination of total and bioavailable nicotine concentration in tobacco products*

The determination of the total nicotine concentration was carried out by placing depending on the experiment, used or unused solid tobacco product or their parts (tobacco, paper and filter) in a 250 mL Erlenmeyer flask. Then 20 mL water, 40 mL hexane containing the 500 mg L^{-1} n-hexadecane as the internal standard, and 10 mL of a 2 M NaOH water solution were added and the mixture was shaken in a Unimax 1010 shaker (Heidolph, Essex, UK) for 1 h at 245 rpm and protected from light. After shaking, the mixture was left unattended until phase separation occurred. The organic phase was filtered using a 0.45 μm Nylon syringe filter and 1 μL was injected in a Shimadzu Gas Chromatograph equipped with a Flame Ionization Detector (GC-FID) in the split mode (1:10) using a standard procedure [1]. The GC run was isothermal at 170 ºC for 10 min with a 1.5 mL min^{-1} helium flow rate. The temperatures of the injector and detector were set at 270 ºC.

The bioavailable nicotine concentration was determined by adding in a 250 mL Erlenmeyer flask a preset volume (20 mL for HnBs and 10 mL for CC) of the leachate produced from the corresponding used or unused tobacco products or their parts, 40 mL hexane (containing 500 mg L^{-1} of n-hexadecane as the internal standard) and 10 mL of 2 M NaOH solution. The mixture was shaken for 1 h at 245 rpm in a Unimax 1010 shaker, protected from light. The two phases were left to separate by gravity, the organic phase was filtered using a 0.45 μm Nylon syringe filter and 1 μL was the injected and analyzed in the GC-FID using the same chromatographic conditions.

Reference

[1] World Health Organization (WHO), WHO TobLabNet Official Method SOP 04 – Standard operating procedure for determination of nicotine in cigarette tobacco filler, (2014) 18.

Table S.9 Composition of the natural water samples used in this work.

	River water	Seawater	Rain water
Cl (mg L^{-1})	13	24990	16
N-NO_3(mg L^{-1})	0.53	2.12	0.53
SO_4(mg L^{-1})	1.1	3329	1.4
P-PO_4 (mg L^{-1})	0.02	0.35	0.07
HCO_3(mg L^{-1})	103.8	965.8	19.2
N-NH_3(mg L^{-1})	0.06	0.15	0.05
N-NO_2(mg L^{-1})	<0.002	<0.002	<0.002
F (mg L^{-1})	0.12	2.94	0.03
$CaCO_3$ (mg L^{-1})	84.7	788.6	15.6
IC (mg L^{-1})	21.4	209.0	3.8
TN (mg L^{-1})	0.64	2.5-3.0	0.58
EC (µS cm^{-1})	253	56600	65.3
pH	7.99	7.91	6.44

Table S.10 Degradation products identified during the direct nicotine photolysis using LC/MS and TD-GC/ITMS.

Product	**Retention time (min)**		**Identification Ions**	**Tentative identification**
	LC/MS	**TD-GC/ITMS**		
Nicotine	1.592		163	
		14.310	161, 133, 84	
Cotinine	1.409		177	Cotinine
P105		7.347	105, 78, 51	3-ethenylpyridine
P135	4.590		136	3-Propionylperazine
P181	1.046		182,163	3, 4-Dihydroxy-1-(pyridin-3-yl)butan-1-one
P208	1.087		209	2-Hydroxy-N-methyl-4-oxo-4-(pyridin-3-yl)butanamide

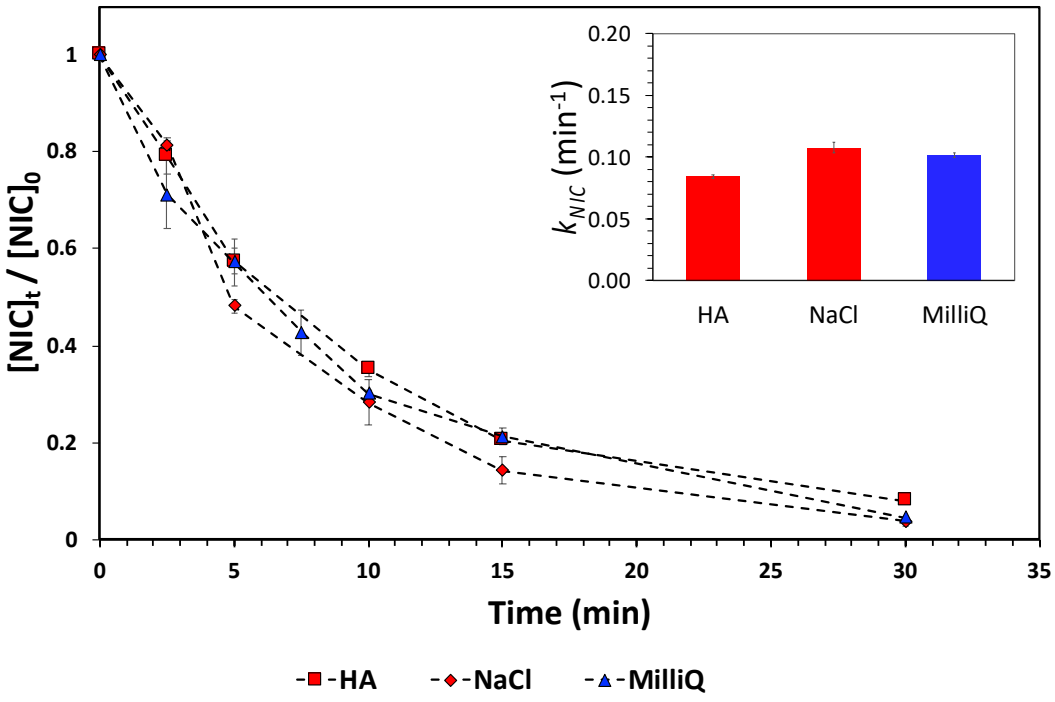

Fig. S.5 Photolysis of 10 mg L^{-1} nicotine solutions in the presence of 2.5 mg L^{-1} humic acids and 3.5 % w:v NaCl under UV_{254} irradiation. Inset graph: apparent rate constants for each dissolved species tested. The photolysis of 10 mg L^{-1} nicotine in ultrapure water (MilliQ) is also given for comparison.

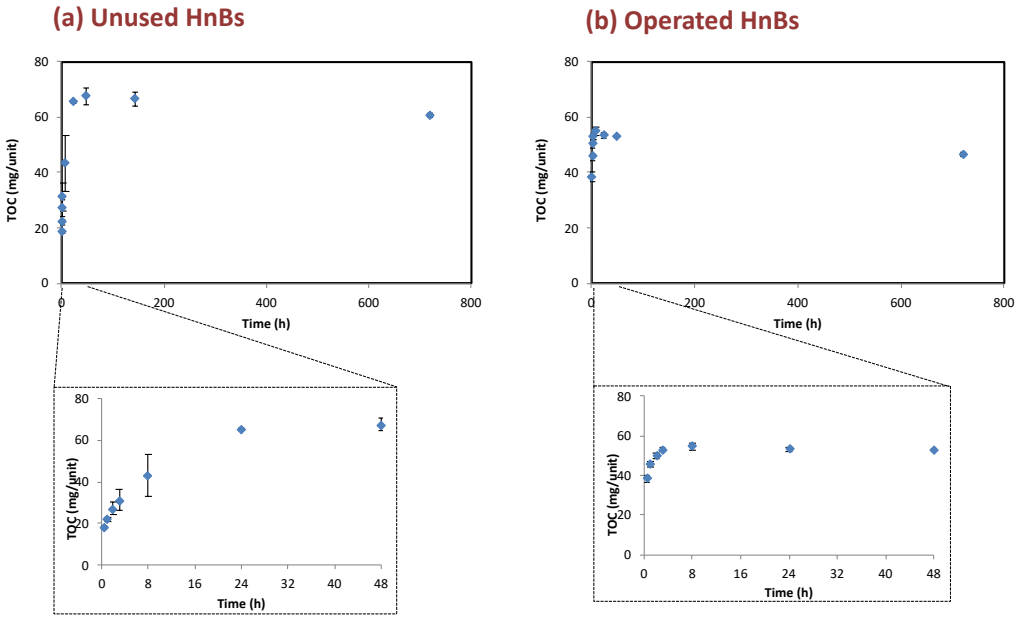

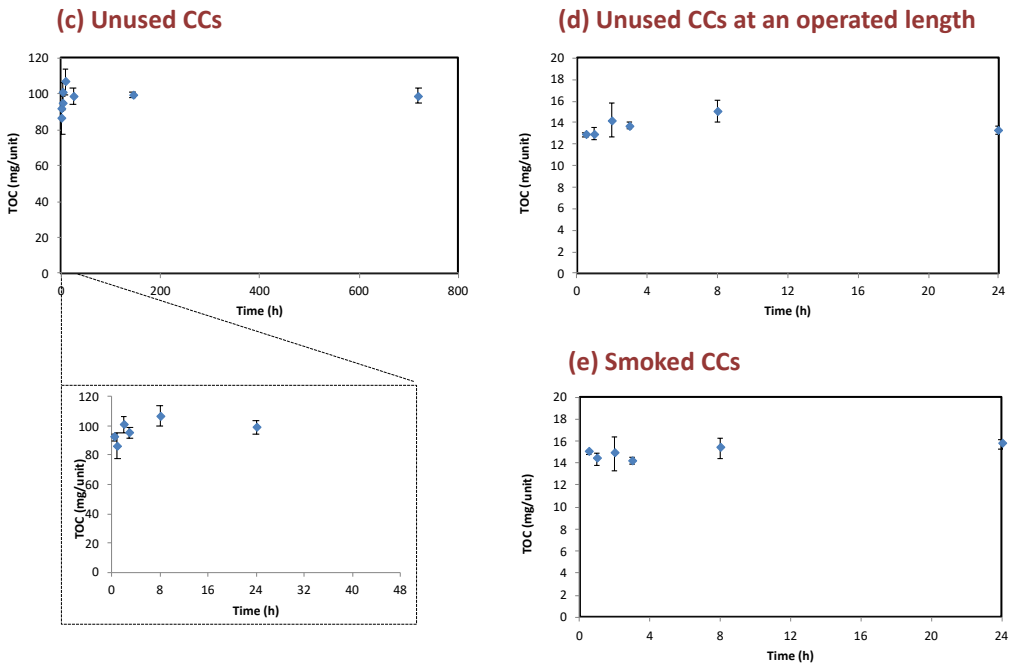

Fig. S.6 Leaching kinetic curves obtained for (a) unused, and (b) operated HnBs and (c) unused CCs at the full length and an operated length (filter plus 3 mm of the tobacco plug) and (d) smoked CCs in ultrapure water.

Table S.11 Total and bioavailable (24 h of soaking) nicotine concentration in used and unused HnB and CC and their different parts (paper, filter and tobacco). The error values correspond to the standard deviation of three-replicate samples. LOD and LOQ stand for limit of detection and quantification respectively.

	Total nicotine content (mg unit^{-1})				**Bioavailable nicotine at 24 h (mg unit^{1})**			
	Whole	**Paper**	**Filter**	**Tobacco**	**Whole**	**Paper**	**Filter**	**Tobacco**
Unused HnB	4.67±0.09	<LOQ	<LOQ	4.71±0.14	3.90±0.21	<LOQ	<LOD	4.55±0.05
Used HnB	3.20±0.09	0.40±0.02	1.17±0.10	1.46±0.04	2.88±0.07	0.43±0.03	1.32±0.08	1.33±0.09
Unused CC	9.46±0.34	<LOQ	<LOQ	10.1±0.4	10.3±0.3	<LOD	<LOD	10.0±0.4
Used CC	1.55±0.11	0.126±0.003	0.60±0.02	1.23±0.02	1.74±0.15	0.130±0.002	0.65±0.05	1.21±0.06

Table S.12 Effect of pH, NaCl (3.5 % w:v) and humic acids (HA; 2.5mg L^{-1}) content on nicotine leaching from used and unused HnB and CCs at 24 h soaking time. Error values correspond to the standard deviation of three replicated analysis.

	UNUSED (mg unit^{-1})					USED (mg unit^{-1})				
	pH=4	**pH=6**	**pH=8**	**HA**	**NaCl**	**pH=4**	**pH=6**	**pH=8**	**HA**	**NaCl**
HnB	3.67±0.22	3.90±0.21	3.60±0.32	4.05±0.30	3.69±0.20	2.75±0.03	2.88±0.07	2.89±0.45	2.65±0.04	2.95±0.18
CCs	10.3±0.2	10.3±0.3	10.3±0.5	10.1±0.4	10.7±0.4	1.60±0.24	1.74±0.15	1.74±0.02	1.81±0.07	1.84±0.01

Table S.13 Bioavailable nicotine concentrations in ultrapure water (MilliQ) and natural water samples (sea water, rain water and river water) from used and unused HnBs and CCs at 24 h soaking time. Error values correspond to the standard deviation of three replicated analysis. The composition of the natural water is given in Table S.9.

	UNUSED (mg unit^{-1})				USED (mg unit^{-1})			
	Milli Q	**Sea**	**Rain**	**River**	**Milli Q**	**Sea**	**Rain**	**River**
HnB	3.90±0.21	4.2±0.3	4.3±0.2	4.4±0.2	2.88±0.07	2.80±0.09	2.85±0.09	2.8±0.2
CCs	10.3±0.3	9.1±0.7	8.9±0.1	9.0±0.2	1.74±0.15	1.82±0.02	1.75±0.08	1.62±0.01

7.4. APPENDIX 4: UVC-INDUCED DEGRADATION OF CILASTATIN IN NATURAL WATER AND TREATED WASTEWATER

Table S.14 Composition of the water samples used in this work.

	River water	Tap water	WW
Cl^- (mg L^{-1})	13	150	13
N-NO_3^- (mg L^{-1})	0.54	5.97	0.53
SO_4^{-2} (mg L^{-1})	12.4	105.3	1.1
P-PO_4^{-3} (mg L^{-1})	0.02	1.68	0.02
HCO_3^- (mg L^{-1})	103.4	144.6	103.8
N-NH_3(mg L^{-1})	0.10	0.24	0.06
N-NO_2^- (mg L^{-1})	0.004	0.320	<0,002
F^- (mg L^{-1})	0.24	0.53	0.12
$CaCO_3$ (mg L^{-1})	84.4	118.1	84.7
IC (mg^C L^{-1})	22.5	33.1	21.4
TN (mg^N L^{-1})	0.98	11.50	0.64
EC (µS cm^{-1})	274.00	932.00	253.00
pH	7.32	7.14	7.68

Table S.15 k and R_o values for the different UV-irradiated aqueous solutions of cilastatin (CIL). The error values correspond to the standard deviation of replicate experiments rounded to significant digits.

Description of the UV-irradiated water solution	***k*, (min^{-1})**	***Ro*, (× 10^{-7} mol L^{-1} s^{-1})**
Effect of concentration		
2.5 mg L^{-1} CIL H_2O solution	0.20 ± 0.02	0.22 ± 0.02
25 mg L^{-1} CIL H_2O solution	0.11 ± 0.01	1.18 ± 0.10
50 mg L^{-1} CIL H_2O solution	0.09 ± 0.00	1.89 ± 0.05
100 mg L^{-1} CIL H_2O solution	0.06 ± 0.00	2.43 ± 0.06
Effect of pH		
pH=3; 100 mg L^{-1} CIL H_2O solution	0.16 ± 0.00	6.79 ± 0.12
pH=5; 100 mg L^{-1} CIL H_2O solution,	0.07 ± 0.01	3.09 ± 0.40
pH=7; 100 mg L^{-1} CIL H_2O solution	0.05 ± 0.01	2.29 ± 0.27

pH=9; 100 mg L^{-1} CIL H_2O solution	0.04 ± 0.00	1.71 ± 0.20
Effect of additives		
t-butanol; 100 mg L^{-1} CIL H_2O solution	0.05 ± 0.00	1.97 ± 0.10
2.5 mg L^{-1} HA; 2.5 mg L^{-1} CIL H_2O solution	0.10 ± 0.01	0.11 ± 0.01
Natural and treated water samples		
Tap water spiked at 2.5 mg L^{-1} with CIL	0.19 ± 0.04	0.22 ± 0.04
WW effluent spiked at 2.5 mg L^{-1} with CIL	0.07 ± 0.00	0.07 ± 0.00
River water spiked at 2.5 mg L^{-1} with CIL	0.11 ± 0.01	0.12 ± 0.01

Table S.16 Analytical characteristics of CIL and of the identified degradation product eluting during the photolysis of CIL.

Product	**Retention time (min)**	**Identification Ions (m/z)**	**Tentative identification**
CIL	4.491	359	
P374	1.648	375/359/315	CIL oxidized to a sulfoxide group

Table S.17 Molar absorption coefficients at 254 nm (ε_x) and direct photolysis quantum yields for 254-nm irradiation (Φ_x) of the different CIL species. Note that x = H_3A^+, H_2A, HA^- or A^{2-}.

Species *x*	**ε_x, L mol^{-1} cm^{-1}**	**Φ_x, mol E^{-1}**
H_3A^+	2243±30	0.59±0.03
H_2A	2692±25	$(9.3\pm0.4)\times10^{-2}$
HA^-	1646±17	$(4.6\pm0.2)\times10^{-2}$
A^{2-}	1268±62	$(1.3\pm0.1)\times10^{-2}$

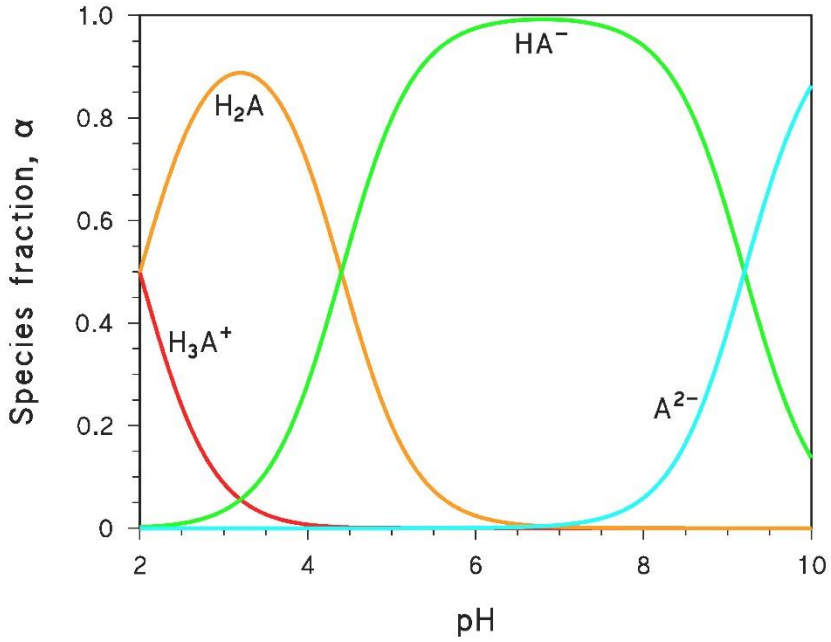

Fig. S.7 Relative abundances of the different CIL species, as a function of pH. The species fractions were derived from **Eqs. (5.1-5.4)**, using $[H^+] = 10^{-pH}$.

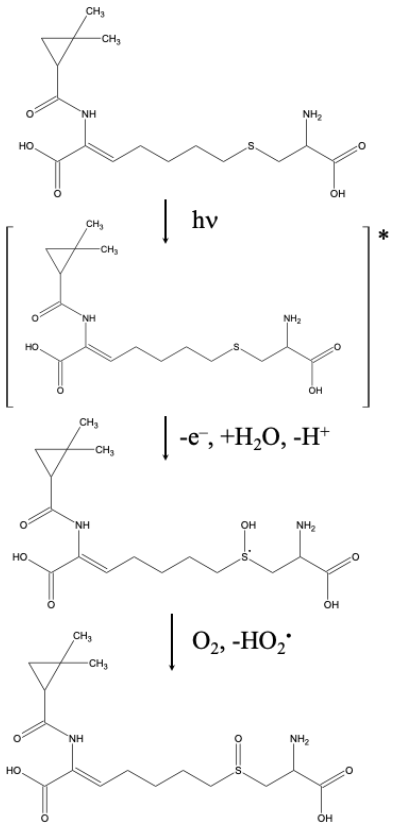

Fig. S.8 Tentative mechanism for the oxidation of the sulfide moiety of CIL to a sulfoxide group.

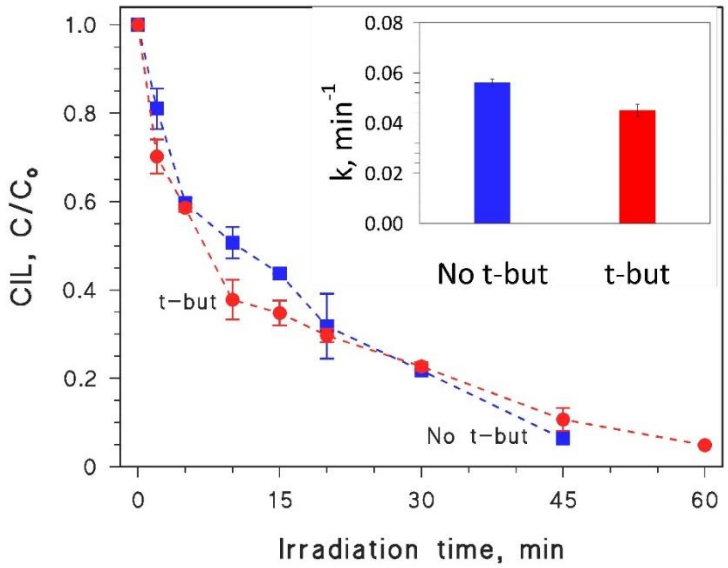

Fig. S.9 Time trends of 100 mg L^{-1} CIL upon 254-nm irradiation at near-neutral pH, alone and upon addition of 100 mg L^{-1} t-butanol. Data points are linked with dashed lines to visualize trends. **Inset:** respective pseudo-first order photodegradation rate constants, together with their sigma-level error bounds. Some error bars are too small to be visible.